

PDF hosted at the Radboud Repository of the Radboud University Nijmegen

The following full text is a publisher's version.

For additional information about this publication click this link.

<http://hdl.handle.net/2066/84459>

Please be advised that this information was generated on 2017-12-06 and may be subject to change.

**New *patches* in the molecular understanding of
renal magnesium handling**

Jenny van der Wijst

The research presented in this thesis was performed at the department of Physiology, Radboud University Nijmegen Medical Centre (RUNMC), the Netherlands, and financially supported by the Netherlands Organisation for Scientific Research (NWO).

ISBN 978-90-9025940-6

Cover design: Appeltje-S

Printed by CPI WÖHRMANN Print service

***New patches* in the molecular understanding of renal magnesium handling**

Een wetenschappelijke proeve
op het gebied van de Medische Wetenschappen

Proefschrift

ter verkrijging van de graad van doctor
aan de Radboud Universiteit Nijmegen
op het gezag van de rector magnificus prof. mr. S.C.J.J. Kortmann
volgens besluit van het college van decanen
in het openbaar te verdedigen op vrijdag 25 februari 2011
om 10:00 uur precies

door

Jenny Annet Jozé van der Wijst
geboren op 25 september 1983
te Oss

Promotores:

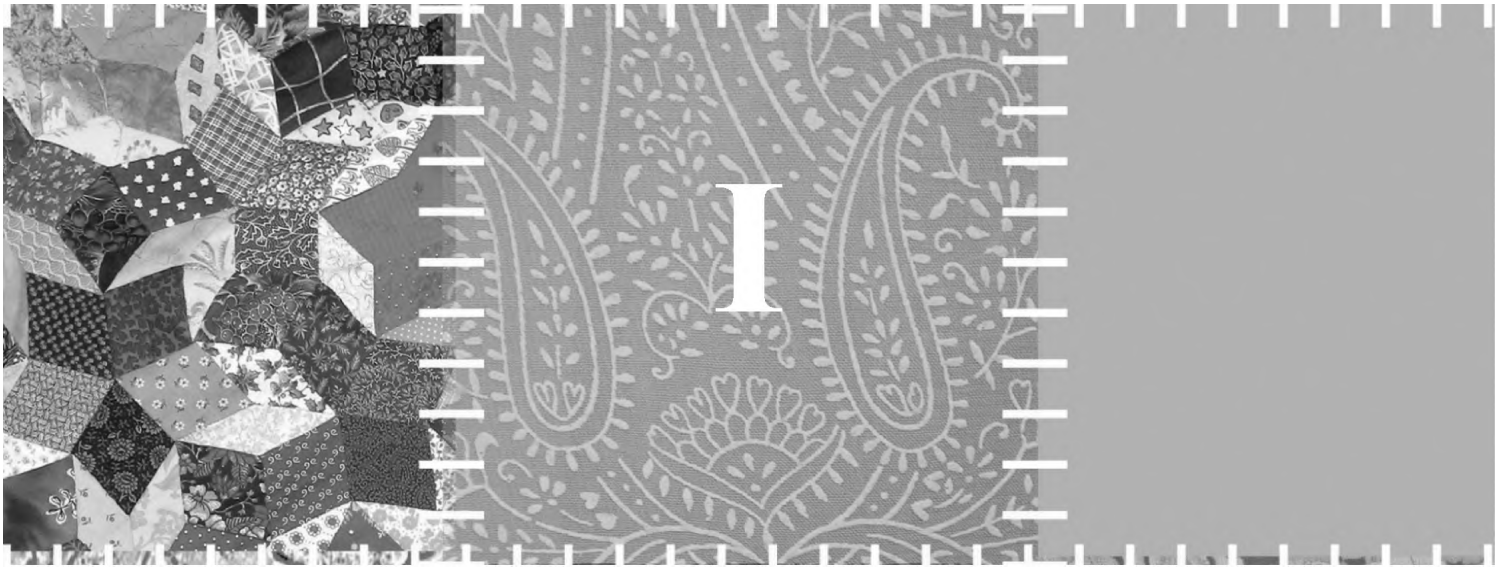
Prof. dr. R.J.M. Bindels
Prof. dr. J.G.J. Hoenderop

Manuscriptcommissie:

Prof. dr. H. van Bokhoven
Prof. dr. E.J. van Zoelen
Dr. M. Merkx (TU Eindhoven)

Table of contents

Chapter 1	7
General introduction	
Chapter 2	35
RACK1 inhibits TRPM6 activity via phosphorylation of the fused α -kinase domain	
Chapter 3	61
Regulation of the epithelial Mg^{2+} channel TRPM6 by estrogen and the associated Repressor protein of Estrogen receptor Activity (REA)	
Chapter 4	81
Methionine sulfoxide reductase B1 (MsrB1) recovers TRPM6 channel activity during oxidative stress	
Chapter 5	99
Effects of the Epidermal Growth Factor Receptor (EGFR) kinase inhibitor Erlotinib on renal and systemic Mg^{2+} handling	
Chapter 6	117
A missense mutation in the Kv1.1 voltage-gated potassium channel-encoding gene <i>KCNA1</i> is linked to human autosomal dominant hypomagnesemia	
Chapter 7	135
Functional analysis of the Kv1.1 N255D mutation associated with autosomal dominant hypomagnesemia	
Chapter 8	153
General discussion and summary	
Chapter 9	183
Nederlandse samenvatting	185
List of abbreviations	191
Curriculum vitae	193
List of publications	194
Dankwoord	195



General introduction

Ion channels

An estimated 100 trillion cells of different size and function build up the human body. Each cell is to some extent self-maintaining and can, therefore, be seen as the smallest entity of life [1]. All cells are surrounded by a plasma membrane, which separates the intracellular compartment from its environment. The plasma membrane is made from a double layer of hydrophobic lipids and hydrophilic phosphorus molecules, therefore also named phospholipid bilayer. It functions as a barrier controlling the movement of hydrophilic and charged molecules, mainly ions. By the early 70's it had become clear that integral membrane proteins exist that underlie the electrical signaling in nerve and muscle tissue. These integral membrane proteins, known as ion channels, provide a high conducting, hydrophilic passageway for the ions to flow down their electrochemical gradient. The 1950s and 1960s were important decennia for exciting discoveries concerning ion channels, though that term came in use later. In 1952, Alan Hodgkin and Andrew Huxley were the first to determine the elementary current properties of membranes as part of their research on excitation and inhibition of the nerve cell membrane. They received the Nobel Prize in physiology and medicine for their findings in 1963 (Table 1). Following, Bernard Katz obtained the Nobel Prize in physiology and medicine in 1970 for his research on the biochemistry and action of neurotransmitters and synapse properties (Table 1). He noticed an interesting noise on the recorded signal with acetylcholine application. Together with Ricardo Miledi, he worked on this noise analysis and provided information about how single ion channels behave. During this work, Bert Sakmann started working in Katz's laboratory and he did set up an electrical recording technique known as the "patch clamp". This fortuitous discovery was recognized by the Nobel Prize in 1991 to Erwin Neher and Bert Sakmann (Table 1). In the last decennia, research in the ion channel field led to the discovery of hundreds of different ion channels. They are classified according to their gating mechanism into voltage-gated, ligand-gated, pH-gated, or mechanically gated. In combination with ion selectivity and sequence similarity, these groups are further subdivided into several subtypes:





Voltage-gated potassium channels

The family of voltage-gated potassium (K^+) channels covers a functionally heterogeneous group of transmembrane channels specific for potassium. They activate in response to depolarization of the cell's membrane potential. This property makes the voltage-gated K^+ channels essential in shaping action potentials and controlling electric activity in excitable cells [2]. These channels are typically formed by four independent alpha-subunits surrounding the pore region. Each subunit has six transmembrane spanning α -helices (S1-S6) with both the amino (N) and the carboxyl (C) terminal on the intracellular side [3, 4]. The S1-S4 segments form the voltage sensing domain, whereas S5 and S6 along with the intervening re-entrant P-loop form the pore domain [5-7]. It was not until 1998 that the detailed molecular structure of a bacterial K^+ channel and the pore selectivity were unravelled by X-

ray crystallography [8]. Importantly, the X-ray structure of the voltage sensor was resolved in 2003, in a bacterial homolog of voltage-gated K^+ channels for which Roderick MacKinnon received the Nobel Prize in Chemistry in 2003 (Table 1) [9]. These structural discoveries opened a new research field that focuses on the mechanism of conformational changes in response to voltage changes. It is generally accepted that the positively charged amino acids in the S4 helices are responsible for voltage sensing. However, there exist a number of competing models for the orientation and conformation of the voltage-sensor domain relative to the pore domain upon membrane depolarization, i.e. the *canonical* or *helical screw* model, the *transporter* model, the *paddle* model, and the *twisted S4* model (reviewed in [7]).

Table 1. Nobel prize winners in the ion channel research field.

Desiphering ion channels: Nobel prize winners

Laureate	Year	Nobel prize	Discovery
Alan Lloyd Hodgkin Andrew Fielding Huxley 	1963	Physiology and Medicine	"for their discoveries concerning the ionic mechanisms involved in excitation and inhibition in the peripheral and central portions of the nerve cell membrane"
Sir Bernard Katz 	1970	Physiology and Medicine	"for the discoveries concerning the humoral transmitters in the nerve terminals and the mechanism for their storage, release and inactivation"
Erwin Neher Bert Sakmann 	1991	Physiology and Medicine	"for their discoveries concerning the function of single ion channels in cells"
Robert MacKinnon 	2003	Chemistry	"for structural and mechanistic studies of ion channels"

Other potassium channels

Other classes of channels selective for K^+ are the calcium (Ca^{2+})-activated K^+ channels, inwardly rectifying K^+ channels, and tandem pore domain K^+ channels. Ca^{2+} -activated K^+ channels open in response to intracellular calcium and voltage changes. They are subdivided in BK, IK, and SK channels. The inwardly rectifying potassium channels consist of a voltage-dependent block by endogenous polyamines and Mg^{2+} , which is removed upon hyperpolarization. These channels differ from the more typical (outwardly rectifying) voltage-gated K^+ channels in their ability to pass ions more easily into the cell (inwardly rectifying). Tandem pore domain (two-pore domain) K^+ channels are formed by four subunits that all contain two pore loops. They function as 'leak channels' and are gated by oxygen, pH, mechanical stretch and G-proteins. The enormous variety of K^+ channel function arises from the multiplicity of subunits, the formation of heteromultimers within subfamilies and from association with intracellular beta-subunit proteins [10, 11].

Voltage-gated calcium channels

Voltage-gated Ca^{2+} channels mediate Ca^{2+} influx upon membrane depolarization that regulates gene expression, excitation-contraction coupling in cardiac and skeletal muscle fibers, neuronal excitation, hormone secretion, and neurotransmission [12, 13]. Ca^{2+} channels are composed of four or five distinct subunits known as $\alpha 1$, $\alpha 2\delta$, $\beta 1-4$, and γ . The channels arise from multiple $\alpha 1$ subunit, while the other associated subunits are involved in modulation of gating. Mammalian $\alpha 1$ subunits are encoded by at least ten genes and various names had been given to the corresponding gene products, which gave rise to confusing nomenclatures. In 2000, a rational nomenclature was adopted based on the well-defined potassium channel nomenclature. Furthermore, these various subunits led to the formation of channels with different types of Ca^{2+} currents. The L-type Ca^{2+} channels ($Ca_v 1.1$ - $Ca_v 1.4$) are activated by strong depolarization and can be blocked by the organic L-type channel blockers dihydropyridines, phenylalkylamines, and benzothiazepines. These channels play a role in muscle and endocrine cells, where they initiate contraction and hormone secretion. The N-type ($Ca_v 2.2$), R-type ($Ca_v 2.3$), and closely related P/Q-type ($Ca_v 2.1$) Ca^{2+} channels, primarily expressed in neurons, also activate upon strong depolarization. They are mostly unaffected by L-type channel antagonists, but are blocked by specific polypeptide toxins. The T-type Ca^{2+} channels ($Ca_v 3.1$, $Ca_v 3.2$, $Ca_v 3.3$) already activate upon weak depolarization, resistant to the other channel blockers and are expressed more ubiquitously.

Voltage-gated sodium channels

Voltage-gated sodium (Na^+) channels are mainly expressed in excitable cells where they are important for the depolarising phase of action potentials [2]. Voltage-gated Na^+ channels have three types of states: deactivated (closed), activated (open), and inactivated (closed). The channels are likely blocked in the deactivated state. This block is removed upon depolarization that opens the

channel, starting an action potential. Shortly after the channel has been activated, it inactivates via a so-called inactivation gate that blocks the pore region of the channel. The inactivation state lasts for a few milliseconds and is removed during the repolarization phase of the action potential allowing the channel to be activated for the next action potential. The voltage-gated Na^+ channels are formed by a large α subunit that might associate with β subunits. The α subunit consists of four repeated domains (I-IV), all containing six transmembrane spanning segments (S1-S6). Similar to voltage-gated K^+ channels, the S4 segment functions as the voltage sensor and a pore-forming region exists between S5 and S6 [14]. The β subunits are not essential for channel function, but their association with the α subunit complex can alter the channel's voltage dependence or cellular localization [15]. So, the nomenclature is standardized according to the α subunit expression and the family of voltage-gated Na^+ channels contains nine members, named $\text{Na}_v1.1$ - $\text{Na}_v1.9$ [16].

Chloride channels

Chloride (Cl^-) channels belong to a diverse superfamily of anion channels [17]. They differ significantly in structure, gating mechanism, and physiological function. In general, Cl^- channels play an important role in the maintenance of cell volume and are involved in setting the resting membrane potential. So far, three mammalian gene families have been established of which the CLC gene family is best known. This family consists of nine CLC channel members, each build up by 10 or 12 transmembrane domains. The importance of several CLC channels is strikingly illustrated by four human inherited diseases linked to mutations in their genes, namely autosomal and recessive myotonia (CLC-1), osteopetrosis (CLC-7), inherited kidney stone diseases (CLCN5) and Bartter's syndrome type III (CLCNKB) [18-21]. Interestingly, the known Cl^- channel genes do not yet match the large variety of biophysically identified Cl^- channels, indicating that new families of Cl^- channels still need to be identified.

Cyclic nucleotide regulated channels

The cyclic nucleotide-regulated channel family consists of two subfamilies, the cyclic nucleotide-gated (CNG) and the hyperpolarization-activated cyclic nucleotide-gated (HCN) channels. CNG channels activation is mediated by direct binding of intracellular cAMP or cGMP [22]. They play important roles in sensory transduction and are mainly expressed in cilia of olfactory neurons and in photoreceptor neurons. CNG channels form heterotetramers by combining A subunits (CNGA1-CNGA4) and B subunits (CNGB1 and CNGB3) [23]. These channels are permeable to monovalent cations as K^+ and Na^+ , which are sensitive to voltage-dependent Ca^{2+} blockage [24]. HCN channels are activated upon hyperpolarization and channel activity is enhanced by cAMP and cGMP since they shift the activation to more positive potential. The mammalian HCN channel family contains four members (HCN1-HCN4) [25]. Homo- or heterotetrameric channels are formed of four HCN subunits,

each containing six transmembrane spanning helices (S1-S6) [26, 27]. HCN channels are widely expressed in heart and brain tissue, where they function as ‘pacemaker channels’ to control cardiac and neuronal rhythmicity [26, 28].

Ligand-gated channels

The ligand-gated ion channels are regulated by binding of a chemical messenger or ligand. They are generally selective to one or more ions like Na^+ , K^+ , Ca^{2+} , or Cl^- . The channel is a complicated pentameric structure, composed of five subunits, each with an extracellular ligand-binding domain and a transmembrane domain. The transmembrane domain consists of four transmembrane helices [29]. Ligand-gated ion channels can be subdivided into three superfamilies:

- Cys-loop receptors (nicotinic acetylcholine receptors, 5-HT₃ receptors, GABA_A and GABA_C receptors, glycine receptors, anionic glutamate receptors, histamine-gated receptors, and serotonin-activated anionic channels) are composed of five subunits, each with an extracellular ligand-binding domain and a transmembrane domain. The transmembrane domain consist of four transmembrane helices [29].
- Ionotropic glutamate receptors (AMPA receptors, NMDA receptors, and kainate receptors) are made of four subunits, each containing two transmembrane segments.
- ATP gated channels (ATP2x receptors) consist of three homologous subunits with three transmembrane segments.

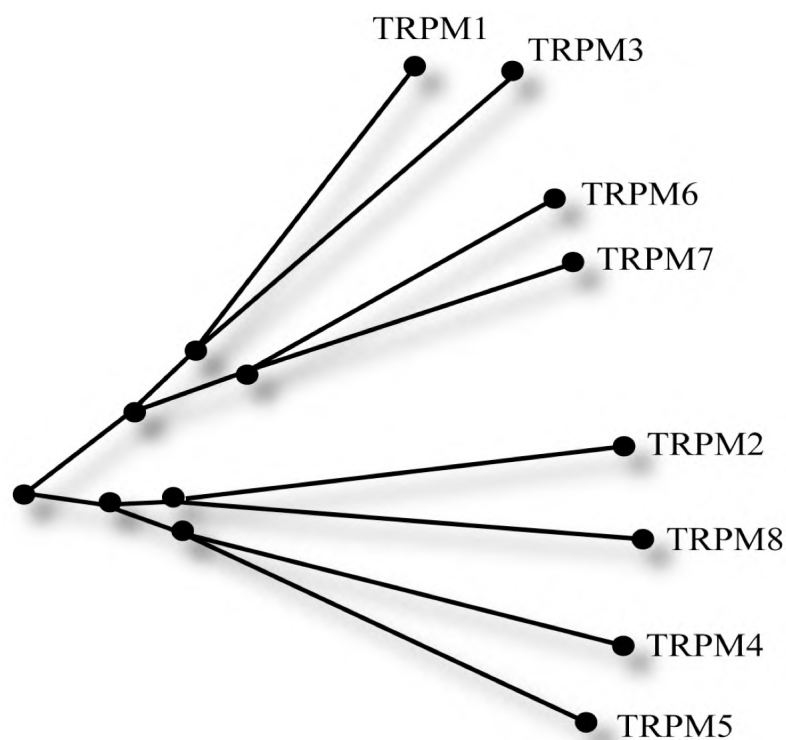


Figure.1 Phylogenetic tree of the mammalian Transient Receptor Potential Melastatin (TRPM) channel subfamily. (adapted from Nilius *et al.*, 2006) .

Transient Receptor Potential channels

The Transient Receptor Potential (TRP) channels are a family of cation channels that are permeable to both monovalent and divalent cations. TRP channels were initially discovered in *trp* mutant strain of the fruit fly *Drosophila melanogaster* [30]. In 1989, the *trp* gene was cloned [31] and it was shown that the encoded TRP protein constitutes a Ca^{2+} -permeable channel [32]. Subsequently, 28 mammalian TRP channels have been cloned that can be subdivided into six subfamilies: canonical (TRPC), vanilloid (TRPV), polycystin (TRPP), mucolipin (TRPML), ankyrin (TRPA), and melastatin (TRPM) [33]. The TRPM subfamily contains eight members (Fig. 1), which are expressed in many cell types and tissues [33, 34]. They are activated by a wide variety of stimuli including voltage, Ca^{2+} , temperature, cell swelling, and several endogenous and exogenous compounds [34, 35]. TRPM proteins are composed of six transmembrane spanning helices, a pore-forming region, and large intracellular N- and C-termini (Fig. 2A). The six transmembrane units are assembled around a central pore in a homo- or heterotetrameric configuration [33] (Fig. 2B).

The magnesiotropic TRP channels

Within the TRPM subfamily, two members, TRPM6 and TRPM7 have been identified as important molecular players in Mg^{2+} homeostasis. These channels share the unique feature of combining an atypical protein kinase domain in the C-termini with an ion channel domain, which gave them the name ‘chanzyme’ [36-38] (Fig. 2A).

Mg^{2+} homeostasis

The tight control of blood magnesium (Mg^{2+}) is of central importance for various essential physiological processes, since it functions as a cofactor in multiple enzymatic reactions involved in energy metabolism, DNA and protein synthesis [39-41]. Clinical manifestations of altered Mg^{2+} homeostasis are multifold. Hypermagnesemia can cause lethargy, confusion, coma and extreme cases can result in cardiac arrest [42]. Hypomagnesemia may lead to similar symptoms as tetany, seizures, and cardiac arrhythmias [42, 43]. Furthermore, disturbances in the Mg^{2+} balance have been associated with diabetes mellitus, osteoporosis, asthma, and heart and vascular disease [44-48]. Consequently, plasma Mg^{2+} levels are maintained within a narrow range (0.7-1.1 mM) by the joint action of intestinal absorption, exchange with bone, and renal excretion. The kidney is the most important organ for the regulation of total body Mg^{2+} homeostasis as fine-tuning of Mg^{2+} excretion via the urine ultimately preserves a constant Mg^{2+} concentration in the blood. Approximately 80% of total plasma Mg^{2+} is filtered by the glomeruli [49, 50], the majority of which is absorbed along the nephron [41, 51]. Most of filtered Mg^{2+} is reabsorbed in the proximal tubule (~20%) and thick ascending limb (TAL) of the loop of Henle (~70%) via passive paracellular transport [52, 53]. The remaining 10% of filtered Mg^{2+} is reabsorbed by an active transcellular mechanism in the distal convoluted tubule

(DCT). This process defines the amount of Mg^{2+} excreted in the urine, as no reabsorption occurs beyond this segment [41]. Finally, on a normal diet, the fractional Mg^{2+} excretion is between 3 and 5% [54] (Fig. 3).

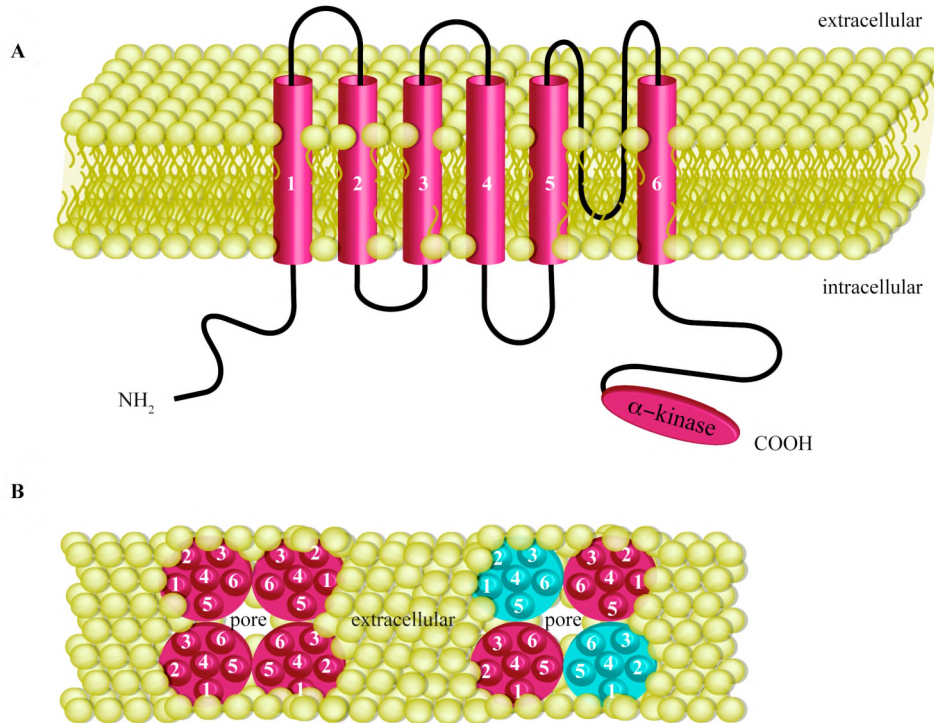


Figure 2. Structural organization of TRPM6. *A.* Side view: The protein consists of six transmembrane spanning segments with large intracellular amino (NH₂) and carboxyl (COOH) termini. There is a putative pore-forming region between the fifth and sixth transmembrane segments. Uniquely, TRPM6 and its closest homologue TRPM7 contain an atypical protein kinase in the carboxyl terminus. *B.* Top view: Four of these six transmembrane subunits will form a functional channel, either in homomeric configuration (red) or by heteromeric formation with TRPM7 subunits (red/blue).

Transcellular transport: distal convoluted tubule

Mg^{2+} reabsorption in the DCT occurs in a transcellular manner. Mg^{2+} enters the epithelial cell through the epithelial Mg^{2+} channel TRPM6 [55]. This uptake from the pro-urine is driven by a favourable transmembrane potential [41]. Then, Mg^{2+} will diffuse through to cell to be extruded actively across the basolateral membrane. This Mg^{2+} efflux is suggested to occur via a secondarily active process, involving Na^+ -dependent exchange or an ATP-dependent Mg^{2+} pump [40, 41]. So far, intracellular Mg^{2+} buffering proteins have not been identified. Interestingly, parvalbumin and calbindin-D_{28k} have an overlapping expression with TRPM6 and both proteins have a Mg^{2+} binding affinity [55, 56]. In addition to these proteins, the γ -subunit of the basolateral Na^+,K^+ -ATPase has been implicated in active Mg^{2+} reabsorption in DCT. Mutations in the *FYXD2* gene, encoding the γ -subunit of the Na^+,K^+ -ATPase, were found in patients with isolated dominant hypomagnesemia with hypocalciuria (IDHH) [57, 58]. This protein is primarily expressed in the kidney with highest expression levels at the basolateral membrane of DCT and medullary TAL [59]. However, the

molecular mechanism by which the γ -subunit affects the Mg^{2+} reabsorption remains to be ascertained. The Na^+, Cl^- cotransporter (NCC) is another protein exclusively expressed in DCT [60] and indirectly involved in transcellular Mg^{2+} reabsorption. Patients with Gitelman syndrome (GS) suffer from hypokalemic metabolic alkalosis with hypomagnesemia and hypocalciuria, which has been associated with mutations in the *SLC12A3* gene, encoding NCC [60]. Inhibition of NCC by thiazide treatment mostly results in hypomagnesemia as well [61]. Importantly, NCC knockout mice, an animal model for GS, and mice treated with thiazide diuretics have decreased expression of TRPM6 [62], which could explain the Mg^{2+} wasting in this disorder. However, at present it is unknown what signals the observed TRPM6 down-regulation (Fig. 3).

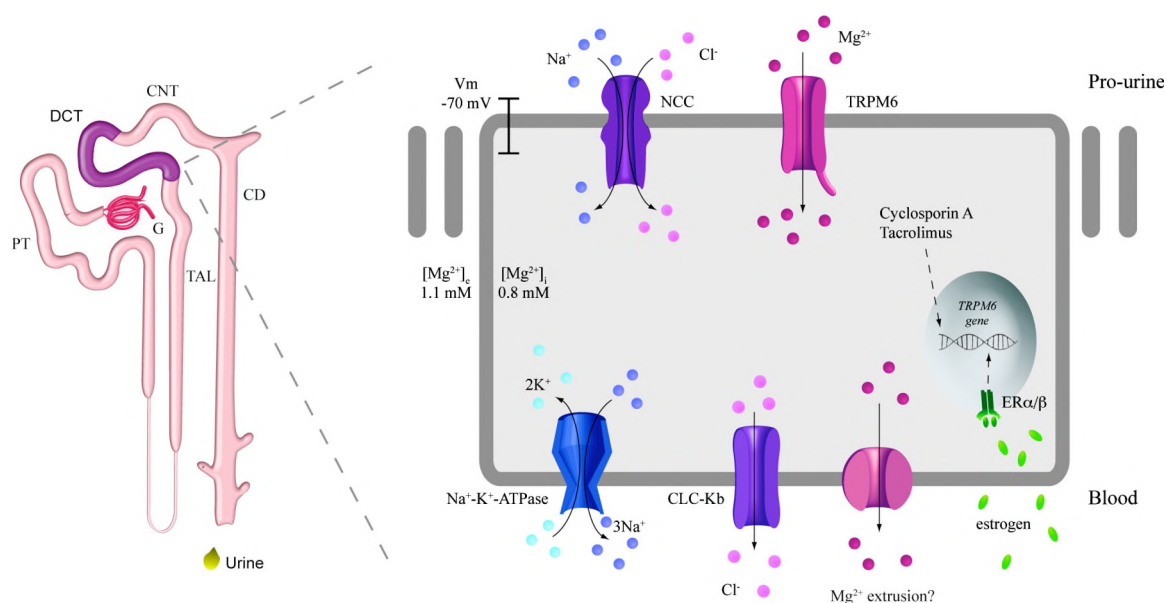


Figure 3. Mg^{2+} reabsorption along the nephron. Mg^{2+} is filtered in the glomerulus, followed by passive reabsorption in the proximal tubule (PT) (~20%) and thick ascending limb (TAL) of the loop of Henle (~70%). The remaining 10% of filtered Mg^{2+} is reabsorbed in active manner in the distal convoluted tubule (DCT). This segment can be further subdivided into an early (DCT1) and late (DCT2) portion. TRPM6 is located in the apical membrane, which facilitates Mg^{2+} transport from the pro-urine into the cell. TRPM6 expression is shown to be regulated by estrogen, cyclosporin, and tacrolimus. Diffusion of Mg^{2+} in the cytoplasm and extrusion to the interstitium occurs through so far unidentified proteins. NCC is exclusively expressed at the apical membrane of DCT, where it cotransports Na^+ and Cl^- from the pro-urine into the cell. The gradient for Na^+ transport is provided by the basolateral Na^+, K^+ -ATPase. Cl^- is extruded at the basolateral membrane via CLC-Kb.

TRPM6

The *TRPM6* gene contains 39 exons encoding a protein of 2022 amino acids [63, 64]. A variety of splice variants have been identified including three alternative first exons [65]. However, the biological relevance of these multiple variants remains to be investigated. TRPM6 shows approximately 50% homology with its closest homologue TRPM7 [36, 38]. Mutations in TRPM6 were found to be causative for autosomal recessive hypomagnesemia with secondary hypocalcemia (HSH), characterized by a defect in intestinal Mg^{2+} transport and impaired renal Mg^{2+} reabsorption [63, 64]. In kidney, TRPM6 is expressed along the apical membrane of DCT, the main site of active

Mg²⁺ reabsorption [55]. Furthermore, TRPM6 is detected in the brush border membrane of absorptive epithelial cells of the ileum and colon [55, 63]. This restricted expression pattern, together with the Mg²⁺ leak in HSH patients, is supportive for an important role of TRPM6 in transcellular Mg²⁺ transport.

TRPM7

The *TRPM7* gene is also made up of 39 exons and encodes a protein of 1865 amino acids. The protein was originally discovered by three independent studies using different techniques: identification by screening databases for homologues of human eukaryotic elongation factor 2 kinase [66], *via* a yeast two-hybrid screen using the C2 domain of phospholipase C as a bait [36], and through a bioinformatics approach aimed at identifying novel ion channels expressed in immune cells [37]. TRPM7 is ubiquitously expressed and represents the only ion channel known that is essential for cellular viability [37, 67]. Cellular knockout of TRPM7 has been shown to induce cell death, which can be rescued by Mg²⁺ supplementation [67]. Interestingly, providing these TRPM7^{-/-} cells with Ca²⁺ or Mn²⁺ in the extracellular medium did not lead to cell survival. Furthermore, TRPM7 plays a role in anoxic neuronal death [68], actomyosin contractility and cell adhesion [69, 70]. The study of zebrafish touchtone/nutria with mutations in TRPM7 showed a requirement for this protein in skeletogenesis [71]. Taken together, these data point towards a critical role of TRPM7 in cellular Mg²⁺ homeostasis.

Channel properties

TRPM6, like TRPM7, is defined as a Mg²⁺-permeable channel and electrophysiological analysis of TRPM6-expressing HEK293 cells demonstrated a typical outwardly rectifying current-voltage (I-V) relationship [55]. The I-V curve is linear in the absence of extracellular divalent cations. So, the outwardly rectifying currents are reflected by the outward flux of monovalent cations and the small inward flux of divalent cations. The small inward currents are intriguing as they occur within the typical range of physiological membrane potentials [55]. The unique permeation rank order of the inward current is Ba²⁺ ≥ Ni²⁺ > Mg²⁺ > Ca²⁺ [55]. So, the pore of TRPM6 has a higher affinity for Mg²⁺ than for Ca²⁺, in contrast to other members the TRP superfamily, which usually display a 10-1000 times lower affinity for Mg²⁺ than for Ca²⁺. TRPM6 is found to be constitutively open, but strongly regulated by intracellular levels of Mg²⁺ ([Mg²⁺]_i), shown by flash experiments with a photolabile Mg²⁺ chelator, 1-(2-nitro-4,5-dimethoxyphenyl)-N,N,N',N'-tetrakis[(oxycarbonyl)methyl]-1,2-ethanediamine (DM-nitrophen) [55]. Thus, in order to allow current development, TRPM6-expressing cells are dialyzed by high concentrations of the chelator ethylenediaminetetraacetate (EDTA) in the intracellular solution. Monovalent currents are highly sensitive to ruthenium red in a voltage-dependent manner. It causes a strong inhibition of inward monovalent currents without affecting outward currents [55]. This inhibition is likely a direct block of the channel pore within the

transmembrane electrical field. The inhibition of ruthenium red on TRPM6 is unspecific since it is a potent blocker of other TRPV channels [72, 73] as well as Ca^{2+} -activated K^+ channels [74]. The channel properties of TRPM6, such as outward rectifying I-V curve, intracellular Mg^{2+} regulation, and the lack of voltage dependence, were found to be indistinguishable from those of TRPM7 [36, 37, 55]. This raises the important question whether the TRPM6 currents are mediated by TRPM6 itself or represent the combined activity of TRPM6 and TRPM7.

Homo/Heteromultimerization

The TRPM6 and TRPM7 channels can form homo- or heterotetramers. Fluorescence resonance energy transfer (FRET) analysis has indicated that TRPM6 can interact with itself and with TRPM7 [65]. Based on experiments in *Xenopus laevis* oocytes and HEK293 cells, it has been suggested that co-expression of TRPM7 is required for plasma membrane expression of TRPM6 and channel activity [65]. This idea was supported by the analysis of the TRPM6 S141L mutant, observed in HSH. TRPM6 S141L was found to hamper the interaction between TRPM6 and TRPM7 resulting in intracellular retention [65]. Another study also demonstrated that plasma membrane trafficking of TRPM6 strongly depends on TRPM7 co-expression [75]. In contrast, Voets *et al.* was able to express TRPM6 in human embryonic kidney (HEK293) cells and measure its channel activity without co-expressing TRPM7 [55]. In line, another group has detected TRPM6, TRPM7 and TRPM6/TRPM7 channels with distinct biophysical characteristics [76]. They demonstrated a greater permeability of TRPM6 to Ni^{2+} , a differential response of TRPM7 to the IP_3 -inhibitor, 2-aminoethoxydiphenyl borate, and a larger unitary conductance of TRPM6 relative to TRPM7 [76]. Further studies are needed to clarify the exact functional channel composition in native tissues.

Channel regulation

Both TRPM6 and TRPM7 are regulated by intracellular free Mg^{2+} ions and Mg^{2+} -complexed nucleotides. The endogenous correlate of TRPM7, identified in several cell lines, has been named MagNuM (Mg^{2+} -nucleotide-inhibited metal) or MIC (Mg^{2+} -inhibited cation) [37, 77-79]. The native MIC current was shown to be suppressed by internal free Mg^{2+} and not by MgATP [80], while other studies pointed towards the Mg^{2+} -nucleotide-mediated regulation of TRPM7. Nadler *et al.* observed that increasing intracellular MgATP concentrations, while keeping free Mg^{2+} levels constant, steadily decreased the TRPM7 activation [37]. This regulation is not mediated by the free nucleotide as NaATP causes TRPM7 activation, which was suggested to occur via ATP-dependent phosphorylation by the kinase domain [36, 37, 81]. However, free Mg^{2+} was also shown to be an important regulator of TRPM7 activity [37] and addition of NaATP reduced the level of free Mg^{2+} thereby causing strong channel activation. Next to the Mg^{2+} -dependent regulation, several studies have shown that phosphatidylinositol bisphosphate (PIP_2) is essential to maintain TRPM7 activity [82-84]. PIP_2 breakdown by receptor-mediated stimulation of phospholipase C (PLC) results in channel

inactivation, which can be recovered by PIP₂ perfusion [83]. Another study suggested that TRPM7 activity is regulated, in kinase activity-dependent manner, by receptor-mediated changes in cyclic AMP (cAMP) and protein kinase A (PKA) levels [85]. Interestingly, Langeslag *et al.* recently used perforated patch clamping to maintain a more physiological internal environment for cellular signaling and could not demonstrate TRPM7 activation upon increased cAMP levels [86]. Furthermore, it was demonstrated that TRPM7 can be activated by stimulation of endogenous PLC-activating receptors in perforated patch configuration [86]. A feedback mechanism was proposed in which PIP₂ depletion counteracts or limits the PLC-mediated activation of TRPM7 [86]. The regulation of TRPM6 by PIP₂, PLC, and cAMP remains to be examined.

Systemic control of TRPM6

The Mg²⁺ excretion and TRPM6 expression in kidney are strongly regulated by Mg²⁺ intake. It has been shown by mice studies that reduction in dietary Mg²⁺ results in hypomagnesemia and renal Mg²⁺ and Ca²⁺ conservation, whereas a high dietary Mg²⁺ content has the opposite effect. The Mg²⁺ restricted diet led to a significant increase in renal TRPM6 abundance, while the enriched diet tended to decrease renal TRPM6 mRNA levels [87]. Variation in dietary Mg²⁺ content did not alter TRPM7 mRNA expression levels. These data support the idea of TRPM6 being the gatekeeper of transepithelial Mg²⁺ transport. Early knowledge about renal Mg²⁺ handling is derived from micropuncture and microperfusion studies. Several hormones have been implicated in the regulation of renal Mg²⁺ reabsorption, including parathyroid hormone (PTH), calcitonin, and glucagon. Importantly, these effects have only been shown in a mouse distal convoluted tubule (mDCT) cell line and need further confirmation in a more physiologically relevant model [88, 89]. Further, Groenesteghe *et al.* demonstrated that 17β-estradiol regulates TRPM6 expression as it could restore the decreased renal TRPM6 mRNA levels in ovariectomized rats, in contrast to 1,25-dihydroxyvitamin D₃ and PTH [87]. However, stimulation with these hormones in the mDCT cell line resulted in increased Mg²⁺ influx and cellular cAMP accumulation (reviewed in [41, 90]). This suggests that their effect on Mg²⁺ reabsorption is not mediated by the TRPM6 transcriptional level, but through altered channel activity. Insulin has also been shown to stimulate Mg²⁺ uptake in mDCT cells [91]. Moreover, a disturbed Mg²⁺ balance has been related to insulin resistance and type 2 diabetes mellitus. Streptozotocin (STZ)-induced diabetic rats display an increased renal TRPM6 mRNA expression, which may represent a compensatory mechanism for the increased Mg²⁺ load to the DCT. Insulin administration reversed this increased abundance in TRPM6 and corrected the hypermagnesiuria observed in these rats [92]. So, diabetes is associated with renal Mg²⁺ wasting, but the responsible molecular mechanism remains elusive so far. Additionally, Mg²⁺ handling can be affected by changes in acid base status via TRPM6 regulation. Mice with chronic metabolic acidosis display increased Mg²⁺ excretion, reduced renal TRPM6 expression, and decreased serum Mg²⁺ [93]. The reverse effects occur during chronic metabolic alkalosis. In line with these findings, Li *et al.* demonstrated that acidic

pH increased TRPM6 inward currents, potentially by decreasing the divalent affinity of the channel [76]. Finally, hypomagnesemia can be caused by use of the immunosuppressive agents cyclosporin A and tacrolimus (FK506) [94, 95] and anticancer drugs like cetuximab and cisplatin [96, 97]. The effect of FK506 can be explained by downregulation of renal TRPM6 expression [98], while the molecular mechanisms of the other compounds are not known yet.

The α -kinase domain

TRPM6 and TRPM7 are unique since they contain an atypical serine/threonine kinase domain, which has similarities with members of the α -kinase family [36, 66, 99]. Apart from containing a zinc-finger domain [99, 100], the α -kinases share little sequence homology with conventional eukaryotic protein kinases [101]. The role of this α -kinase domain in the activation and regulation of these channels is highly debated. On one hand, the TRPM7 kinase has been presented as an essential factor for channel gating [36], while other studies support a regulatory role of the kinase in modulating Mg^{2+} and Mg^{2+} -nucleotide sensitivity [67, 81], and it has even been proposed to be uncoupled from the channel function [102]. Based on the channel's dependence on ATP and the absence of TRPM7 currents in two putative phosphotransferase-deficient mouse TRPM7 mutants, it was suggested that the α -kinase domain is required for channel activation [36]. However, the lack of channel activity in the TRPM7 mutants is likely due to impaired protein expression, since other studies showed normal TRPM7 activation in mutated human TRPM7 channels without phosphotransferase activity (K1648R and G1799D) [67, 102]. The latter group observed a similar Mg^{2+} sensitivity for mutant and wildtype TRPM7 channels, from which they concluded that α -kinase domain and channel activity are dissociated [102]. However, this statement was based on two relatively high Mg^{2+} concentrations (4 and 6 mM). A complete dose-response analysis of the mutant TRPM7 channels demonstrated a significant right shift in their $Mg^{2+}/MgATP$ sensitivity compared to wildtype TRPM7 [67]. Interestingly, The TRPM7- Δ -kinase mutant showed a markedly increased sensitivity to both Mg^{2+} and $MgATP$ with almost full ablation of channel activity at 1 mM $Mg^{2+}/MgATP$ [67]. Further study suggested that the α -kinase domain enclosed a $MgATP$ binding site which acts synergistically with a separate Mg^{2+} -binding site extrinsic to the domain that regulates TRPM7 channel activity [81]. Another interesting issue is whether the nucleotide binding alone regulates channel activity or whether the kinase activity also plays a role, since TRPM6/TRPM7 are able to undergo autophosphorylation and phosphorylate other substrates. TRPM6 is capable of cross-phosphorylating TRPM7, but not vice versa [75]. Annexin 1 and myosin IIA have been identified as endogenous phosphorylation targets of the TRPM7 α -kinase [69, 103]. Recently, it has been demonstrated that TRPM7 regulates the myosin IIA filament stability and localization via a kinase-dependent mechanism [104]. TRPM6 and TRPM7 share exogenous substrates, as myosin IIA, IIB, and IIC, which were not phosphorylated by the functionally distant eEF2-kinase [105]. Furthermore,

Clark *et al.* provided a model where substantial autophosphorylation of the cytosolic C-termini of both TRPM6 and TRPM7 leads to increased substrate phosphorylation via enhancing the kinase-substrate interactions [106]. Finally, the α -kinase domain might play a role as modulator of TRPM6 and TRPM7 via regulation by interaction partners, which have not been discovered so far. Further experiments should help to elucidate the role of the α -kinase domain in regulating TRPM6/TRPM7 channel activity.

Channelomics

Channelomics is a new term for proteomics of ion channels. It includes all aspects of ion channel research such as transcriptional and translational regulation, post-translational consequences on the protein composition and modulatory effects of hormones, drugs, and toxins on the structure and function of ion channels. In this section several biochemical, biophysical and electrophysiological technologies, which are frequently employed to study the channelomics, will be highlighted.

Cell surface biotinylation

Biotinylation is a rapid method of covalently attaching a biotin tag to cell surface proteins, while intracellularly located proteins are not stained. The technique uses a cell-impermeable, cleavable biotinylation reagent (Sulfo-NHS-SS-Biotin) to label exposed amines of proteins on the surface of mammalian cells. As long as the cell remains intact, only the amines exposed on the surface will be biotinylated by Sulfo-NHS-SS-Biotin. Subsequently, the cells are harvested and lysed, and the labeled surface proteins are affinity-purified with avidin containing beads. Avidin is a glycoprotein found in egg whites and oviducts of birds, reptiles and amphibians. It contains four identical subunits, each able to bind a single biotin molecule [107]. Avidin is highly useful for protein purification and detection as most chemical modifications have barely any effect on the avidin activity. Subsequently, antibody labelling or a fluorescent dye can detect the biotin-avidin protein complex, which is used in ELISA (enzyme-linked immunosorbent assay) assays, western blots, and other immunoanalytical methods. In the light of ion channel research, the cell surface biotinylation assay is valuable for differentiation of plasma membrane proteins from those localized to organelle membranes, distribution of membrane proteins in polarized epithelial cells, and internalization and recycling of cell surface proteins.

Tags

Protein tags are peptide sequences genetically attached to a recombinant protein. The various tags can be grouped according to their purposes: *i*) Affinity tags, such as glutathione-S-transferase (GST), are used for purification of proteins from their biological source; *ii*) solubilization tags assist proper protein folding and prevent precipitating, when the recombinant protein is expressed in chaperone-

deficient species such as *E. coli*; *iii*) chromatography tags, like a FLAG-tag, can alter chromatographic properties of the protein to provide different resolution using a particular separation technique; *iv*) epitope tags are short peptide sequences, usually derived from viral genes, that are predominantly used for western blotting and immunoprecipitation studies. Epitope tags involve V5-tag, c-myc-tag, and HA-tag; *v*) fluorescence tags are used to visualize a protein, mostly during live cell imaging. The green fluorescent protein (GFP) and its derivatives (i.e. BFP, YFP) are the most frequently used fluorescence tags. Combinations of protein tags are even used to achieve multifunctional control of the protein. However, an important risk with addition of tags is the alteration or ablation of the native function of the protein.

Fluorescence microscopy

Ion channels are dynamic in nature: they are continuously formed, trafficked to the plasma membrane, inserted in the plasma membrane, and removed to be degraded or recycled. So, ion channel function is not just dependent on electrophysiological channel properties, but on channel trafficking as well. The development of molecular techniques to tag channels with fluorescent proteins, and of advanced microscopic imaging techniques such as fluorescence resonance energy transfer (FRET), fluorescence recovery after photobleaching (FRAP), and total internal reflection fluorescence (TIRF) microscopy, generated new opportunities to study the intracellular movement of channels to and from the plasma membrane.

FRET (fluorescent resonance energy transfer)

FRET, also known as Förster resonance energy transfer, is a mechanism of energy transfer between two chromophores. This mechanism is named after the German scientist Theodor Förster. The term ‘fluorescence resonance energy transfer’ is often used instead, since the chromophores are fluorescent (fluorophores). The non-radiative transfer of photon energy from an electronic excited fluorophore (the donor) to another fluorophore (the acceptor) occurs when both are located within close proximity (1–10 nm). The donor and acceptor fluorophores for FRET analysis come from a class of green fluorescent proteins (GFPs). Importantly, the GFPs should be selected on the basis of sufficient separation in excitation spectra to stimulate only the donor GFP, an overlap (>30%) between the donor emission spectrum and the acceptor excitation spectrum for efficient energy transfer, and adequate separation in emission spectra between donor and acceptor GFPs to independently measure the fluorescence of each fluorophore [108]. If FRET occurs, the donor fluorophore signal will be quenched and the acceptor fluorophore signal will be sensitized or increased. Current advances in fluorescence microscopy, together with the development of new fluorescent probes, make FRET a great technique for studying molecular interactions within living cells. It can be used to examine protein-protein interactions, such as heteromeric assembly of ion channels [109]. The binding of intracellular signalling molecules to ion channel domains, as well as

the downstream pathway of receptor or channel activation like the cAMP signaling, can be studied by this technique [110, 111]. Furthermore, FRET is used to monitor conformational rearrangements associated with channel gating [112].

FRAP (fluorescence recovery after photobleaching)

FRAP microscopy is introduced in the 1970s for imaging intracellular molecular dynamics. Similar as to FRET, fluorophores as GFP will be tagged to the protein of interest, which results in an intracellular fluorescence signal upon protein expression. A special illumination step is used to perturb the steady-state fluorescence distribution within single cells. After this high intensity illumination had permanently photobleached the fluorescent dye in a small selected region, surrounding molecules that are still fluorescent migrate into this blackened area recovering the fluorescence distribution. In this way, the trafficking of proteins to the plasma membrane can be measured by the time and amount of fluorescent recovery. More recently, the technique is now used to study channel subunits, isoforms, or accessory proteins that modulate trafficking and membrane localization [113, 114].

Total internal reflection fluorescence (TIRF)

TIRF microscopy was developed by Daniel Axelrod in the early 1980s [115]. With this type of microscopy a thin region of cells can be visualized. It employs the phenomenon of total internal reflection, which occurs at the glass-water interface of the glass coverslip containing a bath solution with cells that lies under the microscope. At large angle of incidence, the excitation light reflects back into glass and generates at the interface with water a so-called evanescent wave. The evanescent wave selectively illuminates and excites fluorophores in small region of approximately 100-200 nm from the interface. Thus, TIRF allows high resolution imaging of features and events occurring close to the plasma membrane of living cells. In contrast to conventional fluorescence microscopy, TIRF can be used to examine the fluorescence of single molecules. Similar to FRAP, TIRF is only recently used to study channel trafficking and function [116, 117]. In addition, TIRF is used together with FRET to detect channel assembly, the effect of small molecule binding, and conformational channel rearrangement at the plasma membrane level [118-120].

Patch clamp technique

Studies in artificial lipid membranes showed that certain proteins isolated from bacteria and other antibiotic polypeptides were able to induce discrete changes in membrane conductance [121, 122]. These conductance changes were of the same order of magnitude as single channel conductances measured in current fluctuations by voltage clamp of neuromuscular junction and in nodes of Ranvier [123, 124]. The voltage clamp allows the membrane voltage to be controlled independent of ionic currents across a lipid membrane [125]. However, background noise in these voltage clamp setups

was mostly higher than the single channel signals to be measured. Therefore, a small area of the membrane (“patch”) should be isolated for localized electrical measurements by placing a glass micropipette on the surface of the voltage-clamped cell. Erwin Neher and Bert Sakmann developed the patch clamp technique and could measure single channel currents from the acetylcholine-activated receptor [126]. Subsequently, the technique was improved significantly with the phenomenon now called gigaseal formation [127, 128].

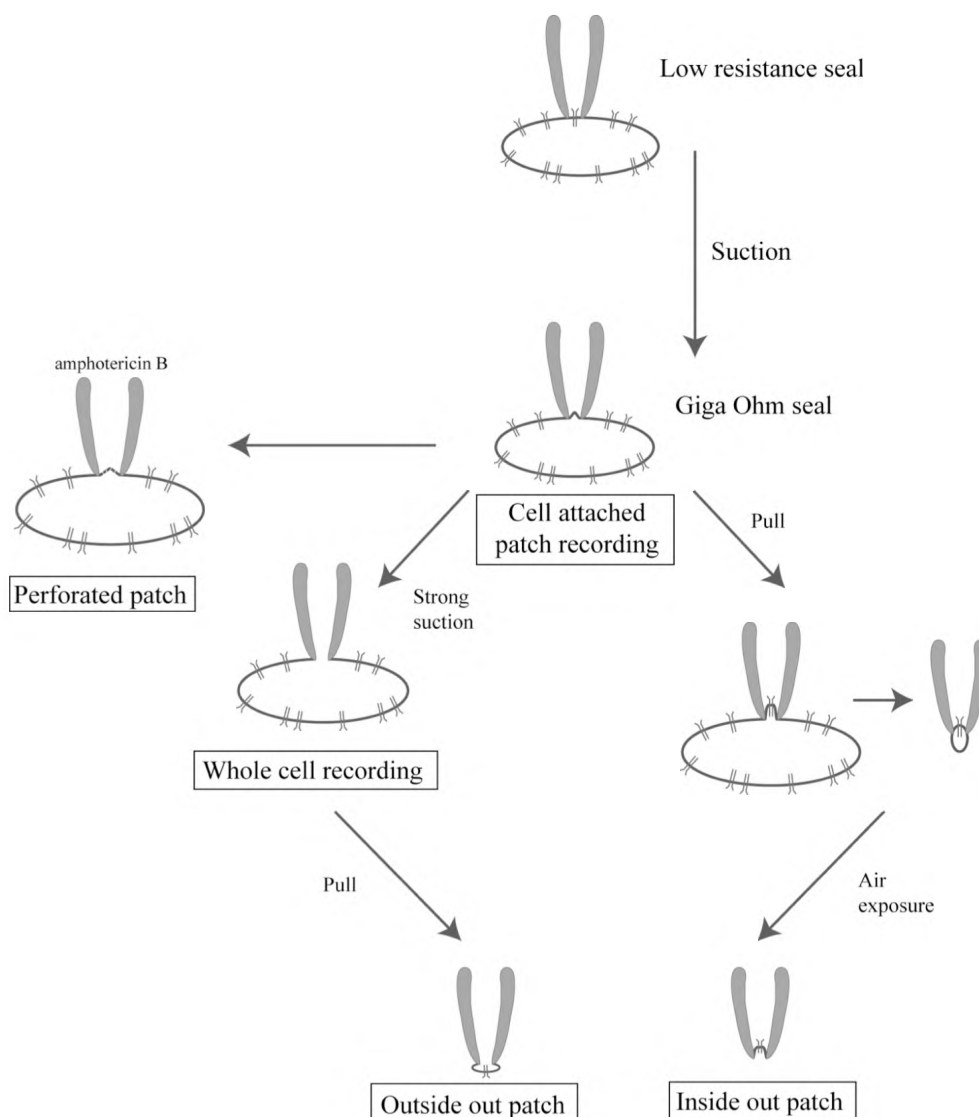


Figure 4. Schematic representation of the patch clamp configurations. Applying slight suction to the back of the pipette results in a tight seal between pipette and membrane, which is called the cell-attached patch recording method. Rupture of the membrane patch within the pipette, through short strong suction, gives access to the cytoplasm of the cell, whole-cell recording method. From the cell-attached configuration, the pipette can be retracting and a small vesicle of membrane remains attached to the pipette. By exposing the tip of the pipette to air, this vesicle opens, leading to the inside-out patch recording configuration. The intracellular surface of the membrane is exposed to the extracellular medium). On the other hand, retracting the pipette in the whole-cell configuration, a membrane patch will form a vesicle that is exposed to the extracellular medium. This is called the outside-out recording configuration.

Following formation of the gigaseal, a variety of recording configurations can be established (Fig. 4):

- i) Cell-attached patch recording. In this recording configuration, the cell remains intact. Following gigaseal formation, single channel currents through ion channels trapped within the patch of membrane can be recorded.
- ii) Inside-out patch. A patch of the membrane can be pulled off the cell by withdrawing the pipette after gigaseal formation. The cytoplasmic membrane is then facing the bath solution, allowing manipulation of the intracellular environment of ion channels during single channel measurements.
- iii) Whole-cell recording. Following a gigaseal, the patch of membrane under the pipette can be ruptured by application of strong suction. Patch rupture is detected as a sudden increase in capacitive current in response to a test potential step. This configuration results in electrical contact and diffusional exchange between the pipette electrode and the cytoplasm, which allows optimal control of the intracellular compartment.
- iv) Outside-out patch. This configuration can be achieved by pulling away the pipette during a whole-cell recording. The patch of membrane withdrawn from the cell will reseal on the pipette such that the extracellular membrane surface can be exposed to different solutions during a single channel measurement.
- v) Perforated-patch recording. A disadvantage of whole-cell recording is the loss of cytoplasmic ions, nucleotides and other signaling molecules. Therefore a gigaseal can be formed with a pipette filled with pore-forming antibiotic molecules. These antibiotics form small perforations in the membrane, providing electrical access to the cell, without dialyzing the interior of the cell.

The variety of patch clamp configurations, combined with the single channel resolution, offers a powerful experimental tool, from the molecular level of altered channel gene expression, to the cellular level, where signaling mechanisms are unravelled, to the tissue level, in which cellular interactions in slice preparations are revealed.

Outline of this thesis

As illustrated in the aforementioned paragraphs, ion channels are essential proteins for all living organisms. They regulate the flow of ions across the plasma membrane of each cell in the body and are involved in a wide variety of biological processes. The epithelial Mg^{2+} channel TRPM6 is the gatekeeper of transcellular Mg^{2+} (re)absorption, and thus an important component for the control of body Mg^{2+} homeostasis. However, the molecular mechanism for active Mg^{2+} reabsorption is largely unknown. The aim of this thesis was, therefore, to provide more insight in the physiological and molecular regulation of renal ion channels in general and in particular of the epithelial Mg^{2+} channel TRPM6 and the voltage-operated K^+ channel Kv1.1. **Chapter 2** describes the identification of the first TRPM6-associated protein, named receptor for activated c-kinase 1 (RACK1). RACK1 was found as an interaction partner of the TRPM6 α -kinase by yeast two-hybrid screening and via a combination of GST pull-down and Fourier transform ion cyclotron resonance mass spectrometry (FTMS). The function of RACK1 was further studied using biochemical and electrophysiological analysis. The identification of a new α -kinase interaction partner, repressor of estrogen receptor

activity (REA), and its role on TRPM6 regulation are outlined in **chapter 3**. The chapter also points out a rapid stimulatory effect of 17β -estradiol on TRPM6. Next, **chapter 4** portrays the identification of a third protein interacting with the TRPM6 α -kinase domain, called Methionine Sulfoxide Reductase B1 (MsrB1). It highlights the effect of oxidative stress on TRPM6 channel activity and partial recovery via MsrB1, involving a methionine residue in the peripheral region of the TRPM6 α -kinase domain. The study presented in **chapter 5** illustrates the effect of the widely used anti-cancer drug Erlotinib on Mg^{2+} handling. By combining mice studies with biochemical and electrophysiological data, the effect on TRPM6 expression and channel activity was examined. **Chapter 6** reports the identification of a mutation in the *KCNA1* gene as cause for autosomal dominant hypomagnesemia in a Brazilian family. The mutation results in the amino acid change $N^{255}D$ in the encoded K^+ channel Kv1.1. This study provides a new coupling between renal K^+ handling and active Mg^{2+} reabsorption as Kv1.1 co-localizes with TRPM6 along the apical membrane of DCT. Furthermore, hypomagnesemia is presented as a new phenotypic characteristic associated with a mutation in *KCNA1*. Functional analysis demonstrated that this mutation in Kv1.1 results in a non-functional channel. The effect of the mutation on Kv1.1 channel function was further examined in the study described in **chapter 7**. Combining structural modelling with patch clamp recordings was used to investigate the result of substituting N^{255} by other amino acids ($N^{255}E$, $N^{255}Q$, $N^{255}A$, $N^{255}V$, $N^{255}T$, $N^{255}H$).). Finally, the studies of this thesis and the physiological implications of the finding are discussed and summarized in **chapter 8**.

References

1. Alberts B: *Molecular Biology of the Cell*, 4th ed. New York, Garland Science, 2002
2. Hille B: *Ion channels of excitable membranes*, 3rd ed. Sunderland, Sinauer Associates, 2001
3. Grottesi A, Sands ZA, Sansom MS: Potassium channels: complete and undistorted. *Curr Biol* 15:R771-774, 2005
4. Long SB, Campbell EB, Mackinnon R: Crystal structure of a mammalian voltage-dependent Shaker family K⁺ channel. *Science* 309:897-903, 2005
5. Aggarwal SK, MacKinnon R: Contribution of the S4 segment to gating charge in the Shaker K⁺ channel. *Neuron* 16:1169-1177, 1996
6. Armstrong CM: Voltage-gated K channels. *Sci STKE* 2003:re10, 2003
7. Sands Z, Grottesi A, Sansom MS: Voltage-gated ion channels. *Curr Biol* 15:R44-47, 2005
8. Doyle DA, Morais Cabral J, Pfuetzner RA, *et al.*: The structure of the potassium channel: molecular basis of K⁺ conduction and selectivity. *Science* 280:69-77, 1998
9. Jiang Y, Lee A, Chen J, *et al.*: X-ray structure of a voltage-dependent K⁺ channel. *Nature* 423:33-41, 2003
10. Christie MJ: Molecular and functional diversity of K⁺ channels. *Clin Exp Pharmacol Physiol* 22:944-951, 1995
11. Dolly JO, Parcej DN: Molecular properties of voltage-gated K⁺ channels. *J Bioenerg Biomembr* 28:231-253, 1996
12. Catterall WA, Perez-Reyes E, Snutch TP, *et al.*: International Union of Pharmacology. XLVIII. Nomenclature and structure-function relationships of voltage-gated calcium channels. *Pharmacol Rev* 57:411-425, 2005
13. Yamakage M, Namiki A: Calcium channels--basic aspects of their structure, function and gene encoding; anesthetic action on the channels--a review. *Can J Anaesth* 49:151-164, 2002
14. Yu FH, Catterall WA: Overview of the voltage-gated sodium channel family. *Genome Biol* 4:207, 2003
15. Isom LL: Sodium channel beta subunits: anything but auxiliary. *Neuroscientist* 7:42-54, 2001
16. Catterall WA, Goldin AL, Waxman SG: International Union of Pharmacology. XLVII. Nomenclature and structure-function relationships of voltage-gated sodium channels. *Pharmacol Rev* 57:397-409, 2005
17. Jentsch TJ, Stein V, Weinreich F, *et al.*: Molecular structure and physiological function of chloride channels. *Physiol Rev* 82:503-568, 2002
18. Simon DB, Bindra RS, Mansfield TA, *et al.*: Mutations in the chloride channel gene, CLCNKB, cause Bartter's syndrome type III. *Nat Genet* 17:171-178, 1997
19. Lloyd SE, Pearce SH, Fisher SE, *et al.*: A common molecular basis for three inherited kidney stone diseases. *Nature* 379:445-449, 1996
20. Kornak U, Kasper D, Bosl MR, *et al.*: Loss of the CIC-7 chloride channel leads to osteopetrosis in mice and man. *Cell* 104:205-215, 2001
21. Koch MC, Steinmeyer K, Lorenz C, *et al.*: The skeletal muscle chloride channel in dominant and recessive human myotonia. *Science* 257:797-800, 1992
22. Matulef K, Zagotta WN: Cyclic nucleotide-gated ion channels. *Annu Rev Cell Dev Biol* 19:23-44, 2003
23. Bradley J, Frings S, Yau KW, *et al.*: Nomenclature for ion channel subunits. *Science* 294:2095-2096, 2001
24. Frings S, Seifert R, Godde M, *et al.*: Profoundly different calcium permeation and blockage determine the specific function of distinct cyclic nucleotide-gated channels. *Neuron* 15:169-179, 1995
25. Ludwig A, Zong X, Jeglitsch M, *et al.*: A family of hyperpolarization-activated mammalian cation channels. *Nature* 393:587-591, 1998
26. Robinson RB, Siegelbaum SA: Hyperpolarization-activated cation currents: from molecules to physiological function. *Annu Rev Physiol* 65:453-480, 2003

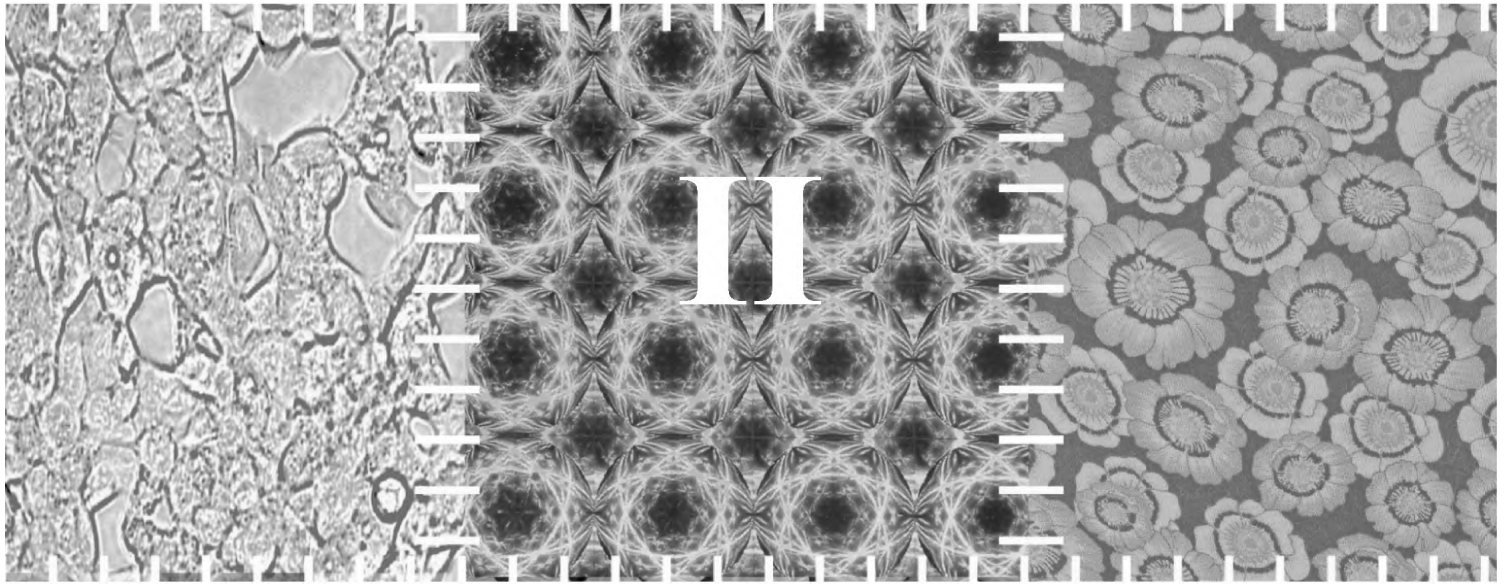
27. Zagotta WN, Olivier NB, Black KD, *et al.*: Structural basis for modulation and agonist specificity of HCN pacemaker channels. *Nature* 425:200-205, 2003
28. Kaupp UB, Seifert R: Molecular diversity of pacemaker ion channels. *Annu Rev Physiol* 63:235-257, 2001
29. Cascio M: Structure and function of the glycine receptor and related nicotinic receptors. *J Biol Chem* 279:19383-19386, 2004
30. Cosens DJ, Manning A: Abnormal electroretinogram from a *Drosophila* mutant. *Nature* 224:285-287, 1969
31. Montell C, Rubin GM: Molecular characterization of the *Drosophila* *trp* locus: a putative integral membrane protein required for phototransduction. *Neuron* 2:1313-1323, 1989
32. Hardie RC, Minke B: The *trp* gene is essential for a light-activated Ca²⁺ channel in *Drosophila* photoreceptors. *Neuron* 8:643-651, 1992
33. Clapham DE, Runnels LW, Strubing C: The TRP ion channel family. *Nat Rev Neurosci* 2:387-396, 2001
34. Fleig A, Penner R: The TRPM ion channel subfamily: molecular, biophysical and functional features. *Trends Pharmacol Sci* 25:633-639, 2004
35. Clapham DE: TRP channels as cellular sensors. *Nature* 426:517-524, 2003
36. Runnels LW, Yue L, Clapham DE: TRP-PLIK, a bifunctional protein with kinase and ion channel activities. *Science* 291:1043-1047, 2001
37. Nadler MJ, Hermosura MC, Inabe K, *et al.*: LTRPC7 is a Mg-ATP-regulated divalent cation channel required for cell viability. *Nature* 411:590-595, 2001
38. Montell C: Mg²⁺ homeostasis: the Mg²⁺-nifcent TRPM chanzymes. *Curr Biol* 13:R799-801, 2003
39. Flatman PW: Magnesium transport across cell membranes. *J Membr Biol* 80:1-14, 1984
40. Flatman PW: Mechanisms of magnesium transport. *Annu Rev Physiol* 53:259-271, 1991
41. Dai LJ, Ritchie G, Kerstan D, *et al.*: Magnesium transport in the renal distal convoluted tubule. *Physiol Rev* 81:51-84, 2001
42. Topf JM, Murray PT: Hypomagnesemia and hypermagnesemia. *Rev Endocr Metab Disord* 4:195-206, 2003
43. Agus ZS: Hypomagnesemia. *J Am Soc Nephrol* 10:1616-1622, 1999
44. Alamoudi OS: Hypomagnesaemia in chronic, stable asthmatics: prevalence, correlation with severity and hospitalization. *Eur Respir J* 16:427-431, 2000
45. Chakraborti S, Chakraborti T, Mandal M, *et al.*: Protective role of magnesium in cardiovascular diseases: a review. *Mol Cell Biochem* 238:163-179, 2002
46. Nieves JW: Osteoporosis: the role of micronutrients. *Am J Clin Nutr* 81:1232S-1239S, 2005
47. Sales CH, Pedrosa Lde F: Magnesium and diabetes mellitus: their relation. *Clin Nutr* 25:554-562, 2006
48. Beyer FR, Dickinson HO, Nicolson DJ, *et al.*: Combined calcium, magnesium and potassium supplementation for the management of primary hypertension in adults. *Cochrane Database Syst Rev* 3:CD004805, 2006
49. Brunette MG, Crochet ME: Fluorimetric method for the determination of magnesium in renal tubular fluid. *Anal Biochem* 65:79-88, 1975
50. Grimellec CL, Poujeol P, Rouffignia C: 3H-inulin and electrolyte concentrations in Bowman's capsule in rat kidney. Comparison with artificial ultrafiltration. *Pflugers Arch* 354:117-131, 1975
51. Quamme GA, de Rouffignac C: Epithelial magnesium transport and regulation by the kidney. *Front Biosci* 5:D694-711, 2000
52. Murayama Y, Morel F, Le Grimellec C: Phosphate, calcium and magnesium transfers in proximal tubules and loops of Henle, as measured by single nephron microperfusion experiments in the rat. *Pflugers Arch* 333:1-16, 1972
53. Quamme GA: Control of magnesium transport in the thick ascending limb. *Am J Physiol* 256:F197-210, 1989
54. Quamme GA: Laboratory evaluation of magnesium status. Renal function and free intracellular magnesium concentration. *Clin Lab Med* 13:209-223, 1993

55. Voets T, Nilius B, Hoefs S, *et al.*: TRPM6 forms the Mg²⁺ influx channel involved in intestinal and renal Mg²⁺ absorption. *J Biol Chem* 279:19-25, 2004
56. Yang W, Lee HW, Hellinga H, *et al.*: Structural analysis, identification, and design of calcium-binding sites in proteins. *Proteins* 47:344-356, 2002
57. Meij IC, Koenderink JB, van Bokhoven H, *et al.*: Dominant isolated renal magnesium loss is caused by misrouting of the Na(+),K(+)-ATPase gamma-subunit. *Nat Genet* 26:265-266, 2000
58. Meij IC, Saar K, van den Heuvel LP, *et al.*: Hereditary isolated renal magnesium loss maps to chromosome 11q23. *Am J Hum Genet* 64:180-188, 1999
59. Wetzel RK, Sweadner KJ: Immunocytochemical localization of Na-K-ATPase alpha- and gamma-subunits in rat kidney. *Am J Physiol Renal Physiol* 281:F531-545, 2001
60. Simon DB, Nelson-Williams C, Bia MJ, *et al.*: Gitelman's variant of Bartter's syndrome, inherited hypokalaemic alkalosis, is caused by mutations in the thiazide-sensitive Na-Cl cotransporter. *Nat Genet* 12:24-30, 1996
61. Moore MJ: Thiazide-induced hypomagnesemia. *Jama* 240:1241, 1978
62. Nijenhuis T, Vallon V, van der Kemp AW, *et al.*: Enhanced passive Ca²⁺ reabsorption and reduced Mg²⁺ channel abundance explains thiazide-induced hypocalciuria and hypomagnesemia. *J Clin Invest* 115:1651-1658, 2005
63. Schlingmann KP, Weber S, Peters M, *et al.*: Hypomagnesemia with secondary hypocalcemia is caused by mutations in TRPM6, a new member of the TRPM gene family. *Nat Genet* 31:166-170, 2002
64. Walder RY, Landau D, Meyer P, *et al.*: Mutation of TRPM6 causes familial hypomagnesemia with secondary hypocalcemia. *Nat Genet* 31:171-174, 2002
65. Chubanov V, Waldegger S, Mederos y Schnitzler M, *et al.*: Disruption of TRPM6/TRPM7 complex formation by a mutation in the TRPM6 gene causes hypomagnesemia with secondary hypocalcemia. *Proc Natl Acad Sci U S A* 101:2894-2899, 2004
66. Riazanova LV, Pavur KS, Petrov AN, *et al.*: [Novel type of signaling molecules: protein kinases covalently linked to ion channels]. *Mol Biol (Mosk)* 35:321-332, 2001
67. Schmitz C, Perraud AL, Johnson CO, *et al.*: Regulation of vertebrate cellular Mg²⁺ homeostasis by TRPM7. *Cell* 114:191-200, 2003
68. Aarts M, Ihara K, Wei WL, *et al.*: A key role for TRPM7 channels in anoxic neuronal death. *Cell* 115:863-877, 2003
69. Clark K, Langeslag M, van Leeuwen B, *et al.*: TRPM7, a novel regulator of actomyosin contractility and cell adhesion. *Embo J* 25:290-301, 2006
70. Su LT, Agapito MA, Li M, *et al.*: TRPM7 regulates cell adhesion by controlling the calcium-dependent protease calpain. *J Biol Chem* 281:11260-11270, 2006
71. Elizondo MR, Arduini BL, Paulsen J, *et al.*: Defective skeletogenesis with kidney stone formation in dwarf zebrafish mutant for *trpm7*. *Curr Biol* 15:667-671, 2005
72. Caterina MJ, Schumacher MA, Tominaga M, *et al.*: The capsaicin receptor: a heat-activated ion channel in the pain pathway. *Nature* 389:816-824, 1997
73. Nilius B, Prenen J, Vennekens R, *et al.*: Pharmacological modulation of monovalent cation currents through the epithelial Ca²⁺ channel ECaC1. *Br J Pharmacol* 134:453-462, 2001
74. Wu SN, Jan CR, Li HF: Ruthenium red-mediated inhibition of large-conductance Ca²⁺-activated K⁺ channels in rat pituitary GH3 cells. *J Pharmacol Exp Ther* 290:998-1005, 1999
75. Schmitz C, Dorovkov MV, Zhao X, *et al.*: The channel kinases TRPM6 and TRPM7 are functionally nonredundant. *J Biol Chem* 280:37763-37771, 2005
76. Li M, Jiang J, Yue L: Functional characterization of homo- and heteromeric channel kinases TRPM6 and TRPM7. *J Gen Physiol* 127:525-537, 2006
77. Kozak JA, Kerschbaum HH, Cahalan MD: Distinct properties of CRAC and MIC channels in RBL cells. *J Gen Physiol* 120:221-235, 2002
78. Prakriya M, Lewis RS: Separation and characterization of currents through store-operated CRAC channels and Mg²⁺-inhibited cation (MIC) channels. *J Gen Physiol* 119:487-507, 2002

79. Hermosura MC, Monteilh-Zoller MK, Scharenberg AM, *et al.*: Dissociation of the store-operated calcium current I(CRAC) and the Mg-nucleotide-regulated metal ion current MagNuM. *J Physiol* 539:445-458, 2002
80. Kozak JA, Cahalan MD: MIC channels are inhibited by internal divalent cations but not ATP. *Biophys J* 84:922-927, 2003
81. Demeuse P, Penner R, Fleig A: TRPM7 channel is regulated by magnesium nucleotides via its kinase domain. *J Gen Physiol* 127:421-434, 2006
82. Kozak JA, Matsushita M, Nairn AC, *et al.*: Charge screening by internal pH and polyvalent cations as a mechanism for activation, inhibition, and rundown of TRPM7/MIC channels. *J Gen Physiol* 126:499-514, 2005
83. Runnels LW, Yue L, Clapham DE: The TRPM7 channel is inactivated by PIP(2) hydrolysis. *Nat Cell Biol* 4:329-336, 2002
84. Gwanyanya A, Sipido KR, Vereecke J, *et al.*: ATP and PIP2 dependence of the magnesium-inhibited, TRPM7-like cation channel in cardiac myocytes. *Am J Physiol Cell Physiol* 291:C627-635, 2006
85. Takezawa R, Schmitz C, Demeuse P, *et al.*: Receptor-mediated regulation of the TRPM7 channel through its endogenous protein kinase domain. *Proc Natl Acad Sci U S A* 101:6009-6014, 2004
86. Langeslag M, Clark K, Moolenaar WH, *et al.*: Activation of TRPM7 channels by phospholipase C-coupled receptor agonists. *J Biol Chem* 282:232-239, 2007
87. Groenestege WM, Hoenderop JG, van den Heuvel L, *et al.*: The epithelial Mg²⁺ channel transient receptor potential melastatin 6 is regulated by dietary Mg²⁺ content and estrogens. *J Am Soc Nephrol* 17:1035-1043, 2006
88. Bailly C, Roinel N, Amiel C: Stimulation by glucagon and PTH of Ca and Mg reabsorption in the superficial distal tubule of the rat kidney. *Pflugers Arch* 403:28-34, 1985
89. Elalouf JM, Roinel N, de Rouffignac C: Stimulation by human calcitonin of electrolyte transport in distal tubules of rat kidney. *Pflugers Arch* 399:111-118, 1983
90. Quamme GA: Renal handling of magnesium: drug and hormone interactions. *Magnesium* 5:248-272, 1986
91. Dai LJ, Ritchie G, Bapty BW, *et al.*: Insulin stimulates Mg²⁺ uptake in mouse distal convoluted tubule cells. *Am J Physiol* 277:F907-913, 1999
92. Lee CT, Lien YH, Lai LW, *et al.*: Increased renal calcium and magnesium transporter abundance in streptozotocin-induced diabetes mellitus. *Kidney Int* 69:1786-1791, 2006
93. Nijenhuis T, Renkema KY, Hoenderop JG, *et al.*: Acid-base status determines the renal expression of Ca²⁺ and Mg²⁺ transport proteins. *J Am Soc Nephrol* 17:617-626, 2006
94. Lote CJ, Thewles A, Wood JA, *et al.*: The hypomagnesaemic action of FK506: urinary excretion of magnesium and calcium and the role of parathyroid hormone. *Clin Sci (Lond)* 99:285-292, 2000
95. Thompson CB, June CH, Sullivan KM, *et al.*: Association between cyclosporin neurotoxicity and hypomagnesaemia. *Lancet* 2:1116-1120, 1984
96. Schrag D, Chung KY, Flombaum C, *et al.*: Cetuximab therapy and symptomatic hypomagnesemia. *J Natl Cancer Inst* 97:1221-1224, 2005
97. Schilsky RL, Anderson T: Hypomagnesemia and renal magnesium wasting in patients receiving cisplatin. *Ann Intern Med* 90:929-931, 1979
98. Nijenhuis T, Hoenderop JG, Bindels RJ: Downregulation of Ca(2+) and Mg(2+) transport proteins in the kidney explains tacrolimus (FK506)-induced hypercalciuria and hypomagnesemia. *J Am Soc Nephrol* 15:549-557, 2004
99. Ryazanova LV, Dorovkov MV, Ansari A, *et al.*: Characterization of the protein kinase activity of TRPM7/ChaK1, a protein kinase fused to the transient receptor potential ion channel. *J Biol Chem* 279:3708-3716, 2004
100. Yamaguchi H, Matsushita M, Nairn AC, *et al.*: Crystal structure of the atypical protein kinase domain of a TRP channel with phosphotransferase activity. *Mol Cell* 7:1047-1057, 2001
101. Ryazanov AG, Ward MD, Mendola CE, *et al.*: Identification of a new class of protein kinases represented by eukaryotic elongation factor-2 kinase. *Proc Natl Acad Sci U S A* 94:4884-4889, 1997

102. Matsushita M, Kozak JA, Shimizu Y, *et al.*: Channel function is dissociated from the intrinsic kinase activity and autophosphorylation of TRPM7/ChaK1. *J Biol Chem* 280:20793-20803, 2005
103. Dorovkov MV, Ryazanov AG: Phosphorylation of annexin I by TRPM7 channel-kinase. *J Biol Chem* 279:50643-50646, 2004
104. Clark K, Middelbeek J, Lasonder E, *et al.*: TRPM7 regulates myosin IIA filament stability and protein localization by heavy chain phosphorylation. *J Mol Biol* 378:790-803, 2008
105. Clark K, Middelbeek J, Dorovkov MV, *et al.*: The alpha-kinases TRPM6 and TRPM7, but not eEF-2 kinase, phosphorylate the assembly domain of myosin IIA, IIB and IIC. *FEBS Lett* 582:2993-2997, 2008
106. Clark K, Middelbeek J, Morrice NA, *et al.*: Massive autophosphorylation of the Ser/Thr-rich domain controls protein kinase activity of TRPM6 and TRPM7. *PLoS One* 3:e1876, 2008
107. Hiller Y, Gershoni JM, Bayer EA, *et al.*: Biotin binding to avidin. Oligosaccharide side chain not required for ligand association. *Biochem J* 248:167-171, 1987
108. Pollok BA, Heim R: Using GFP in FRET-based applications. *Trends Cell Biol* 9:57-60, 1999
109. Kerschensteiner D, Soto F, Stocker M: Fluorescence measurements reveal stoichiometry of K⁺ channels formed by modulatory and delayed rectifier alpha-subunits. *Proc Natl Acad Sci USA* 102:6160-6165, 2005
110. Adams SR, Harootunian AT, Buechler YJ, *et al.*: Fluorescence ratio imaging of cyclic AMP in single cells. *Nature* 349:694-697, 1991
111. Erickson MG, Alseikhan BA, Peterson BZ, *et al.*: Preassociation of calmodulin with voltage-gated Ca(2+) channels revealed by FRET in single living cells. *Neuron* 31:973-985, 2001
112. Corry B, Rigby P, Liu ZW, *et al.*: Conformational changes involved in MscL channel gating measured using FRET spectroscopy. *Biophys J* 89:L49-51, 2005
113. O'Connell KM, Tamkun MM: Targeting of voltage-gated potassium channel isoforms to distinct cell surface microdomains. *J Cell Sci* 118:2155-2166, 2005
114. Vicente R, Villalonga N, Calvo M, *et al.*: Kv1.5 association modifies Kv1.3 traffic and membrane localization. *J Biol Chem* 283:8756-8764, 2008
115. Axelrod D, Thompson NL, Burghardt TP: Total internal reflection fluorescence microscopy. *J Microsc* 129:19-28, 1983
116. Stein AT, Ufret-Vincenty CA, Hua L, *et al.*: Phosphoinositide 3-kinase binds to TRPV1 and mediates NGF-stimulated TRPV1 trafficking to the plasma membrane. *J Gen Physiol* 128:509-522, 2006
117. Demuro A, Parker I: Optical single-channel recording: imaging Ca²⁺ flux through individual ion channels with high temporal and spatial resolution. *J Biomed Opt* 10:11002, 2005
118. Bal M, Zhang J, Zaika O, *et al.*: Homomeric and heteromeric assembly of KCNQ (Kv7) K⁺ channels assayed by total internal reflection fluorescence/fluorescence resonance energy transfer and patch clamp analysis. *J Biol Chem* 283:30668-30676, 2008
119. Bal M, Zaika O, Martin P, *et al.*: Calmodulin binding to M-type K⁺ channels assayed by TIRF/FRET in living cells. *J Physiol* 586:2307-2320, 2008
120. Raveh A, Riven I, Reuveny E: The use of FRET microscopy to elucidate steady state channel conformational rearrangements and G protein interaction with the GIRK channels. *Methods Mol Biol* 491:199-212, 2008
121. Bean RC, Shepherd WC, Chan H, *et al.*: Discrete conductance fluctuations in lipid bilayer protein membranes. *J Gen Physiol* 53:741-757, 1969
122. Hladky SB, Haydon DA: Discreteness of conductance change in bimolecular lipid membranes in the presence of certain antibiotics. *Nature* 225:451-453, 1970
123. Anderson CR, Stevens CF: Voltage clamp analysis of acetylcholine produced end-plate current fluctuations at frog neuromuscular junction. *J Physiol* 235:655-691, 1973
124. Conti F, Hille B, Nonner W: Non-stationary fluctuations of the potassium conductance at the node of ranvier of the frog. *J Physiol* 353:199-230, 1984
125. Hodgkin AL, Huxley AF: Resting and action potentials in single nerve fibres. *J Physiol* 104:176-195, 1945
126. Neher E, Sakmann B: Single-channel currents recorded from membrane of denervated frog muscle fibres. *Nature* 260:799-802, 1976

127. Sigworth FJ, Neher E: Single Na⁺ channel currents observed in cultured rat muscle cells. *Nature* 287:447-449, 1980
128. Hamill OP, Marty A, Neher E, *et al.*: Improved patch-clamp techniques for high-resolution current recording from cells and cell-free membrane patches. *Pflugers Arch* 391:85-100, 1981



RACK1 inhibits TRPM6 activity via phosphorylation of the fused α -kinase domain

Gang Cao^{1*}, Stéphanie Thébault^{1*}, **Jenny van der Wijst**¹, AnneMiete van der Kemp¹, Edwin Lasonder², René J.M. Bindels¹, Joost G.J. Hoenderop¹
* contributed equally to this work

¹Department of Physiology, Radboud University Nijmegen Medical Centre, Nijmegen, The Netherlands

²Centre for Molecular and Biomolecular Informatics, Radboud University Nijmegen Medical Centre, Nijmegen, The Netherlands

Summary

Background: The maintenance of the body's Mg^{2+} balance is of great importance because of its involvement in numerous enzymatic systems and its intervention in neuromuscular excitability, protein synthesis, and nucleic acid stability. Recently, the transient receptor potential melastatin 6 (TRPM6) was identified as the gatekeeper of active Mg^{2+} transport and therefore plays a crucial role in the regulation of Mg^{2+} homeostasis. Remarkably, TRPM6 combines a Mg^{2+} channel with an α -kinase domain whose function remains elusive.

Results: Here, we identify the receptor for activated C-kinase 1 (RACK1) as the first regulatory protein of TRPM6 that associates with the α -kinase domain. RACK1 and TRPM6 are both present in renal Mg^{2+} -transporting distal convoluted tubules. We demonstrate that RACK1 inhibits channel activity in an α -kinase activity-dependent manner, whereas small interference (si) RNA-mediated knockdown of RACK1 increases the current. Moreover, threonine¹⁸⁵¹ in the α -kinase domain was identified as an autophosphorylation site of which the phosphorylation state is essential for the inhibitory effect of RACK1. Importantly, threonine¹⁸⁵¹ was crucial for the Mg^{2+} sensitivity of TRPM6 autophosphorylation and channel activity. TRPM6 channel activity was less sensitive to Mg^{2+} when RACK1 was knocked down by siRNA. Finally, activation of protein kinase C by phorbol 12-myristate 13-acetate-PMA prohibited the inhibitory effect of RACK1 on TRPM6 channel activity.

Conclusions: We propose a unique mode of TRPM6 regulation in which the Mg^{2+} influx is controlled by RACK1 through its interaction with the α -kinase and the phosphorylation state of the threonine¹⁸⁵¹ residue.

Introduction

The maintenance of the body's Mg^{2+} balance is of crucial importance for various vital cellular processes [1, 2]. Mg^{2+} homeostasis in mammals depends on the equilibrium between intestinal absorption and renal excretion. The renal distal convoluted tubule (DCT) reabsorbs ~10% of the filtered Mg^{2+} , and the reabsorption rate in this segment defines the final urinary Mg^{2+} concentration [3]. Mg^{2+} reabsorption in DCT is active and transcellular in nature, but the molecular details and regulation of this pathway remain largely unknown. Recently, transient receptor potential melastatin 6 (TRPM6) was identified as a pivotal component in active Mg^{2+} (re)absorption, mutations of which cause hypomagnesemia with secondary hypocalcemia (HSH) [4, 5]. TRPM6 is localized along the apical membrane of DCT and intestinal cells. It confines a Mg^{2+} -permeable channel, the activity of which is strongly regulated by the intracellular Mg^{2+} concentration ($[Mg^{2+}]_i$) [2]. Expression of TRPM6 is regulated by dietary Mg^{2+} , whereas TRPM7 is unaffected, supporting the idea of an important role of TRPM6 in transepithelial Mg^{2+} transport [6].

Remarkably, TRPM6 and TRPM7 contain a unique carboxyl (C)-terminal serine/threonine protein kinase domain belonging to the α -kinase family [7-9]. This distinctive combination of a

channel and an enzyme domain within a single molecule raises still unsolved questions concerning the regulatory role of this catalytic domain on channel activity. While it has been demonstrated that the TRPM7 α -kinase is able to autophosphorylate the channel and downstream substrates such as myosin IIA heavy chain and annexin I [10-13], the role of this α -kinase activity in modulating channel function is far from clear. Previous studies indicated that the α -kinase activity is not essential for TRPM7 activation [11, 13] and that regulation of TRPM7 activity by intracellular Mg^{2+} is dissociated from autophosphorylation or α -kinase activity [13]. Other groups demonstrated regulation of TRPM7 activity by intracellular Mg^{2+} and nucleotides as well as the cAMP/protein kinase A pathway, which required the α -kinase [14, 15]. It was reported that deletion of the TRPM7 α -kinase domain or phosphotransferase-deficient kinase mutants results in nonfunctional channels [9]. Compared to TRPM7, little is known about the α -kinase function of TRPM6. So far, only one study reported that the α -kinase of TRPM6 is capable of crossphosphorylation of TRPM7, but not vice versa, underlying the functional nonredundancy of these two “chanzymes” [12].

The aim of the present study was, therefore, to investigate the role of the α -kinase domain in TRPM6 channel activity through the identification of regulatory proteins specifically interacting with the α -kinase domain.

Results

RACK1 associates with TRPM6

To identify potential TRPM6-interacting proteins, two independent approaches were used, i.e., the yeast two-hybrid screening of a mouse kidney cDNA library with the complete C-tail of TRPM6 and the combination of a GST pull-down with the α -kinase domain of TRPM6 in mouse kidney lysate followed by Fourier transform ion cyclotron resonance mass spectrometry (FTMS). RACK1, a scaffold protein originally discovered as an adaptor for protein kinase C (PKC) [16], was identified as a TRPM6 interacting protein in both approaches. Figure 1A shows that RACK1 interacted with TRPM6, whereas no interaction was observed in the absence of either RACK1 or the TRPM6 C-tail. To further establish this interaction, GST pull-down binding assays were performed, which demonstrated that RACK1 interacts specifically with the α -kinase domain, but not with GST alone (Fig. 1B). Next, the association between TRPM6 and RACK1 was substantiated in mammalian HEK293 cells. RACK1 coprecipitated with the GST-kinase and GST-TRPM6-C-tail, but not with GSTTRPM6-C-tail- Δ -kinase and GST alone (Fig. 1C). Furthermore, coprecipitation experiments also demonstrated that the endogenously expressed RACK1 in HEK293 cells is associated with the TRPM6 α -kinase domain (Fig. 1D). Finally, coimmunoprecipitation studies of RACK1 with full-length TRPM6 or TRPM6 Δ -kinase in HEK293 cells showed that wild-type TRPM6 but not TRPM6 Δ -kinase co-precipitates with RACK1 (Fig. 1E).

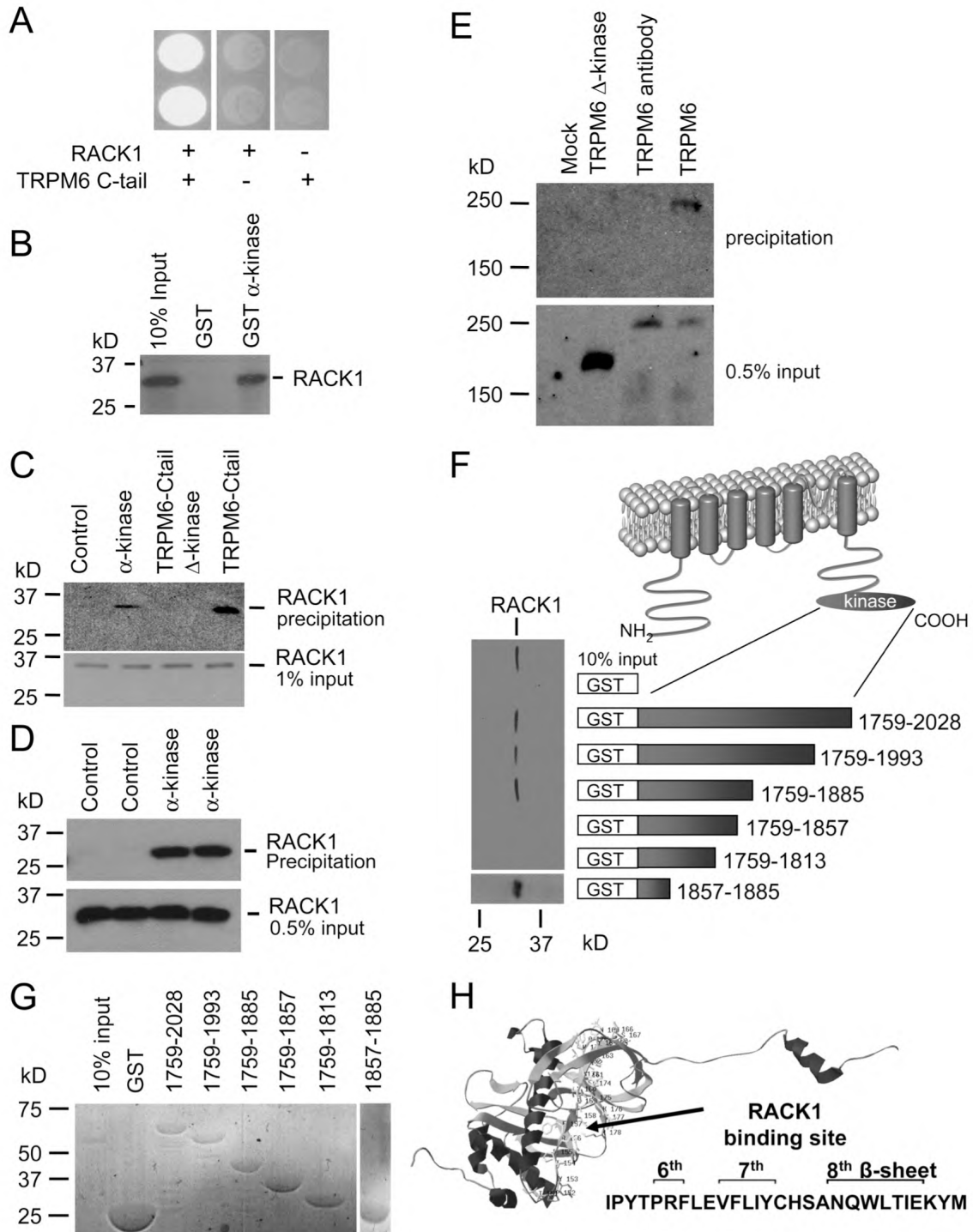


Figure 1. RACK1 interacts with α -kinase domain in TRPM6. *A.* The C-terminus of TRPM6 and the empty pAS1 vector were co-expressed with full-length RACK1 into the Y153 yeast strain and grown on media without tryptophan, leucine and histidine. *B.* GST-pull down assay between [³⁵S]-methionine-labeled RACK1 protein and GST or GST fused to the α -kinase domain. *C.* Co-precipitation studies of GST-kinase, GST-TRPM6-C-tail- Δ -kinase and GST-TRPM6-C-tail in RACK1-expressing HEK293 cells (top panel). RACK1 input (1%) expression was analyzed by immunoblotting (bottom panel). *D.* Co-precipitation studies of GST and GST- α -kinase with endogenous RACK1 in HEK293 cells (top panel). RACK1 input (0.5%) expression was analyzed by immunoblotting (bottom panel). *E.* Co-immunoprecipitation studies of RACK1 with GFP-TRPM6 or GFP-TRPM6 Δ -kinase in HEK293 cells (top panel). Input (0.5%) expression was analyzed by immunoblotting (bottom panel). *F.* Mapping of the RACK1 binding site within the α -kinase domain. Schematic diagram of the GST-fusion proteins containing different truncations of the α -kinase. *G.* Coomassie staining of the SDS/PAGE gel. *H.* RACK1 binding site in the predicted 3D-structure model of the α -kinase domain.

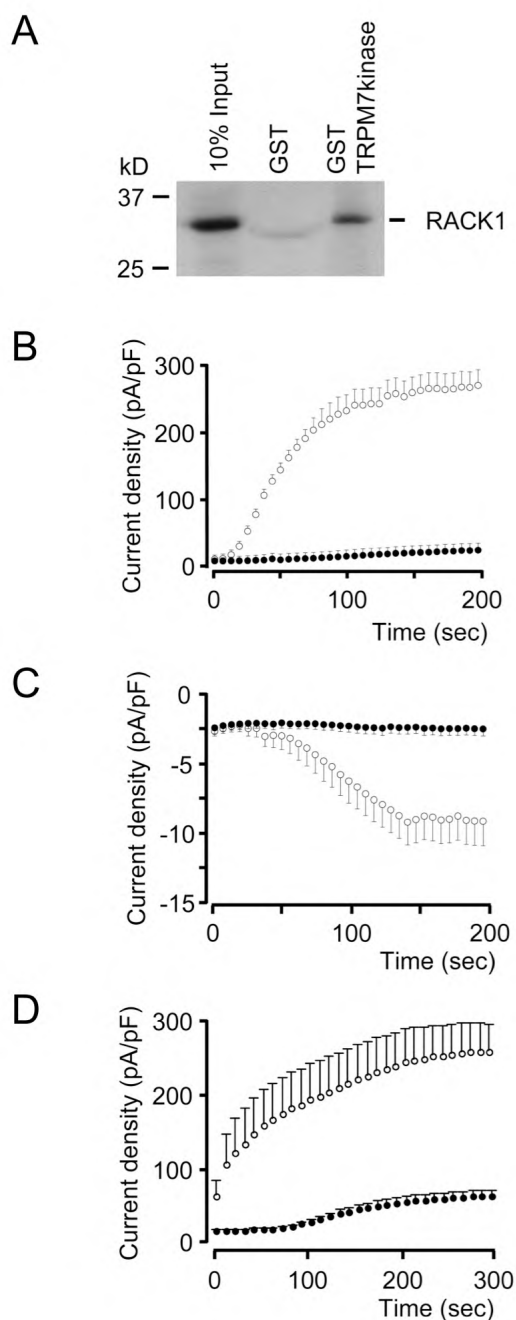


Figure 2. *A.* [35 S]-methionine-labeled RACK1 protein was incubated with GST or GST-fused to the TRPM7 α -kinase domain immobilized on glutathione-sepharose 4B beads. Bound RACK1 was separated by SDS/PAGE and visualized by autoradiography. *B.* Time course of the current density (pA/pF) at +80 mV of TRPM6 (\circ); TRPM6 and RACK1 (0.5 μ g, \bullet) transfected HEK293 cells. *C.* Corresponding time course at -80 mV. *D.* Time course of the current density at +80 mV of TRPM6 (\bullet , $n = 9$) and mock (\circ , $n = 4$) TRPM6-transfected HEK293 cells (selected from the MIC-developing HEK293 cells).

Mapping of the RACK1 binding site in TRPM6

To determine the RACK1 binding site within TRPM6, a series of deletion mutants in the α -kinase domain of the channel was constructed and evaluated for their interaction with [35 S]-methionine-labeled RACK1 protein using pull-down experiments (Fig. 1F). The interaction between the two proteins was abolished when TRPM6 was truncated at position 1857, whereas truncation at position 1885 had no effect on the interaction with RACK1. Moreover, a GST-fusion protein containing only the short stretch between the amino acids 1857 and 1885 of the TRPM6-kinase domain bound to RACK1 (Fig. 1F). Therefore, the RACK1 binding site within TRPM6 is restricted to the region between the positions 1857 and 1885. The integrity and quantity of the GST-fusion proteins was analyzed and confirmed by Coomassie staining (Fig. 1G). To explore the RACK1 binding site in the TRPM6 α -kinase domain, the tertiary structure of TRPM6 α -kinase domain was modeled by SWISS-MODEL (<http://swissmodel.expasy.org/SWISS-MODEL.html>) (Fig. 1H), based on the homology between the TRPM6 α -kinase and the crystallized TRPM7 α -kinase domain [17]. Due to the high homology between the TRPM7 and TRPM6 α -kinase domains (84%), these two α -kinase s share a highly conserved secondary structure. Indeed, the GST pull-down assay showed that RACK1 also interacts with the TRPM7 α -kinase domain (Fig. 2A). The surface and accessibility analysis of the RACK1 binding site (6th, 7th, and 8th β sheets) suggested that, among the 28 amino acids of the RACK1 binding site, 18 are localized at the surface of the TRPM6 α -kinase domain (see <http://www.cmbi.ru.nl/whvensela/trpm6/>).

RACK1 and TRPM6 co-express in kidney

To study the localization of RACK1 in kidney, immunohistochemistry was performed on kidney sections using the thiazide-sensitive Na^+/Cl^- cotransporter (NCC) as a DCT marker. These analyses indicated immunopositive staining for RACK1 in the NCC-expressing DCT cells (Fig. 3A, top panel). TRPM6 completely colocalized with NCC [2] along the apical membrane in DCT, indicating the presence of RACK1 in the TRPM6-expressing DCT segment (Fig. 3A, bottom panel). Subsequent immunohistochemical stainings confirmed the colocalization of RACK1 and TRPM6 in the DCT (Fig. 3B).

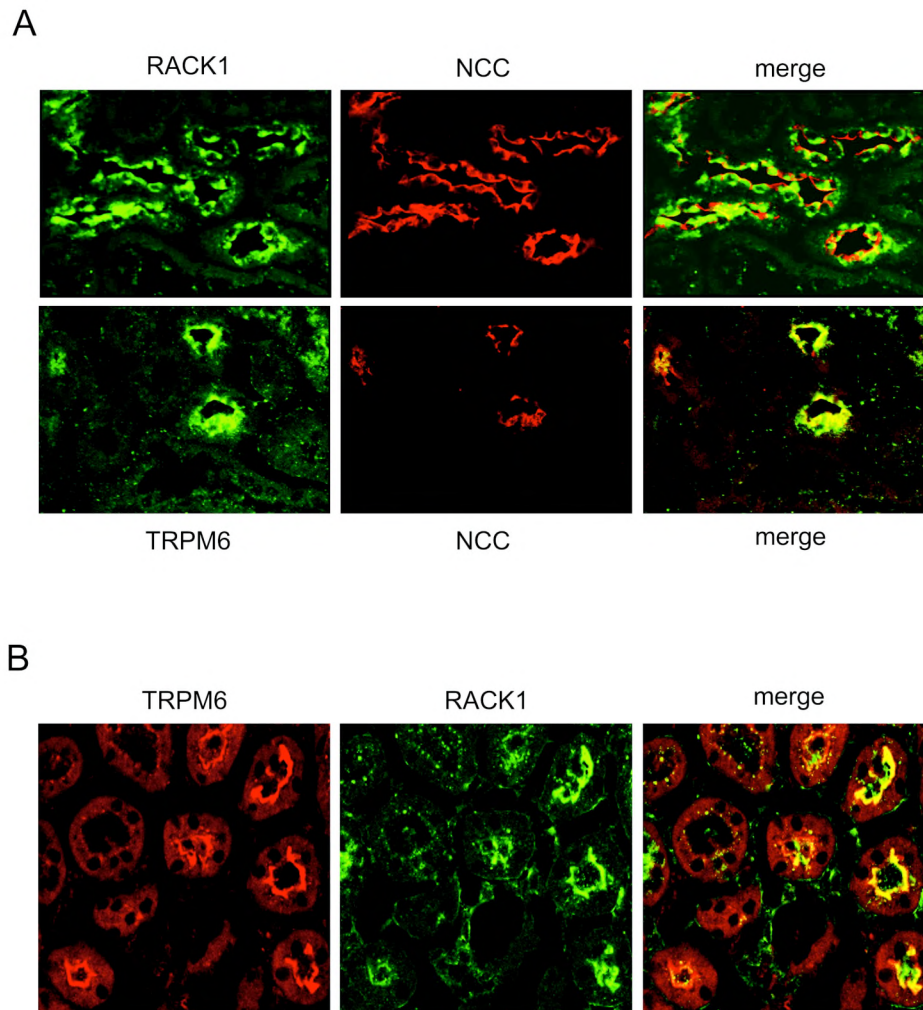


Figure 3. Localization of RACK1 in kidney. *A.* Immunohistochemical analysis of RACK1 and NCC in kidney sections (top panel). Kidney sections were co-stained with antibodies against TRPM6 and NCC. *B.* Immunohistochemical analysis of TRPM6 and RACK1 in rat kidney sections.

RACK1 inhibits TRPM6 channel activity

The functional role of RACK1 on TRPM6 current was investigated in HEK293 cells by whole-cell recordings. In mock-transfected HEK293 cells, dialyzed with a Mg^{2+} -free pipette solution, around 40% of the cells developed small albeit significant currents, generally referred to as the Mg^{2+} -inhibited cation current (MIC current) [18, 19]. This endogenous current was approximately ten times smaller

and developed over a longer time period compared to the TRPM6 current (Fig. 2D). We demonstrated that co-expression of RACK1 with TRPM6 significantly inhibited the TRPM6-mediated current amplitude in a dose-dependent manner.

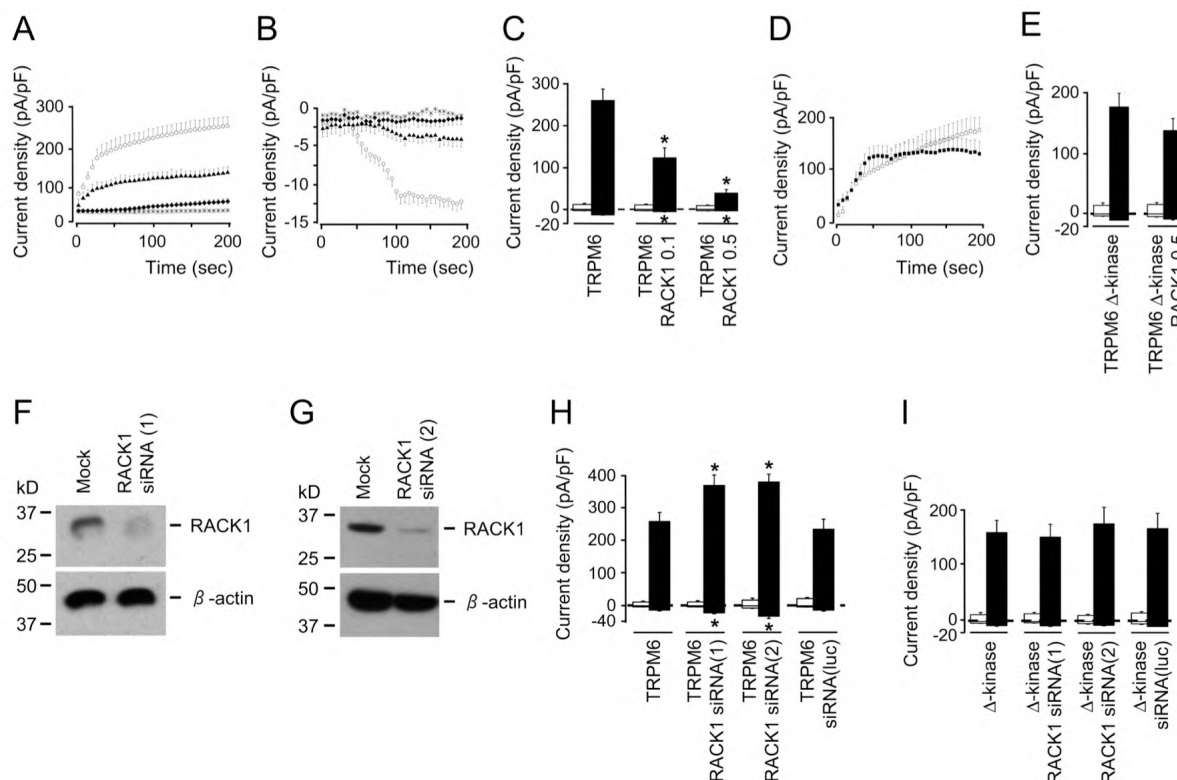


Figure 4. Functional effect of RACK1 on TRPM6 activity. *A.* Time course of the current density (pA/pF) at +80 mV of TRPM6 (○), TRPM6 and RACK1 (0.5 μg, ◆), TRPM6 and RACK1 (0.1 μg, ▲), and mock TRPM6 (*) transfected HEK293 cells. *B.* Corresponding time course at -80 mV. *C.* Averaged values of the current density at +80 and -80 mV after 200 s of mock TRPM6 (n=10), TRPM6 (n=22), mock TRPM6 and RACK1 (0.1 μg, n=11), TRPM6 and RACK1 (0.1 μg, n=18), mock TRPM6 and RACK1 (0.5 μg, n=13), and TRPM6 and RACK1 (0.5 μg, n=24). Open bars correspond to cells transfected with mock transfected DNA and closed bars to cells transfected with TRPM6 in the absence and presence of RACK1. * indicates $P = 0.001$ compared to TRPM6 current. *D.* Time course of the current density at +80 mV of TRPM6 Δ-kinase (□); and TRPM6 Δ-kinase and RACK1 (0.5 μg, ■) transfected HEK293 cells. *E.* Averaged values of the current density at +80 and -80 mV after 200 s of mock TRPM6 Δ-kinase (n=9); TRPM6 Δ-kinase (n=22); mock TRPM6 Δ-kinase and RACK1 (0.5 μg, n=10) and TRPM6 Δ-kinase and RACK1 (0.5 μg, n=19) transfected HEK293 cells. Open and closed bars correspond to cells transfected with mock TRPM6 Δ-kinase and TRPM6 Δ-kinase, respectively, in the absence and presence of RACK1. *F,G.* Immunoblot analysis of RACK1 and β-actin expression in mock, siRNA-RACK1(1) and siRNA-RACK1(2) transfected HEK293 cells. *H.* Averaged values of the current density at +80 and -80 mV after 200 s of mock TRPM6 (n=9), TRPM6 (n=19), mock TRPM6 and siRNA-RACK1(1) (0.5 μg, n=17), TRPM6 and siRNA-RACK1(1) (0.5 μg, n=21, $P = 0.029$), mock TRPM6 and siRNA-RACK1(2) (0.1 μg, n=18), TRPM6 and siRNA-RACK1(2) (0.1 μg, n=23, $P = 0.001$), mock TRPM6 and siRNA(luc) (0.5 μg, n=13), and TRPM6 and siRNA(luc) (0.5 μg, n=17, $P = 1.000$). * indicates $P < 0.05$ compared to the TRPM6 current. Open bars correspond to cells are transfected with mock DNA whereas closed bars to cells transfected with TRPM6 in the absence and presence of siRNA-RACK1 or luciferase. *I.* Similarly to Figure 3H, averaged values of mock TRPM6 Δ-kinase (n=10), TRPM6 Δ-kinase (n=23), mock TRPM6 Δ-kinase and siRNA-RACK1(1) (0.5 μg, n=12), TRPM6 Δ-kinase and siRNA-RACK1(1) (0.5 μg, n=19, $P = 1.000$), mock TRPM6 Δ-kinase and siRNA-RACK1(2) (0.1 μg, n=17), TRPM6 Δ-kinase and siRNA-RACK1(2) (0.1 μg, n=22, $P = 1.000$), mock TRPM6 Δ-kinase and siRNA(luc) (0.5 μg, n=18), and TRPM6 Δ-kinase and siRNA(luc) (0.5 μg, n=25, $P = 1.000$) current densities. P values are relative to the TRPM6 Δ-kinase current.

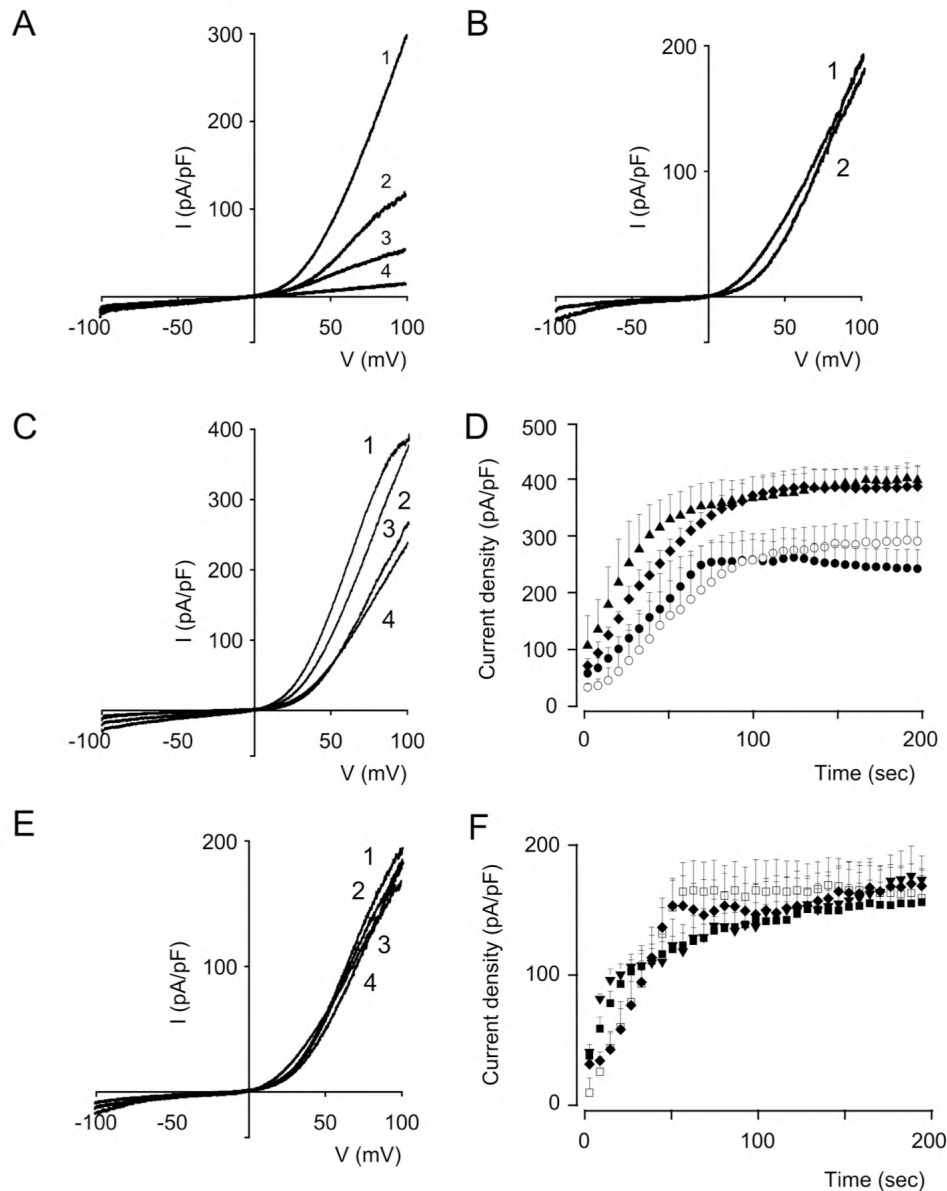


Figure 5. *A.* Current recorded after 200 sec stimulation by a voltage ramp between -100 and $+100$ mV of TRPM6 (1), TRPM6 and RACK1 ($0.1 \mu\text{g}$, 2), TRPM6 and RACK1 ($0.5 \mu\text{g}$, 3), and mock TRPM6 (4) transfected HEK293 cells. *B.* Current recorded after 200 sec stimulation by a voltage ramp between -100 and $+100$ mV of TRPM6 Δ -kinase (1), and TRPM6 Δ -kinase and RACK1 ($0.5 \mu\text{g}$, 2) transfected HEK293 cells. *C.* Current recorded after 200 sec stimulation by a voltage ramp between -100 and $+100$ mV of TRPM6 (3), TRPM6 and siRNA-RACK1(1) ($0.5 \mu\text{g}$, 2), TRPM6 and siRNA-RACK1(2) ($0.1 \mu\text{g}$, 1), and TRPM6 and siRNA(luc) ($0.5 \mu\text{g}$, 4) transfected HEK293 cells. *D.* Time course of the current density at $+80$ mV of TRPM6 (\circ), TRPM6 and siRNA-RACK1(1) ($0.5 \mu\text{g}$, \blacklozenge), TRPM6 and siRNA-RACK1(2) ($0.1 \mu\text{g}$, \blacktriangle), and TRPM6 and siRNA(luc) ($0.5 \mu\text{g}$, \bullet) transfected HEK293 cells. *E.* Current of TRPM6 Δ -kinase (1), TRPM6 Δ -kinase and siRNA-RACK1(1) ($0.5 \mu\text{g}$, 2), TRPM6 Δ -kinase and siRNA-RACK1(2) ($0.1 \mu\text{g}$, 3), and TRPM6 Δ -kinase and siRNA-luc ($0.5 \mu\text{g}$, 4) transfected HEK293 cells. *F.* Time course of the current density at $+80$ mV of TRPM6 Δ -kinase (\square), TRPM6 Δ -kinase and siRNA-RACK1(1) ($0.5 \mu\text{g}$, \blacklozenge), TRPM6 Δ -kinase and siRNA-RACK1(2) ($0.1 \mu\text{g}$, \blacktriangle), and TRPM6 Δ -kinase and siRNA-luc ($0.5 \mu\text{g}$, \blacksquare) transfected HEK293 cells.

TRPM6 current was reduced by $56\% \pm 4\%$ and $88\% \pm 3\%$ compared to TRPM6 alone when $0.1 \mu\text{g}$ or $0.5 \mu\text{g}$ RACK1 cDNA, respectively, was co-transfected (Fig. 4A–4C and Fig. 5A). Furthermore, RACK1 also inhibited the TRPM7 channel activity (Fig. 2B and 2C). However, the inhibitory effect of RACK1 on TRPM6/7 current was specific, since RACK1 did not significantly

affect the current in TRPV5-expressing HEK293 cells ($-11\% \pm 3\%$, $-16\% \pm 3\%$, and $-9\% \pm 2\%$ at -80 mV in divalent-free, EDTA, and 10 mM Ca^{2+} solutions, respectively, $n = 10$ – 12 cells as described previously [20]). Importantly, RACK1 co-expression with an α -kinase -deleted TRPM6 mutant (TRPM6 Δ -kinase) failed to suppress the TRPM6 Δ -kinase-mediated current at both $+80$ and -80 mV (Fig. 4D and 4E and Fig. 5B).

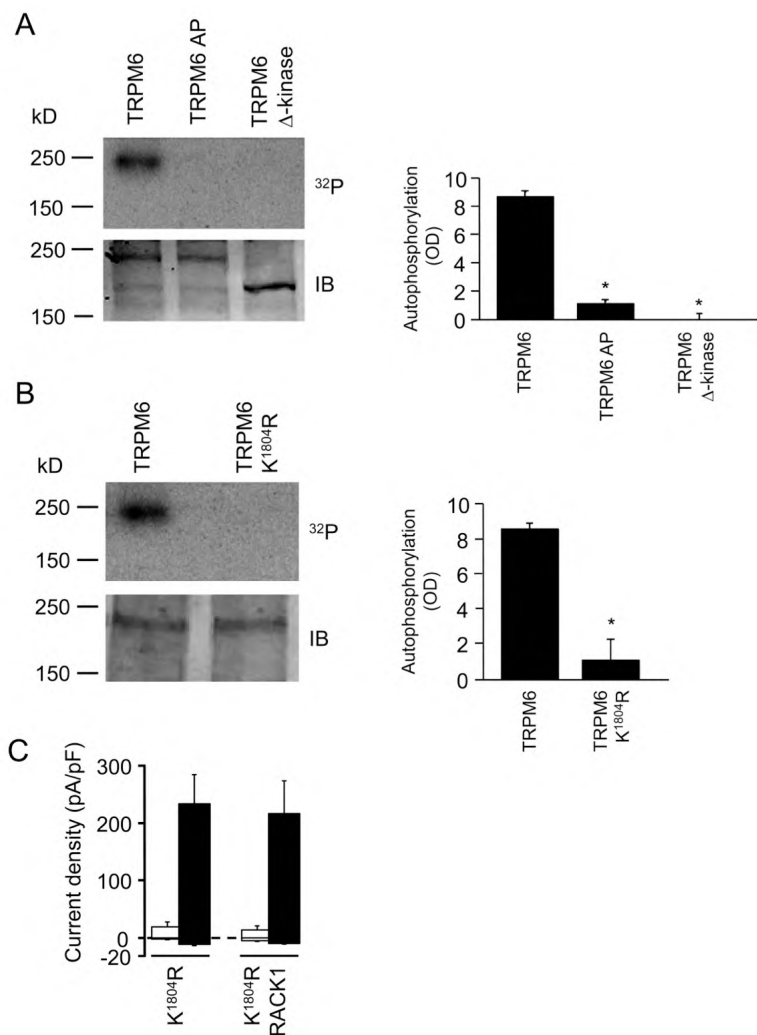


Figure 6. Inhibition of TRPM6 by RACK1 depends on phosphorylation of the α -kinase *A*. *In vitro* protein kinase assay of TRPM6 and the TRPM6 Δ -kinase mutant (^{32}P , top panel). Addition of alkaline phosphatase (AP) was used as a negative control. Immunoblotting (IB, bottom panel) and densitometry quantification (right panel) of TRPM6 and TRPM6 Δ -kinase expression. * indicates $P = 0.001$, $n=3$. *B*. *In vitro* protein kinase assay of TRPM6 and the K¹⁸⁰⁴R mutant (^{32}P , top panel). Immunoblotting (IB, bottom panel) and densitometry quantification (right panel) of TRPM6 and K¹⁸⁰⁴R expression. * indicates $P = 0.001$, $n=3$. *C*. Summary of the current density at $+80$ and -80 mV of K¹⁸⁰⁴R ($n=22$), K¹⁸⁰⁴R and RACK1 (0.5 μg , $n=24$; $P = 1.000$ compared to the K¹⁸⁰⁴R current), mock K¹⁸⁰⁴R ($n=15$) and mock K¹⁸⁰⁴R and RACK1 ($n=16$). Open bars correspond to mock conditions whereas closed bars to cells transfected with K¹⁸⁰⁴R in the absence and presence of RACK1.

Small interference RNA-mediated RACK1 silencing stimulates TRPM6 activity

To further elucidate the molecular mechanism of the RACK1 inhibitory effect, siRNA technology was applied. Immunoblot analysis revealed a significant downregulation of RACK1 protein abundance in HEK293 cells expressing RACK1-targeted siRNA(1) and siRNA(2) in comparison to mock-transfected cells (Fig. 4F and 4G). siRNA(1) and siRNA(2) for RACK1 induced a significant increase of the TRPM6 current amplitude [356 ± 31 pA/pF, -18 ± 1 pA/pF and 397 ± 25 pA/pF, -33 ± 6 pA/pF for RACK1 siRNA(1) and siRNA(2) at $+80$ and -80 mV, respectively, in comparison to 275 ± 26 pA/pF, -13 ± 2 pA/pF for TRPM6 and empty vector, respectively] (Fig. 4H and Fig. 5C and 5D). The siRNA for luciferase, siRNA(luc), did not significantly affect TRPM6 current amplitudes.

Importantly, RACK1 siRNA(1), RACK1 siRNA(2), and siRNA(luc) did not alter the current amplitude of the TRPM6 Δ -kinase mutant (Fig. 4I and Fig. 5E and 5F).

RACK1-mediated inhibition of TRPM6 is kinase activity-dependent

Next, the role of the kinase-mediated autophosphorylation was investigated. TRPM6 α -kinase autophosphorylation activity was first assessed by an *in vitro* protein kinase assay. Figure 6A indicates that TRPM6 is autophosphorylated, whereas deletion of its α -kinase or the addition of alkaline phosphatase prevents channel autophosphorylation. Next, we constructed a phosphotransferase-deficient mutant (K¹⁸⁰⁴R) according to the homologous TRPM7 phosphotransferase-deficient mutant (K¹⁶⁴⁸R) [13]. The *in vitro* phosphorylation assay showed that the kinase activity of the K¹⁸⁰⁴R mutant was abolished, while the mutant was equally expressed compared to wild-type TRPM6 (Fig. 6B). K¹⁸⁰⁴R mutant was still able to bind RACK1, as demonstrated by GST pull-down assay (Fig. 7A).

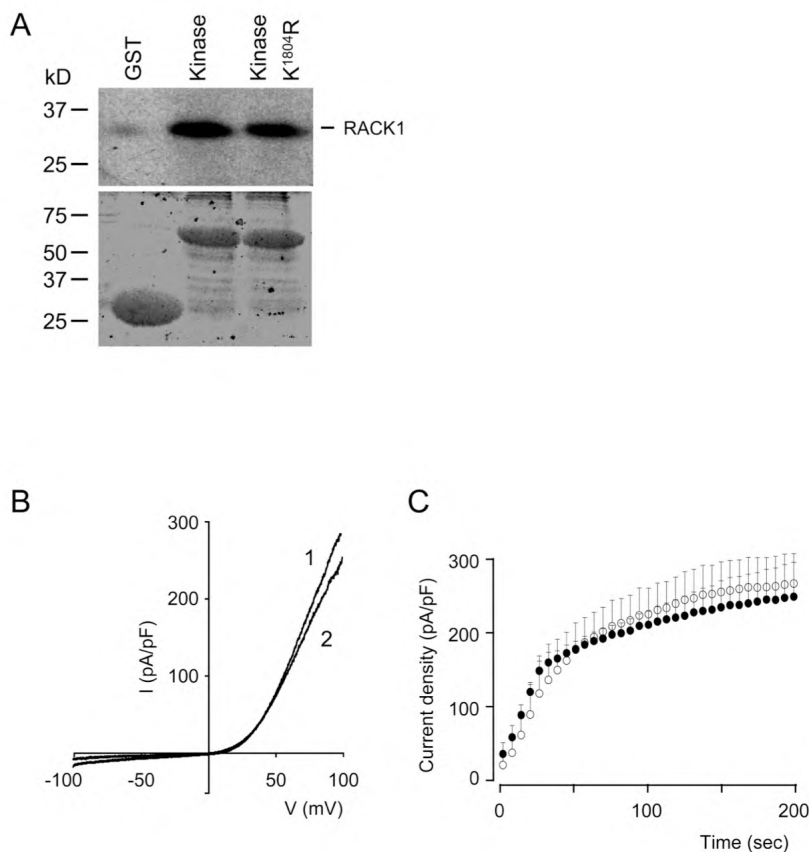


Figure 7. *A.* GST-pull down binding assay between RACK1 protein and GST, GST-fused to the kinase domain of TRPM6 or the K¹⁸⁰⁴R mutant (top panel). Coomassie staining of the corresponding gel (bottom panel). *B.* Current recorded after stimulation by a voltage ramp between -100 and $+100$ mV of K¹⁸⁰⁴R (1), and K¹⁸⁰⁴R and RACK1 (0.5 μ g, 2) transfected HEK293 cells. *C.* Time course of the current density at $+80$ mV of K¹⁸⁰⁴R (\circ), and K¹⁸⁰⁴R and RACK1 (0.5 μ g, \bullet) transfected HEK293 cells.

Autophosphorylation of threonine¹⁸⁵¹ in the kinase domain is essential for the inhibitory effect of RACK1

To address the autophosphorylation site(s) in TRPM6 that are essential for the regulatory effect of RACK1, the purified GST-TRPM6 α -kinase protein was subjected to an *in vitro* phosphorylation

assay and subsequently analyzed by FTMS. Figure 8A revealed a single autophosphorylation site within the α -kinase domain corresponding to the threonine residue at position 1851 (T¹⁸⁵¹). Interestingly, in the tertiary structure model of the TRPM6 α -kinase domain, T¹⁸⁵¹ is located at the end of the fourth α helix adjacent to the RACK1 binding site (Fig. 8B). Subsequently, T¹⁸⁵¹ was either point mutated into an alanine, resulting in a nonphosphorylated residue (T¹⁸⁵¹A), or into an aspartate, mimicking the constitutive autophosphorylated threonine residue (T¹⁸⁵¹D). Both T¹⁸⁵¹A and T¹⁸⁵¹D mutations significantly decreased TRPM6 autophosphorylation in comparison to the wild-type channel (Fig. 8C and Fig. 9A), while GST pull-down assays demonstrated that RACK1 binding to T¹⁸⁵¹A and T¹⁸⁵¹D mutants was not altered (Fig. 9B). Importantly, the expression of the (mutated) TRPM6 proteins was equal (Fig. 8C, lower panel). Furthermore, both mutants (T¹⁸⁵¹A and T¹⁸⁵¹D) displayed currents similar to the wild-type channel (Fig. 8D and 8E and Fig. 9C–9F). However, the T¹⁸⁵¹A mutation prevented the inhibitory effect of RACK1 (Fig. 8D and Fig. 9C and 9D), whereas the RACK1-induced inhibition remained unaltered when coexpressed with the T¹⁸⁵¹D mutant (Fig. 8E and Fig. 9E and 9F).

Threonine¹⁸⁵¹ and RACK1 play an important role in Mg²⁺-dependent channel activity

To explore whether RACK1 and the T1851 residue in the α -kinase domain are important for the inhibitory effect of Mg²⁺ on TRPM6 current, the influence of [Mg²⁺] on TRPM6 and T¹⁸⁵¹A mutant autophosphorylation was investigated. TRPM6 autophosphorylation activity was strongly dependent on the Mg²⁺ concentration and steadily increased in the physiological range of 0.1–1.0 mM Mg²⁺ (Fig. 8F). In contrast, the autophosphorylation activity of the T¹⁸⁵¹A mutant was not affected by the Mg²⁺ concentration (Fig. 8G). Both TRPM6 and T¹⁸⁵¹A mutant channel activities were significantly inhibited by Mg²⁺ in the patch-pipette. However, the T¹⁸⁵¹A mutant channel was less sensitive to the intracellular Mg²⁺ concentration compared to wild-type TRPM6 (IC₅₀ 0.72 ± 0.07 mM versus IC₅₀ 0.51 ± 0.06 mM, respectively) (Fig. 8H). Figure 8I showed that knockdown of endogenous RACK1 by siRNA significantly reduces the Mg²⁺-dependent inhibition of the TRPM6 current. Together, these data suggest that the T¹⁸⁵¹ phosphorylation-dependent inhibitory effect of RACK1 may play an important role in the suppression of the TRPM6 current by intracellular free Mg²⁺.

Coexpression of RACK1 does not affect expression of TRPM6 at the plasma membrane

The influence of RACK1 on the amount of TRPM6 channels expressed at the plasma membrane was investigated by cell surface biotinylation experiments. As shown in Figure 10 (upper panel), coexpression of RACK1 did not affect the amount of TRPM6 channels expressed at the plasma membrane. Of note, TRPM6 was equally expressed in all tested conditions, as determined in the total cell lysates (Fig. 10, bottom panel).

RACK1 inhibits TRPM6 in a PKC-dependent manner

Next, the effect of PKC activation by phorbol 12-myristate 13-acetate-PMA (PMA) [21] on the regulatory effect of RACK1 was studied. PKC activation by preincubation with 100 nM PMA for 5 min prevented the inhibitory effect of RACK1 on the TRPM6 current (Fig. 11B and Fig. 12C and 12D). The current amplitude in the presence of PMA was, however, not modified in cells expressing TRPM6 only (Fig. 11A and Fig. 12A and 12B).

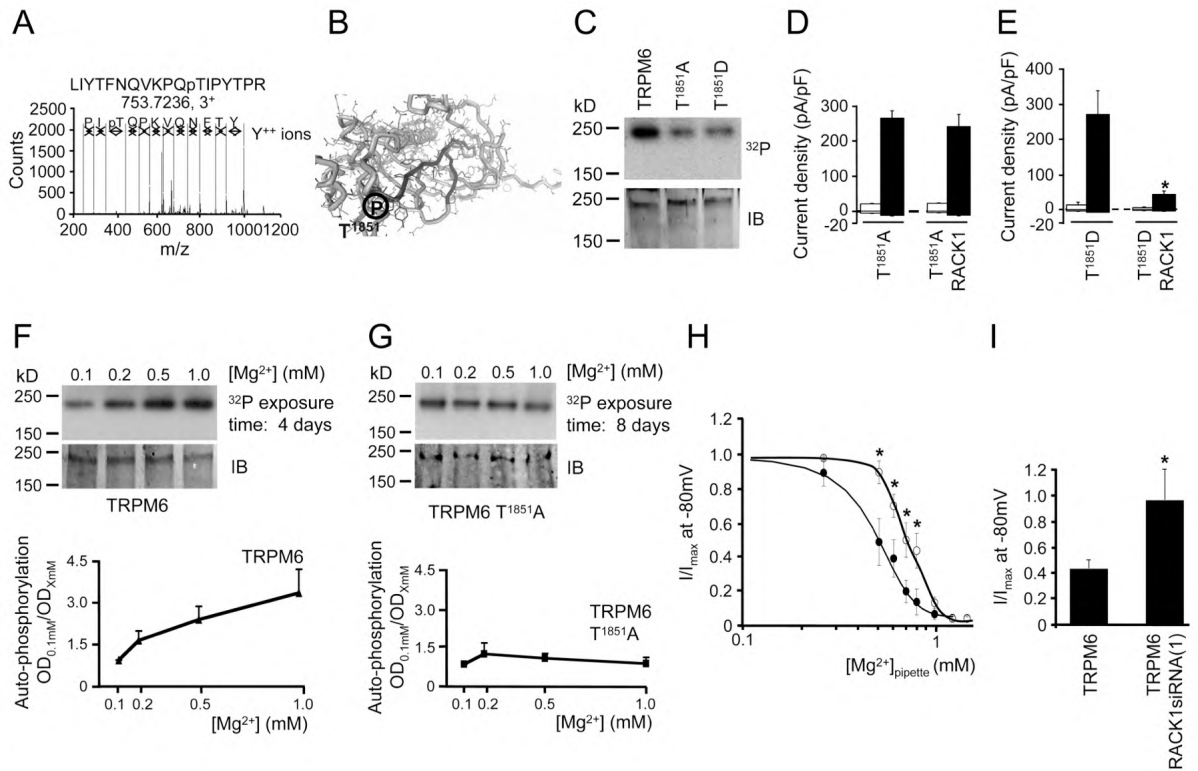


Figure 8. Mapping and function of the auto-phosphorylation site in TRPM6 α -kinase domain. *A.* Analysis of phosphorylated tryptic peptide by LTQ-FT ICR mass spectrometer. For detailed information see materials and methods. *B.* Auto-phosphorylated threonine at position 1851 in the putative 3-D structure of the TRPM6 α -kinase domain, in which the RACK1 binding site is highlighted. *C.* *In vitro* protein kinase assay (^{32}P , top panel) and immunoblotting analysis (IB, bottom panel) of TRPM6, T¹⁸⁵¹A and T¹⁸⁵¹D mutants. *D, E.* Averaged values of the current density at +80 and -80 mV of T¹⁸⁵¹A with (n=23; $P = 1.000$ compared to T¹⁸⁵¹A) or without RACK1 (n=25) (*D*) and T¹⁸⁵¹D with (n=27; $P = 0.001$ compared to T¹⁸⁵¹D) or without RACK1 (n=23) (*E*). Open and closed bars correspond to cells transfected with mock DNA and TRPM6 mutants, respectively, in the absence or presence of RACK1. *F, G.* *In vitro* phosphorylation of TRPM6 (*F*) and TRPM6 T¹⁸⁵¹A (*G*) at different Mg^{2+} concentrations (^{32}P , top panels). Autoradiograms were exposed 4 days for TRPM6 and 8 days for TRPM6 T¹⁸⁵¹A. TRPM6 and TRPM6 T¹⁸⁵¹A expression was determined by immunoblotting (IB, bottom panels). The phosphorylated proteins were quantified and plotted against 0.1 mM [Mg^{2+}] (n=3 for each; $P_{0.2 \text{ mM} [\text{Mg}^{2+}]} = 0.120$; $P_{0.5 \text{ mM} [\text{Mg}^{2+}]} = 0.042$; $P_{1.0 \text{ mM} [\text{Mg}^{2+}]} = 0.049$ for TRPM6 and $P_{0.2 \text{ mM} [\text{Mg}^{2+}]} = 0.442$; $P_{0.5 \text{ mM} [\text{Mg}^{2+}]} = 0.370$; $P_{1.0 \text{ mM} [\text{Mg}^{2+}]} = 0.973$ for TRPM6 T¹⁸⁵¹A). *H.* Effect of the pipette Mg^{2+} concentration on the inhibition of the inward Na^+ current at -80 mV of TRPM6 (\bullet , n=8-11) and the T¹⁸⁵¹A transfected HEK293 cells (\circ , n=9-13). * indicates $P < 0.05$, compared to TRPM6 current in 0 mM [Mg^{2+}]. *I.* Effect of the pipette Mg^{2+} concentration on the inhibition of the inward Na^+ current at -80 mV of TRPM6 (n=10) and TRPM6 and siRNA-RACK1(1) (0.5 μg , n=10, $P = 0.03$) transfected HEK293 cells.

To confirm the specificity of PMA, HEK293 cells coexpressing TRPM6 and RACK1 were incubated with 5 μM chelerythrine chloride, a specific PKC inhibitor [22], for 20 min prior to PMA

treatment. As shown in Figure 11B and Figures 12C and 12D, the stimulatory action of PMA was counteracted by chelerythrine chloride, suggesting that the PMA effect is indeed due to PKC activation. To further elucidate the PKC effect, the TRPM6 C-tail was coexpressed with RACK1 in HEK293 cells, subjected to PKC activation by PMA or vehicle, and subsequently precipitated using glutathione Sepharose 4B beads. The interaction of RACK1 with the TRPM6 C-tail was significantly reduced when PKC was activated (Fig. 11C, upper panel). Importantly, RACK1 was equally expressed in all situations (Fig. 11C, lower panel).

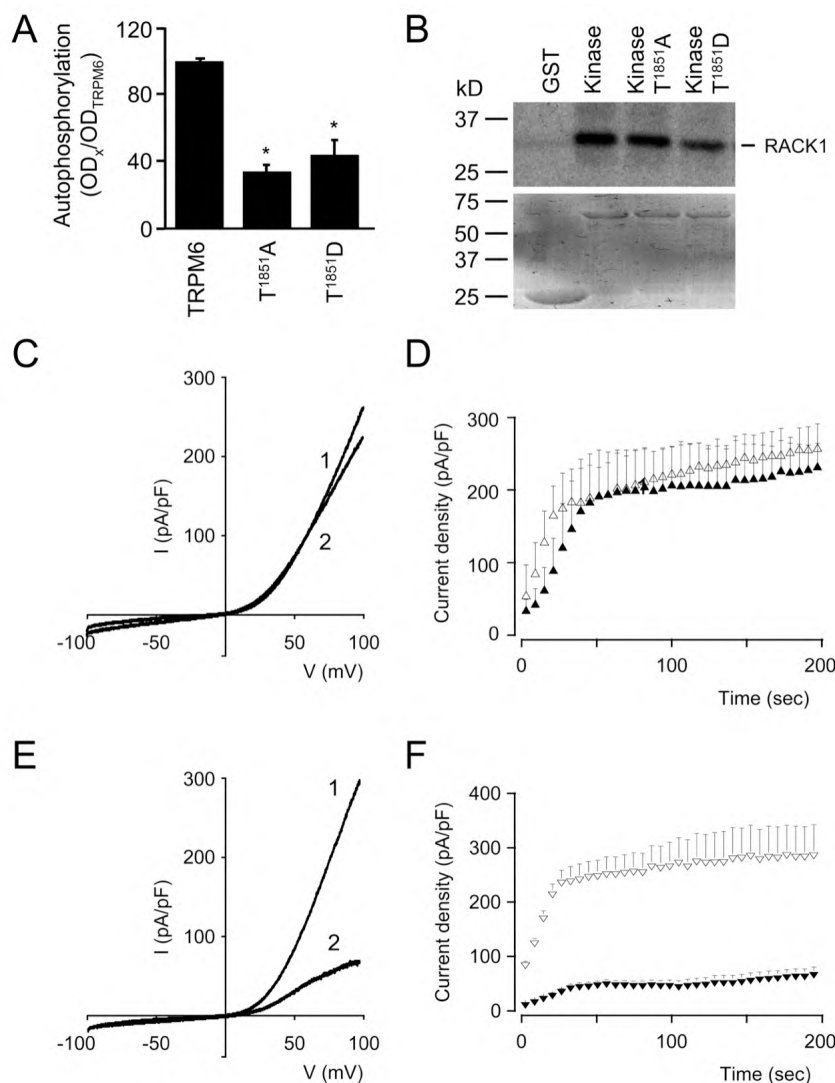


Figure 9. *A.* Densitometry quantification (right panel) of TRPM6, T¹⁸⁵¹A and T¹⁸⁵¹D expression. * indicates $P^{T^{1851}A} = 0.001$ and $P^{T^{1851}D} = 0.002$ compared to wild-type TRPM6, $n=3$ samples). *B.* GST-pull down binding assay between RACK1 protein and GST or GST-fused to the kinase domain of TRPM6, T¹⁸⁵¹A and T¹⁸⁵¹D mutants (top panel). Coomassie staining of the corresponding gel (bottom panel). *C.* Current recorded after stimulation by a voltage ramp between -100 and $+100$ mV of T¹⁸⁵¹A (1), and T¹⁸⁵¹A and RACK1 ($0.5 \mu\text{g}$, 2) transfected HEK293 cells. *D.* Time course of the current density at $+80$ mV of T¹⁸⁵¹A (Δ), and T¹⁸⁵¹A and RACK1 ($0.5 \mu\text{g}$, \blacktriangle) transfected HEK293 cells. *E.* Current recorded after stimulation by a voltage ramp between -100 and $+100$ mV of T¹⁸⁵¹D (1), and T¹⁸⁵¹D and RACK1 ($0.5 \mu\text{g}$, 2) transfected HEK293 cells. *F.* Time course of the current density at $+80$ mV of T¹⁸⁵¹D (open \blacktriangledown), and T¹⁸⁵¹D and RACK1 ($0.5 \mu\text{g}$, \blacktriangledown) transfected HEK293 cells.

Discussion

In the present study, we identified RACK1 as the first TRPM6-associated protein and demonstrated that RACK1 inhibits TRPM6 channel activity depending on the phosphorylation state T¹⁸⁵¹ in the α -kinase domain. First, RACK1 binds to the TRPM6 α -kinase domain and shares a similar expression pattern with TRPM6 in the kidney. Second, overexpression of RACK1 inhibits TRPM6

activity, and conversely, silencing of RACK1 by siRNA increases the TRPM6 current. Third, the RACK1-mediated inhibition of TRPM6 is prevented by deletion of the α -kinase domain. Fourth, inactivation of the α -kinase abrogates the inhibitory effect of RACK1. Fifth, T¹⁸⁵¹ is identified as an important autophosphorylation site in TRPM6-modulating channel activity by RACK1. Sixth, T¹⁸⁵¹ was crucial for the Mg²⁺ sensitivity of TRPM6 autophosphorylation and channel activity. Finally, knockdown of endogenous RACK1 by siRNA significantly reduces the Mg²⁺-dependent inhibition of the TRPM6 current.

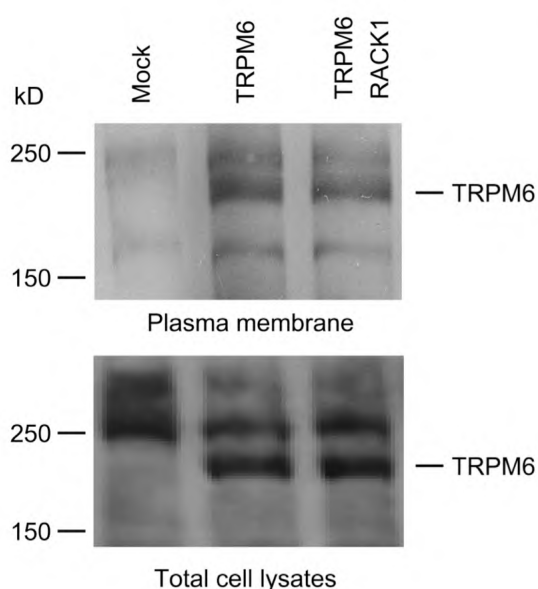


Figure 10. Co-expression of RACK1 does not affect the plasma membrane expression of TRPM6. TRPM6 and RACK1 transfected HEK293 cells were subjected to cell surface biotinylation analysis. TRPM6 expression was analyzed by immunoblotting for the plasma membrane fraction (top panel) and in total cell lysates (bottom panel). As negative control, mock cells were used.

TRPM6 forms the Mg²⁺ influx channel involved in intestinal and renal Mg²⁺ (re)absorption and is so far the only known molecular identity in the process of active transepithelial Mg²⁺ transport. However, TRPM6 regulation remains poorly understood. In this respect, the identification of RACK1 as a TRPM6 regulator provides the first molecular insight into the control of renal Mg²⁺ entry and, therefore, into the maintenance of Mg²⁺ balance. The interaction between RACK1 and TRPM6 was confirmed by GST pull-down assay and coimmunoprecipitation. Unfortunately, similar studies investigating an interaction between endogenous TRPM6 and RACK1 in kidney DCT cells were unsuccessful, possibly due to the low protein abundance of the channel. In addition, we demonstrated that endogenously expressed RACK1 in HEK293 cells interacts with the TRPM6 α -kinase domain. At the molecular level, our results suggest that RACK1 specifically binds to the 6th, 7th, and 8th β sheets of the α -kinase domain. Eighteen amino acids of the RACK1 binding site are located on the peripheral region of the tertiary structure of the TRPM6 α -kinase domain, which may facilitate the association between RACK1 and TRPM6. Importantly, we showed that RACK1 is abundantly present in TRPM6-expressing tubules, which further suggests the physiological relevance of the interaction between these proteins in the kidney.

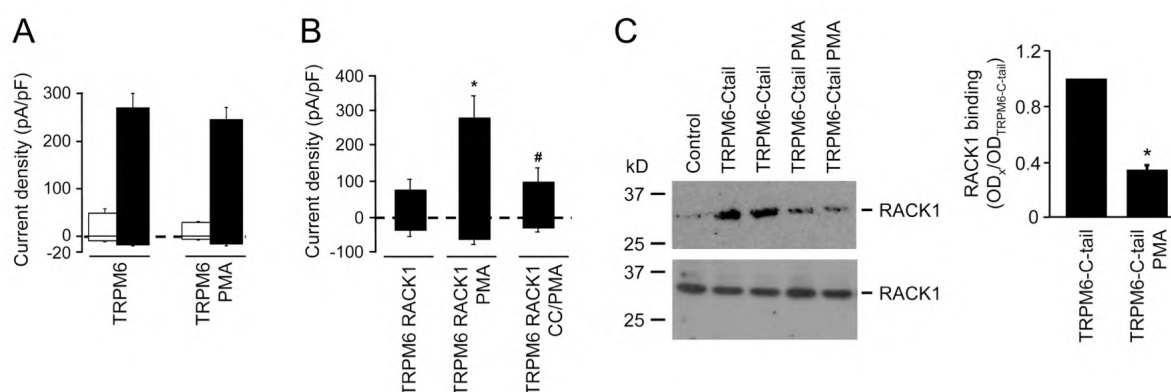


Figure 11. Inhibitory effect of RACK1 is PKC-dependent. *A.* Effect of PKC activation by PMA (100 nM, 5 minutes pre-treatment) on the current density at +80 and -80 mV of mock TRPM6 (n=14) and TRPM6 (n=22). Open bars correspond to cells transfected with mock DNA whereas closed bars to cells transfected with TRPM6. *B.* Effect of PKC activation by PMA and PKC inhibition by chelerythrine chloride (CC, 5 μ M, 20 minutes pre-treatment prior to PMA treatment) on the current density at +80 and -80 mV of TRPM6 and RACK1 (0.5 μ g, n=7-12) transfected HEK293 cells. * indicates $P = 0.01$ compared to TRPM6 and RACK1 without pre-treatment and # indicates $P = 0.02$ compared to TRPM6 and RACK1 pretreated with PMA. *C.* Effect of PKC activation on RACK1 binding. After PMA or vehicle pre-incubation, RACK1 was co-precipitated with GST-fused C-tail, separated by SDS/PAGE and visualized using the anti-RACK1 antibody (top panel). Immunoblotting (bottom panel) and densitometry quantification (right panel) of TRPM6-C-tail and RACK1 binding. * indicates $P = 0.001$ compared to TRPM6-C-tail.

RACK1, a member of the WD-40 family of proteins, is regarded as a scaffolding protein in multiple intracellular signal transduction pathways, including ion channel proteins such as the IP₃ receptor, NMDA receptor, and GABA_A receptor channels [23-25]. RACK1-mediated decline of the TRPM6 current was dose-dependent, and depletion of endogenously expressed RACK1 in HEK293 cells resulted in increased TRPM6 currents. The inhibitory effect of RACK1 requires the α -kinase domain with functional phosphotransferase activity. This was supported by the analysis of the TRPM6 Δ -kinase and the phosphotransferase-deficient (K¹⁸⁰⁴R) mutants, which were both insensitive to RACK1. While the autophosphorylation activity of the α -kinase domain has been well documented [10-13], the regulatory role of this catalytic domain on channel activity remains elusive. Previously, it has been demonstrated that the balance between phosphorylation and dephosphorylation operates as a key mechanism to regulate ion channel activity [26, 27]. However, the phosphotransferase-deficient K¹⁸⁰⁴R mutant displayed currents indistinguishable from wild-type TRPM6. Interestingly, the mutants T¹⁸⁵¹A and T¹⁸⁵¹D displayed currents similar to the wild-type channel but exhibited a significant albeit reduced autophosphorylation, while the autophosphorylation of mutant K¹⁸⁰⁴R was fully abolished. These data suggest that, besides T¹⁸⁵¹, additional autophosphorylation sites are present in TRPM6. Our findings support the conclusion that TRPM6 α -kinase autophosphorylation events are not vital for TRPM6 channel activation. Consistently, previous studies showed that TRPM7 phosphotransferase activity is not essential for channel activation [11, 12]. In contrast, the inhibitory action of RACK1

requires functional phosphotransferase activity. This notion is supported by the fact that the current of the phosphorylation-impaired mutants (K¹⁸⁰⁴R and T¹⁸⁵¹A) is insensitive to RACK1. Furthermore, the constitutive phosphorylated mutant T¹⁸⁵¹D was still inhibited by RACK1. Based on these observations, an increased channel activity for the phosphorylation-impaired mutants (K¹⁸⁰⁴R and T¹⁸⁵¹A) and the TRPM6 Δ -kinase mutant was expected. However, functional analysis of these mutated channel proteins did not indicate elevated channel activity. It has been demonstrated that the α -kinase domain can regulate TRPM7 channel activity via other signaling pathways besides RACK1. For instance, previous studies [13-15] indicated that the TRPM7 activity controlled by intracellular Mg²⁺, nucleotides, and the cAMP/protein kinase A pathway requires the α -kinase domain or kinase activity. Therefore, it is conceivable that removing the α -kinase domain or suppressing its phosphotransferase activity may abolish associated regulation(s) of TRPM6 channel activity. This could compensate a potential upregulation of TRPM6 activity caused by removal of the inhibitory RACK1 action. In reminiscence of the adjacent location of the autophosphorylation site in the α -kinase and the RACK1 binding site, we hypothesize that the phosphorylation state of T¹⁸⁵¹ plays a key role in controlling channel activity via RACK1.

Together, our results convincingly demonstrate a novel indirect model of regulation in which RACK1 functions as a mediator linking autophosphorylation of the α -kinase domain to channel activity. In this way, TRPM6 channel activity is controlled efficiently to manage constitutively active epithelial Mg²⁺ channels. Furthermore, cell-surface biotinylation experiments demonstrated that coexpression of RACK1 does not affect the amount of TRPM6 channels expressed at the plasma membrane. These data suggest that the inhibitory effect of RACK1 on TRPM6 is likely due to channel gating. Association of RACK1 and TRPM6 seems a dynamic process that can be abolished by PKC activation, thereby preventing the inhibitory effect of RACK1. An increased TRPM6 current upon PMA treatment in TRPM6-overexpressed HEK293 cells was anticipated, since PKC activation prevents the RACK1 inhibitory effect in TRPM6 and RACK1-overexpressing HEK293 cells. However, this inhibitory effect was not observed, which might be due to the fact that the amount of endogenous RACK1 is insufficient to inhibit the overexpressed TRPM6.

TRPM6 and TRPM7 confine a Mg²⁺-permeable channel of which the activity is strongly regulated by [Mg²⁺]_i [2, 9, 11, 14, 28]. Channel inactivation by elevated [Mg²⁺]_i may function as negative-feedback machinery to balance the Mg²⁺ homeostasis. Matsushita and coworkers postulated that regulation of TRPM7 channel activity by [Mg²⁺]_i is disassociated from its α -kinase activity [11], whereas other studies suggested the involvement of the α -kinase domain [13, 14]. In our study, the T¹⁸⁵¹A mutant is less sensitive to [Mg²⁺]_i, which is in agreement with previous studies showing that TRPM7 phosphotransferase activity influences the Mg²⁺-dependent inhibition of channel activity [13, 14].

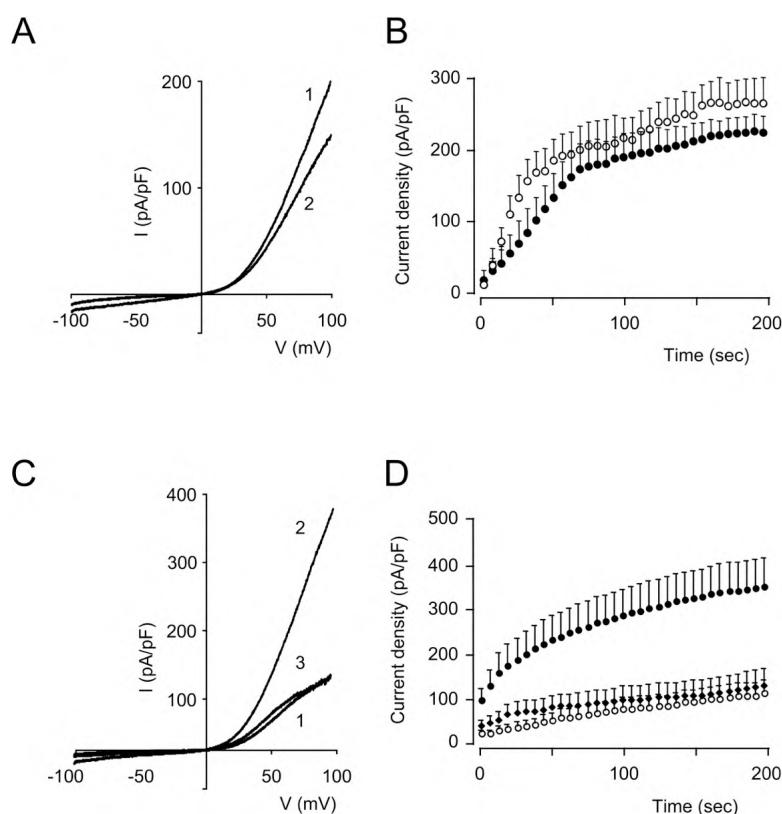


Figure 12. *A.* Current recorded after stimulation by a voltage ramp between -100 and $+100$ mV of TRPM6 transfected HEK293 cells in non-treated conditions (1) or pre-treated with PMA (2). *B.* Time course of the current density at $+80$ mV of TRPM6 transfected HEK293 cells in none-treated conditions (\circ) or pre-treated with PMA (\bullet). *C.* Current recorded after stimulation by a voltage ramp between -100 and $+100$ mV of TRPM6 transfected HEK293 cells in non-treated conditions (1), pre-treated with PMA alone (2) or with chelerythrine chloride (CC) and PMA (3). *D.* Time course of the current density at $+80$ mV of TRPM6 transfected HEK293 cells in none-treated conditions (\circ) and pre-treated with PMA alone (\bullet) or with CC and PMA (\blacklozenge).

This shift in Mg^{2+} sensitivity could have significant impact on TRPM6 activity during transepithelial Mg^{2+} transport because the channel is tightly controlled by $[Mg^{2+}]_i$ [2]. The T¹⁸⁵¹A mutant is still inhibited by high $[Mg^{2+}]_i$, suggesting that additional Mg^{2+} -sensing site(s) are present within TRPM6. Our data indicated that wild-type TRPM6 autophosphorylation activity is gradually enhanced by increasing the Mg^{2+} concentration, in contrast to autophosphorylation of the T¹⁸⁵¹A mutant for which the Mg^{2+} sensitivity is abolished. Thus, residue T¹⁸⁵¹ seems crucial in the Mg^{2+} sensitivity of TRPM6 autophosphorylation. In line with our study, Minagawa and coworkers demonstrated that the Mg^{2+} sensitivity of PhoQ phosphorylation, vital for Escherichia coli Mg^{2+} homeostasis, relies on a single residue, D¹⁷⁹ [29]. Over the last decade, the idea was that the free $[Mg^{2+}]_i$ is more or less constant. However, more recent studies provided evidence that the free $[Mg^{2+}]_i$ concentration varies significantly [30, 31]. Enzymes like adenylate kinases and TRPM7 kinase are dependent on the $[Mg^{2+}]_i$ [13, 32, 33]. Moreover, we showed that siRNA-mediated downregulation of endogenous RACK1 significantly reduced the inhibition of the TRPM6 current by Mg^{2+} . These findings suggest that RACK1 is involved in the Mg^{2+} sensitivity of TRPM6 channel activity.

Together, we suggest that TRPM6-mediated Mg^{2+} influx induces phosphorylation of T¹⁸⁵¹ located in the α -kinase domain. Subsequently, the phosphorylation of T¹⁸⁵¹ will activate the inhibitory effect of RACK1. This latter step may act as an intracellular feedback regulation to control TRPM6-mediated Mg^{2+} influx and avoid Mg^{2+} overload during renal epithelial Mg^{2+} transport. Our data

contribute to a further understanding of molecular mechanisms involved in renal Mg^{2+} handling and to the α -kinase-dependent regulation of TRPM6 channel activity.

Material and methods

DNA Constructs and cRNA Synthesis- The C-tail of human TRPM6 (1075–2022) was cloned in the pAS-1 yeast expression vector. The kinase domain of mouse TRPM6 (1759–2028) and human (1750–2022) was cloned into pGEX6p-2 (Amersham Pharmacia Biotech, Uppsala, Sweden) by PCR using mouse kidney cDNA or human TRPM6 in pCINeo/IRES-GFP [2] as template. The C terminus (1075–2022) and the α -kinase domain (1750–2022) of human TRPM6 were subcloned into the pEBG vector [34]. TRPM6-C-tail- Δ -kinase (1075–1749) was subcloned from TRPM6 Δ -kinase-pCINeo/IRES-GFP construct into the pEBG vector by PCR. Full-length mouse RACK1 cDNA was subcloned into pT7Ts, pCB7, and pGEX6p-2 from RACK1-pACT2. Wild-type TRPM6 in the pCINeo/IRES-GFP vector was HA-tagged at the N-terminal tail as described previously [2]. TRPM6 Δ -kinase (L¹⁷⁴⁹X), TRPM6 phosphotransferase-deficient (K¹⁸⁰⁴R), TRPM6-autophosphorylation (T¹⁸⁵¹A and T¹⁸⁵¹D), and GST- α -kinase truncant (TRPM6 1759-1993, 1759-1885, 1759-1857, 1857-1885, and 1759-1813) mutants were created using the QuickChange site-directed mutagenesis kit (Stratagene, La Jolla, CA, USA) according to the manufacturer's protocol. GFP-fused-TRPM6 in pCINeo vector was constructed by site-directed mutagenesis and PCR based on the TRPM6 cDNA in pCINeo/IRES-GFP. Human RACK1 siRNA plasmids were constructed as described previously [35]. The target sequences of siRNA are positioned at bp 195–215 (human RACK1 sequence accession number NM_006098). pSUPER-luciferase construct was used as a control as described previously [36]. All constructs were verified by sequence analysis. Chemically synthesized double-stranded RACK1 siRNA was purchased from Santa Cruz Biotechnology (Delaware, CA, USA). RACK1 cRNA was synthesized in vitro using T7 RNA polymerase as described previously [37].

GST-Fusion Proteins and Pull-Down Assay- TRPM6 α -kinase GST fusion protein was purified as previously described [38]. RACK1 protein was labeled with [³⁵S]-methionine using a reticulocyte lysate system (Promega, Madison, WI, USA) and added to purified GSTfusion proteins, immobilized on glutathione Sepharose 4B beads. After 2 hr of incubation at room temperature (RT), beads were washed extensively with pull-down buffer (10 mM Tris pH 7.4-HCl), 150 mM NaCl, 0.2% (v/v) Triton X-100). The bound proteins were eluted with SDS-PAGE loading buffer, separated on SDS-polyacrylamide gel, and visualized by autoradiography.

Sequence Analysis and Structure Modeling- The structural model of TRPM6 α -kinase domain was built based on the crystal structure of TRPM7 α -kinase domain [17] [Protein DataBank ID codes: 1IAJ (apo), 1IAH (ADP complex), and 1IA9 (AMP•PNP complex)] using SWISS-MODEL

(<http://swissmodel.expasy.org//SWISS-MODEL.html>) and analyzed by DeepView Swiss-PdbViewer (Version 3.7; <http://swissmodel.expasy.org/spdbv/>) and Yasara (<http://www.yasara.org>).

Mapping of Autophosphorylation in the α -kinase Domain by Nano Liquid Chromatography Tandem Mass Spectrometry- Proteins were treated with dithiothreitol (DTT) and iodoacetamide and digested in-gel by trypsin as previously described [39]. Peptide identification experiments by liquid chromatography tandem mass spectrometry were performed using a nano-HPLC Agilent 1100 nanoflow system connected on-line to a 7 Tesla linear quadrupole ion trap-Fourier transform ion cyclotron resonance (LTQ-FT) mass spectrometer (Thermo Electron, Bremen, Germany) as previously described [39]. Peptides and proteins were identified using the Mascot 2.1 (Matrix Science, Boston, MA, USA) algorithm to search a local version of the Uniprot database and an inhouse-created database containing the GST-TRPM6 kinase sequence. First-ranked peptides were parsed from Mascot database search html files with MSQuant to generate unique first-ranked peptide lists and internal calibration of measured ion masses. Assignment of phosphorylated peptides and modification sites were verified manually. The parent ion mass was determined with a mass accuracy of 0.39 ppm and sequenced using CID fragmentation. The assignment of the fragmentation spectrum, mostly as a doubly charged Y ion series, is depicted. The Mascot search engine identified the phosphorylated peptide with a score of 48.

Electrophysiology- Electrophysiological recordings with standard pipette and extracellular solutions were performed as already described [40]. The pipette solutions used for the intracellular Mg^{2+} experiments contained 150 mM NaCl, 10 mM HEPES, pH 7.2-NaOH, 0.1 mM EGTA, and 0.25, 0.5, 0.6, 0.7, 0.8, 1.2, or 1.5 mM $MgCl_2$ as indicated. The extracellular solutions contained (in mM) 150 NaCl and 10 HEPES (titrated to pH 7.4 with NaOH), supplemented or not with 1 mM $CaCl_2$. The standard pipette solution contained (in mM) 150 NaCl, 10 Na-EDTA, and 10 HEPES (titrated to pH 7.2 with NaOH). In all figures, except Figures 5H and 5I, the extracellular solution was supplemented with 1 mM $CaCl_2$. In Figures 5H and 5I, the recordings were conducted in divalent-free solution (150 mM NaCl and 10 mM HEPES) to observe the effect of Mg^{2+} in the patch pipette on the inward current. Transfected cells were identified by their green appearance, and GFP-negative cells from the same batch of cells were used as controls. The current density values presented in the histograms correspond to the current density after full development of the current, i.e., 200 s. In Figure 2D, only mock and TRPM6-transfected HEK293 cells that developed the MIC current (about 40%) were included.

Coimmunoprecipitation- HEK293 cells transfected with RACK1 and pEBG-TRPM6 kinase or pEBGTRPM6-C-tail or pEBG-TRPM6-C-tail- Δ -kinase were lysed for 1 hr on ice in lysis buffer [150 mM NaCl, 5 mM EDTA, 50 mM Tris pH 7.5-NaOH, 10 mM NaF, 0.5 mM Na_3VO_4 , 2.5 mM

$\text{Na}_4\text{P}_2\text{O}_7$, 0.5% (v/v) Triton including the protease inhibitors leupeptin (0.01 mg/ml), pepstatin (0.05 mg/ml), and phenylmethylsulfonyl fluoride (1 mM)]. The supernatants of the lysates were incubated overnight with glutathione Sepharose 4B beads at 4°C for coprecipitations. In the coimmunoprecipitation experiments, HEK293 cells transfected with RACK1 and GFP-TRPM6, GFP-TRPM6 D-kinase, or mock were lysed as indicated above. The anti-RACK1 antibody (IgM) was labeled with biotin and precipitated by neutravidin-agarose beads (Pierce) and subsequently incubated overnight with the supernatants of the lysates. After extensive washing, the bound proteins were eluted with SDS-PAGE loading buffer. The coprecipitation was analyzed using the anti-RACK1 antibody or anti-GFP (Transduction Laboratories, Lexington, KY, USA).

Immunoblotting- Protein samples were denatured by incubation for 30 min at 37°C in Laemmli buffer and then subjected to SDS-PAGE. Immunoblots were incubated with either mouse anti-HA (Sigma), anti-RACK1, anti-GFP (Transduction Laboratories), or anti- β -actin (Sigma) antibodies. Subsequently, blots were incubated with sheep horseradish peroxidase-conjugated anti-mouse IgG (Sigma) or anti-rabbit IgG (Sigma) and then visualized using enhanced chemiluminescence system.

Immunohistochemistry- Immunohistochemistry was performed as described previously [41]. Briefly, rat kidney sections were incubated for 16 hr at 4°C with rabbit anti-thiazide-sensitive Na^+/Cl^- cotransporter (NCC), mouse anti-RACK1, and guinea pig anti-TRPM6 [2]. To visualize RACK1, tyramide signal amplification kit (NEN Life Science Products, Zaventem, Belgium) was used after incubation with biotin-coated goat anti-mouse secondary antibody. Images were taken with a Bio-Rad MRC 100 confocal laser scanning microscope.

Cell-Surface Labeling with Biotin- HEK293 cells were transiently cotransfected with 12 μg HA-TRPM6 and 3 μg RACK1 or PCB7, in poly-L-lysine (Sigma) coated 10 cm dishes. Cell-surface labeling with biotin was performed as described previously [20]. At 72 hr after transfection, the biotinylation assay was performed. Cells were homogenized in 1 ml lysis buffer as described previously [20], using the NHS-LC-LC-biotin (Pierce, Etten-Leur, The Netherlands). Finally, biotinylated proteins were precipitated using neutravidin-agarose beads (Pierce). TRPM6 expression was analyzed by immunoblot for the precipitates (plasma membrane fraction) and for the total cell lysates using the anti-HA antibody.

In Vitro Phosphorylation and Phosphatase Assays- HA-TRPM6 was precipitated by using the anti-HA antibody. The precipitates were incubated in a total volume of 30 μl kinase reaction buffer A (50 mM HEPES pH 7.4-KOH, 4 mM MnCl_2 , 0.5 mM CaCl_2 , 100 μM ATP) or kinase reaction buffer B (50 mM HEPES pH 7.4-KOH, 1 mM MnCl_2 , 0.5 mM CaCl_2 , 100 μM ATP containing different

MgCl₂ concentrations) and 2 μCi of [γ -³²P]ATP for 30 min at 30°C. For in vitro phosphatase assay, 15 units alkaline phosphatase (Roche, Mannheim, Germany) was added to TRPM6 immunoprecipitates before in vitro phosphorylation assays. The reaction was terminated by three washing steps with phosphorylation washing buffer (50 mM HEPES pH 7.4-KOH, 4 mM MnCl₂, 0.5 mM CaCl₂). Phosphorylation was analyzed after gel electrophoresis by autoradiography.

Statistical Analysis- Values are expressed as mean \pm SE. Statistical significance between groups was determined by analysis of variance (ANOVA) followed by pair-wise comparison using the method of Scheffe' for patch-clamp recordings and unpaired Student's t test for immunoblot and phosphorylation quantifications. Differences in means with $p < 0.05$ were considered statistically significant. The statistical analysis was performed using the SPSS software (SPSS Inc, Chicago, Illinois, USA).

Acknowledgements

This work was supported by the Netherlands Organization for Scientific Research (Zon-Mw 016.006.001, ZonMW 9120.6110, TOPCW 05.B.012), EURYI, Human Frontiers Science Program (RGP32/2004), the Dutch Kidney foundation (C03.6017), and the EMBO fellowship (ALTF 727-2005). We would like to thank Dr. S. van de Graaf for valuable discussions and Mr. R. Janssen, Mr. M. de Graaf, Mr. D. van den Berg, and Mr. M. Prinz for technical assistance. The pAS-1 yeast expression vector was kindly provided by Dr. S. Elledge (Baylor College of Medicine, Houston, Texas, USA). The authors would like to thank Drs. H. Venselaar and G. Vriend (Centre for Molecular and Biomolecular Informatics, Nijmegen, The Netherlands) for surface and accessibility analysis of the TRPM6 α -kinase domain.

References

1. Schlingmann KP, Gudermann T: A critical role of TRPM channel-kinase for human magnesium transport. *J Physiol* 566:301-308, 2005
2. Voets T, Nilius B, Hoefs S, *et al.*: TRPM6 forms the Mg²⁺ influx channel involved in intestinal and renal Mg²⁺ absorption. *J Biol Chem* 279:19-25, 2004
3. Dai LJ, Ritchie G, Kerstan D, *et al.*: Magnesium transport in the renal distal convoluted tubule. *Physiol Rev* 81:51-84, 2001
4. Schlingmann KP, Weber S, Peters M, *et al.*: Hypomagnesemia with secondary hypocalcemia is caused by mutations in TRPM6, a new member of the TRPM gene family. *Nat Genet* 31:166-170, 2002
5. Walder RY, Landau D, Meyer P, *et al.*: Mutation of TRPM6 causes familial hypomagnesemia with secondary hypocalcemia. *Nat Genet* 31:171-174, 2002
6. Groenestege WM, Hoenderop JG, van den Heuvel L, *et al.*: The epithelial Mg²⁺ channel transient receptor potential melastatin 6 is regulated by dietary Mg²⁺ content and estrogens. *J Am Soc Nephrol* 17:1035-1043, 2006
7. Drennan D, Ryazanov AG: Alpha-kinases: analysis of the family and comparison with conventional protein kinases. *Prog Biophys Mol Biol* 85:1-32, 2004
8. Montell C: Mg²⁺ homeostasis: the Mg²⁺-nifcent TRPM chanzymes. *Curr Biol* 13:R799-801, 2003
9. Runnels LW, Yue L, Clapham DE: TRP-PLIK, a bifunctional protein with kinase and ion channel activities. *Science* 291:1043-1047., 2001
10. Clark K, Langeslag M, van Leeuwen B, *et al.*: TRPM7, a novel regulator of actomyosin contractility and cell adhesion. *Embo J* 25:290-301, 2006
11. Matsushita M, Kozak JA, Shimizu Y, *et al.*: Channel function is dissociated from the intrinsic kinase activity and autophosphorylation of TRPM7/ChaK1. *J Biol Chem* 280:20793-20803, 2005
12. Schmitz C, Dorovkov MV, Zhao X, *et al.*: The channel kinases TRPM6 and TRPM7 are functionally non-redundant. *J Biol Chem*, 2005
13. Schmitz C, Perraud AL, Johnson CO, *et al.*: Regulation of vertebrate cellular Mg²⁺ homeostasis by TRPM7. *Cell* 114:191-200, 2003
14. Demeuse P, Penner R, Fleig A: TRPM7 Channel Is Regulated by Magnesium Nucleotides via its Kinase Domain. *J Gen Physiol* 127:421-434, 2006
15. Takezawa R, Schmitz C, Demeuse P, *et al.*: Receptor-mediated regulation of the TRPM7 channel through its endogenous protein kinase domain. *Proc Natl Acad Sci U S A* 101:6009-6014, 2004
16. Ron D, Chen CH, Caldwell J, *et al.*: Cloning of an intracellular receptor for protein kinase C: a homolog of the beta subunit of G proteins. *Proc Natl Acad Sci U S A* 91:839-843, 1994
17. Yamaguchi H, Matsushita M, Nairn AC, *et al.*: Crystal structure of the atypical protein kinase domain of a TRP channel with phosphotransferase activity. *Mol Cell* 7:1047-1057, 2001
18. Gwanyanya A, Sipido K, Vereecke J, *et al.*: ATP- and PIP₂-dependence of the magnesium-inhibited, TRPM7-like cation channel in cardiac myocytes. *Am J Physiol Cell Physiol*, 2006
19. Kozak JA, Cahalan MD: MIC channels are inhibited by internal divalent cations but not ATP. *Biophys J* 84:922-927, 2003
20. Gkika D, Topala CN, Hoenderop JG, *et al.*: The immunophilin FKBP52 inhibits the activity of the epithelial Ca²⁺ channel TRPV5. *Am J Physiol Renal Physiol* 290:F1253-1259, 2006
21. Pascale A, Alkon DL, Grimaldi M: Translocation of protein kinase C-betaII in astrocytes requires organized actin cytoskeleton and is not accompanied by synchronous RACK1 relocation. *Glia* 46:169-182, 2004
22. Andrews DA, Yang L, Low PS: Phorbol ester stimulates a protein kinase C-mediated agatoxin-TK-sensitive calcium permeability pathway in human red blood cells. *Blood* 100:3392-3399, 2002
23. Feng J, Cai X, Zhao J, *et al.*: Serotonin receptors modulate GABA(A) receptor channels through activation of anchored protein kinase C in prefrontal cortical neurons. *J Neurosci* 21:6502-6511, 2001

24. Patterson RL, van Rossum DB, Barrow RK, *et al.*: RACK1 binds to inositol 1,4,5-trisphosphate receptors and mediates Ca²⁺ release. *Proc Natl Acad Sci U S A* 101:2328-2332, 2004
25. Yaka R, Thornton C, Vagts AJ, *et al.*: NMDA receptor function is regulated by the inhibitory scaffolding protein, RACK1. *Proc Natl Acad Sci U S A* 99:5710-5715, 2002
26. Levitan IB: Modulation of ion channels by protein phosphorylation and dephosphorylation. *Annu Rev Physiol* 56:193-212, 1994
27. Touyz RM, He Y, Montezano AC, *et al.*: Differential regulation of transient receptor potential melastatin 6 and 7 cation channels by ANG II in vascular smooth muscle cells from spontaneously hypertensive rats. *Am J Physiol Regul Integr Comp Physiol* 290:R73-78, 2006
28. Nadler MJ, Hermosura MC, Inabe K, *et al.*: LTRPC7 is a Mg.ATP-regulated divalent cation channel required for cell viability. *Nature* 411:590-595., 2001
29. Minagawa S, Okura R, Tsuchitani H, *et al.*: Isolation and molecular characterization of the locked-on mutant of Mg²⁺ sensor PhoQ in *Escherichia coli*. *Biosci Biotechnol Biochem* 69:1281-1287, 2005
30. Murphy E: Mysteries of magnesium homeostasis. *Circ Res* 86:245-248, 2000
31. Romani AM, Matthews VD, Scarpa A: Parallel stimulation of glucose and Mg(2+) accumulation by insulin in rat hearts and cardiac ventricular myocytes. *Circ Res* 86:326-333, 2000
32. Igamberdiev AU, Kleczkowski LA: Implications of adenylate kinase-governed equilibrium of adenylates on contents of free magnesium in plant cells and compartments. *Biochem J* 360:225-231, 2001
33. Igamberdiev AU, Kleczkowski LA: Equilibration of adenylates in the mitochondrial intermembrane space maintains respiration and regulates cytosolic metabolism. *J Exp Bot* 57:2133-2141, 2006
34. Okada T, Inoue R, Yamazaki K, *et al.*: Molecular and functional characterization of a novel mouse transient receptor potential protein homologue TRP7. Ca(2+)-permeable cation channel that is constitutively activated and enhanced by stimulation of G protein-coupled receptor. *J Biol Chem* 274:27359-27370., 1999
35. Mamidipudi V, Zhang J, Lee KC, *et al.*: RACK1 regulates G1/S progression by suppressing Src kinase activity. *Mol Cell Biol* 24:6788-6798, 2004
36. Gkika D, Topala CN, Chang Q, *et al.*: Tissue kallikrein stimulates Ca(2+) reabsorption via PKC-dependent plasma membrane accumulation of TRPV5. *Embo J* 25:4707-4716, 2006
37. Hoenderop JG, van der Kemp AW, Hartog A, *et al.*: The epithelial calcium channel, ECaC, is activated by hyperpolarization and regulated by cytosolic calcium. *Biochem Biophys Res Commun* 261:488-492, 1999
38. van de Graaf SF, Hoenderop JG, Gkika D, *et al.*: Functional expression of the epithelial Ca(2+) channels (TRPV5 and TRPV6) requires association of the S100A10-annexin 2 complex. *Embo J* 22:1478-1487, 2003
39. Olsen JV, Ong SE, Mann M: Trypsin cleaves exclusively C-terminal to arginine and lysine residues. *Mol Cell Proteomics* 3:608-614, 2004
40. Topala CN, Groenestege WT, Thebault S, *et al.*: Molecular determinants of permeation through the cation channel TRPM6. *Cell Calcium*, 2006
41. Hoenderop JG, Dardenne O, Van Abel M, *et al.*: Modulation of renal Ca²⁺ transport protein genes by dietary Ca²⁺ and 1,25-dihydroxyvitamin D₃ in 25-hydroxyvitamin D₃-1 α -hydroxylase knockout mice. *Faseb J* 16:1398-1406, 2002



Regulation of the epithelial Mg^{2+} channel TRPM6 by estrogen and the associated repressor of estrogen receptor activity (REA)

Jenny van der Wijst^{1*}, Gang Cao^{1*}, AnneMiete van der Kemp¹, Femke van Zeeland¹, René J.M. Bindels¹, Joost G.J. Hoenderop¹

*** contributed equally to this work**

¹Department of Physiology, Radboud University Nijmegen Medical Centre, Nijmegen, The Netherlands

Summary

The maintenance of the body's Mg^{2+} balance is essential for neuromuscular excitability, protein synthesis, nucleic acid stability and numerous enzymatic systems. The Transient Receptor Potential Melastatin 6 (TRPM6) functions as the gatekeeper of transepithelial Mg^{2+} transport. However, the molecular regulation of TRPM6 channel activity remains elusive. Here, we identified the Repressor of Estrogen receptor Activity (REA) as an interacting protein of TRPM6 that binds to the 6th, 7th and 8th β -sheets in its α -kinase domain. Importantly, REA and TRPM6 are coexpressed in renal Mg^{2+} -transporting distal convoluted tubules (DCT). We demonstrated that REA significantly inhibits TRPM6, but not its closest homologue TRPM7, channel activity. This inhibition occurs in a phosphorylation-dependent manner, since REA has no effect on the TRPM6 phosphotransferase-deficient mutant (K¹⁸⁰⁴R), while it still binds to this mutant. Moreover, activation of protein kinase C by phorbol 12-myristate 13-acetate-PMA potentiated the inhibitory effect of REA on TRPM6 channel activity. Finally, we showed that the interaction between REA and TRPM6 is a dynamic process, as short-term 17β -estradiol treatment disassociates the binding between these proteins. In agreement with this, 17β -estradiol treatment significantly stimulates the TRPM6-mediated current in HEK293 cells. These results suggest a rapid pathway for the effect of estrogen on Mg^{2+} homeostasis in addition to its transcriptional effect. Together, these data indicate that REA operates as a negative feedback modulator of TRPM6 in the regulation of active Mg^{2+} (re)absorption and provides new insight into the molecular mechanism of renal transepithelial Mg^{2+} transport.

Introduction

Mg^{2+} is a central electrolyte important for many biological functions by its intervention in gene transcription, protein synthesis, nucleic acid stability, channel regulation, cell cycle and numerous enzymatic systems [1-4]. In most species, serum Mg^{2+} levels are kept within a narrow range between 0.8–1.1 mM, while the free intracellular Mg^{2+} concentration $[Mg^{2+}]_i$ has been estimated around 0.5–1.0 mM [5]. Regulation of the Mg^{2+} balance principally resides within the kidney where Mg^{2+} excretion tightly matches the intestinal absorption of Mg^{2+} [5]. The majority of Mg^{2+} in the renal ultrafiltrate is reabsorbed passively in the proximal tubule and the thick ascending limb of the loop of Henle, while the final Mg^{2+} excretion is determined in the distal convoluted tubule (DCT) via an active reabsorption process [5].

The Transient Receptor Potential Melastatin 6 (TRPM6) localizes along the apical membranes of DCT and intestinal cells where it plays a crucial role in active Mg^{2+} (re)absorption. Mutations in TRPM6 lead to hypomagnesemia with secondary hypocalcemia (HSH) indicating that this channel is important for the maintenance of the Mg^{2+} balance [6-8]. Previous studies demonstrated that expression of TRPM6 is regulated by dietary Mg^{2+} and its channel activity is strongly inhibited by the intracellular Mg^{2+} concentration ($[Mg^{2+}]_i$) [8, 9]. Generally, Mg^{2+} -free solutions are used to measure

the characteristic outwardly rectifying TRPM6 currents [8, 10, 11]. Remarkably, TRPM6 contains a carboxyl-terminal α -kinase domain, of which the regulatory role on channel activity remains elusive [12-14]. It has been shown that RACK1 can interact with this domain and inhibit channel activity in a phosphorylation-dependent manner [15]. A recent study demonstrated that the ATP binding motif in the α -kinase domain is required for modulation of TRPM6 channel activity by intracellular ATP [16]. Previous studies suggested that Mg^{2+} uptake in DCT is stimulated by hormones, such as parathyroid hormone, calcitonin, arginine vasopressin, insulin and prostaglandins [17]. A recent study reported that Epidermal Growth Factor (EGF) acts as an autocrine/paracrine magnesiotropic hormone via stimulating its receptor on the basolateral membrane of DCT cells, thereby specifically increasing TRPM6 current [18]. Further, Groenestege *et al.* demonstrated that the renal TRPM6 mRNA level in ovariectomized rats was significantly reduced, whereas 17β -estradiol treatment normalized TRPM6 mRNA levels [9]. Next to this classical transcriptional pathway, accumulating evidence suggests also rapid estrogen effects that occur within minutes via a non-transcriptional route [19-22]. Estrogen has the ability to facilitate rapid membrane-initiated signaling cascades through activation of plasma membrane-associated receptors, such as the recently discovered G protein-coupled receptor 30 (GPCR30) [23]. In addition, it has been demonstrated that the classical estrogen receptor alpha ($ER\alpha$) can be localized to the plasma membrane in response to estrogen or by interaction with adaptor proteins like Shc and p130Cas [24, 25].

The aim of the present study was to investigate the regulation of the α -kinase domain on TRPM6 channel activity by identification of proteins specifically interacting with the α -kinase domain. Using a combined approach including biochemical, immunohistochemical, mass spectrometrical and electrophysiological analyses, we demonstrated a novel operation mode for rapid estrogen regulation on TRPM6 channel activity via attenuating the inhibitory effect of the TRPM6 associated protein, Repressor of Estrogen receptor Activity (REA).

Results

REA associates with TRPM6

To identify proteins potentially interacting with the TRPM6 α -kinase domain, the combination of a GST-pull down with the α -kinase domain of TRPM6 in mouse kidney lysate, followed by Fourier Transform Mass Spectrometry (FTMS), was performed. REA, the Repressor of Estrogen receptor Activity [26], was identified as an interacting protein of the TRPM6 α -kinase domain. Next, GST-pull down binding assays were used to confirm the interaction between REA and TRPM6 α -kinase domain. [^{35}S]-methionine-labeled REA protein was incubated with GST and GST- α -kinase immobilized on glutathione-sepharose 4B beads. REA interacted specifically with the GST- α -kinase, but not with GST alone (Fig. 1A). Next, the association between TRPM6 and REA was further substantiated in mammalian cells by co-precipitation studies of GST and GST- α -kinase in REA-

expressing HEK293 cells. REA co-precipitated with the GST- α -kinase, but not with GST alone (Fig. 1B).

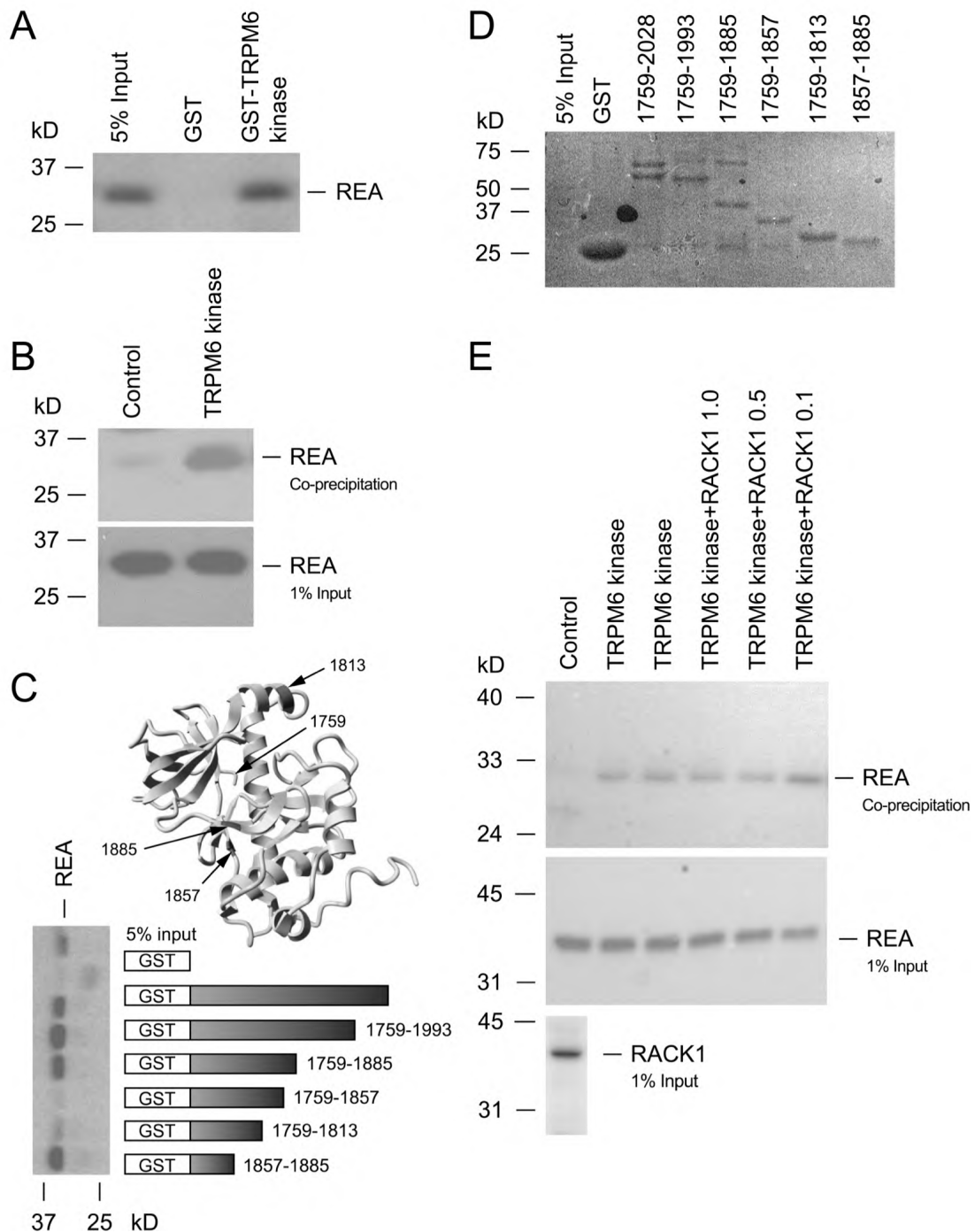


Figure 1. REA interacts with the α -kinase domain in TRPM6. *A.* GST-pull down assay between [35 S]-methionine-labeled REA protein and GST or GST fused to the α -kinase domain. *B.* Co-precipitation studies of GST and GST- α -kinase in REA-expressing HEK293 cells (top panel). REA input (1%) expression was analyzed by immunoblotting (bottom panel). *C.* Mapping of the REA binding site within the α -kinase domain. Predicted 3D structure model of the α -kinase domain with different truncations of the α -kinase. *D.* Coomassie staining of the SDS-PAGE gel. *E.* Co-precipitation studies of GST and GST- α -kinase in REA-expressing HEK293 cells in the presence of different amounts of RACK1 (dilution 1:10 (0.1), 1:2 (0.5), and non-diluted (1.0)) (top panel). REA and RACK1 input (1%) expression was analyzed by immunoblotting (bottom panels).

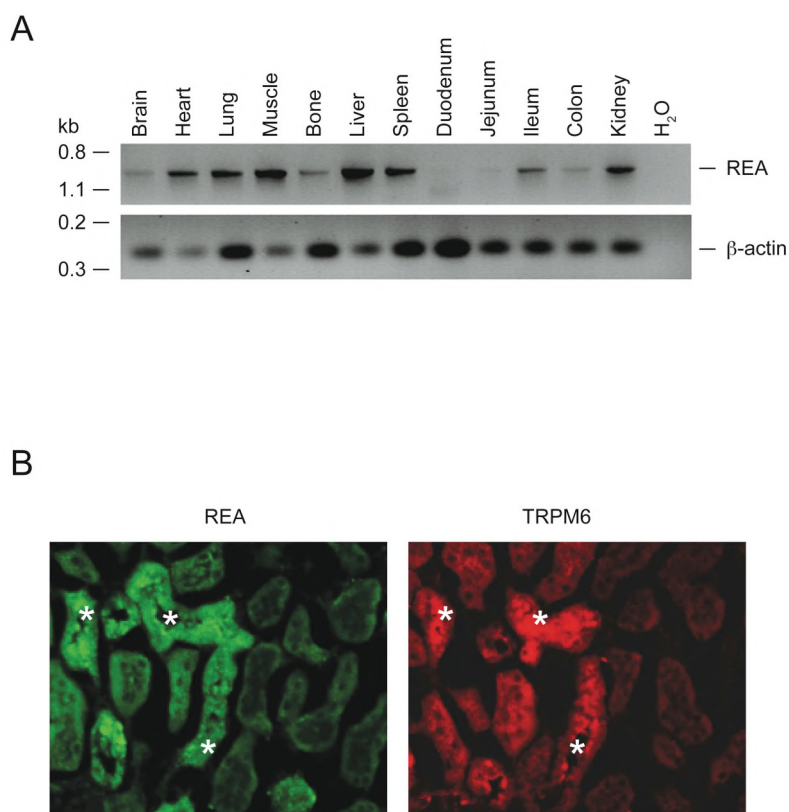


Figure 2. Tissue distribution and localization of REA. *A.* Distribution of REA (top panel) mRNA expression analyzed by RT-PCR on various tissues. β -actin was used as a positive control (bottom panel). *B.* Immunohistochemical analysis of REA (left panel) and TRPM6 (right panel) in mouse kidney serial sections. * indicates overlapping immunopositive tubules for TRPM6 and REA.

REA binds to the 6th, 7th and 8th β -sheets in the TRPM6 α -kinase domain

To determine the REA binding site within TRPM6, a series of deletion mutants in the α -kinase domain was constructed. Truncated TRPM6 α -kinase mutants were expressed as GST-fused proteins and evaluated for their interaction with [³⁵S]-methionine-labeled REA protein (Fig. 1C). Truncation at position 1857 abolished the interaction between the two proteins, whereas truncation at position 1885 had no effect on the interaction with REA. Moreover, a GST-fusion protein containing only the short peptide between the amino acids 1857 and 1885 of the TRPM6 α -kinase domain bound to REA (Fig. 1C). Therefore, the REA binding site within TRPM6 is restricted to the region between the positions 1857 and 1885. The integrity and quantity of the GST-fusion proteins was analyzed and confirmed by Coomassie staining of SDS-PAGE gel (Fig. 1D). The lower abundant product bands of different sizes might be due to binding of so far unknown proteins to the bigger truncation mutants or degradation products. To explore the REA binding site in the TRPM6 α -kinase domain, the tertiary structure of this domain was modeled by SWISS-MODEL (<http://swissmodel.expasy.org/SWISS-MODEL.html>) (Fig. 1D) based on the homology between TRPM6 and TRPM7 α -kinase domains [15, 27]. Due to the significant homology between the TRPM6 and TRPM7 α -kinase domains (84%), these two domains share a well-conserved secondary structure. The surface and accessibility analysis of the REA binding

site (6th, 7th and 8th β -sheets) using Yasara software (<http://www.yasara.org>) suggested that, among the 28 amino acids of the REA binding site, 18 are localized at the surface of the TRPM6 α -kinase domain (see <http://www.cmbi.ru.nl/~hvensela/trpm6/>). Since RACK1 also binds to this region, we investigated whether RACK1 can affect the interaction between TRPM6 and REA. As shown in Fig 1E, REA co-precipitated in similar amounts with GST- α -kinase in the presence and absence of RACK1.

REA co-expresses with TRPM6 in kidney

To address the tissue distribution of REA, reverse transcriptase polymerase chain reaction (RT-PCR) analysis was performed on mouse tissues. The expected DNA fragment of 916 bp for REA was detected in most tested tissues as indicated in Fig. 2A. The β -actin fragment was present in all the tissues evaluated. Of note, REA is present in kidney where TRPM6 is predominantly expressed [8]. To further study the co-expression between REA and TRPM6 in kidney, immunohistochemistry was performed on serial kidney sections. This analysis indicated immunopositive staining for REA in the TRPM6-expressing DCT cells that have been implicated in active Mg^{2+} reabsorption [8] (Fig. 2B).

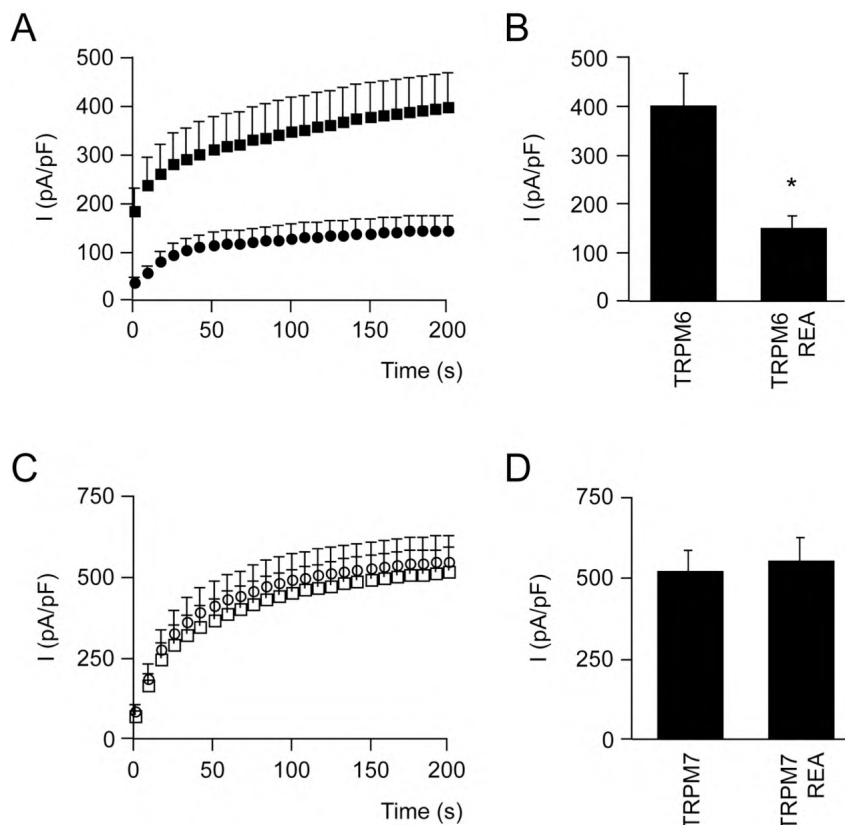


Figure 3. Functional effect of REA on TRPM6 activity. *A.* Time course of the current density (pA/pF) at +80 mV of TRPM6 and mock (■), and TRPM6 and REA (●) transfected HEK293 cells. *B.* Averaged values of the current density at +80 mV after 200 s of TRPM6 and mock (n = 17), and TRPM6 and REA (n = 17). * indicates $P < 0.05$ compared to TRPM6 and mock. *C.* Time course of the current density (pA/pF) at +80 mV of TRPM7 and mock (□), and TRPM7 and REA (○) transfected HEK293 cells. *D.* Averaged values of the current density at +80 mV after 200 s of TRPM7 and mock (n = 18), and TRPM7 and REA (n = 17).

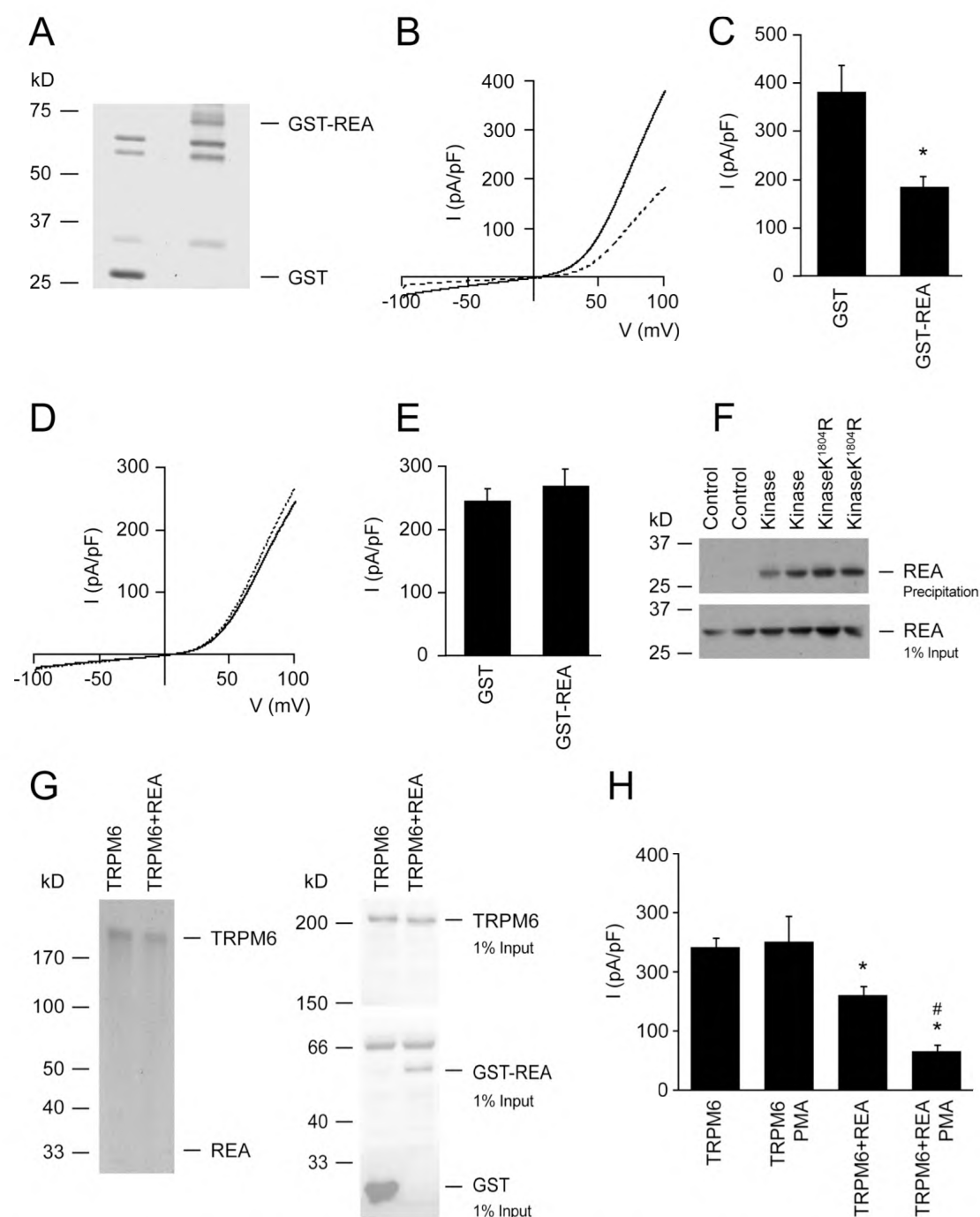


Figure 4. REA inhibits TRPM6 channel activity in a rapid and phosphorylation-dependent manner. *A.* Coomassie staining of purified GST and GST-REA. *B.* Current-voltage (*I/V*) relation of TRPM6 transfected cells infused with GST (solid trace) or GST-REA (dashed trace). *C.* Averaged values of the current density at +100 mV after 600 s of GST infused ($n = 16$) and GST-REA infused ($n = 18$) cells. * indicates $P < 0.05$. *D.* Current-voltage (*I/V*) relations of TRPM6 K¹⁸⁰⁴R transfected cells infused with GST (solid trace) or GST-REA (dashed trace). *E.* Averaged values of the current density at +100 mV after 600 s of GST infused ($n = 26$) and GST-REA infused ($n = 21$) cells. *F.* Co-precipitation studies of GST, GST- α -kinase and GST- α -kinase K¹⁸⁰⁴R in REA-expressing HEK293 cells (top panel). REA input (1%) expression was analyzed by immunoblotting (bottom panel). *G.* *In vitro* protein kinase assay of TRPM6 and TRPM6 and REA (left panel), analyzed for total expression by immunoblotting (right panels). *H.* Effect of PKC activation by PMA (100 nM, 5 min pretreatment) on the current density at +80 after 200 s of TRPM6 and mock ($n = 17-44$), and TRPM6 and REA ($n=17-36$). * indicates $P < 0.05$ compared to TRPM6 and mock without pretreatment, and # indicates $P < 0.05$ compared to TRPM6 and REA without pretreatment.

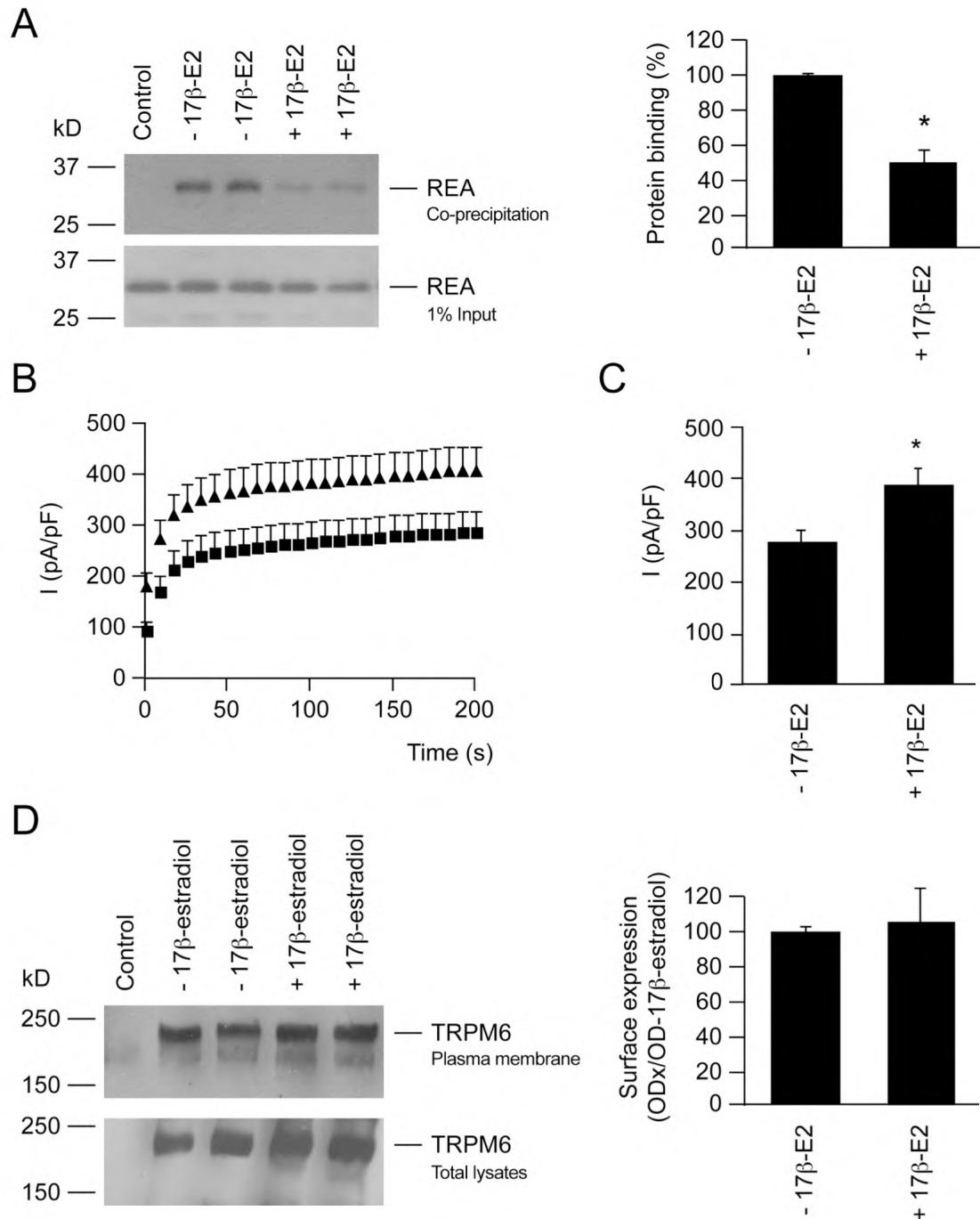


Figure 5. Effect of 17β-estradiol on the binding between REA on TRPM6 and on TRPM6 channel activity. *A.* GST-fused TRPM6 α-kinase domain, GST (control) and REA were co-expressed in HEK293 cells. After treatment with 50 nM 17β-estradiol (17β-E2) or vehicle, REA was co-precipitated with GST-fused α-kinase domain and visualized using the anti-REA antibody (top panel). Immunoblotting (bottom panel) and densitometry quantification (right panel) of binding between TRPM6 α-kinase domain and REA. * indicates $P < 0.05$ compared to vehicle treatment. *B.* Time course of the current density (pA/pF) at + 80 mV of TRPM6 transfected HEK293 cells in control condition (■) and treated with 50 nM 17β-estradiol (E2) for 10 min at 37°C (▲). *C.* Averaged values of the current density at + 80 mV after 200 s of TRPM6 ($n = 37$) and TRPM6 pre-treated with 50 nM of 17β-estradiol (E2) ($n = 37$). * indicates $P < 0.05$ compared to control condition. *D.* TRPM6 expressing HEK293 cells were treated with 50 nM 17β-estradiol (E2) or vehicle and subsequently subjected to cell surface biotinylation assay. TRPM6 expression was analyzed by immunoblot for the plasma membrane fraction (top panel) and for the total cell lysates (bottom panel). Surface expression of TRPM6 was quantified by densitometry (right panel). As negative controls, mock cells were used.

REA inhibits TRPM6 channel activity in a phosphorylation-dependent manner

The functional role of REA on TRPM6 channel activity was investigated by whole-cell patch clamp recordings in HEK293 cells. Steeply outward rectifying currents carried by Na^+ were measured in HEK293 cells co-expressing TRPM6 and empty vector (mock) (Fig. 3A,B). These currents were significantly inhibited in cells co-expressing TRPM6 and REA (Fig. 3A,B). Of note, the inhibitory effect of REA was specific for TRPM6, since REA did not affect the current in TRPM7-expressing HEK293 cells (Fig. 3C,D). To further analyze the inhibitory effect of REA on TRPM6, GST and GST-REA were expressed in HEK293 cells and purified using glutathione-sepharose 4B beads (Fig. 4A). These purified GST and GST-REA proteins were subsequently perfused into TRPM6-expressing HEK293 cells via the patch pipette before whole-cell recording. As shown in Figure 4B,C, REA significantly inhibited the TRPM6-mediated current, but the associated protein did not change the electrophysiological characteristics of the recorded currents. GST alone did not affect the TRPM6-mediated current. Next, the phosphotransferase-deficient mutant (K^{1804}R) was used to investigate the role of TRPM6 phosphorylation activity in this process. REA was unable to inhibit the K^{1804}R mutant-mediated current, similar as GST alone (Fig. 4D,E). Importantly, the co-precipitation assay showed that the K^{1804}R mutation did not influence the binding between TRPM6 and REA (Fig. 4F). Importantly, our *in vitro* phosphorylation assay demonstrated equal autophosphorylation of TRPM6 with or without REA co-expression (Fig. 4G). Next, we investigated the effect of PKC activation by phorbol 12-myristate 13-acetate-PMA (PMA) on the regulatory effect of REA, since it has been shown that RACK1 inhibition can be prevented by 5 min preincubation of 100 nM PMA [15]. Pre-treatment of cells co-expressing TRPM6 and REA significantly decreased TRPM6 channel activity. Of note, the current amplitude in the presence of PMA was not altered in cells expressing TRPM6 alone (Fig. 4H). Finally, we investigated whether REA is a phosphorylation target of TRPM6. The *in vitro* phosphorylation assay showed that REA is not phosphorylated by TRPM6 (Fig. 4G).

17 β -estradiol dissociates the REA-TRPM6 interaction and stimulates channel activity

Given the role of REA in the estrogen signaling pathway [26, 28, 29], the influence of estrogen on the TRPM6 and REA interaction was investigated by co-precipitation experiments. To this end, GST- α -kinase and GST were co-expressed with REA in HEK293 cells, subjected to 17 β -estradiol (50 nM) or vehicle for 10 min at 37 °C, and then precipitated using glutathione-sepharose 4B beads. The interaction between REA and TRPM6 α -kinase domain was significantly reduced by 17 β -estradiol treatment (Fig. 5A, upper panel), whereas REA was equally expressed in all situations (Fig. 5A, lower panel). Next, the influence of estrogen on TRPM6 channel activity was investigated. To this end, HEK293 cells expressing TRPM6 were pre-incubated for 10 min with 17 β -estradiol (50 nM) at 37°C and analyzed by whole-cell patch clamp recordings. As shown in Figure 5B,C, the TRPM6 current was significantly increased when treated with 17 β -estradiol compared to control. Subsequently, the

influence of 17 β -estradiol treatment on the amount of TRPM6 channels expressed at the plasma membrane was investigated by cell surface biotinylation experiments using HEK293 cells. As shown in figure 5D (upper panel), treatment with 17 β -estradiol does not affect the amount of TRPM6 channels expressed at the plasma membrane. Of note, TRPM6 was equally expressed in all tested conditions as determined in the total cell lysates (Fig. 5D, bottom panel).

Discussion

In the present study, we identified REA as a TRPM6-associated protein and demonstrated that this estrogen-responsive protein inhibits the channel activity in a phosphorylation activity-dependent manner. First, REA binds to the TRPM6 α -kinase domain and co-expresses with the Mg²⁺ channel in the renal distal convoluted tubule (DCT). Second, REA specifically inhibits channel activity of TRPM6, but not TRPM7. Third, this inhibition depends on TRPM6 phosphorylation activity, since REA has no effect on the TRPM6 phosphotransferase-deficient K¹⁸⁰⁴R mutant. Fourth, the association between REA and TRPM6 is a dynamic process, which is regulated by 17 β -estradiol treatment. Finally, 17 β -estradiol treatment stimulates TRPM6 activity via a rapid non-transcriptional pathway. TRPM6 functions as the gatekeeper of active transepithelial Mg²⁺ transport [6-8].

Here, REA was identified as a dynamic regulator of TRPM6 channel activity and, therefore, a molecular component in Mg²⁺ homeostasis. REA binds to the α -kinase domain of TRPM6, which was initially identified by the combination of a GST-pull down with the α -kinase domain of TRPM6 in mouse kidney lysate followed by FTMS analysis. This interaction was confirmed by co-precipitation between REA and TRPM6 α -kinase domain in HEK293 cells. Interestingly, our GST-pull down experiment and structure modeling analysis suggest that REA specifically binds to the 6th, 7th and 8th β -sheets in the α -kinase domain, which has been demonstrated as the binding region for RACK1 as well [15]. This might be due to the fact that most amino acids in this area are located on the peripheral region of the tertiary structure of the TRPM6 α -kinase domain, thereby facilitating the interaction with its regulatory proteins. Importantly, we demonstrated that RACK1 has no effect on the binding between REA and the α -kinase domain. This could be explained either by different binding sites within this region or by a higher binding affinity for REA than RACK1. Moreover, we showed that REA is abundantly present in TRPM6-expressing tubules in kidney. The co-expression of REA and TRPM6 in DCT further substantiates the physiological relevance of the interaction between both proteins.

REA was first identified as an interacting protein of the estrogen receptor (ER), where it functions as a selective co-regulator repressing the transcriptional activity of ERs [26]. Genetic deletion of REA significantly enhances estrogen responsiveness *in vivo* [28]. Recently, He *et al.* showed that REA forms a heteromer with prohibitin and acts as a transcriptional co-repressor for ER α [29]. Our study demonstrated a novel role of REA in TRPM6 regulation by showing that the inhibitory effect of REA

on TRPM6 channel activity is not via the long-term transcriptional pathway. This notion is supported by the fact that rapid perfusion of purified GST-REA through the patch pipette into TRPM6 expressing cells induced a significant inhibition of channel activity. Moreover, this inhibitory effect is dependent on the kinase activity of the TRPM6 α -kinase domain since the TRPM6 phosphotransferase-deficient K¹⁸⁰⁴R mutant is insensitive to REA. Of note, REA can still bind to the TRPM6 K¹⁸⁰⁴R mutant. Next, we demonstrated that PKC activation by PMA potentiated the inhibitory effect of REA. Taken together, these data suggest that the phosphorylation activity of TRPM6 α -kinase domain plays a role in the REA effect. Although the phosphorylation activity of the TRPM6 and TRPM7 α -kinase domains has been well established [15, 30-35], the regulatory role of this catalytic domain on channel activity remains elusive. While it has previously been shown that these domains are not essential for TRPM6/7 channel activation [15, 32, 35], several studies have demonstrated an indirect regulatory role in modulation of channel activity [15, 36]. In this line, we previously demonstrated that ATP can regulate TRPM6 channel activity through the ATP binding motif within the α -kinase domain, independent of the TRPM6 α -kinase activity [36]. Moreover, we showed earlier that the inhibitory effect of RACK1 on TRPM6 is dependent on the TRPM6 phosphorylation activity [15]. It has also been illustrated that the phosphorylation-impaired T¹⁸⁵¹A mutant is less sensitive to $[Mg^{2+}]_i$, in agreement with previous studies demonstrating that TRPM7 α -kinase activity influences the Mg^{2+} -dependent inhibition of channel activity [35, 37]. Remarkably, while REA inhibits TRPM6 channel activity, it has no effect on TRPM7, the closest homologue of TRPM6. Based on the structural analysis, the REA binding site in TRPM6 α -kinase domain is highly conserved in TRPM7, therefore REA most likely binds to TRPM7 α -kinase domain as well. However, it has been reported that the α -kinase of TRPM6 is capable of cross-phosphorylation of TRPM7, but not vice versa, suggesting the functional non-redundancy of these two α -kinase domains [33]. One hypothesis is that REA is a specific phosphorylation target of TRPM6, but not TRPM7, and this phosphorylation may function as a switch of the REA regulatory activity on TRPM6. However, we demonstrated that REA could not be phosphorylated by TRPM6. Furthermore, TRPM6 autophosphorylation is not affected in the presence of REA. So, the present study revealed another indirect regulation of TRPM6 channel activity, free from TRPM6 autophosphorylation, but dependent on its α -kinase activity.

REA has been well documented as a regulator in the estrogen signaling pathway [26, 28, 29]. Interestingly, our data showed that the interaction between REA and TRPM6 is a dynamic process that is regulated by estrogen. Treatment with 17 β -estradiol disassociated the interaction between TRPM6 and REA, and attenuated its inhibitory effect on TRPM6 channel activity. According, our electrophysiological data demonstrated that pre-incubation of 17 β -estradiol indeed induced a significant increase of TRPM6-mediated current. It is well known that estrogen can enhance Mg^{2+} utilization and uptake [38-41]. In this line, Groenestege *et al.* demonstrated that the renal TRPM6

mRNA level in ovariectomized rats was significantly reduced, whereas 17 β -estradiol treatment normalized TRPM6 mRNA level, suggesting that estrogen can regulate Mg²⁺ homeostasis via a transcriptional pathway [9]. Accumulating evidence showed that, in addition to the classical transcriptional pathway, estrogen has the ability to facilitate rapid, membrane-initiated, fast signaling cascades via plasma membrane-associated receptors [19-22]. Our current data pointed out a rapid regulatory pathway for estrogen, since the TRPM6-expressing cells were only treated with 17 β -estradiol for 10 min prior to patch clamp analysis. Interestingly, we demonstrated that 17 β -estradiol significantly disassociated the interaction between TRPM6 α -kinase domain and REA. In reminiscence of REA inhibition on TRPM6 channel activity, the molecular mechanism of estrogen stimulation might be due to disassociation of the TRPM6 and REA interaction and subsequent diminishment of the REA inhibition. It would, therefore, be of interest to further elucidate the detailed signaling pathway involved in estrogen stimulation leading to attenuation of the TRPM6 and REA interaction. It is conceivable that estrogen activates an estrogen receptor and its downstream signaling pathway, which might couple to TRPM6 or REA and influence their structure.

Taken together, we presented REA as a novel negative modulator involved in active transepithelial Mg²⁺ transport via regulating TRPM6 channel activity. Furthermore, estrogen disassociated the interaction between TRPM6 and REA and thereby increases TRPM6-mediated Mg²⁺ influx, which may function as a rapid pathway for estrogen to regulate the Mg²⁺ balance. These findings shed new light on the molecular regulation of TRPM6 and contribute to a further understanding of the molecular basis of transepithelial Mg²⁺ (re)absorption.

Material and methods

Cell culture and transfection- HEK293 cells were grown and transfected as previously described [42], and electrophysiological recordings were performed 48 hours post-transfection.

DNA constructs and cRNA synthesis- The kinase domain of mouse (1759-2028) and human (1750-2022) TRPM6 was cloned into pGEX6p-2 (Amersham Pharmacia Biotech, Uppsala, Sweden) by PCR using mouse kidney cDNA or human TRPM6 in pCINeo/IRES-GFP [8] as template. The α -kinase domain (1750-2022) of human TRPM6 was subcloned into the pEBG vector [43]. Full-length mouse REA cDNA was cloned into pT7Ts, pCB7 and pEBG by PCR using mouse kidney cDNA. Wild-type TRPM6 in the pCINeo/IRES-GFP vector was HA-tagged at the N-terminal tail as described previously [8]. GST- α -kinase truncants (TRPM6 1759-1993, 1759-1885, 1759-1857, 1857-1885 and 1759-1813) mutants, TRPM6 phosphotransferase-deficient mutant (K¹⁸⁰⁴R) and GST- α -kinase K¹⁸⁰⁴R mutant were created using the QuickChange site-directed mutagenesis kit (Stratagene, La Jolla, CA, USA) according to the manufacturer's protocol. All constructs were verified by

sequence analysis. REA cRNA was synthesized *in vitro* using T7 RNA polymerase as described previously [44].

Identification of proteins by nano liquid chromatography tandem mass spectrometry- After SDS-PAGE, GST and GST-TRPM6 α -kinase interacting proteins were treated with dithiothreitol (DTT) and iodoacetamide, and digested in-gel by trypsin as previously described [45]. Peptide identification experiments by liquid chromatography tandem mass spectrometry were performed using a nano-HPLC Agilent 1100 nanoflow system connected online to a 7-Tesla linear quadrupole ion trap-Fourier Transform Ion Cyclotron Resonance (LTQ-FT) mass spectrometer (Thermo Electron, Bremen, Germany) as described previously [45]. Peptides and proteins were identified using the Mascot 2.1 (Matrix Science, Boston, MA, USA) algorithm to search a local version of the Uniprot database. First ranked peptides were parsed from Mascot database search html files with MSQuant to generate unique first ranked peptide lists and internal calibration of measured ion masses.

GST-fusion proteins and pull-down assay- TRPM6 α -kinase GST fusion protein was purified as previously described [46]. REA protein was labeled with [³⁵S]-methionine using a reticulocyte lysate system (Promega, Madison, WI, USA) and added to purified GST-fusion proteins, immobilized on glutathione-sepharose 4B beads. After 2 h incubation at room temperature (RT), beads were washed extensively with pull-down buffer (10 mM Tris pH 7.4-HCl), 150 mM NaCl, 0.33% (v/v) Triton X-100). The bound proteins were eluted with SDS-PAGE loading buffer, separated on SDS-PAGE gel and visualized by autoradiography.

Sequence analysis and structure modelling- The structural model of TRPM6 α -kinase domain was built based on the crystal structure of TRPM7 α -kinase domain [27] (Protein DataBank under ID codes: IIAJ (apo), IIAH (ADP complex), and IIA9 (AMP•PNP complex)) using SWISS-MODEL (<http://swissmodel.expasy.org/SWISS-MODEL.html>) and analyzed by DeepView Swiss-PdbViewer (Version 3.7; <http://swissmodel.expasy.org/spdbv/>) and Yasara (www.yasara.org).

RT-PCR- Total RNA isolation from mouse tissue and reverse transcription were performed as described previously [46]. REA and β -actin were amplified by PCR and subsequently analyzed by agarose gel electrophoresis.

Electrophysiology- Patch clamp experiments were performed in the tight seal whole-cell configuration at room temperature using an EPC-10 patch clamp amplifier computer controlled by the Patchmaster software (HEKA Elektronik, Lambrecht, Germany). Electrode resistances were 2–5 M Ω , and capacitance and access resistance were monitored continuously. A ramp protocol, consisting of linear voltage ramps from -100 to +100 mV (within 450 ms), was applied every 2 s from a holding

potential of 0 mV. Current densities were obtained by normalizing the current amplitude to the cell membrane capacitance. The time course of current development was determined by measuring the current at +80 and -80 mV. I/V relations were established from the ramp protocols. The analysis and display of patch clamp data were performed using Igor Pro software (WaveMetrics, Lake Oswego, USA). The standard pipette solution contained 150 mM NaCl, 10mM EDTA, and 10 mM HEPES pH 7.2-NaOH. The extracellular solutions contained 150 mM NaCl, 10 mM HEPES, and 1 mM Ca²⁺ pH 7.4-NaOH. To investigate the effect of purified GST-REA or GST on TRPM6-mediated currents, proteins were added to the standard pipette solution and thereby infused via the patch pipette for 7 min before starting the recordings.

Co-precipitation- HEK293 cells were transiently co-transfected with REA and pEBG-TRPM6 α -kinase or pEBG empty vector. Cells were treated with 50 nM 17 β -estradiol or vehicle for 10 min at 37°C and were lysed for 1 hour on ice in lysis buffer (150 mM NaCl, 5 mM EDTA, 50 mM Tris pH 7.5-NaOH, 0.33% (v/v) triton including the protease inhibitors leupeptin (0.01 mg/ml), pepstatin (0.05 mg/ml) and phenylmethylsulfonyl fluoride (1 mM)). After centrifugation, supernatants of the lysates were incubated overnight with glutathione-sepharose 4B beads at 4°C. After extensive washing in lysis buffer, the bound proteins were eluted and separated by SDS-PAGE. The co-precipitation was analyzed using the anti-REA antibody (Abcam, Cambridge, UK).

Cell surface labeling with biotin- HEK293 cells were transiently transfected with 15 μ g HA-TRPM6 in poly-L-lysine (Sigma, MO, USA) coated 10 cm dishes. 72 hours after transfection, cells were treated with 50 nM 17 β -estradiol or vehicle for 10 min at 37°C. Cell surface labeling with NHS-LC-LC-biotin (Pierce, Etten-Leur, The Netherlands) was performed as previously described [47]. 1 hour after homogenizing, biotinylated proteins were precipitated using neutravidin-agarose beads (Pierce, Etten-Leur, The Netherlands). TRPM6 expression was analyzed by immunoblot for the precipitates (plasma membrane fraction) and for the total cell lysates using the anti-HA antibody (Sigma, MO, USA).

Immunoblotting- Protein samples were denatured by incubation for 30 min at 37°C in Laemmli buffer, and then subjected to SDS-PAGE. Immunoblots were incubated with either mouse anti-HA (Sigma, MO, USA) or rabbit anti-REA (Abcam, Cambridge, UK) antibody. Subsequently, blots were incubated with sheep horseradish peroxidase-conjugated anti-mouse or anti-rabbit IgG (Sigma, MO, USA) and then visualized using the enhanced chemiluminescence system.

Immunohistochemistry- Immunohistochemistry was performed as previously described [48]. Briefly, mouse kidney serial sections were incubated for 16 hours at 4°C with rabbit anti-REA (Abcam, Cambridge, UK) and guinea pig anti-TRPM6 [8]. To visualize TRPM6, tyramide signal

amplification kit (NEN Life Science Products, Zaventem, Belgium) was used after incubation with biotin-coated goat anti-mouse secondary antibody. Images were taken with a Bio-Rad MRC 100 confocal laser scanning microscope.

In vitro phosphorylation assays- HA-TRPM6 was precipitated by using the anti-HA antibody. The precipitates were incubated in a total volume of 30 μ l kinase reaction buffer (50 mM HEPES pH 7.4-KOH, 4 mM $MnCl_2$, 0.5 mM $CaCl_2$, 100 μ M ATP) and 2 μ Ci of [γ ³²P]ATP for 30 min at 30°C. The reaction was terminated by three washing steps with phosphorylation washing buffer (50 mM HEPES pH 7.4-KOH, 4 mM $MnCl_2$, 0.5 mM $CaCl_2$). Phosphorylation was analyzed after gel electrophoresis by autoradiography.

Statistical analysis- Values are expressed as mean \pm SE. Statistical significance between groups was determined by analysis of variance (ANOVA). In case of significance, differences between the means of two groups were analyzed by unpaired *t* test. $P < 0.05$ was considered statistically significant.

Acknowledgements

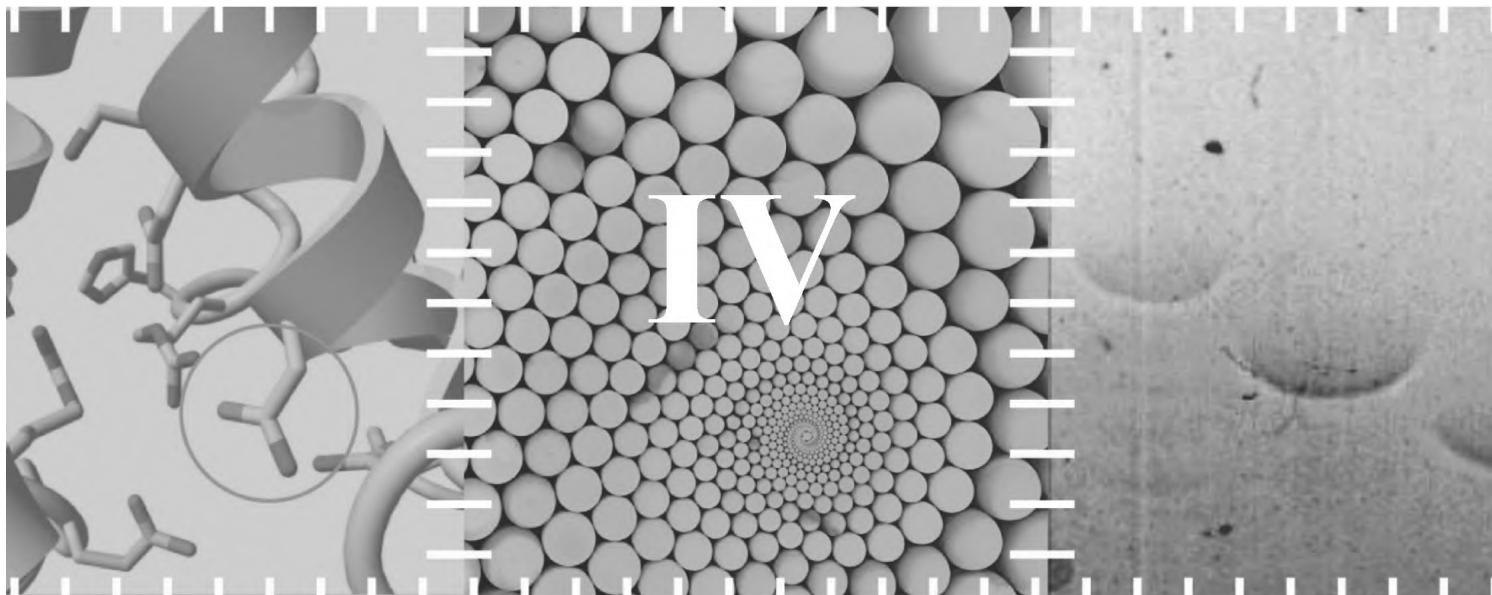
This work was supported by the Netherlands Organization of Scientific Research (ZonMW 9120.6110, ALW818.02.001), EURYI award from the European Science Foundation and the Dutch Kidney foundation (C03.6017, C08.2252). We would like to thank Mr. R. Janssen, Mr. M. de Graaf, Mr. D. van den Berg and Mr. M. Prinz for superb technical assistance.

References

1. Vetter T, Lohse MJ: Magnesium and the parathyroid. *Curr Opin Nephrol Hypertens* 11:403-410, 2002
2. Grubbs RD: Intracellular magnesium and magnesium buffering. *Biometals* 15:251-259, 2002
3. Romani A, Scarpa A: Regulation of cell magnesium. *Arch Biochem Biophys* 298:1-12, 1992
4. Konrad M, Schlingmann KP, Gudermann T: Insights into the molecular nature of magnesium homeostasis. *Am J Physiol Renal Physiol* 286:F599-605, 2004
5. Chubanov V, Gudermann T, Schlingmann KP: Essential role for TRPM6 in epithelial magnesium transport and body magnesium homeostasis. *Pflugers Arch* 451:228-234, 2005
6. Walder RY, Landau D, Meyer P, *et al.*: Mutation of TRPM6 causes familial hypomagnesemia with secondary hypocalcemia. *Nat Genet* 31:171-174, 2002
7. Schlingmann KP, Weber S, Peters M, *et al.*: Hypomagnesemia with secondary hypocalcemia is caused by mutations in TRPM6, a new member of the TRPM gene family. *Nat Genet* 31:166-170, 2002
8. Voets T, Nilius B, Hoefs S, *et al.*: TRPM6 forms the Mg²⁺ influx channel involved in intestinal and renal Mg²⁺ absorption. *J Biol Chem* 279:19-25, 2004
9. Groenestege WM, Hoenderop JG, van den Heuvel L, *et al.*: The epithelial Mg²⁺ channel transient receptor potential melastatin 6 is regulated by dietary Mg²⁺ content and estrogens. *J Am Soc Nephrol* 17:1035-1043, 2006
10. Li M, Du J, Jiang J, *et al.*: Molecular determinants of Mg²⁺ and Ca²⁺ permeability and pH sensitivity in TRPM6 and TRPM7. *J Biol Chem*, 2007
11. Chubanov V, Schlingmann KP, Waring J, *et al.*: Hypomagnesemia with secondary hypocalcemia due to a missense mutation in the putative pore-forming region of TRPM6. *J Biol Chem* 282:7656-7667, 2007
12. Runnels LW, Yue L, Clapham DE: TRP-PLIK, a bifunctional protein with kinase and ion channel activities. *Science* 291:1043-1047., 2001
13. Drennan D, Ryazanov AG: Alpha-kinases: analysis of the family and comparison with conventional protein kinases. *Prog Biophys Mol Biol* 85:1-32, 2004
14. Montell C: Mg²⁺ homeostasis: the Mg²⁺-nificent TRPM channels. *Curr Biol* 13:R799-801, 2003
15. Cao G, Thebault S, van der Wijst J, *et al.*: RACK1 inhibits TRPM6 activity via phosphorylation of the fused alpha-kinase domain. *Curr Biol* 18:168-176, 2008
16. Thebault S, Cao G, Venselaar H, *et al.*: Role of the alpha-kinase domain in TRPM6 channel and regulation by intracellular ATP. *J Biol Chem*, 2008
17. Dai LJ, Ritchie G, Kerstan D, *et al.*: Magnesium transport in the renal distal convoluted tubule. *Physiol Rev* 81:51-84, 2001
18. Groenestege WM, Thebault S, van der Wijst J, *et al.*: Impaired basolateral sorting of pro-EGF causes isolated recessive renal hypomagnesemia. *J Clin Invest* 117:2260-2267, 2007
19. Moriarty K, Kim KH, Bender JR: Minireview: estrogen receptor-mediated rapid signaling. *Endocrinology* 147:5557-5563, 2006
20. Fu XD, Simoncini T: Non-genomic sex steroid actions in the vascular system. *Semin Reprod Med* 25:178-186, 2007
21. Simoncini T, Mannella P, Genazzani AR: Rapid estrogen actions in the cardiovascular system. *Ann N Y Acad Sci* 1089:424-430, 2006
22. Zheng FF, Wu RC, Smith CL, *et al.*: Rapid estrogen-induced phosphorylation of the SRC-3 coactivator occurs in an extranuclear complex containing estrogen receptor. *Mol Cell Biol* 25:8273-8284, 2005
23. Revankar CM, Cimino DF, Sklar LA, *et al.*: A transmembrane intracellular estrogen receptor mediates rapid cell signaling. *Science* 307:1625-1630, 2005
24. Cabodi S, Moro L, Baj G, *et al.*: p130Cas interacts with estrogen receptor alpha and modulates non-genomic estrogen signaling in breast cancer cells. *J Cell Sci* 117:1603-1611, 2004
25. Levin ER: Cellular functions of plasma membrane estrogen receptors. *Steroids* 67:471-475, 2002

26. Montano MM, Ekena K, Delage-Mourroux R, *et al.*: An estrogen receptor-selective coregulator that potentiates the effectiveness of antiestrogens and represses the activity of estrogens. *Proc Natl Acad Sci U S A* 96:6947-6952, 1999
27. Yamaguchi H, Matsushita M, Nairn AC, *et al.*: Crystal structure of the atypical protein kinase domain of a TRP channel with phosphotransferase activity. *Mol Cell* 7:1047-1057, 2001
28. Park SE, Xu J, Frolova A, *et al.*: Genetic deletion of the repressor of estrogen receptor activity (REA) enhances the response to estrogen in target tissues in vivo. *Mol Cell Biol* 25:1989-1999, 2005
29. He B, Feng Q, Mukherjee A, *et al.*: A repressive role for prohibitin in estrogen signaling. *Mol Endocrinol* 22:344-360, 2008
30. Clark K, Langeslag M, van Leeuwen B, *et al.*: TRPM7, a novel regulator of actomyosin contractility and cell adhesion. *Embo J* 25:290-301, 2006
31. Schmitz C, Dorovkov MV, Zhao X, *et al.*: The channel kinases TRPM6 and TRPM7 are functionally nonredundant. *J Biol Chem* 280:37763-37771, 2005
32. Matsushita M, Kozak JA, Shimizu Y, *et al.*: Channel function is dissociated from the intrinsic kinase activity and autophosphorylation of TRPM7/ChaK1. *J Biol Chem* 280:20793-20803, 2005
33. Schmitz C, Dorovkov MV, Zhao X, *et al.*: The channel kinases TRPM6 and TRPM7 are functionally non-redundant. *J Biol Chem*, 2005
34. Runnels LW, Yue L, Clapham DE: TRP-PLIK, a bifunctional protein with kinase and ion channel activities. *Science* 291:1043-1047, 2001
35. Schmitz C, Perraud AL, Johnson CO, *et al.*: Regulation of vertebrate cellular Mg²⁺ homeostasis by TRPM7. *Cell* 114:191-200, 2003
36. Thebault S, Cao G, Venselaar H, *et al.*: Role of the alpha-kinase domain in transient receptor potential melastatin 6 channel and regulation by intracellular ATP. *J Biol Chem* 283:19999-20007, 2008
37. Demeuse P, Penner R, Fleig A: TRPM7 Channel Is Regulated by Magnesium Nucleotides via its Kinase Domain. *J Gen Physiol* 127:421-434, 2006
38. Bogoroch R, Belanger LF: Skeletal effects of magnesium deficiency in normal, ovariectomized, and estrogen-treated rats. *Anat Rec* 183:437-447, 1975
39. McNair P, Christiansen C, Transbol I: Effect of menopause and estrogen substitutional therapy on magnesium metabolism. *Miner Electrolyte Metab* 10:84-87, 1984
40. Muneyyirci-Delale O, Nacharaju VL, Dalloul M, *et al.*: Serum ionized magnesium and calcium in women after menopause: inverse relation of estrogen with ionized magnesium. *Fertil Steril* 71:869-872, 1999
41. Seelig MS: Interrelationship of magnesium and estrogen in cardiovascular and bone disorders, eclampsia, migraine and premenstrual syndrome. *J Am Coll Nutr* 12:442-458, 1993
42. Topala CN, Groenestege WT, Thebault S, *et al.*: Molecular determinants of permeation through the cation channel TRPM6. *Cell Calcium*, 2006
43. Okada T, Inoue R, Yamazaki K, *et al.*: Molecular and functional characterization of a novel mouse transient receptor potential protein homologue TRP7. Ca²⁺-permeable cation channel that is constitutively activated and enhanced by stimulation of G protein-coupled receptor. *J Biol Chem* 274:27359-27370., 1999
44. Hoenderop JG, van der Kemp AW, Hartog A, *et al.*: The epithelial calcium channel, ECaC, is activated by hyperpolarization and regulated by cytosolic calcium. *Biochem Biophys Res Commun* 261:488-492, 1999
45. Olsen JV, Ong SE, Mann M: Trypsin cleaves exclusively C-terminal to arginine and lysine residues. *Mol Cell Proteomics* 3:608-614, 2004
46. van de Graaf SF, Hoenderop JG, Gkika D, *et al.*: Functional expression of the epithelial Ca²⁺ channels (TRPV5 and TRPV6) requires association of the S100A10-annexin 2 complex. *Embo J* 22:1478-1487, 2003
47. Gkika D, Topala CN, Hoenderop JG, *et al.*: The immunophilin FKBP52 inhibits the activity of the epithelial Ca²⁺ channel TRPV5. *Am J Physiol Renal Physiol* 290:F1253-1259, 2006

48. Hoenderop JG, Dardenne O, Van Abel M, *et al.*: Modulation of renal Ca²⁺ transport protein genes by dietary Ca²⁺ and 1,25-dihydroxyvitamin D₃ in 25-hydroxyvitamin D₃-1alpha-hydroxylase knockout mice. *Faseb J* 16:1398-1406, 2002



Methionine sulfoxide reductase B1 (MsrB1) recovers TRPM6 channel activity during oxidative stress

Gang Cao^{1*}, Kyu pil Lee^{1*}, **Jenny van der Wijst**¹, Mark de Graaf¹, AnneMiete van der Kemp¹, René J.M. Bindels¹, Joost G.J. Hoenderop¹
* contributed equally to this work

¹Department of Physiology, Radboud University Nijmegen Medical Centre, Nijmegen, The Netherlands

Summary

Mg^{2+} is an essential ion for many cellular processes, including protein synthesis, nucleic acid stability and numerous enzymatic reactions. Mg^{2+} homeostasis in mammals depends on the equilibrium between intestinal absorption, renal excretion, and exchange with bone. The Transient Receptor Potential Melastatin type 6 (TRPM6) is an epithelial Mg^{2+} channel, which is abundantly expressed in the luminal membrane of the renal and intestinal cells. It functions as the gatekeeper of transepithelial Mg^{2+} transport. Remarkably, TRPM6 combines a Mg^{2+} -permeable channel with an α -kinase domain. Here, by the Ras recruitment system (RRS), we identified methionine sulfoxide reductase B1 (MsrB1) as an interacting protein of the TRPM6 α -kinase domain. Importantly, MsrB1 and TRPM6 are both present in the renal Mg^{2+} -transporting distal convoluted tubules (DCT). MsrB1 has no effect on TRPM6 channel activity in the normoxic conditions. However, hydrogen peroxidase (H_2O_2) decreased TRPM6 channel activity. Co-expression of MsrB1 with TRPM6 attenuated the inhibitory effect of H_2O_2 (TRPM6: $67 \pm 5\%$ of control; TRPM6 + MsrB1: $81 \pm 5\%$ of control). Cell surface biotinylation assays showed that H_2O_2 treatment does not affect the expression of TRPM6 at the plasma membrane. Next, mutation of M¹⁷⁵⁵ to A in TRPM6 reduced the inhibitory effect of H_2O_2 on TRPM6 channel activity (TRPM6 M¹⁷⁵⁵A: $84 \pm 10\%$ of control), thereby mimicking the action of MsrB1. Thus, these data suggest that MsrB1 recovers TRPM6 channel activity by reducing the oxidation of M¹⁷⁵⁵ and could, thereby, function as a modulator of TRPM6 during oxidative stress.

Introduction

To maintain a physiological extra- and intracellular Mg^{2+} concentration is of great importance to keep the accurate function of more than 300 enzymatic systems and the subsequent various biological and physiological processes [1-4]. The kidney is the principal organ responsible for the regulation of the body Mg^{2+} balance. Around 80 % of the total plasma Mg^{2+} is ultrafiltered through the glomeruli and subsequently reabsorbed passively in the proximal tubule and the thick ascending limb of Henle's loop [5]. The final urinary Mg^{2+} concentration is defined by active Mg^{2+} reabsorption in the distal convoluted tubule (DCT) [6].

The Transient Receptor Potential Melastatin type 6 (TRPM6) is a cation channel playing a crucial role in Mg^{2+} homeostasis. Mutations in TRPM6 cause hypomagnesemia with secondary hypocalcemia (HSH) [7, 8]. Interestingly, mice deficient of TRPM6 (TRPM6^{-/-} mice) were essentially embryonically lethal and the incidental TRPM6^{-/-} mice that survived had neural tube defects [9]. TRPM6 and its closest homologue TRPM7, uniquely combine an ion channel pore-forming region with a serine/threonine protein kinase domain. It is located at the carboxyl terminus and has similarities with members of the α -kinase family [10, 11]. Previous studies demonstrated that Receptor for Activated C-Kinase 1 (RACK1) and Repressor of Estrogen Receptor Activity (REA) interact with this domain and inhibit channel activity in an (auto)phosphorylation-dependent manner

[12, 13]. Moreover, modulation of TRPM6 channel activity by intracellular ATP requires the ATP-binding motif in the α -kinase domain [14]. While the phosphorylation activity of the TRPM6/7 α -kinase domains has been well determined, the role of these domains in regulating channel activity remains elusive [12, 15-18].

Over the last years, several studies have implicated TRPM channels in ischemia [19, 20]. Sun *et al.* showed that decreased TRPM7 channel expression significantly reduced neuronal cell death after global ischemia [21]. Furthermore, TRPM4 channel activation in vascular smooth muscle has been shown to contribute to cell death of vascular cells during ischemic injury and TRPM2 has been well studied in relation to oxidative stress [22-25]. Accumulating evidence suggests that reactive oxygen species (ROS) are not only harmful side products of cellular metabolism, but also central players in cell signaling and regulation [26-29]. Interestingly, renal DCT cells contain the largest number of mitochondria. However, the effect of oxidative stress on the epithelial Mg^{2+} channel TRPM6, expressed at the apical membrane of the DCT, has not been studied.

The aim of the present study was to investigate the role of the α -kinase domain in TRPM6 channel activity by the identification of associated proteins. To this end, the Ras recruitment system (RRS), a novel yeast two hybrid screening system, which is designed to screen for partners of plasma membrane proteins, was applied [30]. Here, we identified methionine sulfoxide reductase B1 (MsrB1) as a TRPM6-associated protein, binding to the TRPM6 α -kinase domain. Using biochemical, immunohistochemical and electrophysiological analyses, we demonstrated a novel operation mode for MsrB1 in the regulation of TRPM6 channel activity in oxidative stress through modulating methionine oxidation in TRPM6.

Results

MsrB1 interacts with TRPM6 α -kinase domain

To identify proteins interacting with the α -kinase domain of TRPM6, we applied the RRS. Compared with the conventional yeast two-hybrid, RRS is more appropriate to detect interaction partners of plasma membrane proteins [30]. In this approach, MsrB1, a methionine sulfoxide reductase [31], was identified as an interacting protein of the TRPM6 α -kinase domain. Subsequently, MsrB1 cDNA was co-transformed with the α -kinase domain of TRPM6 into *cdc25-2* yeast strain to confirm the interaction. As shown in Fig 1A, while the *cdc25-2* strains co-transformed with MsrB1 and TRPM6 α -kinase domain grow at 37 °C, yeast co-transformed with the control vector and TRPM6 α -kinase domain only survived at 24 °C. The association between TRPM6 and MsrB1 was further substantiated by co-precipitation studies of glutathion S-transferase (GST) and GST-TRPM6-kinase in MsrB1-expressing HEK293 cells. MsrB1 co-precipitated with the GST- α -kinase, but not with GST alone (Fig. 1B, upper panel).

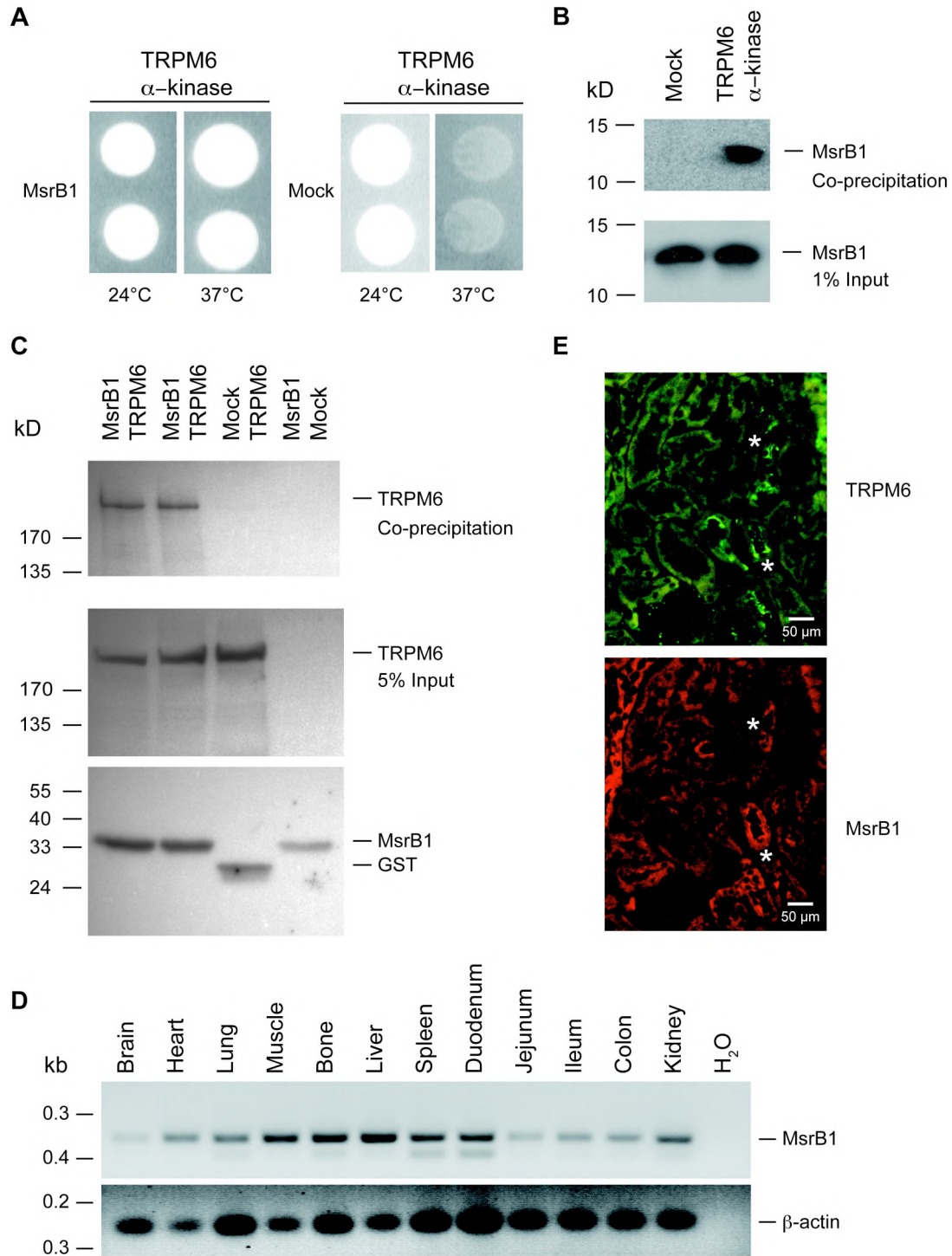


Figure 1. Interaction and co-expression between TRPM6 and MsrB1. *A*. Complementation of the *cdc25-2* mutation through the interaction of TRPM6 α -kinase domain with MsrB1. The temperature-sensitive *cdc25-2* yeast strain was co-transformed with TRPM6 α -kinase domain and MsrB1 or control plasmid (mock), and incubated on galactose-containing plates either at 25 °C or 37 °C. *B*. Co-precipitation studies of GST and GST- α -kinase in MsrB1-expressing HEK293 cells (top panel). MsrB1 input (1%) expression was analyzed by immunoblotting (bottom panel). *C*. Co-precipitation of GST-MsrB1 in TRPM6-expressing HEK293 cells (top panel). TRPM6 input (5%) and MsrB1 precipitation expression were analyzed by immunoblotting (middle panel and bottom panel). *D*. Distribution of MsrB1 (top panel) mRNA expression analyzed by RT-PCR on various tissues. β -actin was used as a positive control (bottom panel). *E*. Immunohistochemical analysis of TRPM6 (upper panel) and MsrB1 (lower panel) in serial mouse kidney sections. * indicates overlapping immunopositive tubules for TRPM6 and MsrB1.

MsrB1 was equally expressed in the tested conditions (Fig. 1B, lower panel). Furthermore, co-precipitation studies of full-length TRPM6 with MsrB1 in HEK293 cells showed that full-length TRPM6 associates with GST-MsrB1 but not with GST alone (Fig. 1C, upper panel). TRPM6 and MsrB1 were expressed in all conditions tested (Fig. 1C, middle and bottom panel).

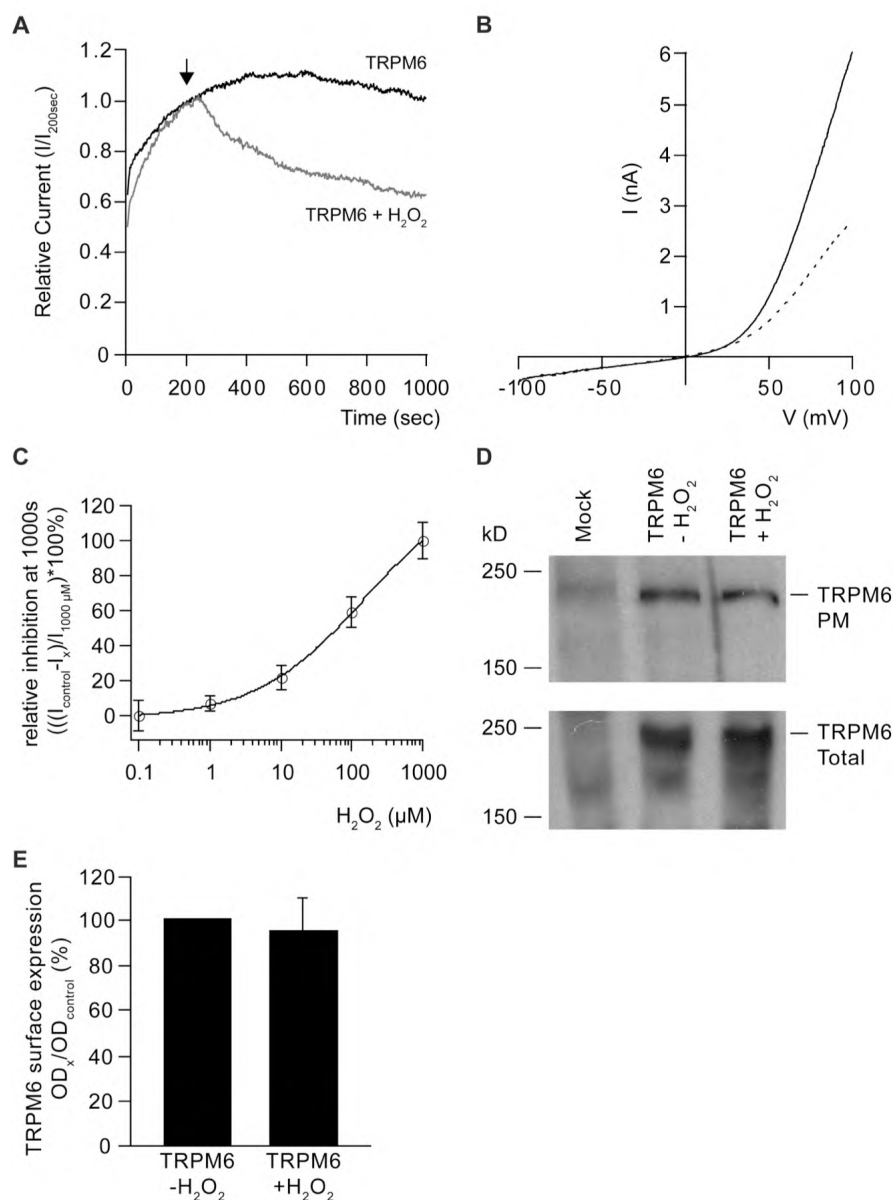


Figure 2. H_2O_2 effect on TRPM6 channel activity and plasma membrane expression. *A.* Time course of the current density (pA/pF) at +80 mV of TRPM6-transfected HEK293 cells, where 1 mM H_2O_2 was added to the bath solution after 200 s (arrow). *B.* Current-voltage (I/V) relation of TRPM6-transfected cells perfused with standard extracellular solution (solid) and 1 mM H_2O_2 (dashed). *C.* Percentage inhibition of the TRPM6 current at +80 mV after 1000 s in response to different H_2O_2 concentrations, normalized to 1 mM H_2O_2 . *D.* TRPM6-expressing HEK293 cells were treated with 1 mM H_2O_2 and subsequently subjected to cell surface biotinylation assays. TRPM6 expression was analyzed by immunoblotting for the plasma membrane fraction (top panel) and for the total cell lysates (bottom panel). Representative immunoblot of 3 independent experiments is shown. As negative controls, mock-transfected cells were used. *E.* Densitometry quantification of TRPM6 surface expression with/without H_2O_2 treatment.

MsrB1 co-expresses with TRPM6 in kidney

To address the tissue distribution of MsrB1, reverse transcriptase polymerase chain reaction (RT-PCR) analysis was performed on a panel of mouse tissues. The expected DNA fragment of MsrB1 was detected in all tissues as indicated in Fig. 1D. The integrity of the cDNA was confirmed by the detection of β -actin. To further study the co-expression of MsrB1 and TRPM6 in kidney, immunohistochemistry was performed on serial mouse kidney sections. This analysis indicated 70% immunopositive staining for MsrB1 in the TRPM6-expressing DCT segment, that has been implicated in active Mg^{2+} reabsorption [32] (Fig. 1E).

H₂O₂ inhibits TRPM6 channel activity

Considering that MsrB1 is a stress protein which mainly exerts its function during oxidative stress [31], we hypothesized that MsrB1 regulates TRPM6 channel activity during oxidative stress. Therefore, we examined the effect of H₂O₂ on TRPM6 channel activity. To this end, HEK293 cells expressing TRPM6 were treated with 1 mM H₂O₂ during whole-cell patch clamp recordings. As shown in Fig. 2A-B, H₂O₂ caused a significant inhibition of the TRPM6-mediated current ($67 \pm 5\%$ of control, $n=13$, $P<0.05$) compared to the non-treated cells ($n=11$). Furthermore, we demonstrate that H₂O₂ inhibits TRPM6 channel activity in a dose-dependent effect with an IC₅₀ of 148 μ M (Fig 2C).

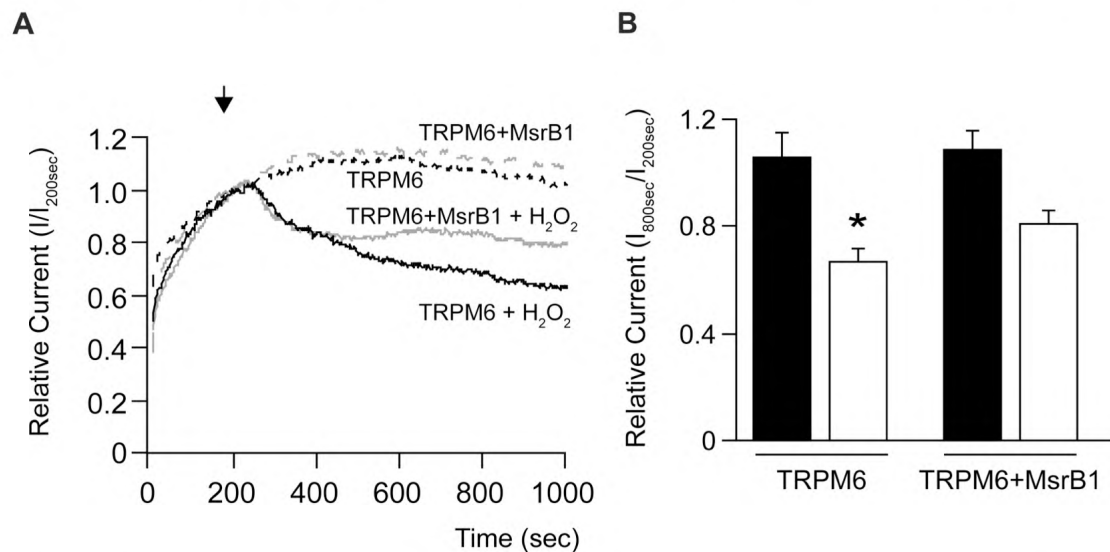


Figure 3. MsrB1 reduces the inhibitory effect of H₂O₂ on TRPM6. *A.* Time course of the current density (pA/pF) at +80 mV of TRPM6 and TRPM6+MsrB1-transfected HEK293 cells, where 1 mM H₂O₂ was added to the bath solution after 200 s (arrow). *B.* Normalized values of the current at +80 mV after 800 s of TRPM6 and TRPM6+MsrB1, treated with (open bars) or without (closed bars) H₂O₂. * indicates $P<0.05$.

H₂O₂ treatment does not affect TRPM6 cell surface expression

Next, the influence of H₂O₂ on the amount of TRPM6 channels at the plasma membrane was investigated by cell surface biotinylation experiments. As shown in Fig. 2D (upper panel), treatment with H₂O₂ did not affect the plasma membrane abundance of TRPM6. Of note, the protein levels of TRPM6 were equal in all tested conditions as verified by the total cell lysates (Fig. 2D, bottom panel).

MsrB1 prevents the inhibitory effect of H₂O₂

Next, the effect of MsrB1 on TRPM6 channel activity was investigated. Patch clamp analysis demonstrated that MsrB1 has no effect on TRPM6 channel activity (TRPM6+empty vector: 250 ± 42 pA/pF and TRPM6+MsrB1: 224 ± 37 pA/pF, $P > 0.2$). To investigate the role of MsrB1 on TRPM6

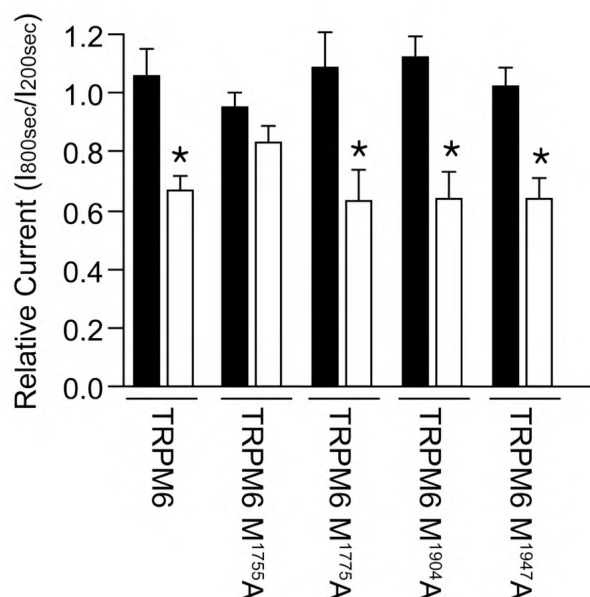
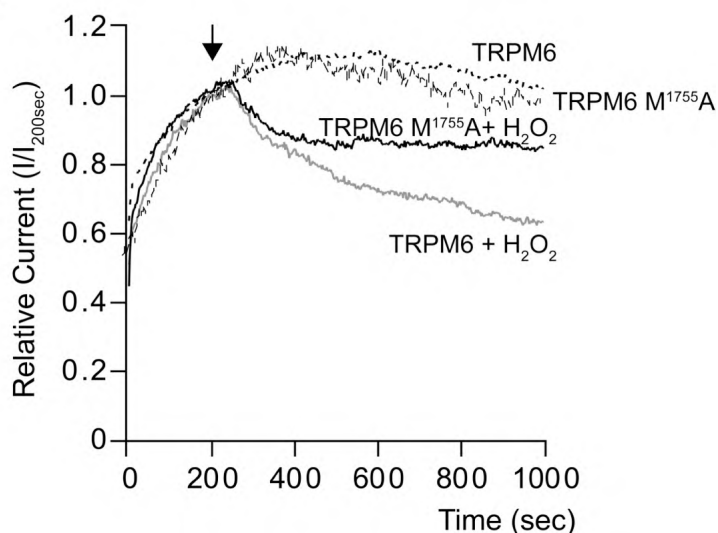
A**B**

Figure 4. TRPM6 M¹⁷⁵⁵A is not significantly inhibited by H₂O₂. *A.* Normalized values of the current at +80 mV after 800 s of TRPM6 and all TRPM6 M-A mutants, treated with (open bars) or without (closed bars) 1 mM H₂O₂. * indicates $P < 0.05$. *B.* Time course of the current density (pA/pF) at +80 mV of TRPM6 and TRPM6 M¹⁷⁵⁵A-transfected HEK293 cells, where 1 mM H₂O₂ was added to the bath solution after 200 s (arrow).

channel activity during oxidative stress, TRPM6 and MsrB1 were co-expressed in HEK293 cells and treated with H₂O₂ during whole-cell patch clamp recordings. Treatment with H₂O₂ significantly decreased TRPM6 current ($67 \pm 5\%$ of control, $n=13$, $P < 0.05$), while co-expression of MsrB1 significantly attenuated this inhibition ($81 \pm 5\%$ of control, $n=13$, $P < 0.05$) (Fig. 3A-B).

Involvement of M¹⁷⁵⁵ in H₂O₂-inhibited TRPM6 activity

Since MsrB1 binds to the TRPM6 α -kinase domain and recovers the inhibitory effect of H₂O₂ on TRPM6 channel activity, we hypothesized that MsrB1 could reduce methionine oxidation of the α -kinase domain. Therefore, the methionine residues located on the peripheral of the TRPM6 α -kinase domain 3D structure (see <http://www.cmbi.ru.nl/~hvensela/trpm6/>) that might be more vulnerable to H₂O₂, were mutated into alanines (namely M¹⁷⁵⁵A, M¹⁷⁷⁵A, M¹⁹⁴⁷A, and M¹⁹⁰⁴A) as analyzed by Yasara software, <http://www.yasara.org>). Subsequent patch clamp analysis showed that only the TRPM6 M¹⁷⁵⁵A

mutant was not significantly inhibited by H₂O₂ (83 ± 6% of control, n=12, P>0.05) (Fig. 4A-B). Of note, the other mutants were significantly inhibited by H₂O₂ (M¹⁷⁷⁵A: 63 ± 10%, n=8; M¹⁹⁰⁴A: 64 ± 9%, n=8; M¹⁹⁴⁷A: 64 ± 7%, n=10) (Fig. 4A).

Discussion

In the present study, we identified MsrB1 as a new TRPM6-associated protein and showed that MsrB1 recovers TRPM6 channel activity *via* reducing the oxidation state of M¹⁷⁵⁵ during oxidative stress. First, MsrB1 directly binds to the TRPM6 α -kinase domain and co-precipitates full-length TRPM6. Second, MsrB1 is co-expressed with TRPM6 in the renal DCT. Third, H₂O₂ inhibits TRPM6 channel activity without affecting the plasma membrane expression. Fourth, MsrB1 prevents the inhibitory effect of H₂O₂ on TRPM6 channel activity. Finally, H₂O₂ has no significant effect on the TRPM6 M¹⁷⁵⁵A mutant.

TRPM6 belongs to the TRPM subfamily of the TRP channels and is so far the only known channel directly mediating active transepithelial Mg²⁺ transport [4, 7, 8, 32]. However, the molecular regulation of this channel remains elusive. Here, we used a novel yeast two-hybrid procedure, RRS, to screen proteins interacting with TRPM6 α -kinase domain. Our data showed that MsrB1 binds to the α -kinase domain of TRPM6 resulting in the recruitment of Ras to the membrane and subsequent complementation of the temperature-sensitive *cdc25-2* mutation. So, we identified MsrB1 as a new interacting protein of the TRPM6 α -kinase domain. This interaction has been confirmed by a subsequent GST co-precipitation assay in HEK293 cells with full-length TRPM6. Importantly, MsrB1 and TRPM6 are co-expressed in the renal DCT, which further substantiates the physiological relevance of the interaction between both proteins.

MsrB1 is an oxidoreductase which catalyzes the thiol-dependent reduction of methionine sulfoxide [31]. MsrB1 belongs to the Msr family composed of MsrA and MsrB. Mammals contain one MsrA and three MsrBs that are highly abundant in kidney, liver, heart and nervous tissue [33-37]. These enzymes protect cells from oxidative stress *via* the repair of oxidative damage to proteins and thereby restore biological activity. They can be involved in ROS-mediated signal transduction through modulation of the function of target proteins [31, 38-40]. Accumulating data showed that reversible methionine oxidation and reduction plays a dynamic role in a variety of cellular signaling pathways [41, 42]. For example, the methionine residues of Helix-3, CamKII, shaker voltage-dependent K⁺ channel and Slo1 K⁺ channels can be oxidized and hereby regulate their function [42-45]. It has been shown that oxidation of a methionine residue in the shaker voltage-dependent K⁺ channel disrupts its inactivation. This effect can be reversed by co-expression with MsrA1 [43].

In the present study, we showed that MsrB1 interacts with the TRPM6 α -kinase domain, but does not affect the channel activity in normoxic conditions. However, hydrogen peroxide (H₂O₂) is a product during oxidative stress and has been studied in relation to potassium channel function and the

TRPM2 channel (reviewed [46, 47]). Here, we demonstrated that H_2O_2 significantly decreases the TRPM6-mediated current in HEK293 cells in a dose-dependent manner. As H_2O_2 did not change the surface expression of TRPM6, it possibly regulates TRPM6 channel activity directly through modulation of the channel conductance. Importantly, the decreased TRPM6 channel activity can be partly recovered by co-expression with MsrB1. This partial recovery could be explained by the fact that Msrs function optimal at 37 °C [48], while our experiments were performed at room temperature. Another possible explanation is the time lapse of MsrB1 functioning, which is likely slower than the oxidation by H_2O_2 .

Free and protein-bound methionine residues are among the most susceptible to oxidation by ROS [49]. It is proposed that surface exposed methionine residues in a protein constitute an antioxidant defense mechanism since various oxidants can easily react with these residues to form methionine sulfoxide. Reduction back to methionine by methionine sulfoxide reductases could catalytically drive this antioxidant system as has been suggested by several studies [50-52]. Therefore, the methionine residues located on the peripheral of the TRPM6 α -kinase domain 3D structure (see <http://www.cmbi.ru.nl/~hvensela/trpm6/>) were examined. Four methionine residues (M¹⁷⁵⁵, M¹⁷⁷⁵, M¹⁹⁰⁴, and M¹⁹⁴⁷) were mutated into alanines and their channel activity was studied upon H_2O_2 treatment. Mutation of M¹⁷⁵⁵ to A significantly attenuates the effect of H_2O_2 on TRPM6 channel activity, mimicking the MsrB1 effect (co-expression of MsrB1, $81 \pm 5\%$ of control; M¹⁷⁵⁵A, $83 \pm 6\%$ of control). These data suggest that M¹⁷⁵⁵ is a crucial target of H_2O_2 . Notably, renal DCT cells contain the largest number of mitochondria, the major source of endogenous H_2O_2 , per unit length of any cell along the nephron, underlying a vast source of intracellular H_2O_2 [53]. TRPM6 is predominantly expressed in DCT and is inhibited by H_2O_2 . Therefore, it is conceivable that the metabolic state of DCT cells, which influences the abundance of ROS generated from mitochondria, modulates the Mg^{2+} reabsorption *via* TRPM6.

Taken together, our study demonstrated that H_2O_2 inhibits TRPM6 channel activity and pointed out M¹⁷⁷⁵ as an important target for channel oxidation. Moreover, its interacting protein MsrB1 dynamically regulates this oxidative effect on TRPM6. These data provide insight into the molecular basis of TRPM6 channel regulation and transepithelial Mg^{2+} (re)absorption. Our findings present the first example of modulating TRP channel activity by methionine oxidation and contribute to a further understanding of the regulation of TRP channels by novel post-translational modifications.

Material and methods

Cell culture and transfection- Human Embryonic Kidney (HEK) 293 cells were grown and transfected as previously described [54] and electrophysiological recordings were performed 48 h post-transfection.

DNA constructs- The α -kinase domain of mouse (1759-2028) TRPM6 was cloned into the pMet425-Myc-Ras (kind gift from Dr. A. Aronheim, Haifa, Israel) by PCR using mouse kidney cDNA as template. The α -kinase domain of human (1759-2022) TRPM6 was cloned into the pEBG vector using human TRPM6 in pCINeo/IRES-GFP [32] as template. Full-length mouse MsrB1 cDNA was cloned into pCB7 by PCR using mouse kidney cDNA, and Flag-tagged at the N-terminal tail. Wild-type human TRPM6 in the pCINeo/IRES-GFP vector was HA-tagged at the N-terminal tail as described previously [32]. TRPM6 M¹⁷⁵⁵A, TRPM6 M¹⁷⁷⁵A, TRPM6 M¹⁹⁰⁴A and TRPM6 M¹⁹⁴⁷A mutants were created using the QuickChange site-directed mutagenesis kit (Stratagene, La Jolla, CA, USA) according to the manufacturer's protocol. All constructs were verified by sequence analysis.

RRS Screening- RRS screening was performed as previously described [30]. Briefly, *cdc25-2* strains (kind gift from Dr. A. Aronheim) were co-transformed with the pMet425-Myc-Ras-TRPM6 α -kinase domain and mouse kidney cDNA library. Transformants were grown on selectable minimal glucose plates for 5 days at 25 °C, and subsequently replica plating onto minimal galactose plates, incubating for 5–7 days at 37 °C. Library plasmids of positive colonies growing on galactose plates at 37 °C were isolated and further analyzed by DNA sequencing. The positive colonies were co-transformed with the pMet425-Myc-Ras-TRPM6 α -kinase domain into *cdc25-2* cells to confirm specificity of interaction.

RT-PCR- Total RNA isolation from mouse tissue and reverse transcription were performed as described previously [55]. MsrB1 and β -actin were amplified by PCR and subsequently analyzed by agarose gel electrophoresis.

Electrophysiology- Patch clamp experiments were performed in the tight seal whole-cell configuration at room temperature using an EPC-10 patch clamp amplifier computer controlled by the Pulse software (HEKA Elektronik, Lambrecht, Germany). Electrode resistances were 2–5 M Ω , and capacitance and access resistance were monitored continuously. A ramp protocol, consisting of linear voltage ramp from -100 to +100 mV (within 450 ms) was applied every 2 s from a holding potential of 0 mV. Current densities were obtained by normalizing the current amplitude to the cell membrane capacitance. The time course of current development was determined by measuring the current at +80 and -80 mV. I/V relations were established from the ramp protocols. The analysis and display of patch clamp data were performed using Igor Pro software (WaveMetrics, Lake Oswego, USA). The standard pipette solution contained 150 mM NaCl, 10 mM EDTA, and 10 mM HEPES pH 7.2-NaOH. The extracellular solution contained 150 mM NaCl, 10 mM HEPES pH 7.4-NaOH supplemented with 1 mM CaCl₂. To avoid breakdown, H₂O₂ was stored at 4 °C prior to use and added to the perfusate immediately (<1 min) prior to making recordings.

Co-precipitation assay- HEK293 cells were transiently co-transfected with MsrB1 and pEBG-TRPM6- α -kinase or pEBG empty vector. 24 h after transfection, cells were lysed for 1 h on ice in lysis buffer (150 mM NaCl, 5 mM EDTA, 50 mM Tris pH 7.5-NaOH, 0.33% (v/v) Triton X-100 including the protease inhibitors leupeptin (0.01 mg/ml), pepstatin (0.05 mg/ml) and phenylmethylsulfonyl fluoride (1 mM)). After centrifugation, supernatants of the lysates were incubated overnight with glutathione-sepharose 4B beads at 4 °C. In the co-precipitation experiment with full length TRPM6, HEK293 cells were co-transfected with pEBG-MsrB1 and TRPM6 pCIneo/IRES-GFP or pCIneo/IRES-GFP empty vector, and subsequently lysed and incubated on glutathione-sepharose 4B beads as described above. After extensive washing, the bound proteins were eluted with SDS-PAGE loading buffer. The co-precipitation was analyzed using the anti-MsrB1 antibody (kind gift from Dr. J Moskovitz, Lawrence, Kansas, USA), mouse anti-HA (Sigma, MO, USA) antibody, or anti-GST antibody (Sigma, MO, USA).

Cell surface labeling with biotin- HEK293 cells, in poly-L-lysine (Sigma, MO, USA) coated 10 cm dishes, were transiently transfected with 15 μ g HA-TRPM6. 72 h after transfection, cells were treated with 1 mM H₂O₂ for 10 min at 37 °C. Cell surface labeling with NHS-LC-LC-biotin (Pierce, Etten-Leur, The Netherlands) was performed as previously described [56]. 1 h after homogenizing, biotinylated proteins were precipitated using neutravidin-agarose beads (Pierce, Etten-Leur, The Netherlands). TRPM6 expression was analyzed by immunoblot for the precipitates (plasma membrane fraction) and for the total cell lysates using the mouse anti-HA antibody.

Immunoblotting- Protein samples were denatured by incubation for 30 min at 37°C in Laemmli buffer, and then subjected to SDS-PAGE. Immunoblots were incubated with either mouse anti-HA or rabbit anti-MsrB1 antibody. Subsequently, blots were incubated with sheep horseradish peroxidase-conjugated anti-mouse or anti-rabbit IgG (Sigma, MO, USA) and then visualized using the enhanced chemiluminescence system.

Immunohistochemistry- Immunohistochemistry was performed as previously described [57]. Briefly, mouse kidney sections were incubated for 16 h at 4°C with rabbit anti-MsrB1 and guinea pig anti-TRPM6. To visualize TRPM6, tyramide signal amplification kit (NEN Life Science Products, Zaventem, Belgium) was used after incubation with biotin-coated goat anti-mouse secondary antibody. Images were taken with a Bio-Rad MRC 100 confocal laser scanning microscope.

Statistical analysis- Values are expressed as mean \pm SE. Statistical significance between groups was determined by analysis of variance (ANOVA) followed by Bonferroni's Multiple Comparison Test. Differences between the means of two groups were analyzed by an unpaired Student's *t* test. $P < 0.05$ were considered statistically significant.

Acknowledgements

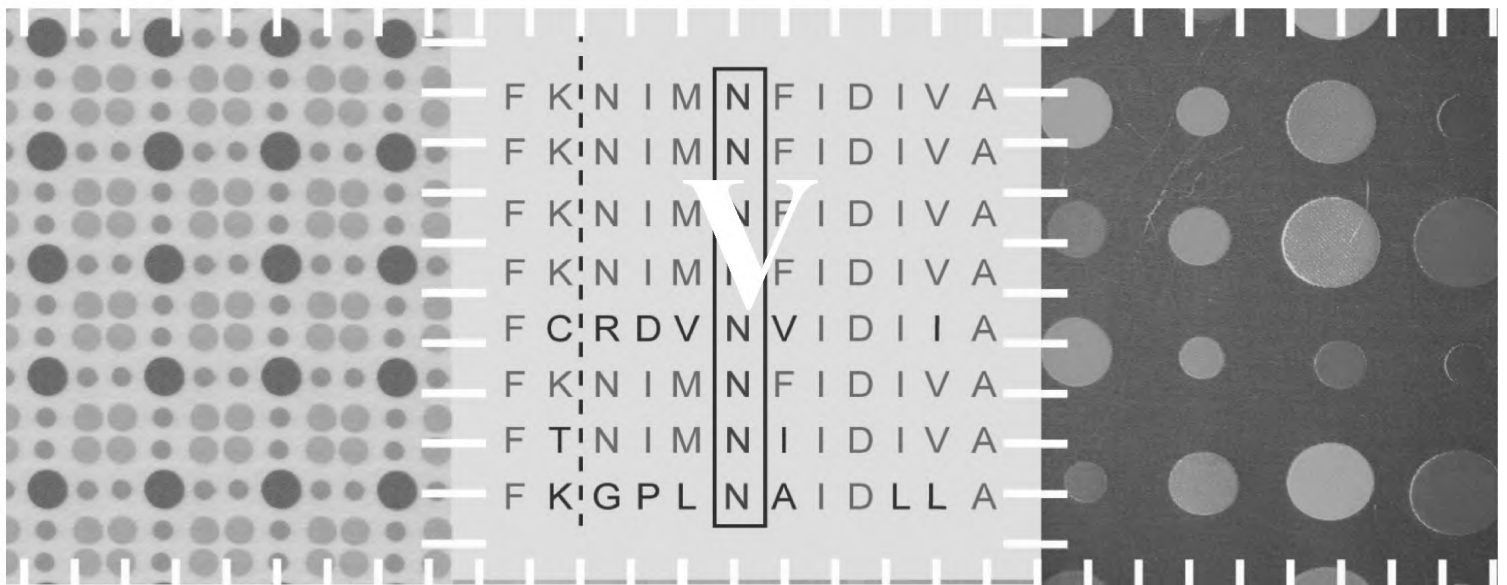
This work was supported by the Netherlands Organization of Scientific Research (ZonMW 9120.6110, ALW818.02.001), EURYI award from the European Science Foundation and the Dutch Kidney foundation (C03.6017, C08.2252). We would like to thank Mr. R. Janssen, Mr. M. de Graaf, Mr. D. van den Berg and Mr. M. Prinz for superb technical assistance.

References

1. Vetter T, Lohse MJ: Magnesium and the parathyroid. *Curr Opin Nephrol Hypertens* 11:403-410, 2002
2. Grubbs RD, Maguire ME: Magnesium as a regulatory cation: criteria and evaluation. *Magnesium* 6:113-127, 1987
3. Romani A, Scarpa A: Regulation of cell magnesium. *Arch Biochem Biophys* 298:1-12, 1992
4. Konrad M, Schlingmann KP, Gudermann T: Insights into the molecular nature of magnesium homeostasis. *Am J Physiol Renal Physiol* 286:F599-605, 2004
5. Grimellec CL, Poujeol P, Rouffignia C: 3H-inulin and electrolyte concentrations in Bowman's capsule in rat kidney. Comparison with artificial ultrafiltration. *Pflugers Arch* 354:117-131, 1975
6. Dai LJ, Ritchie G, Kerstan D, *et al.*: Magnesium transport in the renal distal convoluted tubule. *Physiol Rev* 81:51-84, 2001
7. Walder RY, Landau D, Meyer P, *et al.*: Mutation of TRPM6 causes familial hypomagnesemia with secondary hypocalcemia. *Nat Genet* 31:171-174, 2002
8. Schlingmann KP, Weber S, Peters M, *et al.*: Hypomagnesemia with secondary hypocalcemia is caused by mutations in TRPM6, a new member of the TRPM gene family. *Nat Genet* 31:166-170, 2002
9. Walder RY, Yang B, Stokes JB, *et al.*: Mice defective in *Trpm6* show embryonic mortality and neural tube defects. *Hum Mol Genet* 18:4367-4375, 2009
10. Runnels LW, Yue L, Clapham DE: TRP-PLIK, a bifunctional protein with kinase and ion channel activities. *Science* 291:1043-1047, 2001
11. Ryazanova LV, Dorovkov MV, Ansari A, *et al.*: Characterization of the protein kinase activity of TRPM7/ChaK1, a protein kinase fused to the transient receptor potential ion channel. *J Biol Chem* 279:3708-3716, 2004
12. Cao G, Thebault S, van der Wijst J, *et al.*: RACK1 inhibits TRPM6 activity via phosphorylation of the fused alpha-kinase domain. *Curr Biol* 18:168-176, 2008
13. Cao G, van der Wijst J, van der Kemp A, *et al.*: Regulation of the epithelial MG²⁺ channel TRPM6 by estrogen and the associated repressor protein of estrogen receptor activity (REA). *J Biol Chem*, 2009
14. Thebault S, Cao G, Venselaar H, *et al.*: Role of the alpha-kinase domain in TRPM6 channel and regulation by intracellular ATP. *J Biol Chem*, 2008
15. Schmitz C, Dorovkov MV, Zhao X, *et al.*: The channel kinases TRPM6 and TRPM7 are functionally nonredundant. *J Biol Chem* 280:37763-37771, 2005
16. Clark K, Middelbeek J, Dorovkov MV, *et al.*: The alpha-kinases TRPM6 and TRPM7, but not eEF-2 kinase, phosphorylate the assembly domain of myosin IIA, IIB and IIC. *FEBS Lett* 582:2993-2997, 2008
17. Clark K, Middelbeek J, Morrice NA, *et al.*: Massive autophosphorylation of the Ser/Thr-rich domain controls protein kinase activity of TRPM6 and TRPM7. *PLoS ONE* 3:e1876, 2008
18. Matsushita M, Kozak JA, Shimizu Y, *et al.*: Channel function is dissociated from the intrinsic kinase activity and autophosphorylation of TRPM7/ChaK1. *J Biol Chem* 280:20793-20803, 2005
19. Rempe DA, Takano T, Nedergaard M: TR(I)Pping towards treatment for ischemia. *Nat Neurosci* 12:1215-1216, 2009
20. McNulty S, Fonfria E: The role of TRPM channels in cell death. *Pflugers Arch* 451:235-242, 2005
21. Sun HS, Jackson MF, Martin LJ, *et al.*: Suppression of hippocampal TRPM7 protein prevents delayed neuronal death in brain ischemia. *Nat Neurosci* 12:1300-1307, 2009
22. Fonfria E, Marshall IC, Benham CD, *et al.*: TRPM2 channel opening in response to oxidative stress is dependent on activation of poly(ADP-ribose) polymerase. *Br J Pharmacol* 143:186-192, 2004
23. Hara Y, Wakamori M, Ishii M, *et al.*: LTRPC2 Ca²⁺-permeable channel activated by changes in redox status confers susceptibility to cell death. *Mol Cell* 9:163-173, 2002

24. Zhang W, Chu X, Tong Q, *et al.*: A novel TRPM2 isoform inhibits calcium influx and susceptibility to cell death. *J Biol Chem* 278:16222-16229, 2003
25. Naziroglu M: New molecular mechanisms on the activation of TRPM2 channels by oxidative stress and ADP-ribose. *Neurochem Res* 32:1990-2001, 2007
26. Thannickal VJ, Fanburg BL: Reactive oxygen species in cell signaling. *Am J Physiol Lung Cell Mol Physiol* 279:L1005-1028, 2000
27. Ushio-Fukai M: Vascular signaling through G protein-coupled receptors: new concepts. *Curr Opin Nephrol Hypertens* 18:153-159, 2009
28. Kohchi C, Inagawa H, Nishizawa T, *et al.*: ROS and innate immunity. *Anticancer Res* 29:817-821, 2009
29. Eckers A, Klotz LO: Heavy metal ion-induced insulin-mimetic signaling. *Redox Rep* 14:141-146, 2009
30. Aronheim A: Protein recruitment systems for the analysis of protein +/- protein interactions. *Methods* 24:29-34, 2001
31. Grimaud R, Ezraty B, Mitchell JK, *et al.*: Repair of oxidized proteins. Identification of a new methionine sulfoxide reductase. *J Biol Chem* 276:48915-48920, 2001
32. Voets T, Nilius B, Hoefs S, *et al.*: TRPM6 forms the Mg²⁺ influx channel involved in intestinal and renal Mg²⁺ absorption. *J Biol Chem* 279:19-25, 2004
33. Moskovitz J, Weissbach H, Brot N: Cloning the expression of a mammalian gene involved in the reduction of methionine sulfoxide residues in proteins. *Proc Natl Acad Sci U S A* 93:2095-2099, 1996
34. Kuschel L, Hansel A, Schonherr R, *et al.*: Molecular cloning and functional expression of a human peptide methionine sulfoxide reductase (hMsrA). *FEBS Lett* 456:17-21, 1999
35. Fomenko DE, Novoselov SV, Natarajan SK, *et al.*: MsrB1 (methionine-R-sulfoxide reductase 1) knock-out mice: roles of MsrB1 in redox regulation and identification of a novel selenoprotein form. *J Biol Chem* 284:5986-5993, 2009
36. Jung S, Hansel A, Kasperczyk H, *et al.*: Activity, tissue distribution and site-directed mutagenesis of a human peptide methionine sulfoxide reductase of type B: hCBS1. *FEBS Lett* 527:91-94, 2002
37. Hansel A, Jung S, Hoshi T, *et al.*: A second human methionine sulfoxide reductase (hMSRB2) reducing methionine-R-sulfoxide displays a tissue expression pattern distinct from hMSRB1. *Redox Rep* 8:384-388, 2003
38. Stadtman ER, Moskovitz J, Berlett BS, *et al.*: Cyclic oxidation and reduction of protein methionine residues is an important antioxidant mechanism. *Mol Cell Biochem* 234-235:3-9, 2002
39. Moskovitz J: Roles of methionine sulfoxide reductases in antioxidant defense, protein regulation and survival. *Curr Pharm Des* 11:1451-1457, 2005
40. Cabreiro F, Picot CR, Friguet B, *et al.*: Methionine sulfoxide reductases: relevance to aging and protection against oxidative stress. *Ann N Y Acad Sci* 1067:37-44, 2006
41. Bigelow DJ, Squier TC: Redox modulation of cellular signaling and metabolism through reversible oxidation of methionine sensors in calcium regulatory proteins. *Biochim Biophys Acta* 1703:121-134, 2005
42. Colombo G, Meli M, Morra G, *et al.*: Methionine sulfoxides on prion protein Helix-3 switch on the alpha-fold destabilization required for conversion. *PLoS ONE* 4:e4296, 2009
43. Ciorba MA, Heinemann SH, Weissbach H, *et al.*: Modulation of potassium channel function by methionine oxidation and reduction. *Proc Natl Acad Sci U S A* 94:9932-9937, 1997
44. Santarelli LC, Wassef R, Heinemann SH, *et al.*: Three methionine residues located within the regulator of conductance for K⁺ (RCK) domains confer oxidative sensitivity to large-conductance Ca²⁺-activated K⁺ channels. *J Physiol* 571:329-348, 2006
45. Erickson JR, Joiner ML, Guan X, *et al.*: A dynamic pathway for calcium-independent activation of CaMKII by methionine oxidation. *Cell* 133:462-474, 2008
46. Eisfeld J, Luckhoff A: Trpm2. *Handb Exp Pharmacol*:237-252, 2007
47. Liu Y, Gutterman DD: Oxidative stress and potassium channel function. *Clin Exp Pharmacol Physiol* 29:305-311, 2002

48. Moskovitz J, Berlett BS, Poston JM, *et al.*: The yeast peptide-methionine sulfoxide reductase functions as an antioxidant in vivo. *Proc Natl Acad Sci U S A* 94:9585-9589, 1997
49. Stadtman ER, Levine RL: Free radical-mediated oxidation of free amino acids and amino acid residues in proteins. *Amino Acids* 25:207-218, 2003
50. Levine RL, Mosoni L, Berlett BS, *et al.*: Methionine residues as endogenous antioxidants in proteins. *Proc Natl Acad Sci U S A* 93:15036-15040, 1996
51. Yao Y, Yin D, Jas GS, *et al.*: Oxidative modification of a carboxyl-terminal vicinal methionine in calmodulin by hydrogen peroxide inhibits calmodulin-dependent activation of the plasma membrane Ca-ATPase. *Biochemistry* 35:2767-2787, 1996
52. Nabuchi Y, Fujiwara E, Ueno K, *et al.*: Oxidation of recombinant human parathyroid hormone: effect of oxidized position on the biological activity. *Pharm Res* 12:2049-2052, 1995
53. Madsen KM VJ, Tisher CC.: Relationship between structure and function in distal tubule and collecting duct. *J Electron Microscop Tech.* 9:187-208, 1988
54. Topala CN, Groenestege WT, Thebault S, *et al.*: Molecular determinants of permeation through the cation channel TRPM6. *Cell Calcium* 41:513-523, 2007
55. van de Graaf SF, Hoenderop JG, Gkika D, *et al.*: Functional expression of the epithelial Ca(2+) channels (TRPV5 and TRPV6) requires association of the S100A10-annexin 2 complex. *Embo J* 22:1478-1487, 2003
56. Gkika D, Topala CN, Chang Q, *et al.*: Tissue kallikrein stimulates Ca(2+) reabsorption via PKC-dependent plasma membrane accumulation of TRPV5. *Embo J* 25:4707-4716, 2006
57. Hoenderop JG, Dardenne O, Van Abel M, *et al.*: Modulation of renal Ca²⁺ transport protein genes by dietary Ca²⁺ and 1,25-dihydroxyvitamin D₃ in 25-hydroxyvitamin D₃-1 α -hydroxylase knockout mice. *Faseb J* 16:1398-1406, 2002



Effects of Epidermal Growth Factor Receptor (EGFR) kinase inhibitor Erlotinib on renal and systemic Mg²⁺ handling

Henrik Dimke¹, **Jenny van der Wijst**¹, Todd R. Alexander, Inez M.J. Meijer², Gemma M. Mulder³, Harry van Goor³, Sabine Tejpar³, Joost G.J. Hoenderop¹, René J.M. Bindels¹

¹Department of Physiology, Radboud University Nijmegen Medical Centre, Nijmegen, The Netherlands

²Department of Cell Biology, Faculty of Science, Radboud University Nijmegen Medical Centre, Nijmegen, The Netherlands

³Department of Pathology and Medical Biology, University Medical Centre Groningen, The Netherlands

Summary

A mutation in pro-EGF causes isolated hypomagnesemia. Further, monoclonal antibodies targeting the extracellular EGFR domain have been implicated in the regulation of epithelial Mg^{2+} transport. However, the effect of the widely used EGFR tyrosine kinase inhibitor, Erlotinib, on Mg^{2+} homeostasis remains unknown. To investigate the potential role of Erlotinib on Mg^{2+} handling, C57BL/6 mice were given intraperitoneal injections for 23 days. In Erlotinib-injected mice, a small but significant decrease in serum Mg^{2+} concentrations was observed at day 16 and 23, while the fractional excretion of Mg^{2+} remained unchanged after 23 days. Semi-quantitative immunohistochemical evaluation did not reveal detectable changes in renal Transient Receptor Potential Melastatin 6 (TRPM6) protein expression. The effect of Erlotinib on TRPM6 was investigated in HEK293 cells. Patch clamp analysis in TRPM6 expressing cells demonstrated that Erlotinib inhibited EGF-induced changes in TRPM6 current density at a concentration of 30 μ M. At lower concentrations (0.3 μ M), Erlotinib failed to inhibit EGF-mediated TRPM6 stimulation. Likewise, EGF-induced tyrosine phosphorylation of its receptor was only blocked by 30 μ M of Erlotinib. In addition, 30 μ M Erlotinib inhibited EGF-stimulated increases in the mobile fraction of endomembrane TRPM6 channels. In this mouse model, Erlotinib does influence Mg^{2+} handling. However, the effect on the systemic Mg^{2+} concentration seems less potent than that observed with antibody-based EGFR inhibitors *in vivo*. Currently, clinical data detailing the effect of Erlotinib on Mg^{2+} handling is lacking. Based on the doses given to cancer patients it is unlikely that Erlotinib severely affects serum Mg^{2+} concentrations in these individuals.

Introduction

Overall maintenance of serum Mg^{2+} concentration is essential for many cellular processes, including adequate function of neurological and cardiovascular systems. The Transient Receptor Potential Melastatin subtype 6 (TRPM6) was originally identified as the causative gene for the rare autosomal recessive disorder; hypomagnesemia with secondary hypocalcemia [1, 2]. TRPM6, which is expressed in kidney and colon [1, 3, 4], constitutes the gatekeeper and postulated rate-limiting entry step for active Mg^{2+} (re-) absorption.

The effect of EGF on TRPM6 has been firmly established. Application of EGF readily increases TRPM6 current density [5, 6]. Additional evidence suggests that EGF provokes trafficking of the channel to the plasma membrane, via activation of the Rho GTPase, Rac1 [5]. These discoveries were prompted by the observations that anti-cancer treatments with monoclonal antibodies (Cetuximab), targeting an extracellular epitope on the epidermal growth factor receptor (EGFR), causes hypomagnesemia in patients with colorectal cancer. In addition, genetic linkage and sequence analysis implicated the pro-EGF gene in isolated recessive renal hypomagnesemia [6-8]. The

observed decline in serum Mg^{2+} is accompanied by renal Mg^{2+} wasting, as these patients maintain an inappropriately high fractional Mg^{2+} excretion [6].

While mostly patients with colorectal cancer are treated with monoclonal EGFR inhibitors, numerous patient groups suffering from cancer receive tyrosine kinase inhibitors, such as Erlotinib or Gefitinib. These include individuals being treated for non-small cell lung cancer as well as pancreatic cancer [9]. Erlotinib has been grouped with platinum compounds in most trials, a combination that may potentiate the effects on serum Mg^{2+} concentrations [10]. At present, there are no published clinical reports detailing the potential effect of tyrosine kinase inhibitors on systemic and renal Mg^{2+} handling. Given the pronounced effect of Cetuximab on Mg^{2+} homeostasis, we sought to ascertain whether Erlotinib alters Mg^{2+} handling. Thus Mg^{2+} homeostasis and TRPM6 expression levels were investigated in wild-type mice receiving Erlotinib for 23 days, and the effect of Erlotinib on current density and mobility of TRPM6 was studied in HEK293 cells transiently overexpressing the channel.

Results

Erlotinib reduces serum Mg^{2+} concentration in C57Bl/6 mice

C57BL/6 mice were injected intraperitoneally with a high dose of Erlotinib or vehicle for 23 day (2 mg/mouse/day) (n=9 per group). Blood samples were obtained at day 16, by puncturing a vascular bundle in the sub-mandibular area. Serum Mg^{2+} concentration showed a significant decline in the Erlotinib-injected group ($p < 0.05$) (Figure 1A), while no difference was detected in serum Ca^{2+} concentration between groups ($p > 0.5$) (Figure 1B). Upon sacrifice after 23 days of Erlotinib injections, similar results were found, namely a slight but significant decline in the serum Mg^{2+} concentration in the Erlotinib-injected group ($p < 0.05$) (Figure 1C). Erlotinib did not affect the systemic Ca^{2+} concentration at day 23 ($p > 0.2$) (Figure 1D). No difference was observed in the urinary excretion of Mg^{2+} ($p > 0.5$), (Figure 2A) and the urinary Ca^{2+} excretion ($p > 0.2$) (Figure 2B) after 23 days of Erlotinib administration. The glomerular filtration rate remained within normal limits ($p > 0.2$) (Figure 2C). Importantly, no change in the fractional excretion of Mg^{2+} was observed in mice receiving Erlotinib ($p > 0.2$) (Figure 2D). The fractional excretion of Ca^{2+} ($p > 0.5$) remained unchanged after chronic administration of Erlotinib (Figure 2E). These results suggest that Erlotinib-treated mice waste Mg^{2+} , as serum Mg^{2+} is decreased while a compensatory reduction in the fractional Mg^{2+} excretion is absent.

Renal TRPM6 protein expression is unchanged in erlotinib-injected mice

As mice injected with Erlotinib develop a modest reduction in serum Mg^{2+} , without appropriate compensation by the kidney, a possible effect could be on the expression level of TRPM6. Therefore, TRPM6 mRNA abundance was determined in the Erlotinib-and vehicle-injected mice. Chronic administration of Erlotinib caused a significant 0.67 fold decrease in the mRNA expression of

TRPM6 ($p < 0.02$, $n = 9$) (Figure 3A). TRPM6 protein abundance was determined by semi-quantification of fluorescence, from anti-TRPM6 immunolabeled kidney sections. However, using this method no change in TRPM6 fluorescence was found ($p > 0.5$, $n = 9$) (Figure 3B). As TRPM6 is abundantly expressed in colon, the main site for active Mg^{2+} absorption in the intestine, the effect of Erlotinib on colonic TRPM6 mRNA expression was investigated. No change in the abundance of colonic TRPM6 was observed between Erlotinib- and vehicle- injected mice ($p > 0.2$, $n = 9$) (Figure 3C).

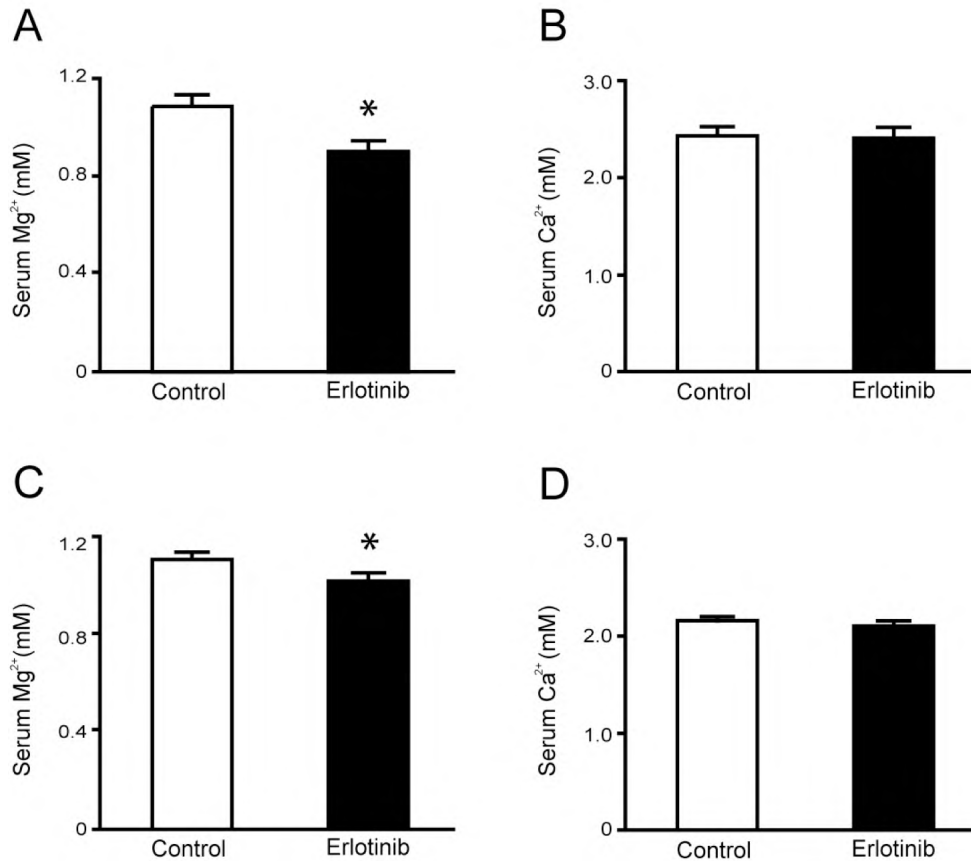


Figure 1. Effect of Erlotinib on serum Mg^{2+} and Ca^{2+} concentrations. *A-B.* Changes in serum Mg^{2+} and Ca^{2+} concentrations after 16 days, in mice receiving daily injections with Erlotinib or vehicle. *C-D.* Effect of Erlotinib or vehicle on serum Mg^{2+} and Ca^{2+} concentrations after 23 days. Values are presented as means \pm SEM ($n = 9$). * $p < 0.05$ is considered statistically significant.

Renal EGFR expression is increased in mice injected with erlotinib

To investigate whether changes in the renal EGF system were apparent after chronic administration of Erlotinib, renal mRNA expression of EGF and the EGFR was determined. A 1.6 fold increase in the mRNA abundance of the EGFR receptor was observed in Erlotinib-injected mice ($p < 0.05$, $n = 9$) (Figure 4A). Additionally, no change in renal mRNA expression of EGF was observed after injection of Erlotinib ($p > 0.05$, $n = 9$) (Figure 4B). To evaluate changes in the secretion of EGF after administration of Erlotinib, the urinary excretion of EGF was measured in the experimental groups. No differences were observed in the total urinary excretion of EGF between vehicle- and Erlotinib-injected animals (Figure 4C). In addition, no changes were detected when the values were

corrected for the urinary creatinine excretion (Figure 4D). As the colonic EGF system may be affected in a similar way, as observed in the kidney, the abundance of the EGFR and the EGF mRNA was investigated in samples extracted from colon. However, no differences in the colonic expression of the EGFR ($p>0.5$, $n=9$) (Figure 4E) and EGF ($p>0.2$, $n=9$) (Figure 4F) were detectable between vehicle- and Erlotinib-injected animals.

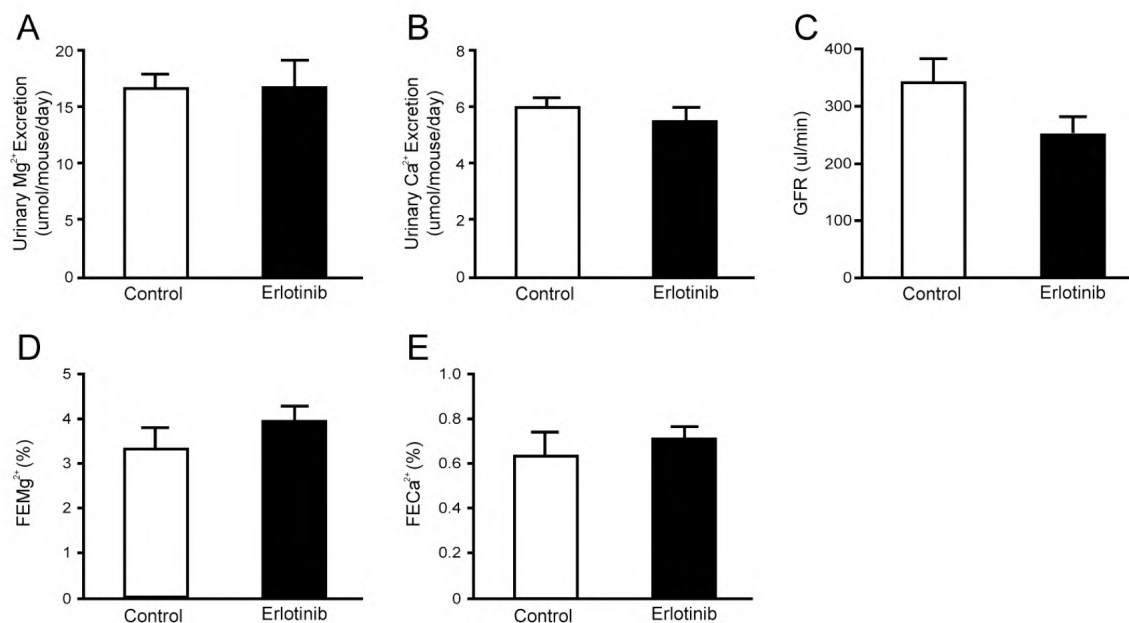


Figure 2. Functional data after 23 days of Erlotinib injections. *A-B*. Daily urinary excretion of Mg²⁺ and Ca²⁺ in mice injected with Erlotinib for 23 days. *C*. Creatinine clearance (estimated glomerular filtration rate) in Erlotinib- and vehicle- injected mice as well as *D-E*. the corresponding fractional excretions of Mg²⁺ (FEMg) and Ca²⁺ (FECa). Values are presented as means \pm SEM ($n = 9$). * $p<0.05$ is considered statistically significant.

Supraphysiological concentrations of erlotinib are necessary to inhibit TRPM6 channel activity

HEK293 cells expressing TRPM6 were subjected to whole cell patch-clamp analysis. Using this technique a TRPM6 specific outward current was detectable. Pretreatment with Erlotinib alone did not significantly affect channel currents from controls ($p>0.05$). Application of EGF (10 nM) significantly increased channel activity compared to control ($p<0.001$) (Figure 5A-C). Pretreatment with Erlotinib (30 μ M) completely prevented the EGF-induced increase in TRPM6 current density ($p<0.01$). However, at lower Erlotinib concentrations (0.3 μ M), Erlotinib did not significantly inhibit EGF-stimulated TRPM6 channel currents (Figure 5A-C). Tyrosine phosphorylation of the immunoprecipitated EGFR was evaluated under the same experimental conditions as aforementioned (Figure 5D). In the presence of EGF, tyrosine phosphorylation of the immunoprecipitated receptor was markedly increased. Preincubation of HEK293 cells with Erlotinib at 30 μ M blunted the EGF-induced EGFR tyrosine phosphorylation. However, incubation with 0.3 μ M of Erlotinib was not sufficient to effectively block EGFR phosphorylation. Cells incubated in the absence of EGF showed no detectable tyrosine phosphorylation of the EGFR.

Erlotinib inhibits EGF-stimulated mobility of endomembrane TRPM6

Fluorescence recovery after photobleaching (FRAP) was used to estimate the mobility and mobile fraction of GFP-tagged TRPM6 channels in HEK293 cells. The electrophysiological properties of GFP-TRPM6 have previously been shown to display comparable currents to that of wild-type TRPM6 in the presence or absence of EGF.[5] In line with this, an increase in the maximal recovery was found after EGF application ($p < 0.05$) (Figure 6 D-E). Pretreatment with Erlotinib (at 30 μM) prevented the EGF-stimulated increase in the mobile fraction of TRPM6 channels ($p < 0.05$) (Figure 6 D-E).

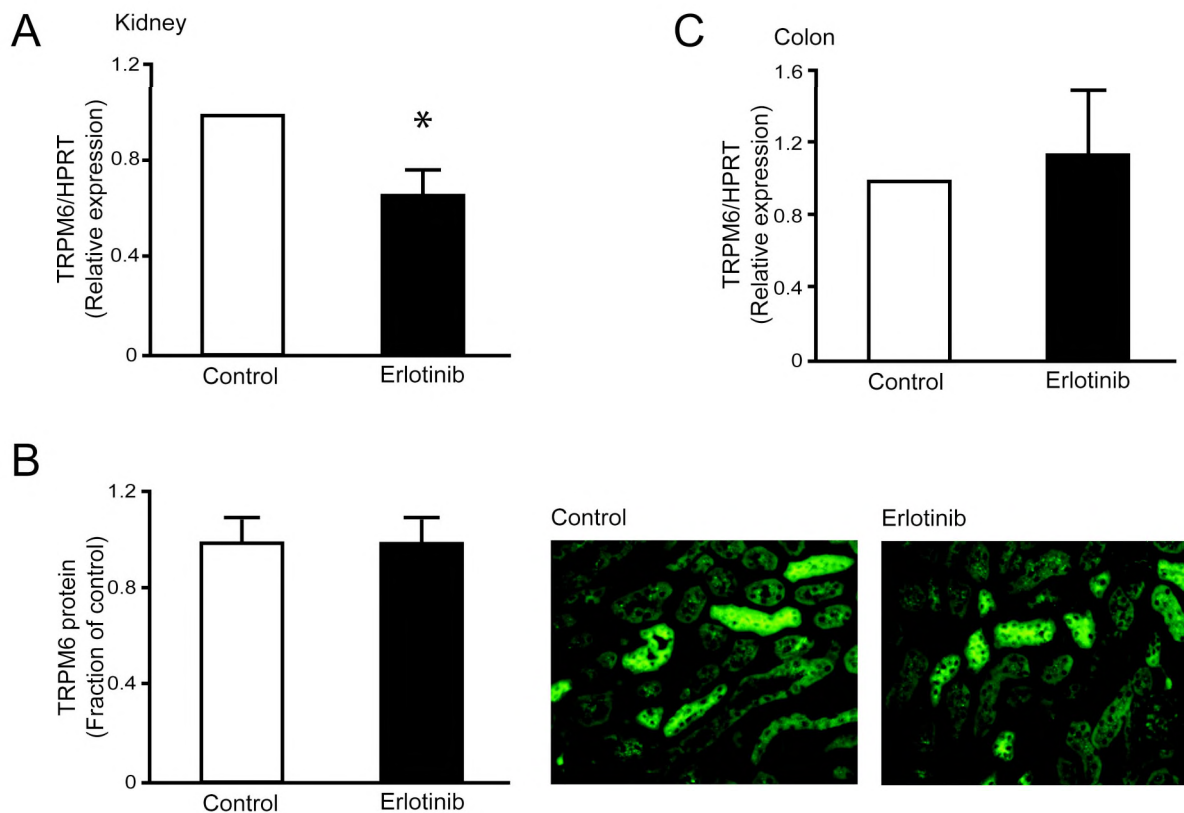


Figure 3. Effect of Erlotinib on mRNA and protein abundance of TRPM6. *A.* Semi-quantitative real-time PCR was used to determine the abundance of TRPM6 mRNA extracted from kidney. *B.* Histogram depicting TRPM6 protein abundance determined by computerized analysis of immunohistochemical images. Representative immunohistochemical pictures of TRPM6 in vehicle- and Erlotinib- injected mice. *C.* Semi-quantitative real-time PCR determination of TRPM6 mRNA expression in colon. Data is presented as means \pm SEM. * $p < 0.05$ is considered statistically significant.

Discussion

The current study shows that Erlotinib is capable of affecting TRPM6 regulation and thereby altering Mg^{2+} handling. This conclusion is based on: *i*) mice receiving supraphysiological doses of Erlotinib for 23 days develop a decrease in their serum Mg^{2+} concentration; *ii*) Erlotinib-injected mice fail to reduce the fractional renal excretion of Mg^{2+} in response to a decreased serum Mg^{2+} concentration; *iii*) whole-cell patch clamp analysis in HEK293 cells shows that Erlotinib significantly inhibited EGF-stimulated TRPM6 channel activity.

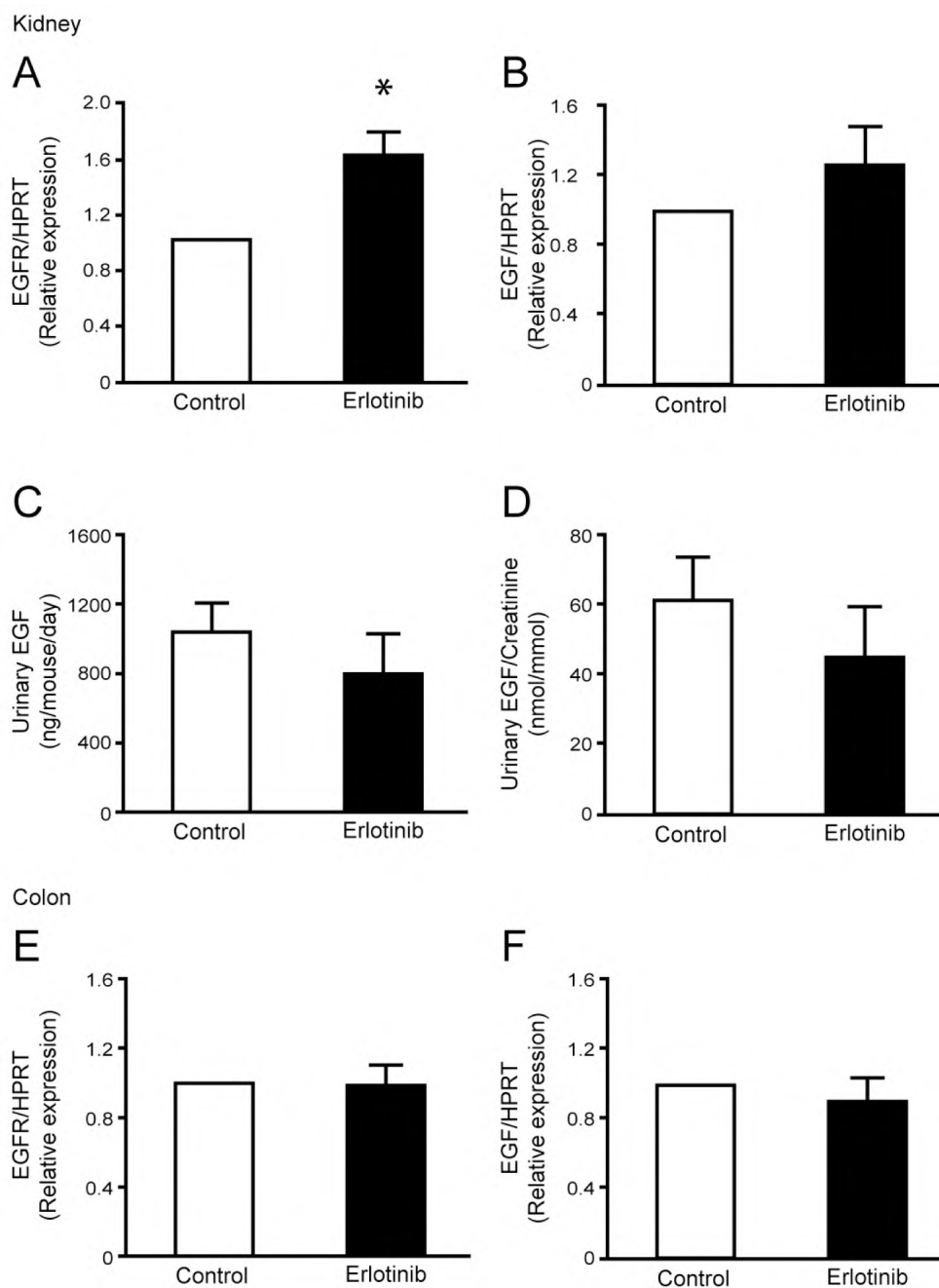


Figure 4. Erlotinib modulates EGFR mRNA expression. *A-B.* Semi-quantitative determination of the mRNA abundance of EGFR and EGF in kidney of vehicle and Erlotinib-injected mice. *C-D.* Measurements of urinary EGF excretion as well as the urinary EGF/creatinine ratio. *E-F.* Colonic mRNA abundance of EGFR and EGF. Data is presented as means \pm SEM. * $p < 0.05$ is considered statistically significant.

Administration of 92 mg/kg Erlotinib (~ 2.3 mg/ 25 g mouse) intraperitoneally yielded a plasma concentration of approximately 40 μM after 1 hr in mice [11]. A virtually identical dose was employed in our mice study (2 mg/mouse/day), thus we can expect similar plasma concentrations of Erlotinib. HEK293 cells received dosages in the same range (30 μM of Erlotinib). Given the moderate effects of Erlotinib *in vivo*, application of the compound could still block EGF-stimulated TRPM6 currents and routing in HEK293 cells. This can possibly be explained by the bioavailability of the compound. It has been estimated that 92-95% of the administered Erlotinib is bound to plasma

proteins [12], thus the estimated free concentration in our mouse model would approximate 2-3 μM , a dose that likely would impose less inhibition on EGF-stimulated TRPM6 activity *in vitro*.

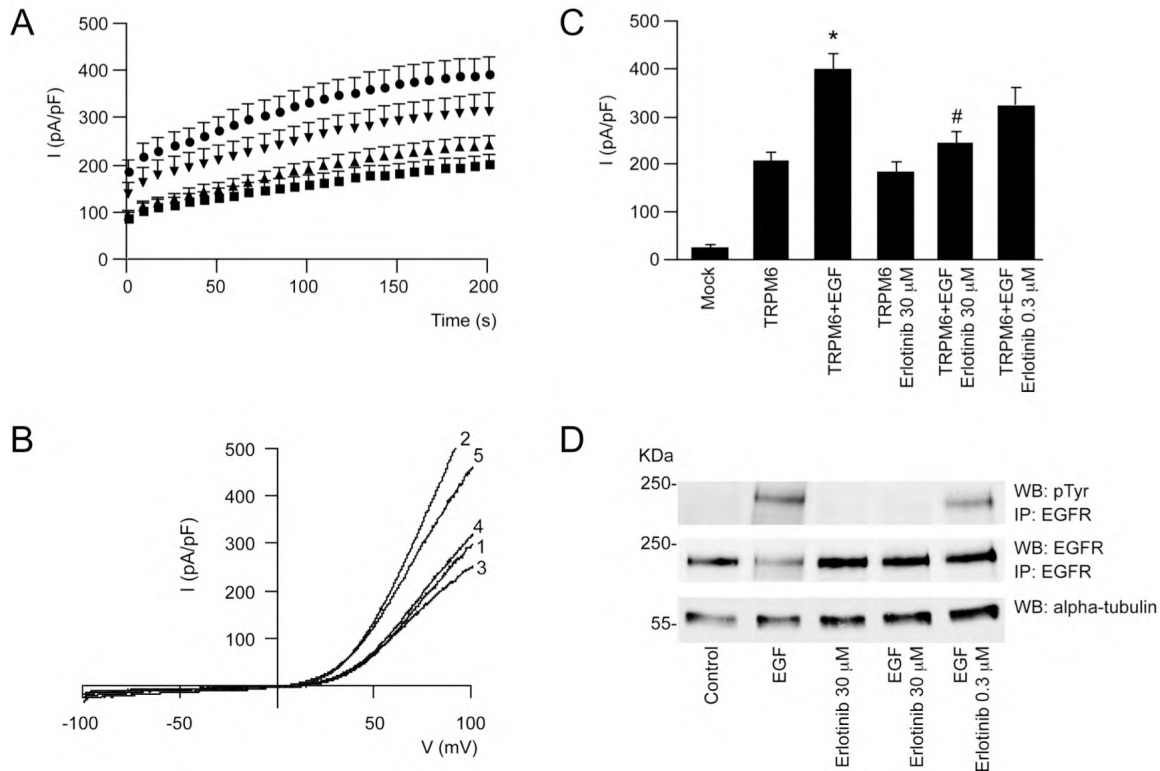


Figure 5. EGFR blockade by Erlotinib can prevent EGF-induced changes in TRPM6 current density. *A.* Time course of the current development (pA/pF) at +80 mV of TRPM6 (■) transfected HEK293 cells, pretreated with EGF (●) and Erlotinib 30 μM (▲) or 0.3 μM (▼) *B.* Current recorded after 200 sec stimulation by a voltage ramp between -100 and +100 mV of TRPM6 transfected HEK293 cells (1), pretreated with EGF (2) or Erlotinib (3) alone, or pretreated with EGF and Erlotinib 30 μM (4) / 0.3 μM (5) *C.* Histogram summarizing the current density (pA/pF) at +80 of TRPM6 transfected HEK293 cells pretreated with EGF and/or Erlotinib as indicated. * indicates $p < 0.01$ compared to TRPM6 current ($n=12-26$ cells). # indicates $P < 0.05$ compared to TRPM6 pretreated with EGF ($n=12-26$ cells). *D.* The immunoprecipitated EGFR was placed on Western blots for the detection of tyrosine phosphorylation (pTyr) as well as the EGFR itself. In addition, alpha-tubulin was detected in whole cell lysates as a control for total expression.

Individuals receiving a single standard dose of Erlotinib (150 mg) show a maximal plasma concentration amounting to $2.65 \pm 2.02 \mu\text{M}$ (1.14 $\mu\text{g/ml}$) of the compound [12, 13], representing a ~ 10 times lower circulating concentration than the mouse model. Given that the free circulating concentration of Erlotinib is likely to be around 0.3 μM in human patients, we tested whether this concentration would be able to block the effect of EGF on TRPM6 currents. However, we could not detect any significant differences from EGF-stimulated cells. Evaluating EGF-induced tyrosine phosphorylation of its receptor substantiated these data. At Erlotinib concentrations of 30 μM , we were unable to detect any phosphorylation of the EGFR. At lower concentrations (0.3 μM), resembling the free concentration found in humans receiving standard doses of Erlotinib, EGFR phosphorylation was still present after application of EGF. Previous studies show that Erlotinib inhibits ligand-stimulated tyrosine autophosphorylation of the EGFR, with a IC_{50} of approximately 20

nM in cells. However, concentrations of at least a few hundred nM of Erlotinib are necessary to block more than 90% of the ligand-induced autophosphorylation [14, 15].

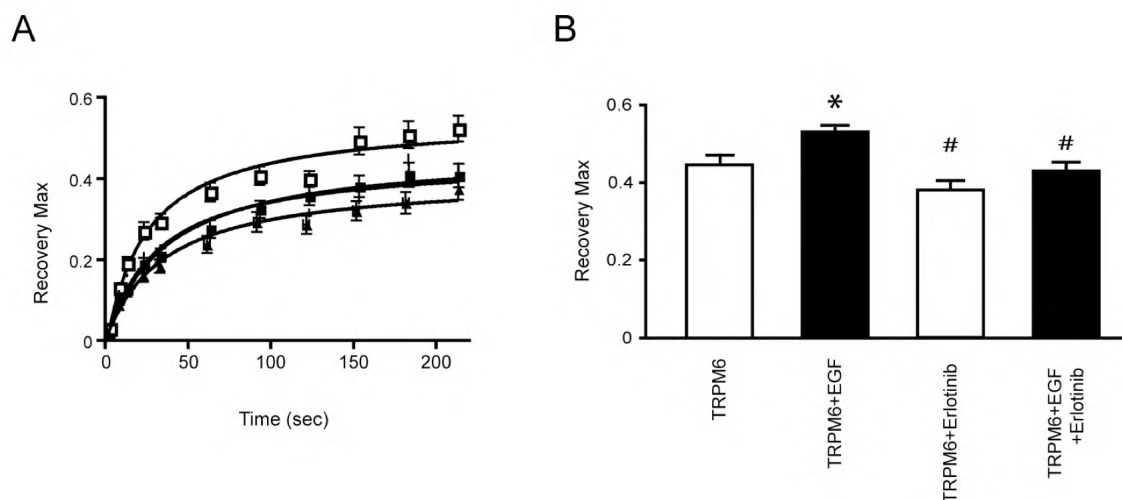


Figure 6. Erlotinib inhibits EGF-stimulated changes in the mobile fraction of TRPM6. *A.* Fluorescence recovery kinetics as a function of time, measured in HEK293 cells transiently transfected with GFP-TRPM6. Cells were pre-incubated with Erlotinib (30 μ M, 30 min) alone (\blacktriangle) or prior to EGF application (10 nM, 30-60 min, \triangle), and compared to control (\blacksquare) or EGF-treated cells (\square). *B.* Histogram representing the maximal recovery of fluorescence (estimated mobile fraction) in HEK293 cells expressing GFP-TRPM6 with or without application of Erlotinib, EGF, or both. Data is presented as means \pm SEM ($n = 9$). * $p < 0.05$ is considered statistically significant from control. # $p < 0.05$ statistically significant from EGF-treated.

The results obtained in this study fits well with the previous observations. Taken together, these data indicate that Erlotinib treatment in human patients is unlikely to induce severe hypomagnesemia as observed with EGFR-directed antibodies. However, it remains unclear whether the cellular concentration of Erlotinib, namely that obtained in the DCT, is similar to what is observed in plasma. Similarly, the bioavailability of monoclonal antibodies may explain why colorectal cancer patients receiving Cetuximab show a pronounced decrease in serum Mg^{2+} concentrations; to such a degree that hypomagnesemia develops.

We also found that inhibition of Mg^{2+} transport by Erlotinib is likely to occur via inhibition of TRPM6 routing, by preventing EGF-mediated changes in the mobile fraction of TRPM6 proteins. After application of Erlotinib, the EGF-stimulated fraction of TRPM6 channels becomes unresponsive. As previously shown, EGF does not only increase the mobile fraction, but also increases the plasma membrane expression of the channel, suggesting that EGF exerts its effect by redistributing TRPM6 from storage vesicles to the membrane [5]. In the experimental animal, where physiological levels of EGF are present, blockade of the EGFR would be expected to retain a bigger fraction of TRPM6 channels in endomembrane compartments, thereby preventing plasma membrane trafficking and hence reduce Mg^{2+} influx. This hypothesis would also explain renal Mg^{2+} wasting, without concomitant changes in renal TRPM6 protein expression.

EGFR inhibition by Erlotinib influences Mg^{2+} handling, by decreasing serum Mg^{2+} content, without providing a compensatory decrease in the fractional renal Mg^{2+} excretion. These data are in good agreement with those obtained from patients receiving Cetuximab, although less pronounced [6, 7]. Thus, the kidney is not able to effectively compensate for the reduction in serum Mg^{2+} concentration. Accordingly, the data insofar support tubular Mg^{2+} wasting, as a potential source of reducing serum Mg^{2+} concentration or at least in keeping serum Mg^{2+} lowered. Systemic and renal Ca^{2+} homeostasis remained unaffected during administration of Erlotinib, suggesting that EGF does not directly affect Ca^{2+} handling. Thus the changes in renal Mg^{2+} handling correlate well with impaired distal tubular transport, where Mg^{2+} transport is mechanistically separated from that of Ca^{2+} . Also, the lack of secondary changes in Ca^{2+} , which often accompany perturbations in Mg^{2+} homeostasis, may be explained by the modest decline in serum Mg^{2+} concentration observed in Erlotinib-injected animals. This is confirmed in patients treated with Cetuximab, as the appearance of hypocalcaemia was limited to individuals presenting with at least grade 2 hypomagnesemia (serum Mg^{2+} between 0.5 to 0.4 mM).[7] The underlying cause of the secondary hypocalcemia during severe hypomagnesemia remains incompletely understood, although impaired release of PTH from the parathyroid gland and desensitization of bone to PTH is likely implicated [16, 17].

Despite a significant decrease in renal TRPM6 mRNA abundance, semi-quantitative comparison of TRPM6 immunofluorescence could not detect a difference in protein expression. These findings may be explained by the observation that TRPM6 is retained in endomembrane vesicles, leading to a decreased degradation of the protein. In such an event, mRNA expression would be expected reduced, as the protein is retained in the cell. In fact, *in vitro* findings in this study support this observation, i.e. impaired mobility of TRPM6 after EGF-stimulation in the presence of Erlotinib.

No change was observed in colonic TRPM6 mRNA abundance. Due to difficulties detecting TRPM6 immunohistochemically in the colon, it is not possible to confirm whether TRPM6 protein abundance remains unchanged. Moreover, it cannot be excluded whether Erlotinib inhibits EGF-stimulated TRPM6 trafficking in the colon, as we observe in HEK293 cells. However, it is currently not possible to effectively estimate Mg^{2+} uptake in the intact animal using tracers, due to the very short half-life of the radioactive $^{28}Mg^{2+}$ isotope. In addition, one would expect an increased TRPM6 expression in the colon during conditions of lowered serum Mg^{2+} , an effect that is not observed here and elsewhere [3]. It is currently unclear how colonic Mg^{2+} absorption is regulated. An increase was found in the renal EGFR mRNA expression, while in the colon no such change could be detected. This response may indicate that particularly in kidney, the EGF axis is affected after Erlotinib treatment. Additionally, the EGF mRNA abundance remained unchanged in both organs. Measurements of EGF in the urine supported these findings, suggesting that EGF secretion is not altered in response to Erlotinib.

The current study is to our knowledge the first to delineate the effects of Erlotinib on Mg^{2+} handling *in vivo*. Taken together, these findings suggest that Erlotinib can inhibit EGF-stimulated

TRPM6 activity and consequently impair Mg^{2+} reabsorption in the kidney. Additionally, it provides an explanation about why hypomagnesemia has not been correlated with Erlotinib treatment in patients undergoing chemotherapy, as has been observed with Cetuximab. However, it should be noted that Erlotinib has the potential to modulate renal and systemic Mg^{2+} handling *in vivo*. Therefore, caution should be given when treating individuals prone to developing hypomagnesemia, and patients receiving combinational treatment with Mg^{2+} lowering compounds.

Material and methods

Experimental protocol- C57BL/6 mice (10 weeks old, n=18) received intraperitoneal injections with Erlotinib or vehicle for 23 days. The animals were kept in a light- and temperature-controlled room with *ad libitum* access to food and water. Erlotinib (Tarceva®, generously provided by Roche Diagnostics GmbH, Penzberg, Germany) was dissolved in 10% dimethyl sulfoxide in saline with 0.1% Pluronic P105 v/v as previously described [11]. The compound was delivered once daily at a dose of 2 mg/mouse/day. Controls received an identical vehicle solution. At day 16, blood was obtained by puncturing the vascular bundle located rear of the jawbone. During the last 24 hrs of the experimental period, mice were placed in metabolic cages and subsequently killed under 1.5% (v/v) isoflurane anesthesia (Nicholas Piramal Limited, London, United Kingdom). Blood was withdrawn by perforating the orbital vessels and serum was extracted afterwards. Additionally, organs were dissected out and immediately frozen in liquid nitrogen. One half kidney was processed for immunohistochemistry by immersion fixation in 2% w/v periodate-lysine-paraformaldehyde (PLP), followed by overnight incubation in 15% w/v sucrose. The animal ethics board of Radboud University Nijmegen approved all experimental procedures.

Analytical Procedures- Serum and urinary Mg^{2+} and Ca^{2+} concentrations were measured using a colorimetric assay kit according to the manufacturer's protocol (Roche Diagnostics, Almere, the Netherlands). Urinary mouse EGF was measured by an enzyme-linked immunosorbent assay (R&D DuoSet® ELISA, DY2028, R&D systems Europe Ltd., United Kingdom). The wells were coated with anti-mouse EGF overnight, blocked with BSA (1 hour, room temperature) and washed with phosphate-buffered saline with 0.05% (v/v) Tween 20 (PBS-T). Urine samples and recombinant mouse EGF, used as standard (diluted in 0.5% (w/v) BSA), were added (2 hours, room temperature). After washing in PBS-T, biotinylated goat anti-mouse EGF was added, followed by horseradish peroxidase-conjugated streptavidin. Color was developed with OPD (o-Phenylenediamine) and stopped with H_2SO_4 (end concentration 0.33 M). Absorbance was measured at 492 nm (Varioskan, Thermo electron corporation, Waltham, USA); data were analyzed using SkanIt Software for Varioskan (Thermo electron corporation, Waltham, USA). Detection range of the ELISA was between 2-577 pg/ml.

Semiquantitative Real-Time PCR Analysis- Tissue RNA was extracted using TriZol Total RNA Isolation Reagent (Life Technologies BRL, Breda, The Netherlands). After DNase treatment (Promega, Madison, WI), 1.5 µg of RNA was reverse transcribed by Molony-Murine Leukemia Virus-Reverse Transcriptase (Invitrogen) as described previously [18]. The cDNA was mixed with Power SYBR® green PCR mastermix (Applied Biosystems, Foster City, CA, USA) and primers against TRPM6 (5'-AAAGCCATGCGAGTTATCAGC-3'; 5'-CTTCACAATGAAAACCTGCCC-3'), EGFR (5'- CAGAACTGGGCTTAGGGAAC-3'; 5'-GGACGATGTCCCTCCACTG-3'), EGF (5'-GAGAATCTACTGGACAGACAGTGG-3'; 5'-CTCGAGATTCTCTCTGGATG-3') or the housekeeping gene hypoxanthine-guanine phosphoribosyl transferase (HPRT; 5'-TTATCAGACTGAAGAGCTACTGTAATGATC-3'; 5'-TTACCAGTGTCAATTATATCTTCAACAATC-3'). The mRNA expression levels were quantified using a single color real-time PCR detection system (MyiQ™, Biorad, Veenendaal, the Netherlands). Data analysis was carried out using the Relative Expression Software Tool (REST©[19]).

Immunohistochemistry- 7 µm PLP fixed cryosections were prepared and stained with anti-TRPM6 (guinea pig antiserum), as described previously [4]. Photographs of TRPM6 staining in kidney cortex were taken through a 25x objective on a Zeiss fluorescence microscope (Sliedrecht, The Netherlands) equipped with a digital photo camera (Nikon DMX1200). Semi-quantitative determination of TRPM6 protein expression was done using Image J (image processing program, NIH, USA), similar to previous publications [20].

Cell culture and transfection- Cells were maintained and transfected using Lipofectamine 2000 (Invitrogen-Life Technologies, Breda, The Netherlands) as previously described [21]. Briefly, HEK293T cells were transiently transfected with a N-terminal HA-tagged TRPM6 in the pCINeo/IRES-GFP vector [4] for patch clamp analysis. HEK293 cells were transfected with TRPM6 N-terminally conjugated to Green Fluorescent Protein (GFP) in the pCINeo vector [5] for FRAP analysis. Experiments were performed 48–72 h post-transfection. Cells were preincubated at 37°C in the presence or absence Erlotinib (30 µM or 0.3 µM) for 60 minutes. Cells were also incubated with or without EGF (10 nM) for 30 minutes.

Electrophysiology- Electrophysiological recordings were made as previously described [4, 5]. Briefly, whole-cell currents were determined in the tight seal whole-cell configuration using a patch clamp amplifier controlled by Patchmaster software (HEKA, Lambrecht, Germany). Cells were kept in an extracellular bath solution (150 mM NaCl, 10 mM HEPES/NaOH, 1 mM CaCl₂, pH 7.4). Electrode resistances were between 2-4 MΩ after filling with standard pipette solution (150 mM NaCl, 10 mM EDTA and 10 mM HEPES/NaOH, pH 7.2). Capacitance and access resistances were

continuously monitored using the automatic capacitance compensation of the Patchmaster software. A linear voltage ramp protocol from -100 to +100 mV (within 450 ms) was applied every 2 s from a holding potential of 0 mV. Extracting the current amplitudes at +80 and -80 mV from individual ramp current records assessed the temporal development of membrane currents. Current densities presented were determined by normalizing the current amplitude to the cell membrane capacitance. All experiments were performed at room temperature. The analysis and display of patch clamp data were performed using Igor Pro software (WaveMetrics, Lake Oswego, USA).

Western blotting and immunoprecipitation- HEK293T cells were incubated with EGF and Erlotinib as described above. Immunoprecipitation and western blotting was performed as previously described.[22] Briefly, cells were incubated in lysis buffer (150 mM NaCl, 25 mM Tris/HCL pH=7.5, 1% Brij97 (Polyethylene Glycol Monooleyl Ether), 5 mM EDTA/NaOH pH=8.0, 1 mM Na₃VO₄, 1 mM NaF, 1 mM phenylmethylsulfonyl fluoride, 1 µg/ml leupeptin, 1 µg/ml aprotinin, 1 µg/ml pepstatin) and spun down at 1000 g for 10 min at 4°C. Lysates were incubated overnight with anti-EGFR directed mouse antibodies (sc-120, Santa Cruz Biotechnology, CA, UAS) coupled to protein A-Sepharose beads. Immunoprecipitates were run on SDS-PAGE gels and blotted onto membranes for detection of tyrosine phosphorylation (4G10, Millipore, MA, USA) and EGFR abundance (sc-03, Santa Cruz Biotechnology). Alpha-tubulin was detected in whole cell lysates and used as a housekeeping control (T6199, Sigma Aldrich, Zwijndrecht, the Netherlands).

Fluorescence recovery after photobleaching (FRAP)- The experiments were performed essentially as described previously [5]. GFP-TRPM6 expressing HEK293 cells were plated onto glass Petri dish chambers (0.17 mm thick Wilco Wells, USA) and mounted on a confocal laser-scanning microscope (Zeiss LSM 510). Cells were kept in a standard solution (130 mM NaCl, 20 mM HEPES/Tris, 5 mM KCl, 5 mM glucose, 1 mM CaCl₂, 1 mM MgCl₂, pH 7.4). After defining two regions of interest (ROI) and subsequent recording two base-line fluorescence measurements, irreversible photobleaching of one ROI was initiated. Following photobleaching, fluorescence of both ROI's was measured over a 4 min period. Recovery in fluorescence was calculated from baseline measurements. The unbleached ROI was used to correct for photobleaching induced by image acquisition. The FRAP data was fitted by nonlinear regression analysis using previously published equations [23]. Between 14-16 cells were measured in each experimental condition.

Statistical analysis- Values are presented as means ± SEM. Comparisons between two groups were made using an unpaired t-test. Statistical significance was determined by ANOVA in the patch clamp and FRAP experiments. p<0.05 is considered statistically significant.

Acknowledgements

This work was supported by the Netherlands Organization for Scientific Research (ZonMw 9120.6110, 91208026), EURYI award from the European Science Foundation, and the Dutch Kidney foundation (C03.6017, C05.4106). We would like to thank Titia Woudenberg-Vrenken, Tom Nijenhuis, Henk Arnts, Annemiete W.C.M van der Kemp, and Jeroen van Leeuwen for technical and scientific contributions to this work.

References

1. Schlingmann KP, Weber S, Peters M, *et al.*: Hypomagnesemia with secondary hypocalcemia is caused by mutations in TRPM6, a new member of the TRPM gene family. *Nat Genet* 31:166-170, 2002
2. Walder RY, Landau D, Meyer P, *et al.*: Mutation of TRPM6 causes familial hypomagnesemia with secondary hypocalcemia. *Nat Genet* 31:171-174, 2002
3. Groenestege WM, Hoenderop JG, van den Heuvel L, *et al.*: The epithelial Mg²⁺ channel transient receptor potential melastatin 6 is regulated by dietary Mg²⁺ content and estrogens. *J Am Soc Nephrol* 17:1035-1043, 2006
4. Voets T, Nilius B, Hoefs S, *et al.*: TRPM6 forms the Mg²⁺ influx channel involved in intestinal and renal Mg²⁺ absorption. *J Biol Chem* 279:19-25, 2004
5. Thebault S, Alexander RT, Tiel Groenestege WM, *et al.*: EGF increases TRPM6 activity and surface expression. *J Am Soc Nephrol* 20:78-85, 2009
6. Groenestege WM, Thebault S, van der Wijst J, *et al.*: Impaired basolateral sorting of pro-EGF causes isolated recessive renal hypomagnesemia. *J Clin Invest* 117:2260-2267, 2007
7. Tejpar S, Piessevaux H, Claes K, *et al.*: Magnesium wasting associated with epidermal-growth-factor receptor-targeting antibodies in colorectal cancer: a prospective study. *Lancet Oncol* 8:387-394, 2007
8. Schrag D, Chung KY, Flombaum C, *et al.*: Cetuximab therapy and symptomatic hypomagnesemia. *J Natl Cancer Inst* 97:1221-1224, 2005
9. Mendelsohn J, Baselga J: Epidermal growth factor receptor targeting in cancer. *Semin Oncol* 33:369-385, 2006
10. Gatzemeier U, Pluzanska A, Szczesna A, *et al.*: Phase III study of erlotinib in combination with cisplatin and gemcitabine in advanced non-small-cell lung cancer: the Tarceva Lung Cancer Investigation Trial. *J Clin Oncol* 25:1545-1552, 2007
11. Pollack VA, Savage DM, Baker DA, *et al.*: Inhibition of epidermal growth factor receptor-associated tyrosine phosphorylation in human carcinomas with CP-358,774: dynamics of receptor inhibition in situ and antitumor effects in athymic mice. *J Pharmacol Exp Ther* 291:739-748, 1999
12. Hidalgo M, Bloedow D: Pharmacokinetics and pharmacodynamics: maximizing the clinical potential of Erlotinib (Tarceva). *Semin Oncol* 30:25-33, 2003
13. Hidalgo M, Siu LL, Nemunaitis J, *et al.*: Phase I and pharmacologic study of OSI-774, an epidermal growth factor receptor tyrosine kinase inhibitor, in patients with advanced solid malignancies. *J Clin Oncol* 19:3267-3279, 2001
14. Moyer JD, Barbacci EG, Iwata KK, *et al.*: Induction of apoptosis and cell cycle arrest by CP-358,774, an inhibitor of epidermal growth factor receptor tyrosine kinase. *Cancer Res* 57:4838-4848, 1997
15. Schaefer G, Shao L, Totpal K, *et al.*: Erlotinib directly inhibits HER2 kinase activation and downstream signaling events in intact cells lacking epidermal growth factor receptor expression. *Cancer Res* 67:1228-1238, 2007
16. Anast CS, Mohs JM, Kaplan SL, *et al.*: Evidence for parathyroid failure in magnesium deficiency. *Science* 177:606-608, 1972
17. Rude RK, Oldham SB, Singer FR: Functional hypoparathyroidism and parathyroid hormone end-organ resistance in human magnesium deficiency. *Clin Endocrinol (Oxf)* 5:209-224, 1976
18. Hoenderop JGJ, Hartog A, Stuver M, *et al.*: Localization of the Epithelial Ca²⁺ Channel in Rabbit Kidney and Intestine. *J Am Soc Nephrol* 11:1171-1178, 2000
19. Pfaffl MW, Horgan GW, Dempfle L: Relative expression software tool (REST) for group-wise comparison and statistical analysis of relative expression results in real-time PCR. *Nucleic Acids Res* 30:e36, 2002
20. Nijenhuis T, Hoenderop JG, Bindels RJ: Downregulation of Ca(2+) and Mg(2+) transport proteins in the kidney explains tacrolimus (FK506)-induced hypercalciuria and hypomagnesemia. *J Am Soc Nephrol* 15:549-557, 2004

21. Topala CN, Groenestegge WT, Thebault S, *et al.*: Molecular determinants of permeation through the cation channel TRPM6. *Cell Calcium* 41:513-523, 2007
22. Alwan HA, van Zoelen EJ, van Leeuwen JE: Ligand-induced lysosomal epidermal growth factor receptor (EGFR) degradation is preceded by proteasome-dependent EGFR deubiquitination. *J Biol Chem* 278:35781-35790, 2003
23. Yguerabide J, Schmidt JA, Yguerabide EE: Lateral mobility in membranes as detected by fluorescence recovery after photobleaching. *Biophys J* 40:69-75, 1982



A missense mutation in the Kv1.1 voltage-gated potassium channel-encoding gene *KCNA1* is linked to human autosomal dominant hypomagnesemia

Jenny van der Wijst^{1*}, Bob Glaudemans^{1*}, Rosana H. Scola², Paulo J. Lorenzoni², Angelien Heiser³, AnneMiete W. van der Kemp¹, Nine V. Knoers³, Joost G.J. Hoenderop¹, René J.M. Bindels¹

* contributed equally to this work

¹Department of Physiology, Radboud University Nijmegen Medical Centre, Nijmegen, The Netherlands

²Neuromuscular Disorders Division, Clinical Hospital, Parana Federal University, Curitiba, Parana, Brazil

³Department of Human Genetics, Radboud University Nijmegen Medical Centre, Nijmegen, The Netherlands

Summary

Primary hypomagnesemia forms a heterogeneous group of disorders characterized by renal or intestinal magnesium (Mg^{2+}) wasting, resulting in tetany, cardiac arrhythmias, and seizures. The kidney plays an essential role in maintaining blood Mg^{2+} levels with a prominent function for the Mg^{2+} -transporting channel TRPM6 in the distal convoluted tubule (DCT). In DCT, Mg^{2+} reabsorption is an active transport process primarily driven by the negative potential across the luminal membrane. Here, by use of a positional cloning approach in a family with isolated autosomal dominant hypomagnesemia we identified a N²⁵⁵D mutation in *KCNA1*, a gene encoding the voltage-gated potassium (K^+) channel Kv1.1. Patch clamp analysis showed that the mutation results in a non-functional channel with a dominant negative effect on wild-type Kv1.1 channel functioning. Cell surface biotinylation experiments demonstrated that wild-type Kv1.1, Kv1.1 N²⁵⁵D and combinations hereof were able to reach the plasma membrane in similar amounts. Furthermore, Kv1.1 is expressed in the kidney, where it co-localizes with the Mg^{2+} -permeable channel TRPM6 along the luminal membrane of DCT. Thus, Kv1.1 is a renal K^+ channel that establishes a favorable luminal membrane potential in DCT cells to control the TRPM6-mediated Mg^{2+} reabsorption.

Introduction

Occurrence of hypomagnesemia (serum Mg^{2+} levels below 0.70 mM) in the general population has been estimated around 2%, while hospitalized patients are more prone to develop hypomagnesemia (12%) [1]. Recent studies of intensive care patients have even estimated frequencies as high as 60% [2]. The blood Mg^{2+} concentration depends on the renal Mg^{2+} excretion in response to altered uptake by the intestine. Hence, the kidney is essential for the maintenance of the Mg^{2+} balance [3]. The majority of filtered Mg^{2+} is reabsorbed along the proximal tubule and the thick ascending limb of Henle's loop via a passive paracellular pathway [4]. However, fine-tuning of Mg^{2+} excretion occurs in the distal convoluted tubule (DCT) in an active transcellular fashion initiated by the Mg^{2+} -permeable Transient Receptor Potential Melastatin subtype 6 channel (TRPM6) [5, 6]. Since the extra- and intracellular Mg^{2+} concentration are both in the millimolar range, it has been hypothesized that the membrane potential across the luminal membrane acts as the primary driving force for Mg^{2+} entry via TRPM6 [6, 7]. Previously, genetic studies in families with hereditary renal Mg^{2+} wasting syndromes revealed several new genes involved in Mg^{2+} homeostasis, including tight junction proteins claudin 16 and 19 [8, 9], the thiazide-sensitive sodium chloride cotransporter (NCC) [10], the γ -subunit of the Na^+,K^+ -ATPase (FXD2) [11], TRPM6 [12, 13] and the recently discovered magnesiotropic hormone epidermal growth factor (EGF) [14]. Despite these discoveries, our knowledge of renal Mg^{2+} handling remains far from complete.

Results

A heterozygous KCNA1 A763G mutation is causative for hypomagnesemia

Here, we identified a large Brazilian family (46 family members of which 21 affected) with autosomal dominant hypomagnesemia (Fig. 1A). Affected individuals showed low serum Mg^{2+} levels (< 0.40 mM, normal range 0.70-0.95 mM), while their urinary Mg^{2+} excretion was normal, suggesting impaired tubular Mg^{2+} reabsorption. The phenotype of the proband (IV-3, Fig. 1A) starting from infancy consists of recurrent muscle cramps, tetanic episodes, tremor and muscle weakness, especially in distal limbs.

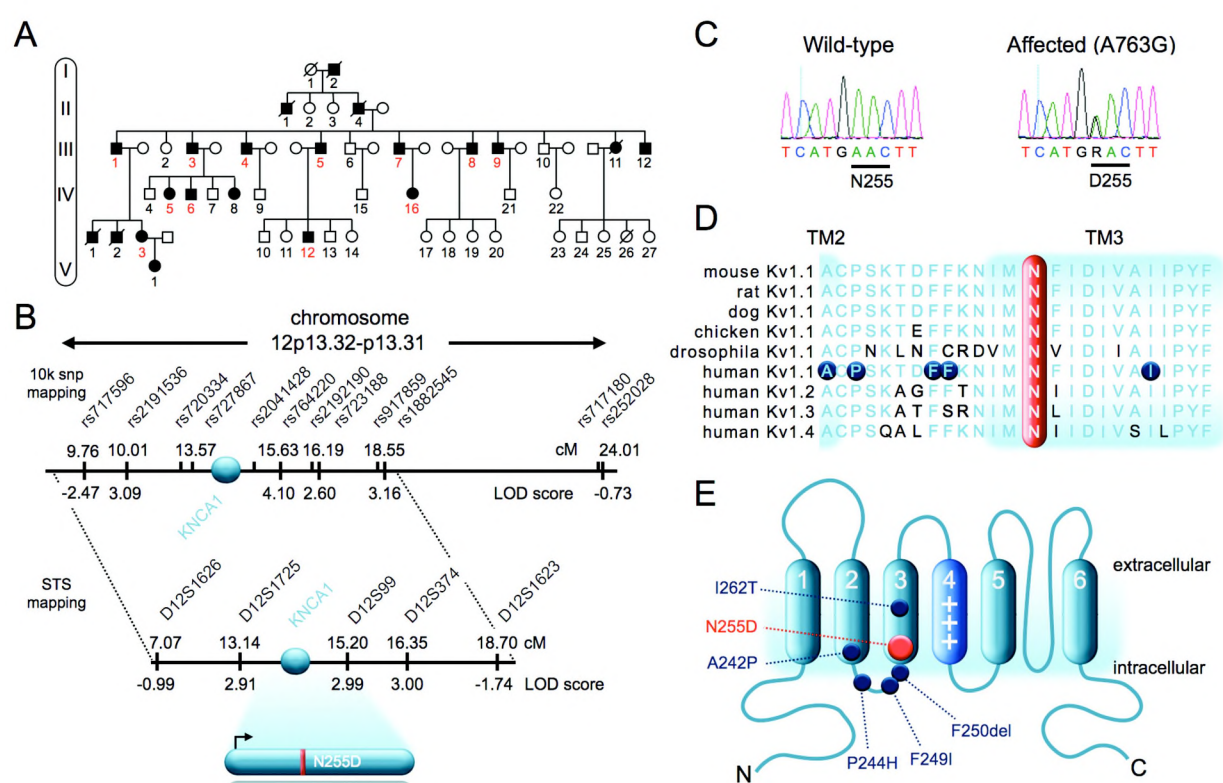


Figure 1. Heterozygous *KCNA1* A763G mutation causes isolated hypomagnesemia. **A.** Pedigree with 5 generations (I-V) of a Brazilian family with autosomal dominant hypomagnesemia. Affected family members are depicted in black, male and female members are shown as squares and circles, respectively. A diagonal line indicates that the individual is deceased. The light gray number indicates individuals included in the STS mapping. **B.** A 10K SNP array-based haplotyping approach was performed that showed linkage to a 14,3 cM region between SNP rs717596 and rs252028 on the short arm of chromosome 12. This region was confirmed and narrowed down to a 11,6 cM region between markers D12S1626 and D12S1623 containing 31 genes, including the *KCNA1* gene. **C.** Mutation analysis of *KCNA1* revealed a heterozygous A763G missense mutation in affected individual III-1. *KCNA1* encodes the voltage-gated potassium channel Kv1.1 where the observed mutation results in a N²⁵⁵D amino acid substitution (underlined). **D.** Multiple alignment analysis shows conservation of the N²⁵⁵ amino acid (gray bar) among species and Kv1 family members. Mutated amino acids in other families with the Kv1.1 genotype are depicted as dark gray dots [16-19]. Gray and black colored letters represent conserved and non-conserved amino acids, respectively. **E.** Schematic representation of the Kv1.1 channel that consists of a voltage sensor in transmembrane segment S4 and a pore forming region (S5 and S6). Localization of the newly identified N²⁵⁵D mutation is denoted by the light gray dot, while other nearby mutations are indicated by dark gray dots.

A single nucleotide polymorphism (SNP)-based linkage analysis identified a 14.3 cM locus on the short arm of chromosome 12 (Fig. 1B) which was subsequently narrowed down by fine mapping with microsatellite markers to an 11.6 cM region containing 31 genes between the markers D12S1626 and D12S1623 (maximum multipoint LOD score 3.0) (Fig. 1B; Fig. 2). Other genes previously associated with hypomagnesemia are located outside this critical region and therefore excluded as a candidate gene in our family. From the identified locus we sequenced *KCNA1* and identified a heterozygous mutation A763G (Fig. 1C) in the affected individual III-1 (Fig. 1A) that co-segregates with the disorder and was absent in 100 control chromosomes (data not shown). *KCNA1* encodes the *Shaker*-related voltage-gated K⁺ channel Kv1.1 in which the identified mutation causes substitution of the highly conserved asparagine at position 255 for an aspartic acid (N²⁵⁵D) (Fig. 1D). The predicted amino acid topology of Kv channels shows six transmembrane spanning α -helical segments (S1-6), with the S4 segment acting as the voltage-sensor and a hydrophobic pore region between S5 and S6 (Fig. 1E) [15]. The newly identified N²⁵⁵D mutation is positioned in the third transmembrane segment (S3) close to the voltage sensor (Fig. 1E).

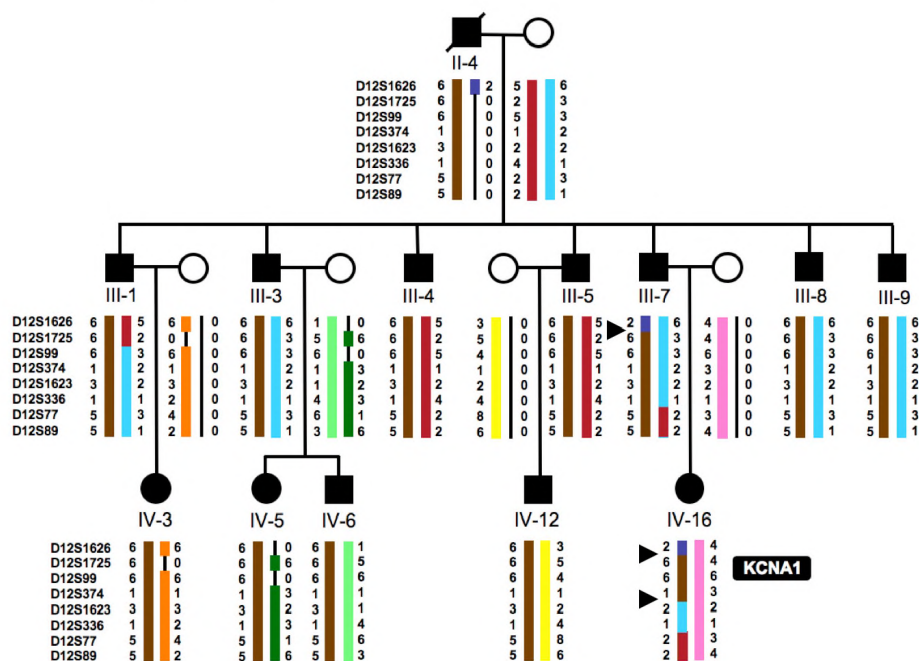


Figure 2. Haplotype analysis of the autosomal dominant hypomagnesemia locus on the short arm of chromosome 12 in the Brazilian family. Affected family members are shown in black; circles and squares refer to female and male individuals, respectively. A diagonal line indicates that the individual is deceased. Microsatellite markers are depicted on the left. The haplotypes are illustrated by different colors. The brown haplotype co-segregates with the disease. Critical recombinations are pinpointed by arrowheads (▶) in individuals III-7 (telomeric) and IV-16 (centromeric). *KCNA1* is located within the critical region between markers D12S1725 and D12S99 (black bar).

Localization of *Kv1.1* in the DCT of the kidney

So far, all proteins implied in familial hypomagnesemia, have been shown to be expressed in kidney underlining the pivotal role of this organ in body Mg²⁺ homeostasis. To study the (sub)cellular

localization of Kv1.1 in kidney, we used a rabbit polyclonal antibody raised against the Kv1.1 channel. Immunopositive staining was observed along the luminal membrane of distinct tubules present in the superficial cortex of the mouse kidney (Fig. 3). Using serial kidney sections, we demonstrated that Kv1.1 co-localizes with the epithelial Mg^{2+} channel TRPM6 in DCT (Fig. 3A). To confirm this localization we co-stained kidney sections for Kv1.1 and calbindin- D_{28K} , showing a partial overlap in Kv1.1 and calbindin- D_{28K} expression (Fig. 3B). This pattern can be explained by earlier observations that calbindin- D_{28K} , besides in DCT, is also expressed in connecting tubule (CNT) [20], confirming that Kv1.1 is localized primarily in DCT. Indeed, co-staining between Kv1.1 and aquaporin-2 (AQP2), a marker for CNT and the collecting duct, was not observed (Fig. 3C). These findings support the restricted localization of Kv1.1 in the Mg^{2+} -transporting DCT segment of the kidney.

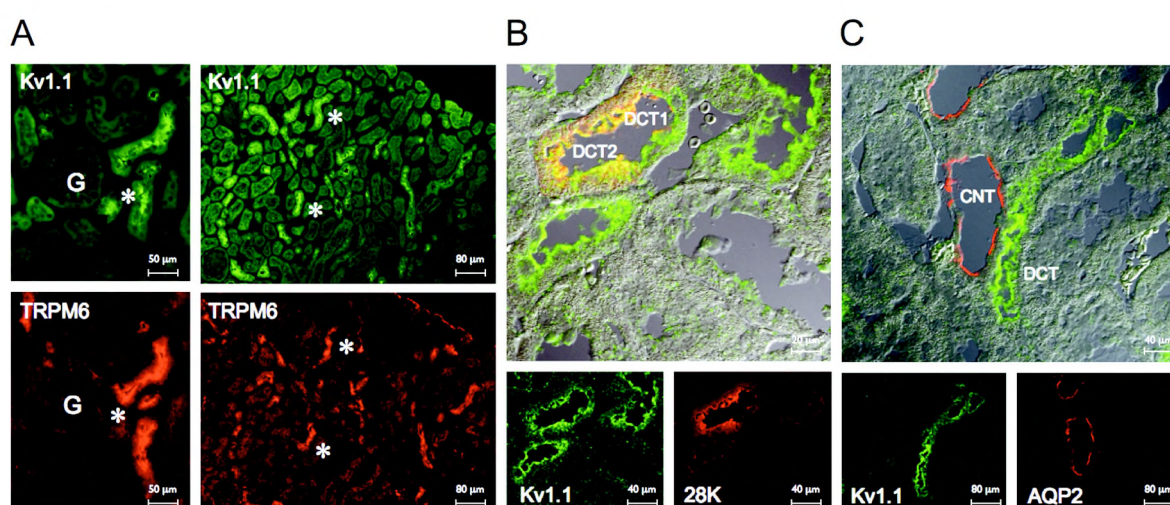


Figure 3. Immunohistochemical analysis of Kv1.1 in kidney. *A.* Staining for Kv1.1 and TRPM6 of mouse serial kidney sections (right panels, overview of a cortical region; left panels, magnified images of immunopositive tubules). The asterisks indicate the same distal tubules on serial sections intensively stained for Kv1.1 and TRPM6. *B.* Mouse kidney sections were co-stained for Kv1.1 and calbindin- D_{28K} (lower panels, immunopositive tubules; upper panel, merged DIC (differential interference contrast) image). *C.* Co-staining of Kv1.1 and aquaporin-2 in mouse kidney sections (lower panels, immunopositive tubules; upper panel, merged DIC image). Abbreviations used: G, glomerulus; DCT, distal convoluted tubule; CNT, connecting tubule; 28K, calbindin- D_{28K} ; AQP2, aquaporin-2. Bar denotes the indicated magnification.

Kv1.1 N255D results in non-functional channels with dominant negative effect on wild-type channel function

To determine the effect of the Kv1.1 N²⁵⁵D mutation on channel activity, Human Embryonic Kidney 293 (HEK293) cells were transiently transfected with mock, wild-type Kv1.1 and/or Kv1.1 N²⁵⁵D. Using the whole-cell patch clamp technique, outward K^+ currents were measured by dialyzing the cells with a pipette solution containing 140 mM K^+ . Cells expressing wild-type Kv1.1 channels produced typical delayed rectifying currents, while Kv1.1 N²⁵⁵D-expressing HEK293 cells showed small currents similar to mock-expressing cells (Fig. 4A,B). Considering the autosomal dominant inheritance in our family, a potential dominant negative effect was investigated by co-transfection of

equal amounts of plasmid DNA encoding wild-type Kv1.1, Kv1.1 N²⁵⁵D or mock in HEK293 cells. The K⁺ current amplitude in HEK293 cells co-expressing wild-type Kv1.1 and Kv1.1 N²⁵⁵D was significantly reduced compared to cells expressing wild-type Kv1.1 alone or co-expressing wild-type Kv1.1 and mock ($P < 0.05$) (Fig. 4C). Next, the influence of Kv1.1 N²⁵⁵D expression on the amount of Kv1.1 channels at the plasma membrane was examined by cell surface biotinylation experiments. As shown in Fig. 4D, co-expression of wild-type Kv1.1 and Kv1.1 N²⁵⁵D in HEK293 cells did not affect the plasma membrane localization of Kv1.1 channels. Of note, Kv1.1 was equally expressed in all conditions as analyzed in the total cell lysates (Fig. 4D, bottom panel). Kv1.1 channels are composed of four subunits and this result suggests that similar amounts of both homotetrameric channels wild-type Kv1.1 and Kv1.1 N²⁵⁵D, and heterotetrameric channels composed of wild-type Kv1.1 with Kv1.1 N²⁵⁵D are located at the plasma membrane.

Kv1.1 regulates TRPM6 Mg²⁺ influx by setting the membrane potential

Since Kv1.1 and TRPM6 are present in the same nephron segment, we investigated by which mechanism Kv1.1 controls Mg²⁺ influx through TRPM6. We studied the potential direct effect of Kv1.1 on TRPM6 activity by patch clamp analysis. To this end, TRPM6 (1.0 µg) was co-transfected with mock (0.1 µg), wild-type Kv1.1 (0.1 µg) or Kv1.1 N²⁵⁵D (0.1 µg) in HEK293 cells. The TRPM6-mediated Na⁺ currents between the three experimental conditions were virtually identical (Fig. 4E). Subsequently, the current clamp mode of the patch clamp technique was used to measure the membrane potential of HEK293 cells expressing wild-type Kv1.1 or Kv1.1 N²⁵⁵D. A significant hyperpolarization ($P < 0.05$) was observed in wild-type Kv1.1-expressing HEK293 cells (-39±3 mV, n=9) compared to mock or Kv1.1 N²⁵⁵D -expressing cells (-3±1 mV, n=7, and -8±2 mV, n=7, respectively). Dendrotoxin K (DTX-K, 10 nM), a specific Kv1.1 channel blocker, significantly depolarized the membrane potential in wild-type Kv1.1-expressing cells (from -39±3 mV to -14±2 mV, n=8, $P < 0.05$) (Fig. 4F). The membrane potential of mock or Kv1.1 N²⁵⁵D -expressing cells was not affected by DTX-K application (Fig. 4F). Furthermore, co-transfection of wild-type Kv1.1 and Kv1.1 N²⁵⁵D resulted in an intermediate hyperpolarization compared to the cells expressing only wild-type Kv1.1 (-23±1 mV vs. -39±3 mV, respectively, n=15, $P < 0.05$). These results suggest that the Kv1.1 N²⁵⁵D channel diminishes the negative membrane potential compared to the normal situation.

Discussion

In this study, we identified a large Brazilian family with autosomal dominant hypomagnesemia. Affected individuals showed low serum Mg²⁺ levels, while serum K⁺ and Ca²⁺ levels, and urinary Ca²⁺ excretion were not affected, which is distinct from previously described forms of inherited hypomagnesemia. For example, families bearing a mutation in claudin 16 and 19 (Familial

Hypomagnesemia with Hypercalciuria and Nephrocalcinosis; OMIM 248250) are hypercalciuric, while mutations in FXYD2 (Isolated Dominant Hypomagnesemia (IDH); OMIM 154020) and TRPM6 (Hypomagnesemia with Secondary Hypocalcemia; OMIM 602014) result in hypocalciuria and hypocalcemia, respectively.

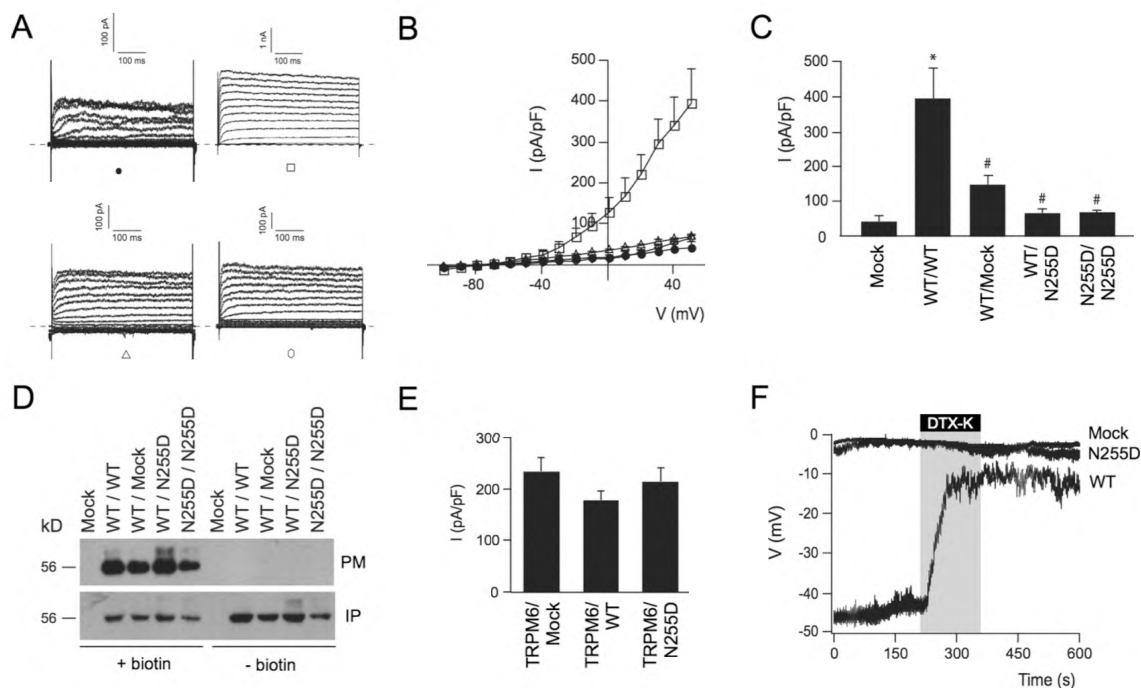


Figure 4. Electrophysiological analysis of mock, wild-type Kv1.1 (Kv1.1 WT) or Kv1.1 N²⁵⁵D transfected HEK293 cells. *A.* Representative original traces of outward K⁺ currents of mock (●), Kv1.1 WT (□), Kv1.1 N²⁵⁵D (Δ), or Kv1.1 WT and mock (◇) elicited by voltage steps from -100 to +50 mV in 10 mV increments, applied from a holding potential of -80 mV, every 10 s. *B.* The I-V relationships of mock (●, n=5), Kv1.1 WT (□, n=11), Kv1.1 N²⁵⁵D (Δ, n=10), Kv1.1 WT and mock (◇, n=9); *C.* Histogram presenting averaged current densities at +50 mV of mock (n=5), Kv1.1 WT (n=11), Kv1.1 WT and mock (n=9), Kv1.1 WT and Kv1.1 N²⁵⁵D (n=9), and Kv1.1 N²⁵⁵D (n=10). Asterisk indicates significance (P < 0.05) compared to mock while hash indicates significance (P < 0.05) compared to Kv1.1 WT. *D.* Cell surface biotinylation of mock, Kv1.1 WT, Kv1.1 WT and mock, Kv1.1 WT and Kv1.1 N²⁵⁵D, and Kv1.1 N²⁵⁵D transfected HEK293 cells. Kv1.1 expression was analyzed by immunoblotting for plasma membrane fraction (PM) and input from the total cell lysates (IP). Representative immunoblot of four independent experiments is shown. *E.* Histogram presenting averaged current densities at +80 mV after 200 s of TRPM6 and mock (n=26), TRPM6 and Kv1.1 WT (n=26), and TRPM6 and Kv1.1 N²⁵⁵D (n=25). *F.* Membrane potential of mock, Kv1.1 WT and Kv1.1 N²⁵⁵D upon acute application of Dendrotoxin K (DTX-K, 10 nM), measured in current clamp mode of whole-cell patch clamp configuration. Representative recordings of eight independent experiments are shown. The error bars denote SEM.

Furthermore, patients with Gitelman Syndrome (GS; OMIM 263800), caused by mutations in NCC, suffer from hypomagnesemia, hypocalciuria and hypokalemia. The phenotype in the proband starting from infancy consists of recurrent muscle cramps, tetanic episodes, tremor and muscle weakness, especially in distal limbs. Serum electrolyte levels were measured during severe attacks of cramps and tetany in two affected family members (proband V-3; V-2), with serum Mg²⁺ levels of 0.37 and 0.25 mM, respectively, while Ca²⁺ and K⁺ concentrations were normal. As a result, all

affected family members received a daily dose of magnesium chloride. Importantly, the proband was recently hospitalized because of a sudden episode of facial myokymia, tremor, severe muscle spasms, muscular pain, cramps, muscular weakness and tetanic contraction episodes, all of which improved shortly after intravenous magnesium treatment. This observation further confirmed that the observed symptoms are a consequence of the low serum Mg^{2+} levels.

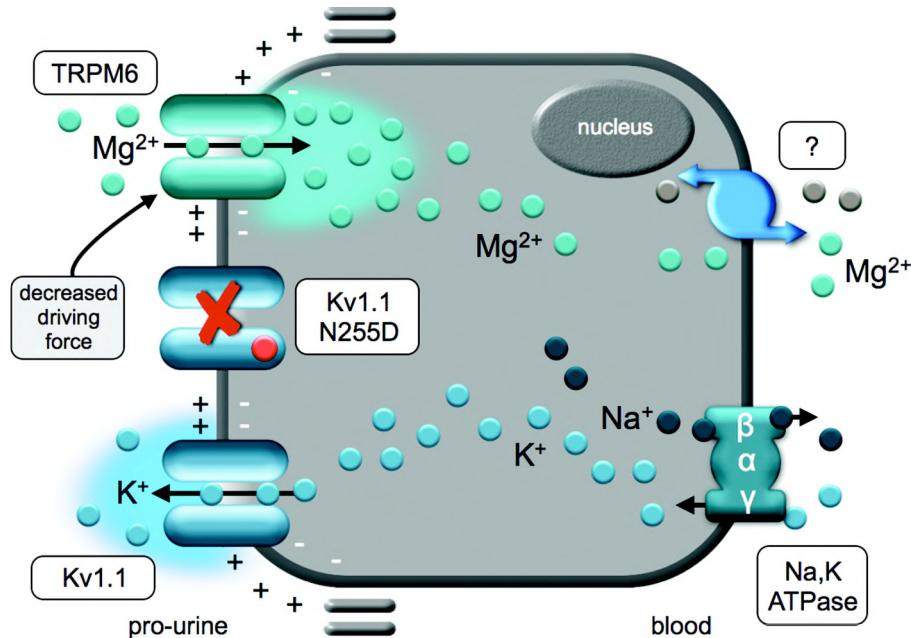


Figure 5. Schematic model of the Mg^{2+} -reabsorbing DCT cell in the kidney. Mg^{2+} uptake from the pro-urine via the epithelial Mg^{2+} channel TRPM6 is primarily driven by the negative potential across the luminal membrane. This luminal membrane potential is maintained by an apical K^+ efflux via Kv1.1 energized by the action of the Na^+,K^+ -ATPase. At the basolateral membrane, Mg^{2+} extrusion to the blood side occurs via an unknown mechanism. The identified $N^{255}D$ mutation results in a non-functional Kv1.1 channel and thereby decreases the driving force for Mg^{2+} influx, thus resulting in renal Mg^{2+} wasting.

By use of a positional cloning approach we revealed a heterozygous mutation in *KCNA1*, encoding the voltage-gate potassium channel Kv1.1, by which the asparagine at amino acid position 255 was converted into an aspartic acid ($N^{255}D$). Remarkably, the Kv1.1 $N^{255}D$ genotype causes hypomagnesemia, whereas mutations in *KCNA1* thus far have been shown to result in episodic ataxia type 1 (EA1). Fig. 1D/E shows the previously identified mutations in close proximity to the $N^{255}D$ mutation [16-19, 21, 22]. EA1 is a dominant human neurological disorder presumably caused by defective Kv1.1 in the cerebellum. Furthermore, abnormal Kv1.1 activity originating in the distal motor axons results in muscle hyperactivity, indicative for myokymia [23, 24]. In addition to the classical description of this disorder, phenotypic variants include EA1 with partial epilepsy [17, 21], EA1 without myokymia [22], and isolated neuromyotonia [17]. We also analyzed the affected members of our Brazilian family for episodic ataxia. On a cerebral MRI of the proband we obtained evidence of a slight atrophy of the cerebral vermis (data not shown). Furthermore, electromyographs of some affected members showed myokymic discharge in line with the previously observed mixed

phenotype (data not shown). Now, we present hypomagnesemia as a new phenotypic characteristic associated with a mutation in *KCNA1*. Thus, it would be highly interesting to perform in the near future a large-scale phenotypical characterisation of patients with identified mutations in the *KCNA1* gene including neurological description, serum Mg^{2+} levels and functional analysis of the corresponding Kv1.1 mutations.

Previously, genetic studies in familial hypomagnesemia revealed several new proteins with a predominant expression in kidney underlining its involvement in Mg^{2+} homeostasis. Our immunohistochemical data clearly demonstrated localization of Kv1.1 along the luminal membrane of TRPM6-expressing DCT cells consistent with a potential link between Kv1.1-mediated K^+ secretion and Mg^{2+} influx by TRPM6. Therefore, we assessed the role of Kv1.1 in controlling Mg^{2+} influx through TRPM6. Electrophysiological analysis of wild-type Kv1.1 and Kv1.1 N²⁵⁵D revealed that the mutation results in a non-functional Kv1.1 channel. Kv1.1 channels consist of four subunits arranged symmetrically around an aqueous pore, forming a so-called tetrameric structure [25, 26]. It has been shown that Kv1.1 channel subunits can assemble with other Kv channel subunits to form heterotetramers [27]. Importantly, hypomagnesemia in the Brazilian family is inherited in an autosomal dominant manner and patients with the N²⁵⁵D mutation are heterozygous. Expression of both alleles likely results in the formation of heterotetrameric channels composed of wild-type and mutated channel subunits leading to a dominant negative effect by the Kv1.1 N²⁵⁵D subunit, as shown in this study. The mutation replaces a neutral amino acid (asparagine) by one with an acidic side-chain (aspartic acid), which may destabilize the secondary or tertiary channel structure and thereby channel formation or trafficking. However, we demonstrated that wild-type Kv1.1 channels, Kv1.1 N²⁵⁵D channels, and the combination hereof are expressed in equal amounts at the plasma membrane.

Considering the striking localization of Kv1.1 in the TRPM6-expressing distal convoluted tubules, we investigated a potential direct functional effect of Kv1.1 on TRPM6 activity. However, wild-type Kv1.1 nor Kv1.1 N²⁵⁵D altered the TRPM6-mediated Na^+ currents and it is, therefore, unlikely that Kv1.1 directly regulates the activity of the Mg^{2+} -permeable channel TRPM6. Mg^{2+} is actively reabsorbed in the DCT. Here, Mg^{2+} influx through TRPM6 is driven by a favorable membrane voltage [6, 7]. This membrane potential is maintained by a so far unidentified apical K^+ efflux pathway, while the K^+ gradient is provided by the basolaterally localized Na^+,K^+ -ATPase. Previously, a mutation in the Na^+,K^+ -ATPase γ subunit was shown to be the underlying cause for autosomal dominant renal Mg^{2+} wasting and secondary hypocalciuria [11]. Interestingly, K^+ efflux through K^+ -permeable channels primarily determines the resting membrane potential. Kv channels are widely expressed in excitable and non-excitable cells, where they play an essential role in the establishment of the electrical properties of the cell, instrumental for many processes [28]. By use of the current clamp mode of the patch clamp technique we demonstrated that Kv1.1 significantly hyperpolarizes the plasma membrane compared to mock or Kv1.1 N²⁵⁵D -expressing cells. This effect was reversible by DTX-K, a specific Kv1.1 channel blocker, confirming the involvement of Kv1.1 in

setting the negative membrane potential. We now hypothesize that the voltage-gated Kv1.1 channel is responsible for the establishment of the negative membrane potential across the luminal membrane of the DCT cell. The N²⁵⁵D mutation leads to depolarization of the luminal membrane, notably diminishing the driving force for Mg²⁺ uptake from the pro-urine (Fig. 5).

In conclusion, a new direct coupling between K⁺ secretion and active Mg²⁺ reabsorption is disclosed by this study, which is highlighted by our discovery of the N²⁵⁵D mutation in the *KCNAl* gene in autosomal dominant hypomagnesemia. The encoded K⁺ channel Kv1.1 co-localizes with the Mg²⁺ influx channel TRPM6 along the luminal membrane of DCT, the main site of active renal Mg²⁺ reabsorption. Kv1.1 channels harboring the N²⁵⁵D mutation show close to background currents impairing their ability to set a favorable membrane potential facilitating TRPM6-mediated Mg²⁺ influx. These findings will open a new window for other studies on the interrelationship of renal K⁺ and Mg²⁺ disturbances.

Material and methods

Subjects- We identified a large family (46 family members, 21 affected) with autosomal dominant hypomagnesemia (Fig 1A). Phenotype in the proband (IV-3) starting from infancy; recurrent muscle cramps, tetanic episodes, tremor and muscle weakness, especially in distal limbs. There were no seizures, recurrent urinary tract infections, polyuria, polydipsia and renal stones. At 4 years, a significant hypomagnesemia (0.37 mM; normal 0.70-0.95 mM) was determined. Serum K⁺ (3.9 mM; normal 3.5-5.0 mM), Ca²⁺ (2.35 mM; normal 2.15-2.50 mM), sodium, phosphate, uric acid, bicarbonate, urea, creatinine, glucose, bilirubin, aminotransferases, alkaline phosphate, lactate dehydrogenase were all normal. Urinary creatinine clearance, urinary Mg²⁺ excretion (2.8 mmol/24h; normal 2.1-6.2 mmol/24h) and Ca²⁺ excretion were also normal. The patient received a daily dose of magnesium chloride, which improved muscular weakness, but slight muscle cramps persisted particularly after physical activity. One of her younger brothers (IV-1, Fig. 1A) died in infancy by a severe attack of cramps and tetany. At that time the serum Mg²⁺ level was as low as 0.28 mM. In addition to these two patients 18 other family members had shown similar clinical manifestations and biochemical features. The proband was tested for signs of cerebellar dysfunction, and admitted to have experienced several periods of uncertainty in walking, where she was not able to walk straight. Objective clinical signs of cerebellar dysfunction, including nystagmus, multistep or overshoot saccades, dysmetria in the finger-nose test, and decomposition of movement of the legs on heel-to-shin test, were absent. However, on a cerebral MRI of the proband we found evidence of slight atrophy of the cerebral vermis (data not shown). Furthermore, electromyographs of some affected members showed myokymic discharge in line with the previously observed mixed phenotype. We collected blood samples of the family members (both affected and non-affected; Fig.1A) for linkage analysis. Subsequently, DNA was extracted according to standard protocols. Control genomic DNA

samples (n=100) were kindly provided by Dr. H. van Bokhoven (Department of Human Genetics, Radboud University Nijmegen Medical Centre, The Netherlands). The study was approved by the Clinical Hospital, Parana Federal University (Curitiba, Parana, Brazil) and written informed consent was obtained from the subjects.

Genetic linkage analysis- A genome-wide linkage approach was performed for 12 family members selected based on simulations in SLINK using the Affymetrix GeneChip[®] mapping 10K 2.0 Array harboring 10,204 SNPs. Sample preparation and hybridization was performed according to the manufacturer's protocol (Affymetrix, Inc., Santa Clara, CA, USA) [29]. Briefly, 250 ng of genomic DNA was digested using 10 units *Xba*I (Westburg, Leiden, The Netherlands) followed by ligation using T4 DNA ligase (Westburg) of universal adaptors to the digested products. Primers complementary to the adaptors were used for amplification of the digested products. After purification of the products using MinElute[™] plates (Qiagen, Venlo, The Netherlands) a fragmentation was performed on 20 µg purified PCR product. Fragmented products were end-labeled and hybridized to the Affymetrix 10K GeneChip[®] overnight. Hybridized arrays were washed and stained using the Fluidics Station 400 (Affymetrix). The GeneChip[®] Scanner 3000 was used to scan the hybridized arrays. Automatic SNP calls were generated using GeneChip DNA analysis software (GDAS; Affymetrix). SNP calls are AA or BB for homozygous SNPs, AB for heterozygous SNPs. When the software was unable to make a call (AA, BB or AB), the SNP was scored as No Call. LOD scores were calculated using Merlin software (www.sph.umich.edu/csg/abecasis/Merlin/index.html). Eight microsatellite markers (D12S1626, D12S1725, D12S99, D12S374, D12S1623, D12S336, D12S77 and D12S89) were selected to fine-map the newly identified hypomagnesemia loci on the short arm of chromosome 12 (<http://genome.ucsc.edu/cgi-bin/hgGateway>). Marker analysis using fluorescently labeled primers was performed according to the protocol for the LMS-MD10 version 2.5 (Applied Biosystems, Nieuwerkerk a/d IJssel, The Netherlands). Reactions for each marker were performed separately, with products being pooled into size and label specific sets before typing. Markers were typed on an ABI 3730 DNA analyzer (Applied Biosystems) using GeneMapper 4.0 software (Applied Biosystems). Allele binning was performed with the Excel 2000 (Microsoft, Redmond, USA) macro Linkage-designer developed by van Camp and coworkers[30], and we checked Mendelian inheritance of alleles with PedCheck 1.0 software (<http://watson.hgen.pitt.edu>) [31]. Multipoint LOD score and haplotype analysis was performed with GeneHunter, version 2.1 release 5, in the easyLINKAGE software package[32] and HaploPainter software (haploPainter.sourceforge.net/html/index.html).

Mutation analysis- From the critical region, we selected the *KCNA1* gene for mutation analysis, using the UCSC genome browser database (<http://genome.ucsc.edu/>). DNA amplification reactions were performed in a thermal cycler with heated lid (MJ Research, PTC-200). The *KCNA1* exon

sequence and flanking regions were amplified from genomic DNA of individual III-1 (Fig. 1A) using multiple overlapping primer sets based on GenBank accession code BC101733 (Table 1). PCR products of correct sizes were selected by DNA agarose gel electrophoresis, following excision and subsequent purification with GenElute™ Gel Extraction Kit (Sigma-Aldrich) according to manufacturer's protocol. The fragments were sequenced on both strands by use of the ABI PRISM Big Dye Terminator Cycle Sequencing V2.0 Ready Reaction kit and the ABI PRISM 3730 DNA analyzer (Applied Biosystems).

Table 1. Overview of primers sets

	Primer sequence	
	Forward (5'-3')	Reverse (5'-3')
KCNA1 set 1	GAGGGGGATTCCAAACTGAG	AACTTCTCCATGGCCTCCTC
KCNA1 set 2	GTACTTCTTCGACCGCAACC	CCCAGCGTGATGAAATAAGG
KCNA1 set 3	CCCTTCTTCATCGTGAAAC	AGCAACTGAGCCTGCTCTTC
KCNA1 set 4	GACAATTGGAGGCAAGATCG	CCCAAATCCTCAATGCAAC

These primer sets, overlapping the human *KCNA1* coding region, were used for mutation analysis based on GenBank accession code BC101733.

Immunohistochemistry- Immunohistochemistry was performed as previously described [33]. In short, either co-immunohistochemical staining or staining of serial sections for Kv1.1 with TRPM6, calbindin-D_{28K} and AQP2, was performed on 7- μ m sections of fixated frozen mouse kidney samples. The mouse kidney cryosections were incubated for 16 hr at 4°C with the primary antibodies: rabbit anti-Kv1.1 (1:300) (Alamone #APC-009), guinea pig anti-TRPM6 (1:1000) [6], guinea pig anti-AQP2 (1:1000) (kindly provided by dr. P.M.T. Deen), and mouse anti-calbindin-D_{28K} (1:750) [34]. For detection of calbindin-D_{28K} and AQP2, sections were incubated with Alexa-conjugated secondary antibodies. The tyramide signal amplification kit (NEN Life Science Products, Zaventem, Belgium) was used after incubation with biotin-coated goat anti-rabbit and goat anti-guinea pig secondary antibodies to visualize Kv1.1 and TRPM6, respectively. Images were taken with a confocal laser scanning imaging system (Olympus Fluoroview, FV1000).

DNA constructs- The *KCNA1* wild-type and N²⁵⁵D mutant sequences were obtained by amplification of genomic DNA from a non-affected and affected family member respectively, using primers 5'-GCCGAATTCGGCCACCATGACGGTGATGTC-3' and 5'-GCCGTCGACATGCAACAACGCATTGACAG-3'. Both PCR products were cloned into pCMV-SPORT6 vectors (Invitrogen, Breda, The Netherlands) using restriction enzymes *EcoRI* and *SalI* following verification by sequence analysis. Subsequently, both the *KCNA1* wild-type and N²⁵⁵D sequences were subcloned via the Gateway® pDONR™221 entry vector into a pCIneo IRES-GFP destination clone creating human *KCNA1* pCIneo IRES GFP (wild-type Kv1.1) and human *KCNA1*

$N^{255}D$ pCIneo IRES GFP (Kv1.1 $N^{255}D$). The pCIneo IRES GFP construct was used as a control (mock) in the experiments. The wild-type TRPM6 pCIneo IRES GFP construct has been described previously (6).

Electrophysiology- HEK293 cells were cultured and transfected as described previously [35]. Whole-cell recordings were performed as described in a previous study [14]. Recorded Kv1.1 currents were evoked as described previously, using the same standard pipette and bath solutions[36]. The membrane potential of transfected HEK293 cells was measured using the current clamp mode, with continuous recording from a holding current of 0 pA. The pipette solution contained (mM): 140 KCl, 1 Na_2 -ATP, 10 HEPES/KOH (pH 7.3). The bath solution contained (mM): 138 NaCl, 5.4 KCl, 1.2 $MgCl_2$, 1 $CaCl_2$, 10 glucose, and 10 HEPES/KOH (pH 7.3). To measure TRPM6-mediated currents, a linear voltage ramp from -100 to +100 mV (within 450 ms) was applied every 2 s from a holding potential of 0 mV. The standard pipette solution contained 150 mM NaCl, 10 mM EDTA, and 10 mM HEPES/KOH (pH 7.2). The extracellular solutions contained 150 mM NaCl, 10 mM HEPES/KOH (pH 7.4). The analysis and display of patch clamp data were performed using Igor Pro software (WaveMetrics, Lake Oswego, USA). Current densities were obtained by normalizing the current amplitude to the cell membrane capacitance.

Cell surface biotinylation- HEK293 cells were transiently transfected using Lipofectamin 2000 (Invitrogen-Life Technologies) with 1 μ g DNA of wild-type Kv1.1, 1 μ g Kv1.1 $N^{255}D$, 1 μ g mock, or co-transfected with 0.5 μ g wild-type Kv1.1 and 0.5 μ g Kv1.1 $N^{255}D$. Cell surface labelling with biotin was performed as described previously [37]. At 48 hours after transfection, the biotinylation assay was performed. Cells were homogenized in 1 ml lysis buffer as described previously [37], using the sulfo-NHS-LC-LC-biotin (Pierce, Etten-Leur, The Netherlands). 1% of the total protein amount was collected as an input sample. Subsequently, biotinylated proteins (plasma membrane fraction) were precipitated using neutravidin-agarose beads (Pierce). Kv1.1 expression was analyzed by immunoblot analysis for the input and the plasma membrane fraction using the monoclonal Kv1.1 antibody (1:1000).

Chemicals and statistical analysis- The guinea pig antibody against AQP2 was kindly provided by Dr. P.M. Deen (Radboud University Nijmegen Medical Centre). Mouse anti-calbindin- D_{28K} was purchased from Sigma. Rabbit polyclonal and mouse monoclonal antibodies specific for Kv1.1 were purchased from Alamone Labs (Jerusalem, Israel) and Neuromab (Davis, CA, USA), for immunohistochemistry and Western Blotting, respectively. Dendrotoxin-K (DTX-K) was purchased from Sigma. Data are shown as mean \pm SEM. Statistical significance was determined using ANOVA Tukey's test. Differences in means with $P < 0.05$ were regarded as statistically significant. Statistical analysis was performed using Prism (GraphPad, San Diego, USA) software.

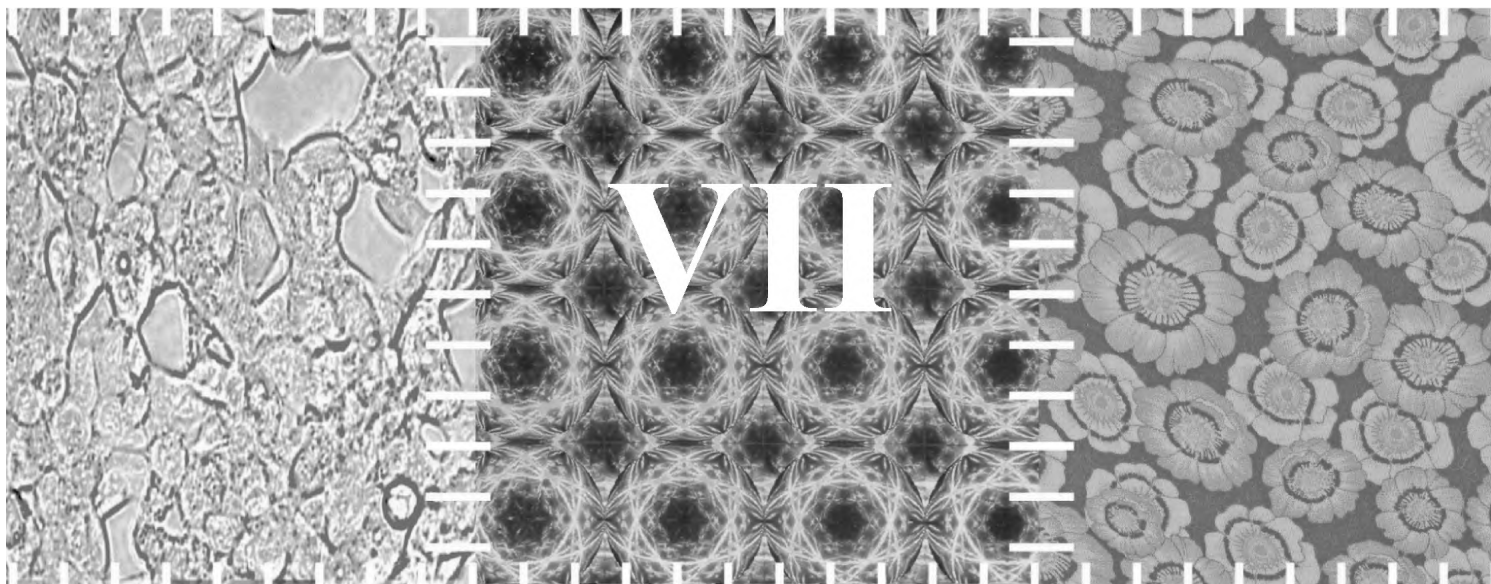
Acknowledgements

The authors thank Dr. H. van Bokhoven for providing genomic control DNA. We are grateful to our colleagues Dr. K. Lee, Mrs. A. Heister, Mrs. F. van Zeeland, Mrs. A. Forst, Mrs. M. Schijvenaars and Mr. R. Makkinje for technical assistance and helpful suggestions and to Drs. C. E. Silvado and L. C. Werneck for recruitment of the patients and their relatives. This study was supported financially by the Netherlands Organization for Scientific Research (ZonMw 9120.6110; ALW 700.55.302), EURYI award from the European Science Foundation and the Dutch Kidney foundation (C03.6017).

References

1. Wong ET, Rude RK, Singer FR, *et al.*: A high prevalence of hypomagnesemia and hypermagnesemia in hospitalized patients. *Am J Clin Pathol* 79:348-352, 1983
2. Chernow B: Hypomagnesemia in intensive care. Correction of units. *Chest* 95:1362, 1989
3. Konrad M, Schlingmann KP, Gudermann T: Insights into the molecular nature of magnesium homeostasis. *Am J Physiol Renal Physiol* 286:F599-605, 2004
4. Quamme GA: Renal magnesium handling: new insights in understanding old problems. *Kidney Int* 52:1180-1195, 1997
5. Dai LJ, Ritchie G, Kerstan D, *et al.*: Magnesium transport in the renal distal convoluted tubule. *Physiol Rev* 81:51-84, 2001
6. Voets T, Nilius B, Hoefs S, *et al.*: TRPM6 forms the Mg²⁺ influx channel involved in intestinal and renal Mg²⁺ absorption. *J Biol Chem* 279:19-25, 2004
7. Schweigel M, Lang I, Martens H: Mg²⁺ transport in sheep rumen epithelium: evidence for an electrodiffusive uptake mechanism. *Am J Physiol* 277:G976-982, 1999
8. Weber S, Hoffmann K, Jeck N, *et al.*: Familial hypomagnesaemia with hypercalciuria and nephrocalcinosis maps to chromosome 3q27 and is associated with mutations in the PCLN-1 gene. *Eur J Hum Genet* 8:414-422, 2000
9. Simon DB, Lu Y, Choate KA, *et al.*: Paracellin-1, a renal tight junction protein required for paracellular Mg²⁺ resorption. *Science* 285:103-106, 1999
10. Simon DB, Nelson-Williams C, Bia MJ, *et al.*: Gitelman's variant of Bartter's syndrome, inherited hypokalaemic alkalosis, is caused by mutations in the thiazide-sensitive Na-Cl cotransporter. *Nat Genet* 12:24-30, 1996
11. Meij IC, Koenderink JB, van Bokhoven H, *et al.*: Dominant isolated renal magnesium loss is caused by misrouting of the Na⁺,K⁺-ATPase gamma-subunit. *Nat Genet* 26:265-266, 2000
12. Schlingmann KP, Weber S, Peters M, *et al.*: Hypomagnesemia with secondary hypocalcemia is caused by mutations in TRPM6, a new member of the TRPM gene family. *Nat Genet* 31:166-170, 2002
13. Walder RY, Landau D, Meyer P, *et al.*: Mutation of TRPM6 causes familial hypomagnesemia with secondary hypocalcemia. *Nat Genet* 31:171-174, 2002
14. Groenestegge WM, Thebault S, van der Wijst J, *et al.*: Impaired basolateral sorting of pro-EGF causes isolated recessive renal hypomagnesemia. *J Clin Invest* 117:2260-2267, 2007
15. Aggarwal SK, MacKinnon R: Contribution of the S4 segment to gating charge in the Shaker K⁺ channel. *Neuron* 16:1169-1177, 1996
16. Browne DL, Gancher ST, Nutt JG, *et al.*: Episodic ataxia/myokymia syndrome is associated with point mutations in the human potassium channel gene, KCNA1. *Nat Genet* 8:136-140, 1994
17. Eunson LH, Rea R, Zuberi SM, *et al.*: Clinical, genetic, and expression studies of mutations in the potassium channel gene KCNA1 reveal new phenotypic variability. *Ann Neurol* 48:647-656, 2000
18. Klein A, Boltshauser E, Jen J, *et al.*: Episodic ataxia type 1 with distal weakness: a novel manifestation of a potassium channelopathy. *Neuropediatrics* 35:147-149, 2004
19. Shook SJ, Mamsa H, Jen JC, *et al.*: Novel mutation in KCNA1 causes episodic ataxia with paroxysmal dyspnea. *Muscle Nerve* 37:399-402, 2008
20. Hoenderop JG, Hartog A, Stuijver M, *et al.*: Localization of the epithelial Ca²⁺ channel in rabbit kidney and intestine. *J Am Soc Nephrol* 11:1171-1178, 2000
21. Zuberi SM, Eunson LH, Spauschus A, *et al.*: A novel mutation in the human voltage-gated potassium channel gene (Kv1.1) associates with episodic ataxia type 1 and sometimes with partial epilepsy. *Brain* 122 (Pt 5):817-825, 1999
22. Lee H, Wang H, Jen JC, *et al.*: A novel mutation in KCNA1 causes episodic ataxia without myokymia. *Hum Mutat* 24:536, 2004
23. da Silva AB, Japp HH, Saldanha A, *et al.*: [Isaacs' syndrome. Report of a case and review of the literature]. *Arq Neuropsiquiatr* 35:139-145, 1977
24. Newsom-Davis J, Mills KR: Immunological associations of acquired neuromyotonia (Isaacs' syndrome). Report of five cases and literature review. *Brain* 116 (Pt 2):453-469, 1993

25. Li M, Jan YN, Jan LY: Specification of subunit assembly by the hydrophilic amino-terminal domain of the Shaker potassium channel. *Science* 257:1225-1230, 1992
26. Baumann A, Grupe A, Ackermann A, *et al.*: Structure of the voltage-dependent potassium channel is highly conserved from *Drosophila* to vertebrate central nervous systems. *Embo J* 7:2457-2463, 1988
27. Shamotienko OG, Parcej DN, Dolly JO: Subunit combinations defined for K⁺ channel Kv1 subtypes in synaptic membranes from bovine brain. *Biochemistry* 36:8195-8201, 1997
28. Armstrong CM, Hille B: Voltage-gated ion channels and electrical excitability. *Neuron* 20:371-380, 1998
29. Matsuzaki H, Dong S, Loi H, *et al.*: Genotyping over 100,000 SNPs on a pair of oligonucleotide arrays. *Nat Methods* 1:109-111, 2004
30. Van Camp G, Coucke PJ, Kunst H, *et al.*: Linkage analysis of progressive hearing loss in five extended families maps the DFNA2 gene to a 1.25-Mb region on chromosome 1p. *Genomics* 41:70-74, 1997
31. O'Connell JR, Weeks DE: PedCheck: a program for identification of genotype incompatibilities in linkage analysis. *Am J Hum Genet* 63:259-266, 1998
32. Collin RW, Kalay E, Oostrik J, *et al.*: Involvement of DFNB59 mutations in autosomal recessive nonsyndromic hearing impairment. *Hum Mutat* 28:718-723, 2007
33. Hoenderop JG, Dardenne O, Van Abel M, *et al.*: Modulation of renal Ca²⁺ transport protein genes by dietary Ca²⁺ and 1,25-dihydroxyvitamin D₃ in 25-hydroxyvitamin D₃-1alpha-hydroxylase knockout mice. *Faseb J* 16:1398-1406, 2002
34. Bindels RJ, Hartog A, Timmermans JA, *et al.*: Immunocytochemical localization of calbindin-D28k, calbindin-D9k and parvalbumin in rat kidney. *Contrib Nephrol* 91:7-13, 1991
35. Chang Q, Hoefs S, van der Kemp AW, *et al.*: The beta-glucuronidase klotho hydrolyzes and activates the TRPV5 channel. *Science* 310:490-493, 2005
36. Jiang B, Sun X, Cao K, *et al.*: Endogenous Kv channels in human embryonic kidney (HEK-293) cells. *Mol Cell Biochem* 238:69-79, 2002
37. Gkika D, Topala CN, Chang Q, *et al.*: Tissue kallikrein stimulates Ca²⁺ reabsorption via PKC-dependent plasma membrane accumulation of TRPV5. *Embo J* 25:4707-4716, 2006



**Functional analysis of the Kv1.1 N²⁵⁵D mutation
associated with autosomal dominant
hypomagnesemia**

**Jenny van der Wijst¹, Bob Glaudemans¹, Hanka Venselaar², Anil Nair¹, Anna-Lena Forst¹, Joost
G.J. Hoenderop¹, René J.M. Bindels¹**

¹Department of Physiology, Radboud University Nijmegen Medical Centre, Nijmegen, The
Netherlands

²Centre for Molecular and Biomolecular Informatics, Radboud University Nijmegen Medical Centre,
Nijmegen, The Netherlands

Summary

Mutations in the voltage-gated K⁺ channel Kv1.1 have been linked with a mixed phenotype of episodic ataxia (EA) and/or myokymia. Recently, we presented autosomal dominant hypomagnesemia as a new phenotypic characteristic associated with a mutation in Kv1.1 (N²⁵⁵D). A conserved asparagine at position 255 in the third transmembrane segment was converted into an aspartic acid, resulting in a non-functional channel. In this study, we explored the functional consequence of this conserved residue by substitution with other hydrophobic, polar or charged amino acids (N²⁵⁵E, N²⁵⁵Q, N²⁵⁵A, N²⁵⁵V, N²⁵⁵T, N²⁵⁵H). Upon overexpression in human embryonic kidney (HEK293) cells, cell surface biotinylation revealed plasma membrane expression of all mutant channels. Next, we used the whole-cell patch clamp technique to demonstrate that the N²⁵⁵E and N²⁵⁵Q mutants were non-functional. Substitution of N255 with other amino acids (N²⁵⁵A, N²⁵⁵V, N²⁵⁵T, and N²⁵⁵H) did not prevent ion conduction and these mutant channels activated at more negative potentials compared to wild-type channels, -41.5 ± 1.6 , -45.5 ± 2.0 , -50.5 ± 1.9 , and -33.8 ± 1.3 mV to -29.4 ± 1.1 mV, respectively. The time constant of activation was significantly faster for the two most hydrophobic mutations, N²⁵⁵A (6.2±0.2 ms) and N²⁵⁵V (5.2±0.3 ms), and the hydrophilic mutant N²⁵⁵T (9.8±0.4 ms) in comparison to wild-type (13.0±0.9 ms). Furthermore, the voltage-dependence of inactivation was shifted ~13 mV to more negative potentials in all mutant channels except for N²⁵⁵H. Taken together, our data showed that an asparagine at position 255 in Kv1.1 is required for normal voltage-dependence and kinetics of channel gating.

Introduction

Voltage-gated K⁺ channels (Kv) are a diverse family of membrane proteins, with the Shaker-related group (Kv1) representing a major sub-family [1-3]. Its members play an important role in excitable cells by setting the resting membrane potential, shaping the action potentials, and by controlling the neuronal excitability [4]. Kv channels comprise of four subunits that encircle a central ion conduction pathway [5, 6]. Each subunit consists of six transmembrane-spanning α -helices (S1-S6) with both the amino (N) and the carboxyl (C) terminal on the intracellular side. The S1-S4 segments form the voltage sensing domain, whereas S5 and S6 along with the intervening re-entrant P-loop form the pore domain [7, 8]. Kv channels are known to switch between the closed and open conformation upon cell depolarization [8, 9]. Several molecular mechanisms on voltage-sensing motion have been described, i.e. the *canonical* or *helical screw* model, the *transporter* model, the *paddle* model, and the *twisted S4* model [8]. It is generally accepted that the array of positive charges on the S4 helix form the principal structural elements responsible for voltage sensing [8].

Kv1.1 was the first mammalian subunit of the Kv family to be cloned and is abundantly expressed in excitable and non-excitable cells [10, 11]. Studies with Kv1.1 knock-out (KO) mice showed that deletion of Kv1.1 results in a seizure disorder similar to epilepsy [12]. Mutations in Kv1.1 in humans

are the cause of periodic episodic ataxia type 1 (EA1) and/or myokymia [13-18]. Electrophysiological analyses of these mutant Kv1.1 channels showed either a significant reduction in current amplitude or altered kinetic properties compared to wild-type Kv1.1 channels [14, 19, 20].

Recently, a novel mutation, in the third transmembrane segment of Kv1.1 was identified in a family with isolated autosomal dominant hypomagnesemia. Surprisingly, hypomagnesemia had thus far not been reported in patients with mutations in Kv1.1. Furthermore, this study demonstrated Kv1.1 expression in the apical membranes of the renal distal convoluted tubule (DCT) segment, where active Mg^{2+} reabsorption takes place. The mutation resulted in the single amino-acid substitution of an asparagine at position 255 for an aspartic acid ($N^{255}D$) [21]. The mutant channel was non-functional with a dominant negative effect on wild-type channel activity. Aim of the present study is to characterize the $N^{255}D$ mutation in Kv1.1. To examine the importance of this position in channel function, we systematically substituted six amino acids with different chemical and physical properties. The mutant Kv1.1 channels were electrophysiology and biochemically analyzed.

Results

Structure analysis of Kv1.1 N^{255}

A few years ago, the crystal structure of the mammalian Kv channel, Kv1.2, has been solved. This crystallized structure has been used to construct a paddle-chimera channel where the Kv2.1 voltage sensor paddle (S3b and S4 helices) has been transferred to Kv1.2 [5, 22]. Based on this latter chimaeric Kv1.2-Kv2.1 structure, homology modeling of Kv1.1 was performed (Fig. 1B; <http://www.cmbi.ru.nl/~hvensela/Kv1.1/>). The sequence identity between Kv1.2-Kv2.1 and Kv1.1 was 75%, which is enough to build a good homology model [23]. Kv1.1 subunits consist of six transmembrane α -helices with both the N- and the C-terminal tails of the protein at the intracellular side (Fig. 1C). Recently, a missense mutation in Kv1.1 was found in patients with isolated autosomal dominant hypomagnesemia, converting the highly conserved asparagine at position 255 (Fig. 1A) into an aspartic acid [21]. This mutation is positioned in the third transmembrane segment (S3) close to the intracellular compartment (Fig. 1B/C). Electrophysiological analysis of the Kv1.1 $N^{255}D$ channel expressed in HEK293 cells demonstrated a significantly reduced current amplitude compared to the wild-type Kv1.1 expressing cells (72.0 ± 3.2 pA/pF vs. 398 ± 83 pA/pF) [21]. Importantly, both channels were expressed at the plasma membrane in equal amounts [21]. To examine the importance of N^{255} in Kv1.1 channel function, we substituted the asparagine by six different amino acids with distinct chemical and physical properties ($N^{255}E$, $N^{255}Q$, $N^{255}A$, $N^{255}T$, $N^{255}V$, and $N^{255}H$). We used the homology model to study the effect of these mutations on the structure of the channel (Fig. 1D; <http://www.cmbi.ru.nl/~hvensela/Kv1.1/>). The asparagine was converted into a glutamic acid or histidine to investigate the involvement of charge in channel function. Further, glutamine was used as a control to test the possible steric hindrance of the extra CH_2 -group in glutamic acid. Next, we

introduced alanine and valine as non-polar amino acids that are not able to participate in hydrogen bonding. Threonine was used as a control for residue size as alanine is a smaller amino acid.

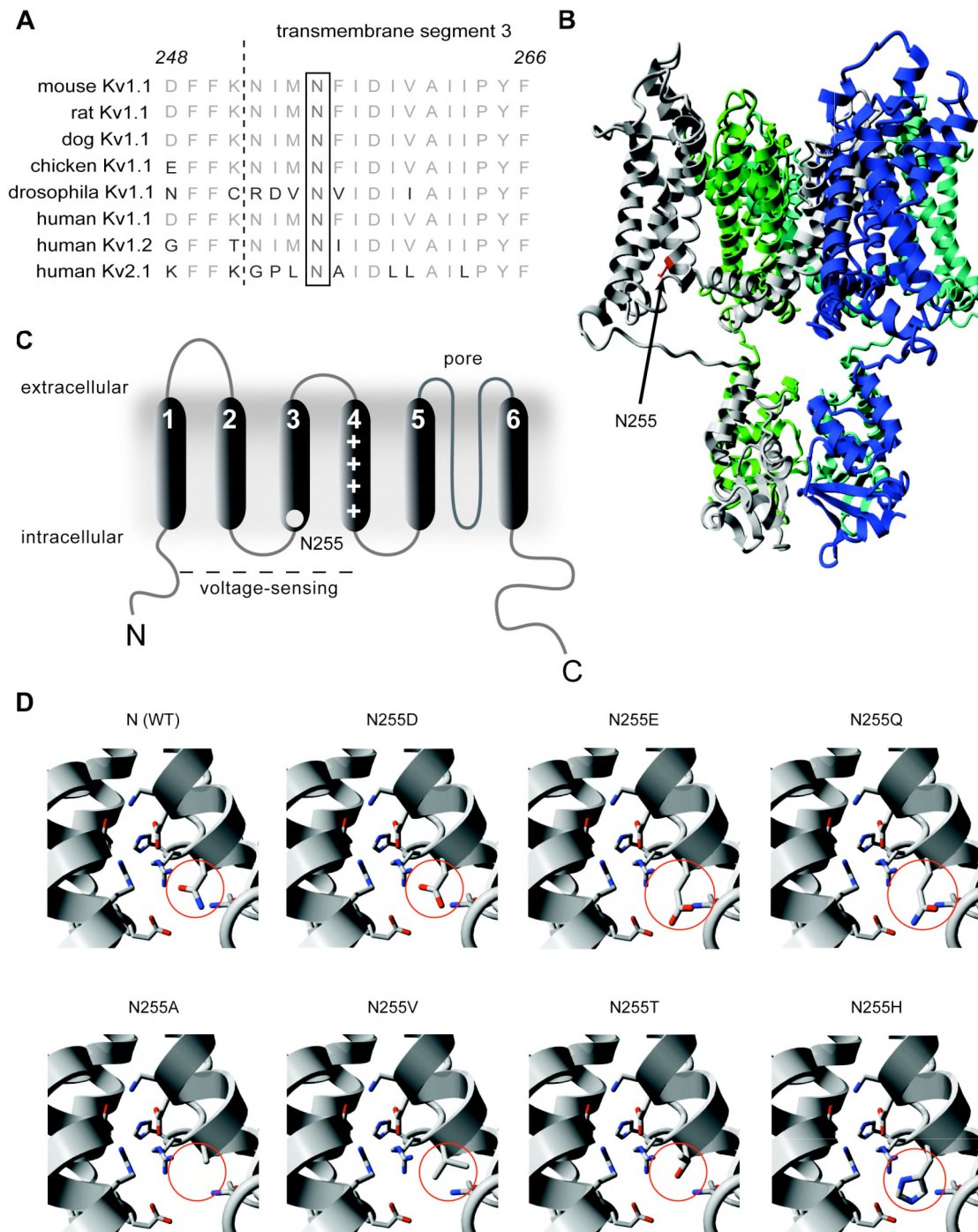


Figure 1. Structural analysis of mutations in Kv1.1 at position 255. *A.* Multiple alignment analysis shows conservation of the N255 amino acid (black bar) among species, and human family members Kv1.2 and Kv2.1. Light gray and dark grey colored letters represent conserved and non-conserved amino acids, respectively. *B.* The predicted 3D-structure model of the tetrameric Kv1.1 channel. *C.* Schematic representation of the Kv1.1 channel, which consists of six transmembrane segments (S1-S6) with S1-S4 functioning as a voltage sensing domain and a pore-forming region between S5 and S6. Localization of the N255 position is denoted by the light gray dot. *D.* Enlarged view of the predicted 3D-structure model showing the side chains of the polar residues surrounding N²⁵⁵ and the mutated amino acids at this position.

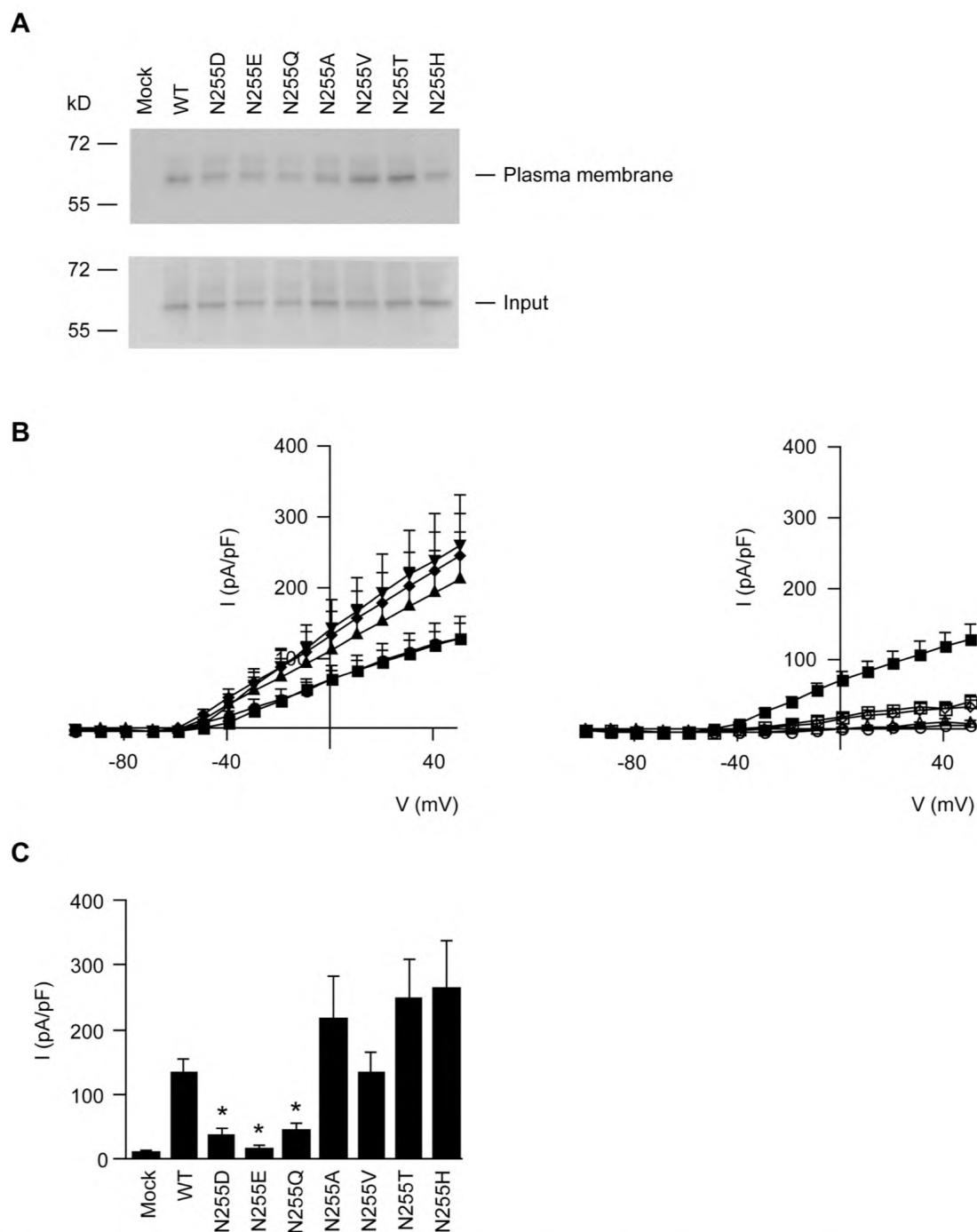


Figure 2. Expression of wild-type and mutant Kv1.1 channels. *A*. Cell surface biotinylation of mock, Kv1.1, Kv1.1 N²⁵⁵D, Kv1.1 N²⁵⁵E, Kv1.1, N²⁵⁵Q, Kv1.1 N²⁵⁵A, Kv1.1 N²⁵⁵V, Kv1.1 N²⁵⁵T, and Kv1.1 N²⁵⁵H expressing HEK293 cells. Kv1.1 expression was analyzed by immunoblotting for plasma membrane fraction and input from the total cell lysates. Representative immunoblot of four independent experiments is shown. *B*. The I–V relationships of the outward K⁺ currents in HEK293 cells expressing mock (○), wild-type Kv1.1 (■), Kv1.1 N²⁵⁵D (◇), Kv1.1 N²⁵⁵E (△), Kv1.1 N²⁵⁵Q (□) (right panel). The I–V relationships of the outward K⁺ currents in HEK293 cells expressing Kv1.1 N²⁵⁵A (▲), Kv1.1 N²⁵⁵V (●), Kv1.1 N²⁵⁵T (◆), and Kv1.1 N²⁵⁵H (▼) (left panel). Mean ± SEM values are shown. *C*. Histogram presenting averaged current densities at +50 mV of mock (n=4), wild-type Kv1.1 (WT, n=11), Kv1.1 N²⁵⁵D (D, n=6), Kv1.1 N²⁵⁵E (E, n=4), Kv1.1 N²⁵⁵Q (Q, n=4), Kv1.1 N²⁵⁵A (A, n=10), Kv1.1 N²⁵⁵V (V, n=7), Kv1.1 N²⁵⁵T (T, n=9), and Kv1.1 N²⁵⁵H (H, n=9) expressing HEK293 cells. Asterisk indicates significance (P < 0.05) in comparison to Kv1.1 wild-type expressing cells. Mean ± SEM values are shown.

Surface expression of the Kv1.1 mutants

The effect of the substituted amino acids on the amount of Kv1.1 channels at the plasma membrane was examined by cell surface biotinylation experiments. As shown in Fig. 2A, the substitution of N²⁵⁵ by other amino acids did not affect the expression of Kv1.1 channels at the plasma membrane.

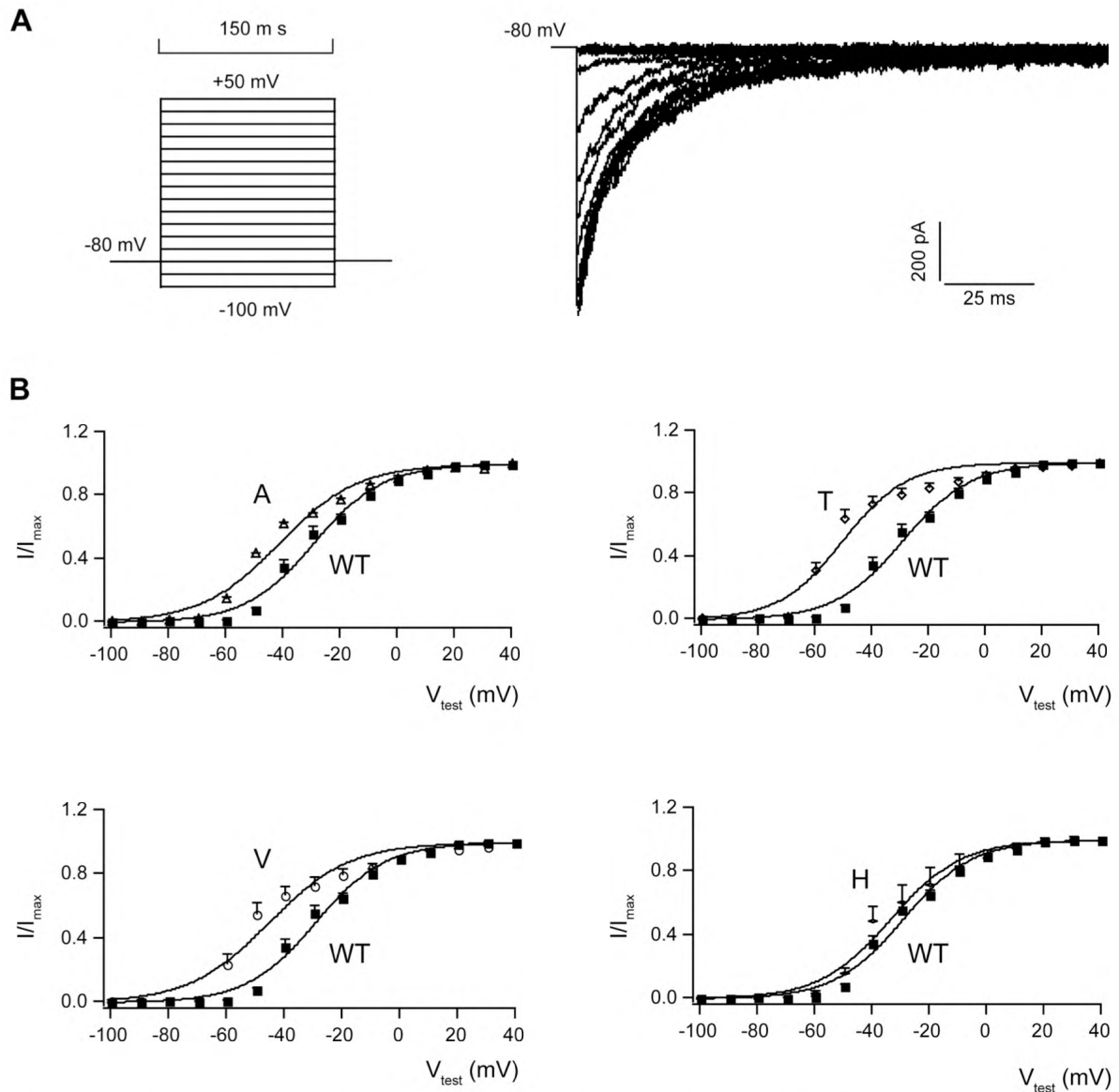


Figure 3. Channel activation of wild-type and mutant Kv1.1 channels. *A.* Representative tail currents of wild-type Kv1.1 at -80 mV, recorded in response to a set of 150 ms voltage steps from -100 to +50 mV in 10 mV increments every 10 s. *B.* The activation curve of the wild-type Kv1.1 (n=5) and Kv1.1 N²⁵⁵A currents (n=4), wild-type Kv1.1 (n=5) and Kv1.1 N²⁵⁵T currents (n=5), wild-type Kv1.1 (n=5) and Kv1.1 N²⁵⁵V currents (n=5), and wild-type Kv1.1 (n=5) and Kv1.1 N²⁵⁵H currents (n=4), respectively. Normalized tail currents are plotted as a function of the pre-pulse potential. The lines reflect the best fits to the averaged current-voltage data points, according to the Boltzmann equation: $I = I_{max} / (1 + \exp((V - V_{1/2}) / k))$, where I is the current measured at each test potential, V , I_{max} is the maximal current; $V_{1/2}$ is the voltage of half-maximal activation; and k is the slope factor.

Electrophysiological characterization of Kv1.1 mutants

Whole-cell patch clamp recordings from HEK293 cells transiently expressing the wild-type Kv1.1 gave typical delayed rectifying currents, in response to a depolarization step from -100 mV to +50 mV (Fig. 2B). We observed in the Kv1.1 mutants a clear difference in current amplitude corresponding to the amino acid substituted. The Kv1.1 N²⁵⁵E and N²⁵⁵Q mutants showed small current amplitudes, similar to mock and the described Kv1.1 N²⁵⁵D mutation [21]. Further, Kv1.1 N²⁵⁵A, N²⁵⁵T, and N²⁵⁵H displayed slightly increased current amplitudes compared to wild-type Kv1.1. The other substituted amino acid (N²⁵⁵V) did not affect the current amplitude of Kv1.1 (Fig. 2B/C).

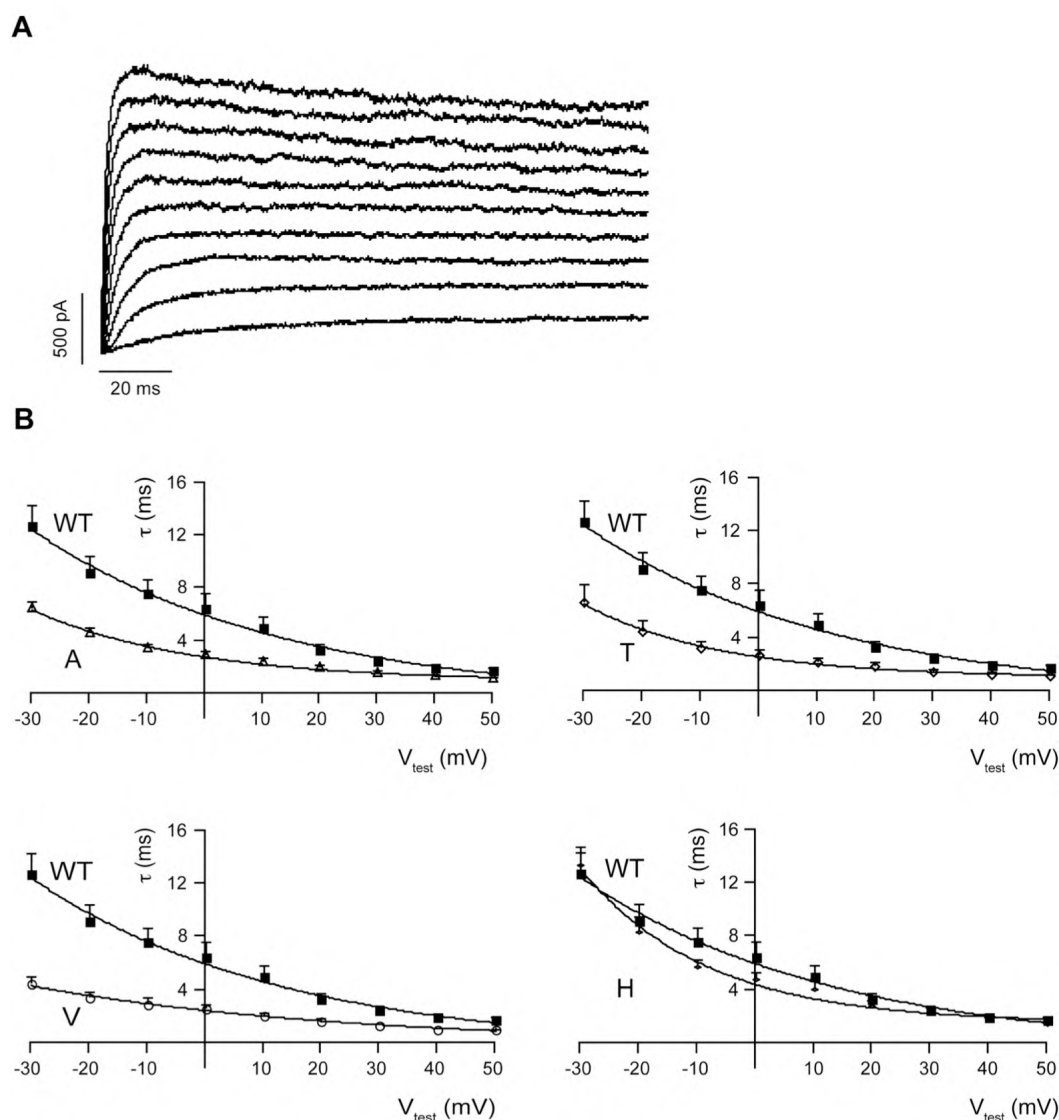


Figure 4. Time dependence of activation from wild-type and mutant Kv1.1 channels. *A*. Representative current traces of wild-type Kv1.1 elicited in response to a set of 150-ms voltage steps from -100 to +40 mV in 10 mV increments every 10 s. These activating traces were fitted with a mono-exponential function. *B*. The time constants of activation for wild-type Kv1.1, Kv1.1 N²⁵⁵A, Kv1.1 N²⁵⁵T, Kv1.1 N²⁵⁵V, and Kv1.1 N²⁵⁵H channels were plotted as a function of pre-pulse potentials and fitted with the equation: $\tau = \tau_{V1/2} \exp(V - V_{1/2}) / k$, where $\tau_{V1/2}$ is the time constant at the half-maximal activation voltage ($V_{1/2}$) of the channels, and k is the slope factor for the voltage-dependence of the time constants.

In order to characterize the activation from the functional mutant and wild-type Kv1.1 channels, tail currents were elicited by 150 ms depolarizing pulses from -100 mV to +50 mV in 10 mV increments every 10 s, from a holding potential of -80 mV (Fig. 3A). The voltage dependence of activation was determined by recording tail currents after pre-pulse voltage steps. The amplitude of the tail currents was normalized to the maximum current and plotted as a function of the conditioning potential. Data points were fitted with a Boltzmann equation to determine the potential of half-maximal activation ($V_{1/2}$) and the slope factor or steepness of voltage dependence (k). This revealed that $V_{1/2}$ for all mutant channels was shifted to more negative potentials compared to wild-type, with extreme shifts of 15 to 20 mV for Kv1.1 N²⁵⁵V and N²⁵⁵T (Fig. 3B; Table 1). The slope factor was not significantly changed for the Kv1.1 mutants compared to wild-type Kv1.1 (Table 1). Mono-exponential functions were used for fitting K⁺ current rise to quantify the time dependence of activation (Fig. 4A). Means of the calculated activation time constants were plotted against the test potentials (Fig. 4B), demonstrating that the mutant channels activated ~2-3 times faster, except for Kv1.1 N²⁵⁵H that was not different from wild-type Kv1.1 (14.6±0.7 ms vs. 13.0±0.9 ms) (Fig. 4B; Table 1).

The inactivation of the total outward currents was determined using a standard double-pulse protocol (Fig. 5A). With the holding potential of -80 mV, 10 s conditioning potentials were given from -90 to +30 mV in 10 mV increments, every 10 s. Then, the membrane was depolarized to +30 mV for 300 ms (Fig. 5A). The rate of inactivation was quantified by measuring the peak current (I_{peak}) and the current at the end of the conditioning pulse (I_{final}). The ratio, $I_{\text{final}}/I_{\text{peak}}$, showed that inactivation kinetics were not altered in the mutant channels compared to wild-type channels (Fig. 5B). Voltage-dependence of inactivation was investigated by plotting the relative amplitudes of the elicited outward currents at +30 mV as function of the potentials. The derived steady-state inactivation curve was fitted to the Boltzmann function, demonstrating the voltage-dependence of inactivation (Fig. 5C). The N²⁵⁵A, N²⁵⁵T, N²⁵⁵V, N²⁵⁵H mutant channels showed 50% inactivation at -46.7±1.8, -46.9±1.8, -46.8±1.5, and -39.6±1.7 mV, respectively, compared to -33.5±1.0 mV for wild-type Kv1.1 (Fig. 5C; Table 1).

Discussion

Voltage-gated potassium (Kv) channels are gated in response to changes in transmembrane voltage [24]. Kv1.1 is abundantly expressed in excitable and non-excitable cells [3, 10, 11]. Recently, a mutation in Kv1.1 (N²⁵⁵D) was found in a large Brazilian family with isolated autosomal dominant hypomagnesemia [21]. In the present study, we investigated the nature of the Kv1.1 N²⁵⁵D mutation and demonstrated that the asparagine at position 255 is essential for normal voltage-dependence and kinetics of channel gating. First, homology modeling of Kv1.1 was performed, based on 75% sequence identity with the crystallized Kv1.2-Kv2.1 chimera. Subsequently, the N²⁵⁵ was substituted

into different amino acids ($N^{255}E$, $N^{255}Q$, $N^{255}A$, $N^{255}V$, $N^{255}T$, $N^{255}H$), which did not affect the expression of the channels at the plasma membrane. Second, the $N^{255}E$ and $N^{255}Q$ mutant channels displayed current amplitude close to the control situation (mock) and $N^{255}D$, and were considered as non-functional.

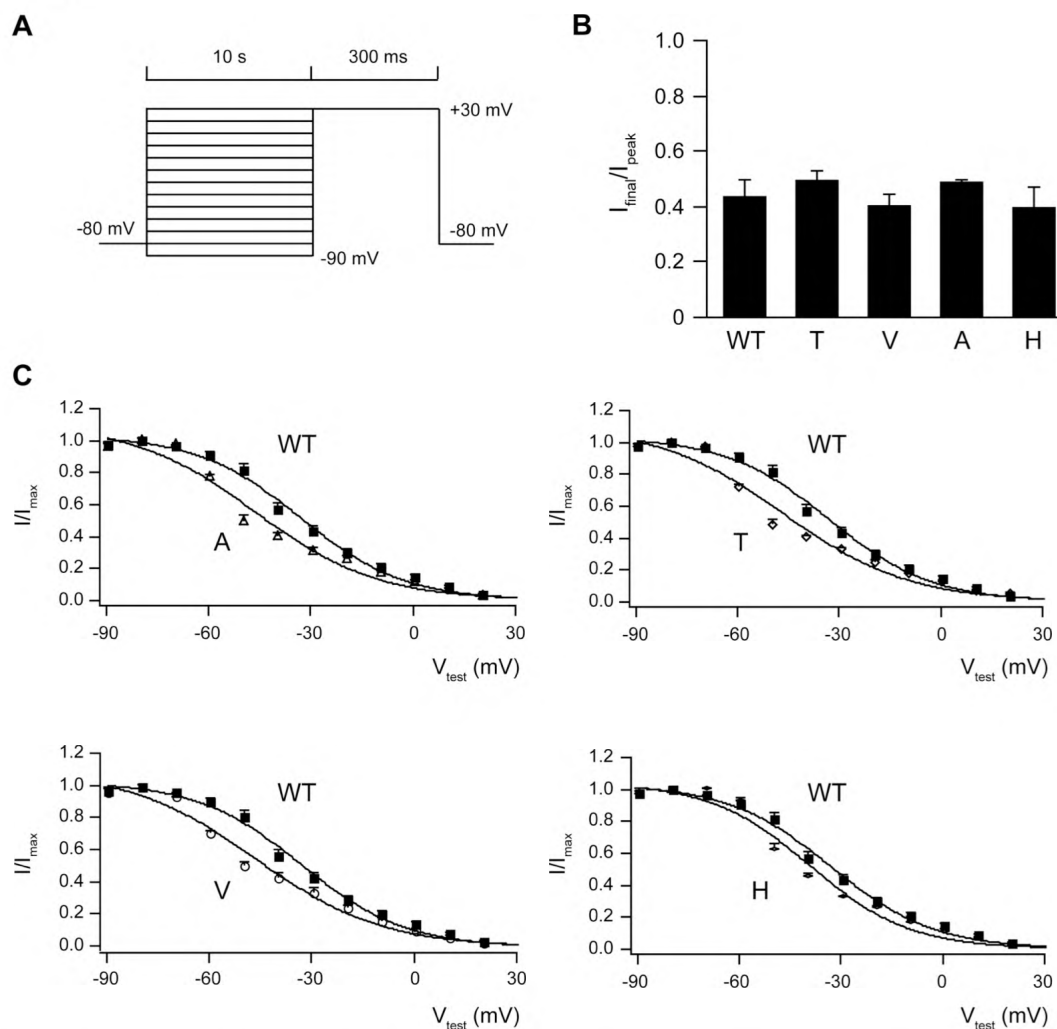


Figure 5. The steady state inactivation of wild-type and mutant Kv1.1 channels. *A*. The representative wild-type Kv1.1 currents recorded with the double-pulse protocol. Outward currents were evoked on membrane depolarizations to +30 mV after (10 s) conditioning pre-pulses to potentials between -90 and +30 mV from a holding potential of -80 mV. *B*. Histogram of current amplitudes at the end of the conditioning voltage step (I_{final}) at +30 mV relative to the peak current amplitude at the beginning of the step (I_{peak}). *C*. The steady-state inactivation curve of the wild-type Kv1.1 ($n=5$) and Kv1.1 $N^{255}A$ currents ($n=5$), wild-type Kv1.1 ($n=5$) and Kv1.1 $N^{255}T$ currents ($n=5$), wild-type Kv1.1 ($n=5$) and Kv1.1 $N^{255}V$ currents ($n=5$), and wild-type Kv1.1 ($n=5$) and Kv1.1 $N^{255}H$ currents ($n=2$), respectively. The peak amplitudes of currents at +30 mV evoked from each conditioning potential were measured in individual cells and normalized to the amplitude of the current evoked after the conditioning pulse at -80 mV. Normalized currents are plotted as a function of the conditioning potential. The lines represent the best Boltzman fits to the data points $I = I_{\text{max}} / (1 + \exp((V - V_{1/2})/k))$, where I is the current measured at each test potential, V ; I_{max} is the maximal current; $V_{1/2}$ is the voltage of half-maximal inactivation; and k is the slope factor.

Third, the other mutants ($N^{255}A$, $N^{255}V$, $N^{255}T$) showed a negative shift in $V_{1/2}$ compared to wild-type Kv1.1 and had a faster time constant of activation except for $N^{255}H$. Fourth, the half-maximal inactivation voltage was shifted to more negative potentials for all mutants, with $N^{255}H$ as the

exception. Affected family members from the Brazilian family with inherited hypomagnesemia showed low plasma Mg^{2+} levels (0.40 mM; normal range, 0.70-0.95 mM) and suffered from muscle cramps, tetanic episodes, tremor, and muscle weakness. Remarkably, mutations in Kv1.1 thus far were known to result in a mixed phenotype of episodic ataxia (EA1) and myokymia [13-16, 18, 21], a neurological phenotype in which hypomagnesemia has not been reported. Kv1.1 was shown to localize to the apical membrane of DCT cells and postulated to be involved in the generation of a favorable apical membrane voltage as a driving force for Mg^{2+} entry [21]. It is puzzling that distinct mutations in nearby amino acid residues in Kv1.1 can result in phenotypes with dysfunction in two different organs (brain and kidney). A possible reason is that the composition of Kv1.1 channels in brain and kidney is different, due to tissue-specific expression of auxiliary β -subunits or co-assembly with other Kv1 subunits that define the functional characteristics of these channels [25-27]. As a result, mutations at close locations within the protein may have tissue-specific effects, giving rise to diverse phenotypic characteristics. Electrophysiological analyses of the EA1/myokymia-related mutant Kv1.1 channels showed either a significant reduction in current amplitude or altered kinetic properties compared to wild-type Kv1.1 channels [14, 19, 20]. The mutation identified in the Brazilian family caused substitution of the asparagine at amino acid position 255 into an aspartic acid (N²⁵⁵D). The asparagine at position 255 is highly conserved among species and Kv1 family members, which suggests its importance in channel function. Indeed, we demonstrated that the change of the neutral asparagine into a negatively charged aspartic acid results in a non-functional channel [21]. In the present study, we investigated the amino acid substitution at position 255 in relation to channel function more extensively.

The tertiary structure of Kv1.1 was modeled by the WHAT-IF server, based on 75% sequence identity with the crystallized Kv1.2-Kv2.1 chimeric channel [5, 22]. The asparagine residue (N²⁵⁵) is located in the third transmembrane segment (S3) close to the S4 voltage-sensor element. S4 contains a long array of positive charges that are shown to sense differences in voltage and start the transition from the closed to open conformation by forming stabilizing hydrogen bonds with the external and internal negative clusters in the voltage-sensing domain [28, 29]. In general, mutations can affect channel activity via loss-of-function at the plasma membrane, protein instability or lack of plasma membrane targeting. Importantly, cell surface biotinylation studies showed that all mutants were expressed at the plasma membrane. Thus, the change in amino acid at position 255 had no effect on channel trafficking. However, the amino acid substitution has a clear effect on channel activity, as we demonstrated that N²⁵⁵E and N²⁵⁵Q channel were non-functional. This indicates that next to the addition of a negative charge at position 255 also an additional CH₂-group in the side-chain influences channel function, likely via affecting conformational rearrangements. Subsequently, the voltage-dependence and kinetics of channel gating of the wild-type functional mutant channels were examined. All mutations stabilized the open state of Kv1.1, measured as negative shifts in the voltage dependence of channel activation. There was no obvious correlation between charge and the

magnitude of the shift in $V_{1/2}$ and k as the effect was not significantly changed for N²⁵⁵H. Depending on the polarity of the side chain, amino acids vary in their hydrophilic or hydrophobic character [30]. These properties are important determinants of the protein structure and the physical properties of the side chains influence the amino acid residues' interactions with other structures, both within a single protein and between proteins. Therefore, the hydrophilic asparagine could be important for structural rearrangements within the channel in response to voltage changes, which can be affected by conversion into hydrophobic amino acids as alanine and valine. Interestingly, the change in activation kinetics was most evident with these two residues as N²⁵⁵A and N²⁵⁵V activated 2 to 3-fold faster than wild-type channels. Furthermore, these mutants significantly shifted the voltage-dependence of activation. However, the magnitude of shift in $V_{1/2}$ was highest for N²⁵⁵T, which suggests that channel gating is independent of hydrogen bonding with the residue at position 255.

Table 1. Electrophysiological characteristics of kv1.1 wild-type and mutant channels.

	WT	A	T	V	H
Voltage-dependence	(n=5)	(n=4)	(n=5)	(n=5)	(n=4)
$V_{1/2}$ (mV)	-29.4±1.1	-41.5±1.6 ^a	-50.5±1.9 ^a	-45.5±2.0 ^a	-33.8±1.3
k (mV)	12.1±1.0	13.7±1.4	11.2±1.7	13.9±1.8	12.3±1.2
Activation	(n=8)	(n=5)	(n=4)	(n=5)	(n=5)
$\tau_{V_{1/2}}$ (ms)	13.0±0.9	6.2±0.2 ^a	9.8±0.4 ^b	5.2±0.3 ^a	14.6 ±0.7
Inactivation	(n=4)	(n=5)	(n=4)	(n=6)	(n=3)
$I_{\text{final}} / I_{\text{peak}}$	0.44±0.07	0.49±0.01	0.50±0.04	0.41±0.04	0.40±0.08
Steady-state inactivation	(n=5)	(n=5)	(n=5)	(n=5)	(n=2)
$V_{1/2}$ (mV)	-33.5±1.0	-46.7±1.8 ^a	-46.9±1.8 ^a	-46.8±1.5 ^a	-39.6±1.7

The voltage-dependent parameters of activation and inactivation ($V_{1/2}$ and k) were obtained from the Boltzmann equation as described in Fig. 3 and Fig. 5, respectively. Activation time constants at $V_{1/2}$ ($\tau_{V_{1/2}}$) were derived from Fig. 4. Inactivation was measured at 30 mV and is presented as the ratio $I_{\text{final}}/I_{\text{peak}}$. Data are presented as mean±SEM, with the number of investigated cells in parenthesis.

^aP < 0.01 (compared to WT)

^bP < 0.05 (compared to WT)

Inactivation, besides activation, is another important property with respect to channel function. Interestingly, the voltage-dependence of inactivation was significantly affected in all mutant Kv1.1 channels compared to wild-type Kv1.1 except for N²⁵⁵H. Substitution of the asparagine with other amino acids shifted the half-point for inactivation to more negative potentials. The acceleration of the inactivation process is also of interest, as it is explained by a constriction mechanism of the outer

mouth of the channel vestibule [31, 32]. It has been demonstrated that negatively charged clusters in the S2 and S3 segments, together with the positive charges in S4, are involved in the opening and closing of Kv1 channels [22]. In line with this, an earlier study showed that mutation of conserved negatively charged residues in the S2 and S3 segments selectively modulate channel gating. Mutation of the aspartic acid at position 258 in Kv1.1 abolished channel activity [33]. Therefore, we suggest that an additional negative charge nearby this cluster in S3 could keep the channel in the inactivated state, which may explain the non-functionality of the mutation found in patients with hypomagnesemia (N²⁵⁵D). However, there were no significant changes in inactivation kinetics between wild-type and mutant channels.

Taken together, we have previously described hypomagnesemia as a new phenotypic variability associated with a mutation in Kv1.1 (N²⁵⁵D) [21]. In this study, we provided more information about the structural arrangement of N²⁵⁵ and its involvement in channel activity. We have demonstrated that N²⁵⁵ is essential for normal channel function, since substitution by other amino acids significantly altered channel activity, voltage-dependence and kinetics of Kv1.1 channels.

Material and methods

DNA constructs- Full-length wild-type KCNA1 and N²⁵⁵D mutant were constructed in the pCIneo-IRES-GFP expression vector as previously described [21]. Other KCNA1 mutants (N²⁵⁵A, N²⁵⁵E, N²⁵⁵Q, N²⁵⁵H, N²⁵⁵T, N²⁵⁵V) were created using the QuickChange site-directed mutagenesis kit (Stratagene, La Jolla, CA, USA) according to the manufacturer's protocol. All constructs were verified by sequence analysis.

Electrophysiology- HEK293 cells were grown in DMEM (Bio Whittaker Europe, Vervier, Belgium) containing 10% (v/v) fetal calf serum, 2 mM l-glutamine and 10 µg/ml Ciproxin at 37 °C in a humidity-controlled incubator with 5% (v/v) CO₂. Cells were transiently transfected with the respective constructs using Lipofectamine 2000 (Invitrogen-Life Technologies, Breda, The Netherlands), as described previously [34], and electrophysiological recordings were performed 48 hours after transfection. Transfected cells were identified by their green fluorescence when illuminated at 488 nm. Non-transfected (GFP-negative) cells from the same batch were used as controls. Patch clamp experiments were performed in the tight seal whole cell configuration at room temperature (20–25°C). An EPC-10 patch clamp amplifier computer was used and controlled by PatchMaster Classic 1.20 software (HEKA Elektronik). Currents were digitized at 20 kHz and digitally filtered at 2.9 kHz. Patch pipettes were pulled from thin-walled borosilicate capillaries (1.5 mm OD, 1.17 mm ID); pipette resistance was typically between 2 and 4 MΩ. The liquid junction potential was not corrected. The pipette solution contained (mM): 140 KCl, 1 MgCl₂, 0.1 CaCl₂, 2 EGTA, 10 HEPES/KOH (pH 7.3), and 1 Na₂-ATP. The bath solution contained (mM): 138 NaCl, 5.4

KCl, 1.2 MgCl₂, 1 CaCl₂, 10 EGTA, 10 HEPES/NaOH (pH 7.3), and 10 glucose. Recordings of Kv1.1 were obtained by voltage steps, applied every 10 sec, consisting of 150 ms steps from -100 mV to +50 mV (10 mV increments). The holding potential was -80 mV. Equimolar pipette and bath solutions of K⁺ (140 mM) were used to determine the voltage dependence of activation. For steady-state inactivation, cells were held at -80 mV, and then subjected to steps from -90 mV to +30 mV (10 mV increments) for 10 s, followed by a depolarizing step to +30 mV. Linear leak and capacitance currents were corrected with a P/5 leak subtraction procedure [35]. The analysis of patch clamp data was performed using Igor Pro software (WaveMetrics, Lake Oswego, USA). Current densities were obtained by normalizing the current amplitude to the cell membrane capacitance.

Cell surface biotinylation- Cell surface labelling with biotin was performed as described previously [36]. HEK293 cells were transiently transfected with 1 µg wild type or mutants Kv1.1 constructs using Lipofectamin 2000 (Invitrogen-Life Technologies), in 6-well plates (1.5 million cells per plate). At 48 hours after transfection, the biotinylation assay was performed using the sulfo-NHS-LC-LC-biotin (Pierce, Etten-Leur, The Netherlands). Cells from each 6 well were homogenized in 1 ml lysis buffer as described previously [37]. Next, 5% of the total protein amount was collected as an input sample. Subsequently, biotinylated proteins (plasma membrane fraction) were precipitated using neutravidin-agarose beads (Pierce). Kv1.1 expression was analyzed by immunoblot analysis for the input and the plasma membrane fraction using the monoclonal Kv1.1 antibody (Neuromab, Davis, CA, USA).

Sequence analysis and structure modelling- The structural model of Kv1.1 was built based on the 3D structure of a chimeric Kv1.2-Kv2.1 channel [22] (PDB-file 2R9R). In order to obtain optimal modeling results, we used a re-refined version of this template from the PDB_REDO data bank [38]. The sequences of the template and Kv1.1 share 75% sequence identity. The WHAT IF server (<http://swift.cmbi.ru.nl>) was used for model building, Yasara [39] was used for loop building, energy minimization and subsequent mutation analysis. The tetrameric model was obtained by superposing four models on the biological subunit of PDB file 2R9R, followed by an energy minimization in Yasara. Visit <http://www.cmbi.ru.nl/~hvensela/Kv1.1/> for more details.

Statistical analysis- Data are shown as mean ± SEM values. Statistical significance was determined using ANOVA followed by Tukey's test. Differences in means with P < 0.05 were regarded as statistically significant. Statistical analysis was performed using Prism (GraphPad, San Diego, USA) software.

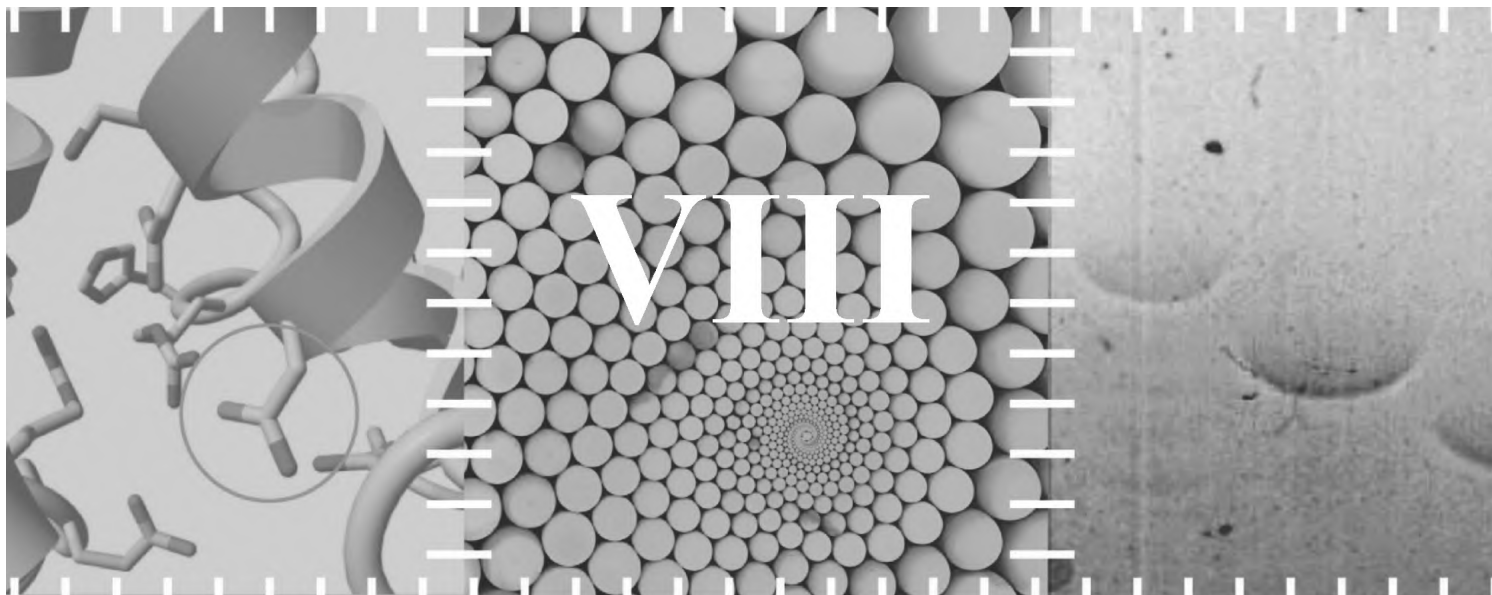
Acknowledgements

The authors would like to thank Dr. KyuPil Lee and Femke van Zeeland for excellent technical assistance and Dr. Gert Vriend for valuable discussion. This work was supported financially by the Netherlands Organization for Scientific Research (ZonMw 9120.6110; NWO-CW 700.55.302, ZonMw 9120.8026), an European Young Investigator award from the European Science Foundation, and the Dutch Kidney foundation (C03.6017, C08.2252).

References

1. Christie MJ: Molecular and functional diversity of K⁺ channels. *Clin Exp Pharmacol Physiol* 22:944-951, 1995
2. Dolly JO, Parcej DN: Molecular properties of voltage-gated K⁺ channels. *J Bioenerg Biomembr* 28:231-253, 1996
3. Armstrong CM: Voltage-gated K channels. *Sci STKE* 2003:re10, 2003
4. Hille B: *Ion Channels of Excitable Membranes* 3ed. Sunderland, MA, Sinauer Associates, Inc., 2001
5. Long SB, Campbell EB, Mackinnon R: Crystal structure of a mammalian voltage-dependent Shaker family K⁺ channel. *Science* 309:897-903, 2005
6. Grottesi A, Sands ZA, Sansom MS: Potassium channels: complete and undistorted. *Curr Biol* 15:R771-774, 2005
7. Aggarwal SK, MacKinnon R: Contribution of the S4 segment to gating charge in the Shaker K⁺ channel. *Neuron* 16:1169-1177, 1996
8. Sands Z, Grottesi A, Sansom MS: Voltage-gated ion channels. *Curr Biol* 15:R44-47, 2005
9. Swartz KJ: Towards a structural view of gating in potassium channels. *Nat Rev Neurosci* 5:905-916, 2004
10. Armstrong CM, Hille B: Voltage-gated ion channels and electrical excitability. *Neuron* 20:371-380, 1998
11. O'Grady SM, Lee SY: Molecular diversity and function of voltage-gated (Kv) potassium channels in epithelial cells. *Int J Biochem Cell Biol* 37:1578-1594, 2005
12. Smart SL, Lopantsev V, Zhang CL, *et al.*: Deletion of the K(V)1.1 potassium channel causes epilepsy in mice. *Neuron* 20:809-819, 1998
13. Browne DL, Gancher ST, Nutt JG, *et al.*: Episodic ataxia/myokymia syndrome is associated with point mutations in the human potassium channel gene, KCNA1. *Nat Genet* 8:136-140, 1994
14. Eunson LH, Rea R, Zuberi SM, *et al.*: Clinical, genetic, and expression studies of mutations in the potassium channel gene KCNA1 reveal new phenotypic variability. *Ann Neurol* 48:647-656, 2000
15. Klein A, Boltshauser E, Jen J, *et al.*: Episodic ataxia type 1 with distal weakness: a novel manifestation of a potassium channelopathy. *Neuropediatrics* 35:147-149, 2004
16. Lee H, Wang H, Jen JC, *et al.*: A novel mutation in KCNA1 causes episodic ataxia without myokymia. *Hum Mutat* 24:536, 2004
17. Shook SJ, Mamsa H, Jen JC, *et al.*: Novel mutation in KCNA1 causes episodic ataxia with paroxysmal dyspnea. *Muscle Nerve* 37:399-402, 2008
18. Zuberi SM, Eunson LH, Spauschus A, *et al.*: A novel mutation in the human voltage-gated potassium channel gene (Kv1.1) associates with episodic ataxia type 1 and sometimes with partial epilepsy. *Brain* 122 (Pt 5):817-825, 1999
19. Chen H, von Hehn C, Kaczmarek LK, *et al.*: Functional analysis of a novel potassium channel (KCNA1) mutation in hereditary myokymia. *Neurogenetics* 8:131-135, 2007
20. Zerr P, Adelman JP, Maylie J: Episodic ataxia mutations in Kv1.1 alter potassium channel function by dominant negative effects or haploinsufficiency. *J Neurosci* 18:2842-2848, 1998
21. Glaudemans B, van der Wijst J, Scola RH, *et al.*: A missense mutation in the Kv1.1 voltage-gated potassium channel-encoding gene KCNA1 is linked to human autosomal dominant hypomagnesemia. *J Clin Invest* 119:936-942, 2009
22. Long SB, Tao X, Campbell EB, *et al.*: Atomic structure of a voltage-dependent K⁺ channel in a lipid membrane-like environment. *Nature* 450:376-382, 2007
23. Sander C, Schneider R: Database of homology-derived protein structures and the structural meaning of sequence alignment. *Proteins* 9:56-68, 1991
24. Sigworth FJ: Voltage gating of ion channels. *Q Rev Biophys* 27:1-40, 1994
25. Gulbis JM: The beta subunit of Kv1 channels: voltage-gated enzyme or safety switch? *Novartis Found Symp* 245:127-141; discussion 141-125, 165-128, 2002

26. Sokolov MV, Shamotienko O, Dhochartaigh SN, *et al.*: Concatemers of brain Kv1 channel alpha subunits that give similar K⁺ currents yield pharmacologically distinguishable heteromers. *Neuropharmacology* 53:272-282, 2007
27. Zhu J, Watanabe I, Gomez B, *et al.*: Heteromeric Kv1 potassium channel expression: amino acid determinants involved in processing and trafficking to the cell surface. *J Biol Chem* 278:25558-25567, 2003
28. Liman ER, Hess P, Weaver F, *et al.*: Voltage-sensing residues in the S4 region of a mammalian K⁺ channel. *Nature* 353:752-756, 1991
29. Pathak MM, Yarov-Yarovoy V, Agarwal G, *et al.*: Closing in on the resting state of the Shaker K(+) channel. *Neuron* 56:124-140, 2007
30. Creighton TH: *Proteins: structures and molecular properties*, in, edited by Freeman WH, San Francisco, 1993
31. Panyi G, Sheng Z, Deutsch C: C-type inactivation of a voltage-gated K⁺ channel occurs by a cooperative mechanism. *Biophys J* 69:896-903, 1995
32. Yellen G, Sodickson D, Chen TY, *et al.*: An engineered cysteine in the external mouth of a K⁺ channel allows inactivation to be modulated by metal binding. *Biophys J* 66:1068-1075, 1994
33. Planells-Cases R, Ferrer-Montiel AV, Patten CD, *et al.*: Mutation of conserved negatively charged residues in the S2 and S3 transmembrane segments of a mammalian K⁺ channel selectively modulates channel gating. *Proc Natl Acad Sci USA* 92:9422-9426, 1995
34. Chang Q, Hoefs S, van der Kemp AW, *et al.*: The beta-glucuronidase klotho hydrolyzes and activates the TRPV5 channel. *Science* 310:490-493, 2005
35. Armstrong CM, Bezanilla F: Charge movement associated with the opening and closing of the activation gates of the Na channels. *J Gen Physiol* 63:533-552, 1974
36. Gkika D, Topala CN, Chang Q, *et al.*: Tissue kallikrein stimulates Ca²⁺ reabsorption via PKC-dependent plasma membrane accumulation of TRPV5. *Embo J* 25:4707-4716, 2006
37. Gkika D, Topala CN, Chang Q, *et al.*: Tissue kallikrein stimulates Ca(2+) reabsorption via PKC-dependent plasma membrane accumulation of TRPV5. *Embo J* 25:4707-4716, 2006
38. Joosten RP, Womack T, Vriend G, *et al.*: Re-refinement from deposited X-ray data can deliver improved models for most PDB entries. *Acta Crystallogr D Biol Crystallogr* 65:176-185, 2009
39. Krieger E, Koraimann G, Vriend G: Increasing the precision of comparative models with YASARA NOVA--a self-parameterizing force field. *Proteins* 47:393-402, 2002



General discussion and summary

Modified after:

“Epithelial Mg^{2+} channel TRPM6: insight into the molecular regulation”

Jenny van der Wijst, Joost G.J. Hoenderop, René J.M. Bindels

Department of Physiology, Radboud University Nijmegen Medical Centre, Nijmegen, The Netherlands

Magnes Res 22:127-132, 2009

Introduction

A key molecule involved in Mg^{2+} handling is the Transient Receptor Potential Melastatin subtype 6 (TRPM6). Mutations of this gene have been associated with the rare monogenetic disorder hypomagnesemia with secondary hypocalcemia (HSH) [1, 2]. The TRPM6 gene contains 39 exons encoding a protein of 2,022 amino acids [1-3]. TRPM6 shares approximately 50% sequence homology with TRPM7. These channels are composed of six membrane-spanning domains with a pore region between the fifth and sixth segment, and large intracellular amino (N) and carboxyl (C) termini. Furthermore, they are thought to form functional homotetramers or heterotetramers, which influences their channel characteristics [4, 5]. TRPM6 functions as a divalent cation channel and it has a higher affinity for Mg^{2+} than for Ca^{2+} [3]. Its channel activity is tightly regulated by intracellular Mg^{2+} levels ($[Mg^{2+}]_i$) and inhibited by ruthenium red in a voltage-dependent manner [3]. Furthermore, micromolar levels of 2-aminoethoxydeiphenyl borate (2-APB) can increase TRPM6 currents [5]. In addition, Li *et al.* [5, 6] demonstrated that TRPM6 inward currents significantly enhanced upon extracellular acidification, which is linked to specific residues in the TRPM6 pore region. In addition to its Mg^{2+} selectivity and sensitivity, TRPM6 has a restricted localization pattern along the luminal membranes of the colon and distal convoluted tubules (DCT) of the kidney, supporting a central role in active Mg^{2+} (re)absorption [3].

TRPM6 regulation by its α -kinase domain

TRPM6, together with its closest homologue TRPM7, is unique by combining an ion channel with a fused α -kinase domain [7, 8]. While it has previously been shown that this catalytic domain is not essential for channel activity, recent studies have revealed an indirect regulatory role in the modulation of channel functioning [9, 10] (**Chapters 2-4**).

Background of the α -kinase domain

In 1999, Ryazanov *et al.* discovered the alpha-kinases as a new class of protein kinases with a catalytic domain. Alpha-kinases were named according to their substrate recognition, as they were shown to phosphorylate amino acids within alpha-helices [11]. They have no detectable sequence homology to the conventional protein kinases (CPKs). To date, six mammalian alpha-kinases have been identified, including elongation factor-2 (eEF-2) kinase, lymphocyte alpha-kinase, heart alpha-kinase, muscle alpha-kinase and TRPM6 and TRPM7 [11-13]. The crystal structure of the TRPM7 kinase has been elucidated, demonstrating structural similarities with CPKs [14]. In particular, the N-terminal lobe shows high homology to the structure in CPKs and is important for anchoring and orientation. The C-terminal tail is mainly important for substrate binding and phosphotransfer. Primary structural differences can be found in this site of catalysis, which leads to diverse substrate specificity and kinase regulation. Another clear distinction between the two kinases is the zinc

binding module in the C-terminus of TRPM7 α -kinase, which is important for structural integrity as cysteine mutations leads to loss of kinase activity [8, 15]. Recently, some studies have revealed phosphorylation targets of the α -kinase domain. TRPM6 and TRPM7 have been shown to share exogenous phosphorylation substrates as myosin IIA, IIB, and IIC [16]. Furthermore, Clark *et al.* [17] showed that the C-terminus of TRPM7 undergoes massive autophosphorylation, thereby increasing the rate of substrate phosphorylation [18]. The TRPM7 autophosphorylation has been mapped to a serine/threonine-rich region close to the α -kinase domain and the TRPM6 α -kinase activity was suggested to be regulated in a comparable fashion [17]. Despite these findings, little is known about the interrelationship between the TRPM6 channel and alpha-kinase. Therefore, we screened for interacting proteins of the TRPM6 α -kinase domain and identified three new modulators of TRPM6, namely the receptor for activated C-kinase 1 (RACK1), repressor of estrogen receptor activity (REA), and methionine sulfoxide reductase B1 (MsrB1) as discussed below.

Autophosphorylation activity of the α -kinase domain – RACK1

RACK1 has been identified as the first TRPM6-associated partner (**Chapter 2**). RACK1 is a 36-kDa scaffold protein containing seven internal Trp-Asp 40 (WD40) repeats and is originally discovered as an adaptor for protein kinase C (PKC) [19, 20]. It is ubiquitously expressed and involved in diverse biological functions (reviewed by McCahill *et al.* [21]). Our study demonstrated that RACK1 co-expresses with TRPM6 in the DCT where active Mg^{2+} reabsorption occurs (**Chapter 2**). RACK1 interacts with the α -kinase domain thereby inhibiting TRPM6 channel activity (Fig.1). The inhibitory effect of RACK1 was shown to be dependent on autophosphorylation of a threonine residue (T¹⁸⁵¹) in the α -kinase domain (**Chapter 2**). Our data suggest that the inhibitory action of RACK1 requires functional phosphotransferase activity. This notion is supported by the fact that the current of the phosphorylation-impaired mutants (K¹⁸⁰⁴R and T¹⁸⁵¹A) is insensitive to RACK1, while the constitutive phosphorylated mutant T¹⁸⁵¹D was still inhibited by RACK1. Based on these observations, an increased channel activity for the phosphorylation-impaired mutants (K¹⁸⁰⁴R and T¹⁸⁵¹A) and the TRPM6 Δ -kinase mutant was expected. However, functional analysis of these mutated channel proteins did not indicate elevated channel activity. It has been demonstrated that the TRPM7 α -kinase domain can regulate channel activity via other signaling pathways. For instance, previous studies indicated that the TRPM7 activity controlled by intracellular Mg^{2+} , nucleotides, and the cAMP/protein kinase A pathway requires the α -kinase domain or kinase activity [10, 22, 23]. It is, therefore, conceivable that removing the α -kinase domain or suppressing its phosphotransferase activity may abolish associated regulation(s) of TRPM6 channel activity. This could compensate for a potential upregulation of TRPM6 activity caused by removal of the inhibitory RACK1 action.

Our findings support the conclusion that TRPM6 α -kinase autophosphorylation events are not vital for TRPM6 channel activation since the phosphotransferase-deficient K¹⁸⁰⁴R mutant displayed

currents indistinguishable from wild-type TRPM6. The mutants T¹⁸⁵¹A and T¹⁸⁵¹D displayed currents similar to the wild-type channel but exhibited a significant albeit reduced autophosphorylation, while the autophosphorylation of mutant K¹⁸⁰⁴R was fully abolished. This suggests that, besides T¹⁸⁵¹, additional autophosphorylation sites are present in TRPM6. However, we hypothesize that T¹⁸⁵¹ plays a key role in controlling channel activity as its phosphorylation state influences the Mg²⁺-dependent inhibition of TRPM6 activity (**Chapter 2**). Channel inactivation by elevated [Mg²⁺]_i may function as negative-feedback machinery to balance the Mg²⁺ homeostasis. Matsushita and coworkers postulated that regulation of TRPM7 channel activity by [Mg²⁺]_i is disassociated from its α -kinase activity [13], whereas other studies suggested the involvement of the α -kinase domain [11, 14]. In our study, the T¹⁸⁵¹A mutant is less sensitive to [Mg²⁺]_i, which is in agreement with previous studies showing that TRPM7 phosphotransferase activity influences the Mg²⁺-dependent inhibition of channel activity [11, 14]. This shift in Mg²⁺ sensitivity could have significant impact on TRPM6 activity during transepithelial Mg²⁺ transport because the channel is tightly controlled by [Mg²⁺]_i [2]. The T¹⁸⁵¹A mutant is still inhibited by high [Mg²⁺]_i suggesting that additional Mg²⁺-sensing site(s) are present within TRPM6. Our data indicated that wild-type TRPM6 autophosphorylation activity is gradually enhanced by increasing the Mg²⁺ concentration [0.1-1.0 mM Mg²⁺]_i, in contrast to autophosphorylation of the T¹⁸⁵¹A mutant for which the Mg²⁺ sensitivity is abolished. Thus, residue T¹⁸⁵¹ seems crucial in the Mg²⁺ sensitivity of TRPM6 autophosphorylation. In line with our study, Minagawa and coworkers demonstrated that the Mg²⁺ sensitivity of PhoQ phosphorylation, vital for *Escherichia coli* Mg²⁺ homeostasis, relies on a single residue, D¹⁷⁹ [29]. Over the last decade, the idea was that the free [Mg²⁺]_i is more or less constant. However, more recent studies provided evidence that the free [Mg²⁺]_i varies significantly [30, 31]. Enzymes like adenylate kinases and the TRPM7 kinase are shown to be dependent on [Mg²⁺]_i [11, 32, 33]. Moreover, it was shown that siRNA-mediated downregulation of endogenous RACK1 significantly reduces the inhibition of the TRPM6 current by Mg²⁺. These findings suggest that RACK1 determines in part the Mg²⁺ sensitivity of TRPM6 channel activity. Together, it is proposed that TRPM6-mediated Mg²⁺ influx induces phosphorylation of T¹⁸⁵¹ located in the α -kinase domain. Subsequently, the phosphorylation of T¹⁸⁵¹ will activate the inhibitory effect of RACK1. This latter step may act as an intracellular feedback regulation to control TRPM6-mediated Mg²⁺ influx and avoid Mg²⁺ overload during renal epithelial Mg²⁺ transport. Experiments with RACK1-knockout mice, which have yet to be generated, could be of interest to further investigate the role of RACK1 in Mg²⁺ handling.

Phosphorylation activity of the α -kinase domain – REA

By using similar screening assays, a new TRPM6-interacting protein, REA, was identified (**Chapter 3**). REA is a 37 kD protein that was first identified as an interacting protein of the estrogen receptor (ER), where it functions as a selective co-regulator repressing the transcriptional activity of

ERs [24]. REA binds to the 6th, 7th, and 8th β -sheets in the α -kinase domain, which is the same region as for RACK1 (**Chapter 2/3**). Most amino acids in this area are located on the peripheral region of the tertiary structure, which facilitates the interaction with regulatory proteins. REA inhibits TRPM6 channel activity in an α -kinase activity-dependent manner, since REA has no functional effect on the TRPM6 phosphotransferase-deficient mutant (K¹⁸⁰⁴R) (**Chapter 3**). However, we demonstrated that REA is not a phosphorylation target of TRPM6, nor was TRPM6 autophosphorylation affected by REA (**Chapter 3**). These data suggest another indirect regulation of TRPM6 activity, independent of autophosphorylation, but reliant on TRPM6 α -kinase activity. REA is also abundantly present in the TRPM6-expressing DCT segment. Taken together, REA acts as another negative modulator involved in renal Mg²⁺ handling via regulating TRPM6-mediated Mg²⁺ influx (Fig. 1).

So far, REA has only been described as co-repressor of the nuclear ERs. In this study, we also demonstrated for the first time a rapid non-genomic estrogen signaling that activates TRPM6 (also see section *Hormonal control of TRPM6*). Further investigation is, therefore, needed to demonstrate a link between REA and the rapid estrogen signals on TRPM6.

Oxidative stress and channel regulation – MsrB1

MsrB1 was identified as an interaction partner of the TRPM6 α -kinase domain, but does not affect the channel activity in normoxic conditions (**Chapter 4**). MsrB1 is an oxidoreductase which catalyzes the thiol-dependent reduction of methionine sulfoxide [25]. It belongs to the Msr family composed of MsrA and MsrB. Mammals contain one MsrA and three MsrBs that are highly abundant in kidney, liver, heart and nervous tissue [26-30]. These enzymes protect cells from oxidative stress via the repair of oxidative damage to proteins and thereby restore biological activity. They can be involved in reactive oxygen species (ROS)-mediated signal transduction through modulation of the function of target proteins [25, 31-33]. Accumulating evidence suggests that ROS are not only harmful side products of cellular metabolism, but also central players in cell signaling and regulation [34-37]. Free and protein-bound methionine residues are among the most susceptible to oxidation by ROS [38]. Surface exposed methionine residues in a protein are proposed to constitute an antioxidant defense mechanism since various oxidants can easily react with these residues to form methionine sulfoxide. Reduction to methionine by methionine sulfoxide reductases could catalytically drive this antioxidant system as has been suggested by several studies [39-41]. So, the reversible methionine oxidation and reduction plays a dynamic role in cellular signaling pathways [42, 43]. Importantly, there should be a cellular balance between ROS production and its removal through antioxidant mechanisms, as overproduction of ROS results in a condition of oxidative stress. Oxidative stress is an important component in several pathophysiological conditions, such as ischemia/reperfusion and diabetes, potentially contributing to cardiac arrhythmia. Over the last years, several studies have implicated TRPM channels in ischemia [44, 45]. Sun *et al.* showed that decreased TRPM7 channel

expression significantly reduced neuronal cell death after global ischemia [46]. Furthermore, TRPM4 channel activation in vascular smooth muscle has been shown to contribute to cell death of vascular cells during ischemic injury and TRPM2 has been well studied in relation to oxidative stress [47-50]. Interestingly, we have demonstrated that H_2O_2 significantly decreases the TRPM6-mediated current in HEK293 cells. As H_2O_2 did not change the surface expression of TRPM6, it possibly regulates TRPM6 channel activity directly through modulation of the channel conductance. Importantly, the decreased TRPM6 channel activity can be partly recovered by co-expression with MsrB1 (**Chapter 4**). Furthermore, we identified four methionine residues located on the peripheral of the TRPM6 α -kinase domain 3D structure (see <http://www.cmbi.ru.nl/~hvensela/trpm6/>), M¹⁷⁵⁵, M¹⁷⁷⁵, M¹⁹⁰⁴, and M¹⁹⁴⁷. Mutation of M¹⁷⁵⁵ to A significantly attenuates the effect of H_2O_2 on TRPM6 channel activity, mimicking the MsrB1 effect (**Chapter 4**). These data suggest that M¹⁷⁵⁵ is a crucial target of H_2O_2 . Notably, renal DCT cells contain the largest number of mitochondria, the major source of endogenous H_2O_2 , per unit length of any cell along the nephron, underlying a vast source of intracellular H_2O_2 [51]. TRPM6 is predominantly expressed in DCT and is inhibited by H_2O_2 . Therefore, it is conceivable that the metabolic state of DCT cells, which influences the abundance of ROS generated from mitochondria, modulates the Mg^{2+} reabsorption via TRPM6.

Regulation by ATP

Next to the associated proteins, ATP was found as a regulatory factor of the α -kinase domain [52]. The functional role of ATP and the α -kinase domain in regulating TRPM6/TRPM7 channel activity is controversial [22, 52-55]. It has been suggested that Mg^{2+} -ATP acts as a source of Mg^{2+} to decrease channel activity rather than inhibition by ATP itself [53]. On the other hand, it was concluded that ATP-dependent regulation of TRPM7 is mediated via a nucleotide-binding site in the α -kinase domain that acts synergistically with a Mg^{2+} -binding site outside this domain [10, 22]. Interestingly, a recent study demonstrated that intracellular ATP can regulate TRPM6 channel activity via its α -kinase domain [52]. By binding to a conserved ATP-binding pocket in this domain, TRPM6-mediated currents are inhibited in a dose-dependent manner by Na^+ -ATP and Mg^{2+} -ATP [52]. Mutation of a conserved residue (G¹⁹⁵⁵D) in the putative motif eradicated the inhibitory ATP action, whereas this effect remained preserved in the TRPM6 K¹⁸⁰⁴R mutant. The inhibition was specific for ATP as the effect could not be mimicked by GTP or CTP. Furthermore, strong Mg^{2+} chelators like EDTA were used to demonstrate that the inhibitory effect is not due to release of Mg^{2+} from Mg^{2+} -ATP [52]. These results indicate another regulatory mechanism of the α -kinase domain via the effect of intracellular ATP on TRPM6 channel activity independent of α -kinase activity [52].

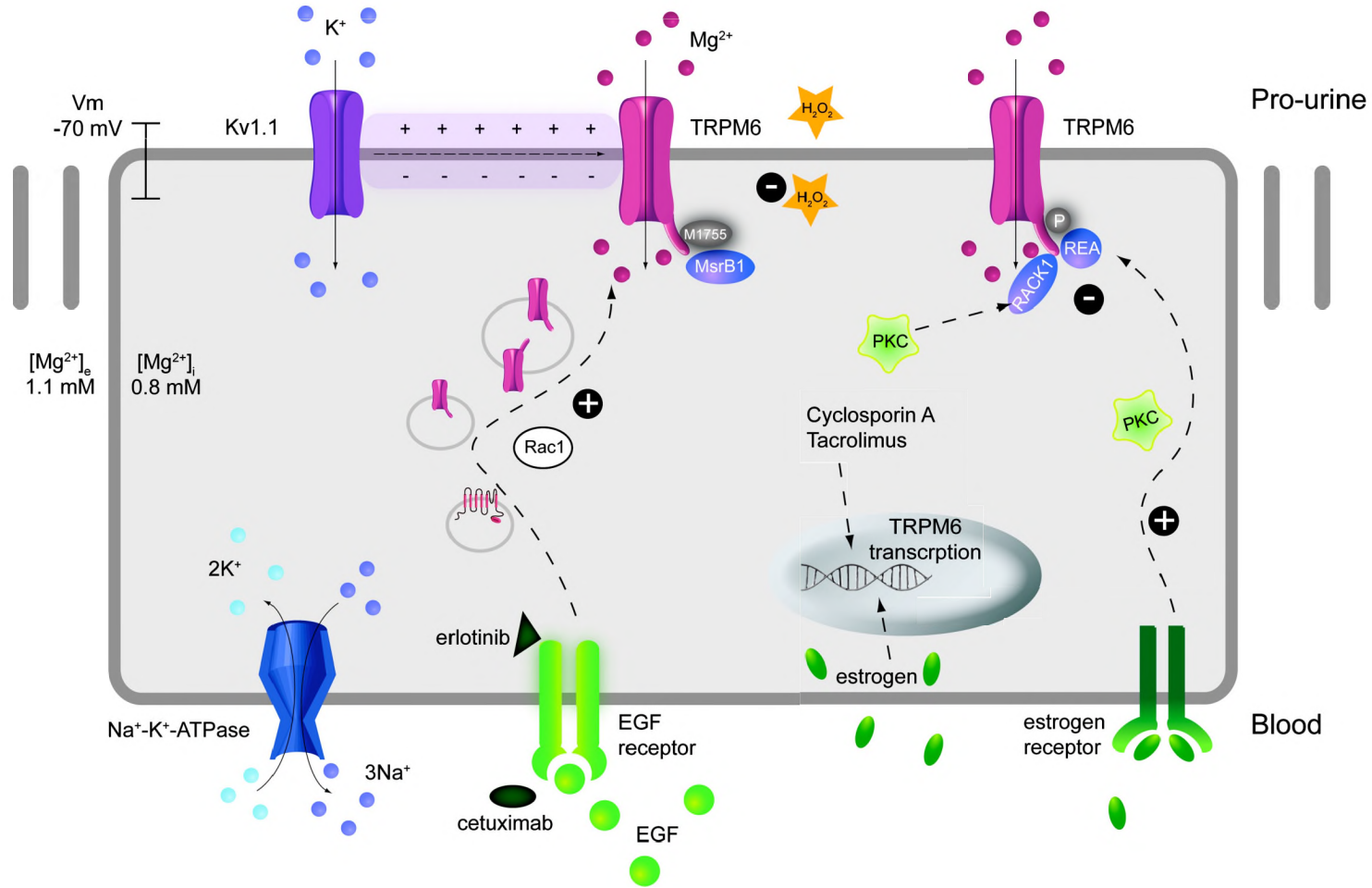


Figure 1. Schematic representation of TRPM6 regulation. TRPM6 channels, located in the luminal membrane, facilitate transport of Mg^{2+} from the pro-urine into the cell, which is primarily driven by the luminal membrane potential established by the voltage-gated K^+ channel, Kv1.1. The intracellular factors RACK1, REA, and MsrB1 were identified as modulators of TRPM6 channel activity, through their binding to the fused alpha-kinase domain. MsrB1 recovers the H_2O_2 inhibitory effect on TRPM6. EGF and estrogen function as magnesiotropic hormones stimulating TRPM6 activity. EGF binds its EGF receptor, thereby activating Rac1-mediated signaling that leads to increased TRPM6 trafficking to the plasma membrane. Estrogen affects TRPM6 via both a genomic and non-genomic pathway. Cetuximab and Erlotinib affect TRPM6 function through inhibition of the EGF receptor.

Conclusion

Taken together, these studies led to new fundamental understanding of the molecular mechanism of transepithelial Mg^{2+} transport and regulation hereof by the TRPM6 alpha-kinase. However, the unique role of alpha-kinase activity on TRPM6 function and vice versa is still unresolved. So, future experiments, using state of the art mass spectrometry and signal transduction technology, should: *i*) identify renal downstream targets of the TRPM6 alpha-kinase domain; *ii*) examine the phosphorylation-control of TRPM6; *iii*) unravel signaling pathways involved in TRPM6 regulation.

Hormonal control of TRPM6

Over the last 10 years several hormones have been suggested to be essential for the maintenance of the Mg^{2+} balance. Previous studies in immortalized mouse DCT cells suggest that parathyroid hormone (PTH), glucagon, and arginine vasopressin (AVP) stimulate Mg^{2+} uptake [56, 57]. However, molecular mechanisms how these hormones affect transepithelial Mg^{2+} transport in the DCT are lacking. In addition, other studies were not able to confirm the stimulatory action of these hormones on Mg^{2+} influx. Recently, two novel regulatory mechanisms involving hormonal control of TRPM6 have been elucidated.

EGF as the first magnesiotropic hormone

Recently, genetic screening of two Dutch sisters with isolated autosomal recessive hypomagnesemia (IRH) led to the discovery of the first magnesiotropic hormone [58]. IRH is due to a mutation in the gene encoding EGF precursor protein pro-EGF (P¹⁰⁷⁰L), which is expressed in DCT together with TRPM6. Physiologically, pro-EGF is sorted to both apical and basolateral membranes where it is cleaved by extracellular proteases into the active molecule EGF [58, 59]. It is suggested that the P¹⁰⁷⁰L mutation, in the cytoplasmic domain, predominantly impairs the release of the hormone to the basolateral site. This disturbs the stimulatory effect of EGF on TRPM6 channel activity and leads to renal Mg^{2+} wasting [58].

Normally, EGF will activate the basolateral EGF receptor (EGFR) following an intracellular signaling cascade to increase TRPM6 surface expression (Fig. 1) [60]. This signaling involves both the Src family of tyrosine kinases and the downstream effector Rac1. Using fluorescence recovery after photo bleaching (FRAP), it was demonstrated that activation of Rac1 increased the mobility of TRPM6 and a constitutively active mutant of Rac1 mimicked the stimulatory action of EGF on TRPM6 mobility and activity [60]. Another study reported that EGF increased the phosphorylation of ERK1/2, leading to upregulation of TRPM6 expression and Mg^{2+} influx, which results in an increase in cell proliferation [61]. Supportive for these studies was the observation that patients treated with the anticancer agent Cetuximab, an EGFR-specific monoclonal antibody, develop hypomagnesemia

[58]. Indeed, pre-incubation with Cetuximab abolished the stimulatory effect of EGF on TRPM6 channel activity.

Erlotinib: A small molecule inhibitor of EGFR

The EGFR is overexpressed in many types of cancer, presumably leading to uncontrolled cell division. Blocking the receptor either using monoclonal antibodies or tyrosine kinase inhibitors would, therefore, slow cancer progression. Instead of Cetuximab, which hinders binding of EGF to its receptor, numerous cancer patients receive tyrosine kinase inhibitors, such as Erlotinib. These compounds bind to the ATP pocket of EGFR and thereby block the downstream signaling. So far, there were no published clinical reports detailing the potential effect of tyrosine kinase inhibitors on systemic and renal Mg^{2+} handling. **Chapter 5** shows that Erlotinib is capable of altering Mg^{2+} handling by affecting TRPM6 regulation. We observed that mice, receiving supraphysiological doses of Erlotinib for 23 days, developed a decrease in their serum Mg^{2+} concentration. In addition, these Erlotinib-injected mice failed to reduce the fractional renal excretion of Mg^{2+} in response to the decreased serum Mg^{2+} concentration. Whole-cell patch clamp analysis revealed that Erlotinib significantly inhibited EGF-stimulated TRPM6 channel activity, through dosages in the same range as the expected plasma concentration in mice (30 μ M of Erlotinib). Although moderate effects of Erlotinib were observed *in vivo*, application of the compound could still inhibit EGF-stimulated TRPM6 channel activity and transport to the plasma membrane. Given that the free circulating concentration of Erlotinib is likely to be around 0.3 μ M in human patients, we tested whether this concentration would be able to block the effect of EGF on TRPM6 channel activity. Here we could not detect any significant differences from EGF-stimulation. Evaluating EGF-induced tyrosine phosphorylation of its receptor substantiated these data. In addition, the inhibitory effect of Erlotinib on Mg^{2+} transport is likely to occur via inhibition of TRPM6 routing, by preventing EGF-mediated changes in the mobile fraction of TRPM6 proteins.

Around 97% of colorectal cancer patients treated with the monoclonal antibody EGFR inhibitors such as Cetuximab develop hypomagnesemia to varying degree [62]. These compounds are currently being considered as first-line treatment for metastatic colorectal cancer. It is now becoming increasingly clear that hypomagnesemia is one of the most commonly reported side effects of these treatments. **Chapter 5** is the first to delineate the effects of Erlotinib on Mg^{2+} handling *in vivo*. The effect on the systemic Mg^{2+} concentration seems less potent than that observed with antibody-based EGFR inhibitors. Still, clinical data concerning the effect of Erlotinib on Mg^{2+} handling is missing. Based on the doses given to cancer patients it is not likely that Erlotinib severely affects serum Mg^{2+} concentrations in these individuals. Furthermore, one could envision that Erlotinib only blocks the overexpressed EGFR often found in tumors, due to its lower affinity for the receptor than EGF and its overall circulating levels in the body. It is, therefore, unlikely to interfere with the normal functions of the EGFR, such as the Mg^{2+} reabsorption in the DCT. However, it should be noted that Erlotinib has

the potential to modulate renal and systemic Mg^{2+} handling *in vivo*. Therefore, caution should be given when treating individuals prone to developing hypomagnesemia, such as patients receiving combinational treatment with Mg^{2+} lowering compounds like cisplatin-based chemotherapy [63].

Table 1. Overview of factors affecting TRPM6

Effect on TRPM6:	mRNA expression	channel activity	Remarks:	Reference:
<u>Intracellular factor:</u>				
$[Mg^{2+}]_i$	-	↓	-	3
pH	-	↑	-	76 (Chapter 1)
H_2O_2	-	↓	-	Chapter 4
ATP	-	↓	-	52
<u>Associated protein:</u>				
RACK1	-	↓	Autophosphorylation-dependent	Chapter 2
REA	-	↓	Kinase activity-dependent	Chapter 3
MsrB1	-	↔	Recovery of oxidative stress	Chapter 4
<u>Hormone:</u>				
EGF	↑	↑	Increases TRPM6 trafficking	60, 61
erlotinib	↓	↔	Blocks EGF-dependent stimulation	Chapter 5
cetuximab	-	↔	Blocks EGF-dependent stimulation	58
Estrogen	↓	↑	-	66 (Chapter 3)
Insulin	↓	-	-	92 (Chapter 1)
<u>Drugs:</u>				
Tacrolimus	↓	-	-	98 (Chapter 1)
Cisplatin	↓	-	-	Unpublished results
Cyclosporin A	↓	-	-	Ikari <i>et al.</i> , 2008
<u>Other:</u>				
<u>Chronic metabolic:</u>				
alkalosis	↓	-	-	93 (Chapter 1)
acidosis	↑	-	-	93 (Chapter 1)
<u>Mg²⁺ diet:</u>				
enriched	↓	-	-	66
restricted	↑	-	-	66

Two estrogen signaling pathways affecting TRPM6

Genomic pathway

Estrogen has also been suggested as magnesiotropic hormone since clinical studies have shown that the hypermagnesiuria in postmenopausal women significantly reduced after estrogen therapy [64, 65]. In addition, Groenestegé *et al.* [66] demonstrated that the renal TRPM6 mRNA level is decreased in ovariectomized rats, which could be restored by supplementation with 17β -estradiol. This effect

can be explained by enhanced transcriptional activity or mRNA stabilization of TRPM6. Thus far, detailed analysis did not result in estrogen-responsive elements in the putative promoter site of TRPM6.

Non-genomic pathway

Next to the classical transcriptional pathway, accumulating evidence suggests also rapid estrogen effects that occur within minutes via a non-transcriptional route [67-69]. Interestingly, our study revealed a rapid stimulatory effect of 17 β -estradiol on TRPM6 (**Chapter 3**). Treatment with 17 β -estradiol disassociated the binding between REA and TRPM6 α -kinase domain, thereby attenuating its inhibitory effect on TRPM6 channel activity (Fig. 1). In agreement with this, 17 β -estradiol significantly stimulated TRPM6 activity, without affecting the plasma membrane trafficking (**Chapter 3**). Estrogen has the ability to facilitate rapid membrane-initiated signaling cascades through activation of plasma membrane-associated receptors, such as the recently discovered G protein-coupled receptor 30 (GPCR30) [70]. In addition, it was demonstrated that the classical estrogen receptor alpha (ER α) is localized to the plasma membrane in response to estrogen or by interaction with adaptor proteins like Shc and p130Cas [71, 72]. Thus, the signaling pathway of estrogen receptor activation leading to increased TRPM6 activity needs to be further investigated.

Link between estrogen signaling and EGFR

Both estrogen and EGF are required for growth and survival, particularly of estrogen-responsive tissues. However, the receptors that mediate the effects of estrogen and EGF utilize apparent different signaling mechanisms. The proliferative effects of estrogen are primarily mediated by nuclear ERs that induce gene transcription in these tissues [73]. In contrast, EGF activates EGFRs, that signal through transmembrane receptor tyrosine kinases (RTKs), which in turn recruit intracellular signaling cascades. However, more evidence is appearing that these divergent signaling mechanisms may cross-communicate. Interestingly, *in vivo* administration of estrogen was shown to upregulate EGFR expression [74, 75]. While this was first shown to be the consequence of ER-mediated gene transcription, other studies reported that estrogen could promote rapid EGF-like effects. This link between estrogen and EGF signaling was highlighted shortly after the discovery of GPR30. GPR30, also referred to as GPER1 (G protein-coupled estrogen receptor1), was identified based on the difference in gene expression in response to estrogen in breast cancer cells [76]. Subsequently, it was shown by several groups that GPR30 is activated by estrogen [70, 77-79].

It has been demonstrated that GPR30 stimulation leads to the activation of the trimeric G protein ($\alpha\beta\gamma$). The α subunit induces activation of adenylate cyclase, which results in the production of cAMP. The β and γ subunits of the G protein activate Src tyrosine kinase that, via several signaling molecules, can activate matrix metalloproteinase (MMP). It should be noted that inactive membrane-

anchored precursors of EGF (pro-EGF) must be cleaved and released by metalloproteinases to generate the active, mature form of the growth factor [80]. So, the activated MMP degrades pro-EGF, which releases EGF that can then activate the EGFR via an autocrine/paracrine mechanism, leading to the activation of PI-3K. The activated EGFR also induces ERK activation [81, 82]. In the past years, transactivation of EGFRs by GPCRs is a recurrent theme in cell signaling [83] and it would be interesting to take this mechanism into account when studying hormonal regulation of TRPM6.

Conclusion

Altogether, these recent studies highlight an important role for EGF and estrogen signaling in the maintenance of Mg^{2+} homeostasis with TRPM6 as a critical player. It would be interesting to investigate the effect of other blocking antibodies and antagonists of the EGFR on Mg^{2+} balance in general and in particular on TRPM6 activity. Furthermore, it would be highly significant to elucidate the estrogen signaling pathway leading to TRPM6 stimulation.

Kv1.1 as new player in TRPM6-mediated Mg^{2+} transport

Voltage-gated K^+ channels (Kv) are a diverse family of membrane proteins, with the Shaker-related group (Kv1) representing a major sub-family [84-86]. Its members play an important role in excitable cells by setting the resting membrane potential, shaping the action potentials, and by controlling the neuronal excitability [87]. Kv channels comprise of four subunits that encircle a central ion conduction pathway [88, 89]. Each subunit consists of six transmembrane-spanning α -helices (S1-S6) with both the amino (N) and the carboxyl (C) terminal on the intracellular side. The S1-S4 segments form the voltage sensing domain, whereas S5 and S6 along with the intervening re-entrant P-loop form the pore domain [90, 91]. Kv channels are known to switch between the closed and open conformation upon cell depolarization [91, 92]. Kv1.1 was the first mammalian subunit of the Kv family to be cloned and is abundantly expressed in excitable and non-excitable cells [93, 94]. Studies with Kv1.1 knock-out (KO) mice showed that deletion of Kv1.1 results in a seizure disorder similar to epilepsy [95].

Genotype – Phenotype

Chapter 6 describes the identification of a novel mutation in the *KCNA* gene, encoding the voltage-gated Kv1.1, in a family with isolated autosomal dominant hypomagnesemia. Affected individuals showed low serum Mg^{2+} levels (< 0.40 mM, normal range 0.70-0.95 mM), while their urinary Mg^{2+} excretion was normal, suggesting impaired tubular Mg^{2+} reabsorption. The phenotype of the proband starting from infancy consists of recurrent muscle cramps, tetanic episodes, tremor and muscle weakness, especially in distal limbs (**Chapter 6**). Previously identified mutations in Kv1.1 are characterized by episodic ataxia 1 (EA1; OMIM 160120), which manifests during the first or second

decade of life [96-110]. Attacks of ataxia are in some cases accompanied by myokymia [96-107, 109], neuromyotonia [99-105, 107] and epilepsy [99, 100, 106]. The diverse phenotype is nicely illustrated by the mutation of the Kv1.1 residue Thr226, which dependent on the mutation causes isolated EA1 (T²²⁶A), isolated myokymia (T²²⁶K) or a mixture of EA1, myokymia and epilepsy that can vary between families and even among family members affected by the same mutation (T²²⁶R).

The affected members of our Brazilian family were also analyzed for episodic ataxia. On a cerebral MRI of the proband we obtained evidence of a slight atrophy of the cerebral vermis (data not shown). Furthermore, electromyographs of some affected members showed myokymic discharge in line with the previously observed mixed phenotype (**Chapter 6**). Now, hypomagnesemia is presented as a new phenotypic characteristic associated with a mutation in *KCNA1*. As it was unknown whether renal Mg²⁺ handling is also affected in patients with other *KCNA1* mutations, serum Mg²⁺ levels were evaluated. Three EA1 patients have been analyzed [103, 104, 109] and their serum Mg²⁺ levels (I²⁶²T: 0.76 mM; L³⁰⁵P: 0.80 mM; V⁴⁰⁴I: 0.73 mM) were within the normal range (0.7-1.1 mM) (unpublished data). Possibly, as observed for EA1, the hypomagnesemia differs in time and should, therefore, be measured at different time points. It would be interesting to perform in the near future a large-scale phenotypical characterisation of patients with identified mutations in the *KCNA1* gene including neurological description, serum Mg²⁺ levels and functional analysis of the corresponding Kv1.1 mutations.

Functional characterization

So far, electrophysiological analyses of these mutant Kv1.1 channels showed either a significant reduction in current amplitude or altered kinetic properties compared to wild-type Kv1.1 channels [98, 100, 111]. The mutation identified in the Brazilian family caused substitution of the asparagine at amino acid position 255 into an aspartic acid (N²⁵⁵D). The asparagine at position 255 is highly conserved among species and Kv1 family members, which suggests its importance in channel function. Indeed, we demonstrated that the change of the neutral asparagine into a negatively charged aspartic acid results in a non-functional channel (**Chapter 6**). It has been shown that Kv1.1 channel subunits can assemble with other Kv channel subunits to form heterotetramers [112]. Importantly, hypomagnesemia in the Brazilian family is inherited in an autosomal dominant manner and patients with the N²⁵⁵D mutation are heterozygous. Expression of both alleles likely results in the formation of heterotetrameric channels composed of wild-type and mutated channel subunits leading to a dominant negative effect by the Kv1.1 N²⁵⁵D subunit (**Chapter 6**). The mutation replaces a neutral amino acid (asparagine) by one with an acidic side-chain (aspartic acid), which may destabilize the secondary or tertiary channel structure and thereby channel formation or trafficking. However, we demonstrated that wild-type Kv1.1 channels, Kv1.1 N²⁵⁵D channels, and the combination hereof are expressed in equal amounts at the plasma membrane (**Chapter 6**).

Interestingly, the newly identified heterozygous Asn²⁵⁵Asp mutation is positioned close to the voltage sensor element (S4). S4 contains a long array of positive charges that are believed to sense differences in voltage and start the transition from the closed to open conformation by forming stabilizing hydrogen bonds with the external and internal negative clusters in the voltage-sensing domain [113, 114]. The evidence of a closely located, complicated hydrogen network together with introduction of an additional charge, led to the hypothesis that the N²⁵⁵D mutation interferes with the voltage sensor characteristics of Kv1.1. Therefore, the tertiary structure of Kv1.1 was modeled by the WHAT-IF server, based on 75% sequence identity with the crystallized Kv1.2-Kv2.1 chimeric channel [88, 115]. Additionally, six mutations were introduced at position 255 to study amino acid substitution at position 255 in relation to channel function more extensively (**Chapter 7**). Depending on the polarity of the side chain, amino acids vary in their hydrophilic or hydrophobic character [116]. These properties are important determinants of the protein structure and the physical properties of the side chains influence the amino acid residues' interactions with other structures, both within a single protein and between proteins. Importantly, the change in amino acid at position 255 had no effect on channel trafficking as all mutant were expressed at the plasma membrane (**Chapter 7**). The hydrophilic asparagine residue could be important for structural rearrangements within the channel in response to voltage changes, which are possibly hampered by the introduction of a negative residue (N²⁵⁵D). To investigate this, another negative glutamic acid (N²⁵⁵E) or positive histidine (N²⁵⁵H) residue were introduced. Compared to asparagine, the glutamic acid contains an extra CH₂-group. As a control for steric hindrance, the non-charged glutamine was introduced (N²⁵⁵Q), which is the same size as Glu. Whole-cell patch clamp analysis demonstrated that N²⁵⁵E and N²⁵⁵Q channels were non-functional, while N²⁵⁵H functions as a normal channel. This indicates that next to the addition of a negative charge at position 255 also an additional CH₂-group in the side-chain influences channel function, likely by conformational rearrangements. Alternatively, introduction of the N²⁵⁵D mutation may block the formation of hydrogen bonds, which reduces the stability of the Kv1.1 channel structure. Therefore, alanine (N²⁵⁵A), valine (N²⁵⁵V), and threonine (N²⁵⁵T) were introduced. Alanine and valine contain both non-polar side chains such that participation in hydrogen bonds is precluded, whereas threonine has an alcoholic group in its side-chain and is, therefore, able to contribute to hydrogen binding. These amino acid substitutions had no effect on Kv1.1 channel activity as shown by patch clamp analysis. Furthermore, the voltage-dependence and kinetics of channel gating of these functional mutants (N²⁵⁵A, N²⁵⁵V, N²⁵⁵T, N²⁵⁵H) was examined (**Chapter 7**). There was no correlation between the size, loss of hydrogen bond or charge and the magnitude of the shift in V_{1/2} for activation or inactivation. Though, the acceleration of the inactivation process is also of interest, as it is explained by a constriction mechanism of the outer mouth of the channel vestibule [117, 118]. The N²⁵⁵H mutation enables the channel to undergo a slightly faster inactivation (**Chapter 7**), which might indicate that the residue at this position takes part in the conformational change during inactivation. So, charged residues at position 255 could be important for conformational changes

since this effect was specific for N²⁵⁵H. It has already been demonstrated that negatively charged clusters in the S2 and S3 segments, together with the positive charges in S4, are involved in the opening and closing of Kv1 channels [115]. In line with this, an earlier study showed that mutation of conserved negatively charged residues in the S2 and S3 segments selectively modulated channel gating. Mutation of the aspartic acid at position 258 in Kv1.1 even abolished channel activity [119]. Therefore, we suggest that an additional negative charge nearby this cluster in S3 could keep the channel in the inactivated state, which may explain the non-functionality of the mutation found in patients with hypomagnesemia (N²⁵⁵D). Altogether, Asn²⁵⁵ is essential for normal channel function, since substitution by other amino acids significantly altered channel activity, voltage-dependence and kinetics of Kv1.1 channels, but more detailed structural information is necessary to specify the involvement of this residue in voltage-sensing and channel opening.

Expression and physiological role of Kv1.1

Kv1.1 was shown to localize to the apical membrane of DCT cells and postulated to be involved in the generation of a favorable apical membrane voltage as a driving force for Mg²⁺ entry. The Mg²⁺ influx via TRPM6 is energized by the local electrochemical gradient. Importantly, the DCT cell lacks a substantial chemical gradient for Mg²⁺. The Mg²⁺ concentration in the pro-urine is likely around 1.1 mM, while the free intracellular Mg²⁺ concentration has been estimated to be 0.5–1.0 mM [120]. The luminal membrane potential in the DCT is approximately -70 mV [121], favouring luminal Mg²⁺ influx. Thus, the movement of Mg²⁺ into the DCT cell seems mainly driven by the electrical gradient. The renal outer medullary potassium channel (ROMK) was proposed to generate the luminal membrane potential via K⁺ efflux. Nevertheless, immunolocalization studies showed specific ROMK staining in the TAL and connecting tubule (CNT), but not the DCT [122]. Alternatively, Kv1.1 has been identified as luminal K⁺ channel in DCT that is believed to establish a favourable luminal membrane potential to control TRPM6-mediated Mg²⁺ reabsorption. Consequently, mutation of Kv1.1 residue Asn²⁵⁵ leads to impairment of renal Mg²⁺ handling [125] (**Chapter 6**). Interestingly, the fact that Kv1.1 channels expressed in DCT cells are not easily activated at the existing membrane potential suggest that their activities are relatively transient, making it difficult to ascribe a functional role. However, there are many examples of Kv channels expressed in epithelial tissue with diverse functions including transepithelial electrolyte transport, cell volume regulation, K⁺ secretion, and apoptosis [94, 123, 124]. Future studies should confirm the exact role of Kv1.1 channels in the DCT cell.

It is, however, still unknown how distinct mutations in nearby amino acid residues in Kv1.1 can result in phenotypes with dysfunction in two different organs (brain and kidney). There are several mechanisms to explain the kidney-associated phenotype, which so far has only been observed for the Kv1.1 N²⁵⁵D mutation: *i*) the composition of Kv1.1 channels in brain and kidney is different, due to tissue-specific expression of auxiliary β -subunits or co-assembly with other Kv1 subunits that define

the functional characteristics of these channels [126-128]; *ii*) the Kv1.1 N²⁵⁵D mutation may have a dominant effect on the function of an unidentified kidney-specific interaction partner, but not on the interaction partners expressed in brain; *iii*) the expression of an alternative tissue-specific Kv1.1 coding sequence. So far, most studies have focused on the neurological phenotype and other kidney-specific transcripts may have been missed. For that reason, it is interesting to investigate whether other Kv1.1 transcripts exist within the kidney; *iv*) post-translational modification processes differ between tissues such as the brain and kidney. In combination with the mutation, this may give rise to a tissue-specific phenotype. Importantly, further experiments are necessary to identify the mechanism that underlies the kidney-specific phenotype.

Kir4.1 as new K⁺ channel in the DCT

Recently, mutations in the *KCNJ10* gene, encoding the K⁺ channel Kir4.1, were identified as the cause for a unique autosomal recessive form of Gitelman-like renal salt wasting disorder [129, 130]. Patients have a complex combination of features that is called EAST syndrome: epilepsy, ataxia, sensorineural deafness, and (a salt-wasting) renal tubulopathy (or seizures, sensorineural deafness, ataxia, mental retardation, and electrolyte imbalance (SeSAME)). Kir4.1 immunostaining has been found at the basolateral membrane of the DCT in human, rat and mice [131, 132]. Here, the Na⁺,K⁺-ATPase facilitates transport of Na⁺ to the interstitium and K⁺ to the intracellular compartment against their respective chemical gradients, generating a driving force for luminal NaCl influx via NCC and basolateral Cl⁻ transport via ClC-Kb. Kir4.1 is suggested to recycle K⁺ into the interstitium to allow a sufficient supply of K⁺ for optimal Na⁺,K⁺-ATPase activity. Another functional adaptation of DCT cells is that they are rich in mitochondria and have deep basolateral infoldings, leading to increased membrane surface. These characteristics were shown to be greatly diminished under conditions with lowered transport activity, as shown in a mouse model for GS [133]. The transport processes in the DCT are similarly affected in patients with EAST syndrome [129].

Conclusion

Taken together, the emerging role for particularly K⁺ channels in controlling the reabsorption of Mg²⁺ and their localization to the same tubule segments is remarkable. Combined disturbances in the K⁺ and Mg²⁺ balance are frequently observed in common pathological conditions. An extensively studied case is Gitelman syndrome, where patients endure hypokalemic metabolic alkalosis with hypomagnesemia and hypocalciuria [134, 135]. Additionally, individuals suffering from hypokalemia often require co-administration of Mg²⁺ and K⁺ in order to correct the hypokalemia successfully [136]. Furthermore, several K⁺ channels, including Kv1.1, are shown to be sensitive to intracellular Mg²⁺ [137]. Future studies should reveal the interrelationship between K⁺ and Mg²⁺ homeostasis.

Intracellular Mg^{2+} detection

As discussed in this thesis, Mg^{2+} is an essential electrolyte for all living organisms. Though, studying the correlation between the biochemical characteristics of Mg^{2+} and its involvement in a plethora of biological functions has been obstructed by missing appropriate techniques to monitor changes in free $[Mg^{2+}]_i$ in the cell. The following paragraphs compose a summary of various methods that are presently used to measure $[Mg^{2+}]_i$ or Mg^{2+} transport in cells.

Atomic absorbance spectrophotometry^[138]

This is the most commonly used method for measuring Mg^{2+} in biological samples, because it has advantages in terms of selectivity, sensitivity, and reproducibility. The determinations are usually carried out in the presence of other cations to minimize complexes with interfering anions. In view of the relatively high cellular Mg^{2+} content, the sensitivity is also a drawback because it requires dilution of samples or determination after culturing under artificially low concentrations of extracellular Mg^{2+} . Other major limitations are that it measures total, rather than free, Mg^{2+} content and that the technique requires lysis of the sample, which limits any kinetic analysis.

Radioactive $^{28}Mg^{2+}$

Radioactive Mg^{2+} can be used in uptake assays, which allow the calculation of the kinetic parameters, like the Michaelis constant (K_m), dissociation constant (K_i) and maximum rate of uptake (V_{max}), to ultimately determine changes in Mg^{2+} content of cells. However, the radioactive half-life of ^{28}Mg , the most stable of the radioactive Mg^{2+} isotopes, is only 21 hours. This fast decay severely restricts the number of possible experiments. In addition to these limitations intrinsic to any isotopic trace determination, ^{28}Mg is not routinely produced and is only available at an exorbitant cost.

^{31}P nuclear magnetic resonance spectroscopy

Nuclear magnetic resonance (NMR) spectrometry was first used to estimate free $[Mg^{2+}]_i$ in 1977 [139]. This method was proven to be useful for estimating free Mg^{2+} content non-invasively in biological samples. It is based on differences in NMR spectral signal of the two major ATP forms in the cell, namely free ATP and Mg-ATP complex. A major drawback is the lack of sensitivity, as the shift observed under normal conditions is only a fraction of the possible spectral shift. This is due to the fact that most cytosolic ATP is in the ATP-Mg form. So, even large changes in intracellular Mg^{2+} content will have only a small effect on the concentrations of ATP-Mg and therefore on the apparent shift. This means that the technique will be relatively insensitive to physiological changes in cytosolic free Mg^{2+} for most mammalian cells. Furthermore, the accuracy of free $[Mg^{2+}]_i$ determination depends on the dissociation constant (K_d) used and on factors that influence this equilibrium, such as pH, temperature and osmolarity in the cell [140].

Mg²⁺-selective electrodes

The first Mg²⁺-selective microelectrode was developed about 30 years ago (ETH1117, [141]). Unfortunately, the cytosolic Mg²⁺ values obtained with this electrode were quite variable, most likely due to lack of selectivity for Mg²⁺ over K⁺. In 1989, a significantly improved Mg²⁺-selective ionophore was developed (ETH 5214, [142]), based on which several new ionophores have been developed in the past years (reviewed by Günzel [143]). These electrodes have been widely used as they have some advantages over other techniques. First, the membrane potential is measured simultaneously, so that the condition of the cell is constantly monitored. Second, these microelectrodes, with very few exceptions, cannot penetrate intracellular organelles, so that their response exclusively reflects concentration changes within the cytoplasm. Once successfully impaled, microelectrodes allow continuous recording as long as the impalement holds, even for up to several hours. However, a major disadvantage is that their use is limited to relatively large, strong cells, like oocytes, in which changes can only be monitored at the specific location of impalement. Furthermore, there is mostly interference from other cellular cations as Na⁺ and K⁺, which requires the simultaneous measurements of many ions via multibarrel microelectrodes [144] followed by appropriate corrections.

Fluorescent indicators

Commercial Mg²⁺ indicators

Fluorescent indicators provide a tool to measure [Mg²⁺]_i levels and transients in individual cells with both spatial and temporal resolution. The first report of a fluorescent indicator that was able to measure Mg²⁺ levels in serum and urine appeared in 1959 [145]. It took thirty years for the development of a new fluorescent Mg²⁺ indicator, named mag-fura-2 (or furaptra by Raju *et al.* [146]). This compound is based on the Ca²⁺ indicator fura-2 (Grynkiewicz *et al.*). In general, the usefulness of fluorescent indicators in measuring [Mg²⁺]_i depends on the ability to load cells with the compound and on the affinity for Mg²⁺. Cell loading with mag-fura-2 and other indicators is generally realized with an acetoxymethylester derivative (mag-fura-2-AM), which diffuses into the cell where cytosolic esterases cleave the acetoxymethyl group such that the indicator gets trapped. Importantly, mag-fura-2 has a higher affinity for Ca²⁺ than for Mg²⁺ (K_d ≈ 50 μM vs. 1.5 mM, respectively [147]). Thus, only the fact that the [Ca²⁺]_i in most cells is in the nanomolar range permits mag-fura-2 to be used as Mg²⁺ indicator. In addition, polyamines, such as putrescine and spermine, have been reported to reduce the response of mag-fura-2 to Mg²⁺ [148]. Similarly, alterations in cell volume during an experiment may produce viscosity changes that can alter mag-fura-2 responses [149]. Based on the discovery of mag-fura-2, several other fluorescent indicators have synthesized with slightly different dissociation constants and characteristics, which are listed in the Molecular Probes catalog [150]. However, they still have a relatively high affinity for Ca²⁺, thereby requiring appropriate corrections that limit their use.

KMG-104

In 2004, Komatsu *et al.* synthesized three novel Mg^{2+} fluorescent indicators KMG-101, -103, and -104 [151]. The compounds of this series feature a charged β -diketone as a binding site specific for Mg^{2+} and a fluorescein residue as the fluorophore that can be excited with an Ar+ laser such as is widely used in confocal scanning microscopy. Among the KMG series, the KMG-104 showed the best properties. It has a suitable dissociation constant ($K_d \approx 2.1$ mM) and had significantly lower affinity for Ca^{2+} ($K_d \approx 7.5$ mM). Furthermore, it appears to be unaffected by pH shifts between 6.0 and 7.6 [151]. This led to the development of the membrane-permeable KMG-104-AM, which can be employed for sensitive and selective Mg^{2+} determination. In the past years, this probe has been used to measure $[Mg^{2+}]_i$ in several mammalian cell types [152-154]. However, the major disadvantage of the KMG series is that their measurement is based on a single wavelength, termed non-ratiometric, which may lead to artificial alterations in the fluorescence signal that could be misinterpreted as changes in Mg^{2+} level. These alterations are most likely due to changes in cell volume in response to osmolarity differences in the intracellular and extracellular milieu. Interestingly, our group has also used KMG-104-AM to measure $[Mg^{2+}]_i$ and demonstrated increase in fluorescence signal in response to increasing Mg^{2+} -containing extracellular solutions. Unfortunately, we were not able to detect any KMG-104 signal when Mg^{2+} -containing solutions were corrected for osmolarity changes, indicating that this putative Mg^{2+} probe is not specifically Mg^{2+} -sensitive but rather too responsive to other cellular responses as cell swelling/shrinking. (unpublished data).

Other possibilities

On one hand, the ideal Mg^{2+} indicator is still not available, while on the other hand, other imaging techniques could also be essential to better exploit the existing indicators. For example, Fluorescence Lifetime Imaging Microscopy (FLIM) can produce an image based on the differences in decay rate of fluorescence. So, the lifetime of the signal, rather than its intensity, is used to create the image in FLIM. As most of the fluorescent indicators undergo a change in fluorescence lifetime upon Mg^{2+} binding, this method could be used for imaging. Furthermore, FLIM can create an image contrast at each point in a two-dimensional image, thereby taking information on cellular changes due to the chemical environment (pH, viscosity) into account during the measurement. A different approach would be the development of FRET-based sensors by inserting a natural Mg^{2+} binding site in the cyan-yellow fluorescent proteins (CFP-YFP), which are commonly used in FRET-based methods. The protein will undergo a conformational change upon Mg^{2+} binding, leading to a FRET change. Importantly, these proteins could also be employed for targeting to specific subcellular locations, allowing detailed Mg^{2+} measurement at the plasma membrane or in certain organelles as mitochondria.

The ultimate challenge is not only to design the probe with ideal characteristics, but also to develop appropriate tools to study Mg^{2+} levels *in vivo*. A combinational approach including chemical,

physical and biological methods will be necessary for the synthesis of new probes and imaging techniques to allow this scenario to come true.

Summary

It can be concluded that none of the above-described techniques is without serious drawbacks, which stresses the need to develop alternative approaches. The possibility to measure $[Mg^{2+}]_i$ in a living organism would highly advance the Mg^{2+} -related research.

Conclusion and future directions

The overall aim of this thesis was to provide more insight in the physiological and molecular regulation of transepithelial Mg^{2+} transport processes. The studies presented in this thesis illustrated the identification of regulators of TRPM6 and the discovery of Kv1.1 as new renal ion channel essential in controlling the body's Mg^{2+} balance. This research has greatly increased our knowledge on the mechanisms that regulate the active Mg^{2+} reabsorption through effects on TRPM6 function. However, the processes of cytosolic Mg^{2+} diffusion and basolateral extrusion are not well studied. In the past years, much of the understanding of mechanisms regulating Mg^{2+} homeostasis has come from studies of inherited forms of Mg^{2+} wasting. So, discovery of new genes by genetic screening studies might help to elucidate these processes further. In addition, several Mg^{2+} transport proteins have been discovered through homology searches with prokaryotic counterparts and screening for genes that were upregulated in cells that were subjected to low $[Mg^{2+}]_e$. Further investigation could unravel a possible physiological role of the protein products of these genes in renal Mg^{2+} handling and improved Mg^{2+} detection methods will certainly help in the classification and validation of these proteins. Moreover, a future challenge would be to further understand the role of the fused α -kinase domain in TRPM6 function. So far, the investigations described in this thesis demonstrated an indirect regulatory role of the α -kinase domain via interaction with proteins that modulate TRPM6 channel activity. New projects should aim to investigate the mechanism of a direct interrelationship between TRPM6 channel function and α -kinase activity by identification of renal downstream target protein of this domain and by unraveling the phosphorylation-dependent control of TRPM6. Altogether, future studies should increase our understanding of the molecular mechanism of transepithelial Mg^{2+} transport and regulation hereof by the TRPM6 channel and its fused alpha-kinase. Subsequently, this can be exploited to develop novel therapies for hypomagnesemia and associated pathologies.

References

1. Schlingmann KP, Weber S, Peters M, *et al.*: Hypomagnesemia with secondary hypocalcemia is caused by mutations in TRPM6, a new member of the TRPM gene family. *Nat Genet* 31:166-170, 2002
2. Walder RY, Landau D, Meyer P, *et al.*: Mutation of TRPM6 causes familial hypomagnesemia with secondary hypocalcemia. *Nat Genet* 31:171-174, 2002
3. Voets T, Nilius B, Hoefs S, *et al.*: TRPM6 forms the Mg²⁺ influx channel involved in intestinal and renal Mg²⁺ absorption. *J Biol Chem* 279:19-25, 2004
4. Chubanov V, Waldegger S, Mederos y Schnitzler M, *et al.*: Disruption of TRPM6/TRPM7 complex formation by a mutation in the TRPM6 gene causes hypomagnesemia with secondary hypocalcemia. *Proc Natl Acad Sci US A* 101:2894-2899, 2004
5. Li M, Jiang J, Yue L: Functional characterization of homo- and heteromeric channel kinases TRPM6 and TRPM7. *J Gen Physiol* 127:525-537, 2006
6. Li M, Du J, Jiang J, *et al.*: Molecular determinants of Mg²⁺ and Ca²⁺ permeability and pH sensitivity in TRPM6 and TRPM7. *J Biol Chem* 282:25817-25830, 2007
7. Montell C: Mg²⁺ homeostasis: the Mg²⁺-nificent TRPM channels. *Curr Biol* 13:R799-801, 2003
8. Runnels LW, Yue L, Clapham DE: TRP-PLIK, a bifunctional protein with kinase and ion channel activities. *Science* 291:1043-1047, 2001
9. Schmitz C, Dorovkov MV, Zhao X, *et al.*: The channel kinases TRPM6 and TRPM7 are functionally nonredundant. *J Biol Chem* 280:37763-37771, 2005
10. Schmitz C, Perraud AL, Johnson CO, *et al.*: Regulation of vertebrate cellular Mg²⁺ homeostasis by TRPM7. *Cell* 114:191-200, 2003
11. Ryazanov AG, Pavur KS, Dorovkov MV: Alpha-kinases: a new class of protein kinases with a novel catalytic domain. *Curr Biol* 9:R43-45, 1999
12. Riazanova LV, Pavur KS, Petrov AN, *et al.*: [Novel type of signaling molecules: protein kinases covalently linked to ion channels]. *Mol Biol (Mosk)* 35:321-332, 2001
13. Ryazanov AG: Elongation factor-2 kinase and its newly discovered relatives. *FEBS Lett* 514:26-29, 2002
14. Yamaguchi H, Matsushita M, Nairn AC, *et al.*: Crystal structure of the atypical protein kinase domain of a TRP channel with phosphotransferase activity. *Mol Cell* 7:1047-1057, 2001
15. Diggle TA, Seehra CK, Hase S, *et al.*: Analysis of the domain structure of elongation factor-2 kinase by mutagenesis. *FEBS Lett* 457:189-192, 1999
16. Clark K, Middelbeek J, Dorovkov MV, *et al.*: The alpha-kinases TRPM6 and TRPM7, but not eEF-2 kinase, phosphorylate the assembly domain of myosin IIA, IIB and IIC. *FEBS Lett* 582:2993-2997, 2008
17. Clark K, Middelbeek J, Morrice NA, *et al.*: Massive autophosphorylation of the Ser/Thr-rich domain controls protein kinase activity of TRPM6 and TRPM7. *PLoS ONE* 3:e1876, 2008
18. Clark K, Middelbeek J, Lasonder E, *et al.*: TRPM7 regulates myosin IIA filament stability and protein localization by heavy chain phosphorylation. *J Mol Biol* 378:790-803, 2008
19. Steele MR, McCahill A, Thompson DS, *et al.*: Identification of a surface on the beta-propeller protein RACK1 that interacts with the cAMP-specific phosphodiesterase PDE4D5. *Cell Signal* 13:507-513, 2001
20. Ron D, Chen CH, Caldwell J, *et al.*: Cloning of an intracellular receptor for protein kinase C: a homolog of the beta subunit of G proteins. *Proc Natl Acad Sci US A* 91:839-843, 1994
21. McCahill A, Warwicker J, Bolger GB, *et al.*: The RACK1 scaffold protein: a dynamic cog in cell response mechanisms. *Mol Pharmacol* 62:1261-1273, 2002
22. Demeuse P, Penner R, Fleig A: TRPM7 channel is regulated by magnesium nucleotides via its kinase domain. *J Gen Physiol* 127:421-434, 2006
23. Takezawa R, Schmitz C, Demeuse P, *et al.*: Receptor-mediated regulation of the TRPM7 channel through its endogenous protein kinase domain. *Proc Natl Acad Sci US A* 101:6009-6014, 2004

24. Montano MM, Ekena K, Delage-Mourroux R, *et al.*: An estrogen receptor-selective coregulator that potentiates the effectiveness of antiestrogens and represses the activity of estrogens. *Proc Natl Acad Sci U S A* 96:6947-6952, 1999
25. Grimaud R, Ezraty B, Mitchell JK, *et al.*: Repair of oxidized proteins. Identification of a new methionine sulfoxide reductase. *J Biol Chem* 276:48915-48920, 2001
26. Moskovitz J, Weissbach H, Brot N: Cloning the expression of a mammalian gene involved in the reduction of methionine sulfoxide residues in proteins. *Proc Natl Acad Sci U S A* 93:2095-2099, 1996
27. Kuschel L, Hansel A, Schonherr R, *et al.*: Molecular cloning and functional expression of a human peptide methionine sulfoxide reductase (hMsrA). *FEBS Lett* 456:17-21, 1999
28. Fomenko DE, Novoselov SV, Natarajan SK, *et al.*: MsrB1 (methionine-R-sulfoxide reductase 1) knock-out mice: roles of MsrB1 in redox regulation and identification of a novel selenoprotein form. *J Biol Chem* 284:5986-5993, 2009
29. Jung S, Hansel A, Kasperczyk H, *et al.*: Activity, tissue distribution and site-directed mutagenesis of a human peptide methionine sulfoxide reductase of type B: hCBS1. *FEBS Lett* 527:91-94, 2002
30. Hansel A, Jung S, Hoshi T, *et al.*: A second human methionine sulfoxide reductase (hMSRB2) reducing methionine-R-sulfoxide displays a tissue expression pattern distinct from hMSRB1. *Redox Rep* 8:384-388, 2003
31. Stadtman ER, Moskovitz J, Berlett BS, *et al.*: Cyclic oxidation and reduction of protein methionine residues is an important antioxidant mechanism. *Mol Cell Biochem* 234-235:3-9, 2002
32. Moskovitz J: Roles of methionine sulfoxide reductases in antioxidant defense, protein regulation and survival. *Curr Pharm Des* 11:1451-1457, 2005
33. Cabreiro F, Picot CR, Friguet B, *et al.*: Methionine sulfoxide reductases: relevance to aging and protection against oxidative stress. *Ann N Y Acad Sci* 1067:37-44, 2006
34. Thannickal VJ, Fanburg BL: Reactive oxygen species in cell signaling. *Am J Physiol Lung Cell Mol Physiol* 279:L1005-1028, 2000
35. Ushio-Fukai M: Vascular signaling through G protein-coupled receptors: new concepts. *Curr Opin Nephrol Hypertens* 18:153-159, 2009
36. Kohchi C, Inagawa H, Nishizawa T, *et al.*: ROS and innate immunity. *Anticancer Res* 29:817-821, 2009
37. Eckers A, Klotz LO: Heavy metal ion-induced insulin-mimetic signaling. *Redox Rep* 14:141-146, 2009
38. Stadtman ER, Levine RL: Free radical-mediated oxidation of free amino acids and amino acid residues in proteins. *Amino Acids* 25:207-218, 2003
39. Levine RL, Mosoni L, Berlett BS, *et al.*: Methionine residues as endogenous antioxidants in proteins. *Proc Natl Acad Sci U S A* 93:15036-15040, 1996
40. Yao Y, Yin D, Jas GS, *et al.*: Oxidative modification of a carboxyl-terminal vicinal methionine in calmodulin by hydrogen peroxide inhibits calmodulin-dependent activation of the plasma membrane Ca-ATPase. *Biochemistry* 35:2767-2787, 1996
41. Nabuchi Y, Fujiwara E, Ueno K, *et al.*: Oxidation of recombinant human parathyroid hormone: effect of oxidized position on the biological activity. *Pharm Res* 12:2049-2052, 1995
42. Bigelow DJ, Squier TC: Redox modulation of cellular signaling and metabolism through reversible oxidation of methionine sensors in calcium regulatory proteins. *Biochim Biophys Acta* 1703:121-134, 2005
43. Colombo G, Meli M, Morra G, *et al.*: Methionine sulfoxides on prion protein Helix-3 switch on the alpha-fold destabilization required for conversion. *PLoS One* 4:e4296, 2009
44. Rempe DA, Takano T, Nedergaard M: TR(I)Pping towards treatment for ischemia. *Nat Neurosci* 12:1215-1216, 2009
45. McNulty S, Fonfria E: The role of TRPM channels in cell death. *Pflugers Arch* 451:235-242, 2005
46. Sun HS, Jackson MF, Martin LJ, *et al.*: Suppression of hippocampal TRPM7 protein prevents delayed neuronal death in brain ischemia. *Nat Neurosci* 12:1300-1307, 2009

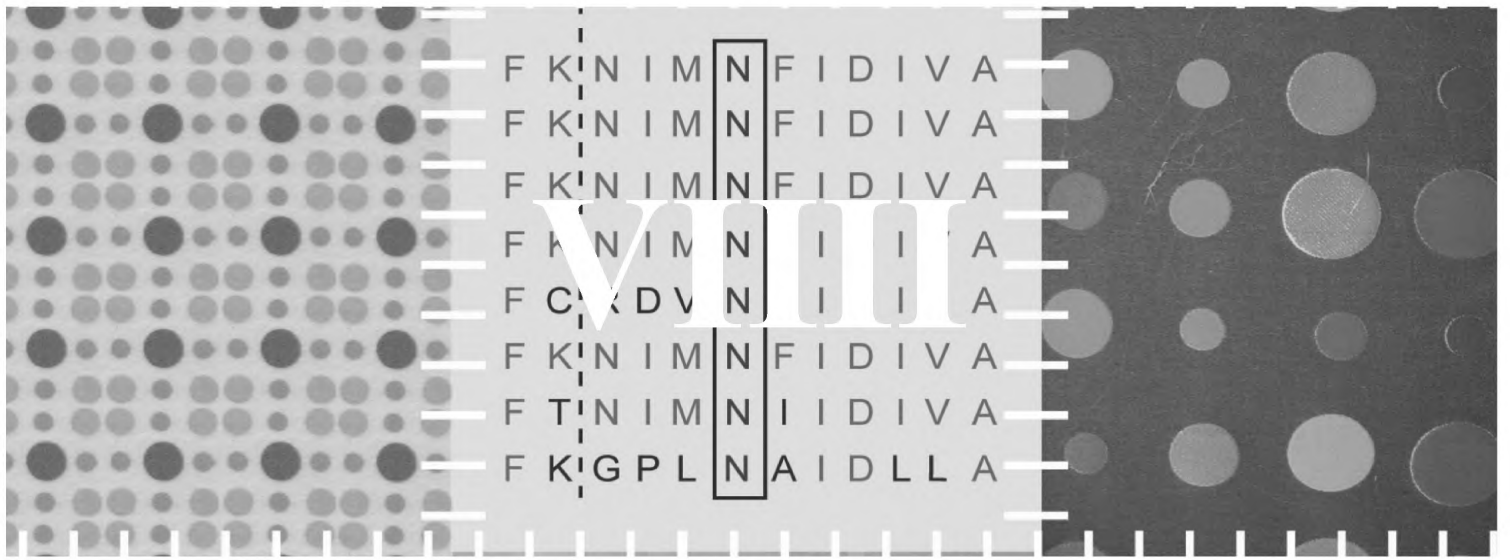
47. Fonfria E, Marshall IC, Benham CD, *et al.*: TRPM2 channel opening in response to oxidative stress is dependent on activation of poly(ADP-ribose) polymerase. *Br J Pharmacol* 143:186-192, 2004
48. Hara Y, Wakamori M, Ishii M, *et al.*: LTRPC2 Ca²⁺-permeable channel activated by changes in redox status confers susceptibility to cell death. *Mol Cell* 9:163-173, 2002
49. Zhang W, Chu X, Tong Q, *et al.*: A novel TRPM2 isoform inhibits calcium influx and susceptibility to cell death. *J Biol Chem* 278:16222-16229, 2003
50. Naziroglu M: New molecular mechanisms on the activation of TRPM2 channels by oxidative stress and ADP-ribose. *Neurochem Res* 32:1990-2001, 2007
51. Madsen KM, Verlander JW, Tisher CC: Relationship between structure and function in distal tubule and collecting duct. *J Electron Microsc Tech* 9:187-208, 1988
52. Thebault S, Cao G, Venselaar H, *et al.*: Role of the alpha-kinase domain in transient receptor potential melastatin 6 channel and regulation by intracellular ATP. *J Biol Chem* 283:19999-20007, 2008
53. Kozak JA, Cahalan MD: MIC channels are inhibited by internal divalent cations but not ATP. *Biophys J* 84:922-927, 2003
54. Gwanyanya A, Sipido KR, Vereecke J, *et al.*: ATP and PIP2 dependence of the magnesium-inhibited, TRPM7-like cation channel in cardiac myocytes. *Am J Physiol Cell Physiol* 291:C627-635, 2006
55. Monteilh-Zoller MK, Hermosura MC, Nadler MJ, *et al.*: TRPM7 provides an ion channel mechanism for cellular entry of trace metal ions. *J Gen Physiol* 121:49-60, 2003
56. Bailly C, Roinel N, Amiel C: Stimulation by glucagon and PTH of Ca and Mg reabsorption in the superficial distal tubule of the rat kidney. *Pflugers Arch* 403:28-34, 1985
57. Dai LJ, Bapty B, Ritchie G, *et al.*: Glucagon and arginine vasopressin stimulate Mg²⁺ uptake in mouse distal convoluted tubule cells. *Am J Physiol* 274:F328-335, 1998
58. Groenestegte WM, Thebault S, van der Wijst J, *et al.*: Impaired basolateral sorting of pro-EGF causes isolated recessive renal hypomagnesemia. *J Clin Invest* 117:2260-2267, 2007
59. Sanderson MP, Dempsey PJ, Dunbar AJ: Control of ErbB signaling through metalloprotease mediated ectodomain shedding of EGF-like factors. *Growth Factors* 24:121-136, 2006
60. Thebault S, Alexander RT, Tiel Groenestegte WM, *et al.*: EGF increases TRPM6 activity and surface expression. *J Am Soc Nephrol* 20:78-85, 2009
61. Ikari A, Okude C, Sawada H, *et al.*: TRPM6 expression and cell proliferation are up-regulated by phosphorylation of ERK1/2 in renal epithelial cells. *Biochem Biophys Res Commun* 369:1129-1133, 2008
62. Tejpar S, Piessevaux H, Claes K, *et al.*: Magnesium wasting associated with epidermal-growth-factor receptor-targeting antibodies in colorectal cancer: a prospective study. *Lancet Oncol* 8:387-394, 2007
63. Schilsky RL, Anderson T: Hypomagnesemia and renal magnesium wasting in patients receiving cisplatin. *Ann Intern Med* 90:929-931, 1979
64. McNair P, Christiansen C, Transbol I: Effect of menopause and estrogen substitutional therapy on magnesium metabolism. *Miner Electrolyte Metab* 10:84-87, 1984
65. Muneyyirci-Delale O, Nacharaju VL, Dalloul M, *et al.*: Serum ionized magnesium and calcium in women after menopause: inverse relation of estrogen with ionized magnesium. *Fertil Steril* 71:869-872, 1999
66. Groenestegte WM, Hoenderop JG, van den Heuvel L, *et al.*: The epithelial Mg²⁺ channel transient receptor potential melastatin 6 is regulated by dietary Mg²⁺ content and estrogens. *J Am Soc Nephrol* 17:1035-1043, 2006
67. Fu XD, Cui YH, Lin GP, *et al.*: Non-genomic effects of 17beta-estradiol in activation of the ERK1/ERK2 pathway induces cell proliferation through upregulation of cyclin D1 expression in bovine artery endothelial cells. *Gynecol Endocrinol* 23:131-137, 2007
68. Moriarty K, Kim KH, Bender JR: Minireview: estrogen receptor-mediated rapid signaling. *Endocrinology* 147:5557-5563, 2006
69. Zheng FF, Wu RC, Smith CL, *et al.*: Rapid estrogen-induced phosphorylation of the SRC-3 coactivator occurs in an extranuclear complex containing estrogen receptor. *Mol Cell Biol* 25:8273-8284, 2005

70. Revankar CM, Cimino DF, Sklar LA, *et al.*: A transmembrane intracellular estrogen receptor mediates rapid cell signaling. *Science* 307:1625-1630, 2005
71. Cabodi S, Moro L, Baj G, *et al.*: p130Cas interacts with estrogen receptor alpha and modulates non-genomic estrogen signaling in breast cancer cells. *J Cell Sci* 117:1603-1611, 2004
72. Levin ER: Cellular functions of plasma membrane estrogen receptors. *Steroids* 67:471-475, 2002
73. Katzenellenbogen JA, Katzenellenbogen BS: Nuclear hormone receptors: ligand-activated regulators of transcription and diverse cell responses. *Chem Biol* 3:529-536, 1996
74. Das SK, Tsukamura H, Paria BC, *et al.*: Differential expression of epidermal growth factor receptor (EGF-R) gene and regulation of EGF-R bioactivity by progesterone and estrogen in the adult mouse uterus. *Endocrinology* 134:971-981, 1994
75. Yarden RI, Lauber AH, El-Ashry D, *et al.*: Bimodal regulation of epidermal growth factor receptor by estrogen in breast cancer cells. *Endocrinology* 137:2739-2747, 1996
76. Carmeci C, Thompson DA, Ring HZ, *et al.*: Identification of a gene (GPR30) with homology to the G-protein-coupled receptor superfamily associated with estrogen receptor expression in breast cancer. *Genomics* 45:607-617, 1997
77. Thomas P, Pang Y, Filardo EJ, *et al.*: Identity of an estrogen membrane receptor coupled to a G protein in human breast cancer cells. *Endocrinology* 146:624-632, 2005
78. Funakoshi T, Yanai A, Shinoda K, *et al.*: G protein-coupled receptor 30 is an estrogen receptor in the plasma membrane. *Biochem Biophys Res Commun* 346:904-910, 2006
79. Filardo E, Quinn J, Pang Y, *et al.*: Activation of the novel estrogen receptor G protein-coupled receptor 30 (GPR30) at the plasma membrane. *Endocrinology* 148:3236-3245, 2007
80. Massague J, Pandiella A: Membrane-anchored growth factors. *Annu Rev Biochem* 62:515-541, 1993
81. Filardo EJ, Quinn JA, Bland KI, *et al.*: Estrogen-induced activation of Erk-1 and Erk-2 requires the G protein-coupled receptor homolog, GPR30, and occurs via trans-activation of the epidermal growth factor receptor through release of HB-EGF. *Mol Endocrinol* 14:1649-1660, 2000
82. Filardo EJ, Quinn JA, Sabo E: Association of the membrane estrogen receptor, GPR30, with breast tumor metastasis and transactivation of the epidermal growth factor receptor. *Steroids* 73:870-873, 2008
83. Prenzel N, Zwick E, Daub H, *et al.*: EGF receptor transactivation by G-protein-coupled receptors requires metalloproteinase cleavage of proHB-EGF. *Nature* 402:884-888, 1999
84. Christie MJ: Molecular and functional diversity of K⁺ channels. *Clin Exp Pharmacol Physiol* 22:944-951, 1995
85. Dolly JO, Parcej DN: Molecular properties of voltage-gated K⁺ channels. *J Bioenerg Biomembr* 28:231-253, 1996
86. Armstrong CM: Voltage-gated K channels. *Sci STKE* 2003:re10, 2003
87. Hille B: *Ion Channels of Excitable Membranes* 3ed. Sunderland, MA, Sinauer Associates, Inc., 2001
88. Long SB, Campbell EB, MacKinnon R: Crystal structure of a mammalian voltage-dependent Shaker family K⁺ channel. *Science* 309:897-903, 2005
89. Grottesi A, Sands ZA, Sansom MS: Potassium channels: complete and undistorted. *Curr Biol* 15:R771-774, 2005
90. Aggarwal SK, MacKinnon R: Contribution of the S4 segment to gating charge in the Shaker K⁺ channel. *Neuron* 16:1169-1177, 1996
91. Sands Z, Grottesi A, Sansom MS: Voltage-gated ion channels. *Curr Biol* 15:R44-47, 2005
92. Swartz KJ: Towards a structural view of gating in potassium channels. *Nat Rev Neurosci* 5:905-916, 2004
93. Armstrong CM, Hille B: Voltage-gated ion channels and electrical excitability. *Neuron* 20:371-380, 1998
94. O'Grady SM, Lee SY: Molecular diversity and function of voltage-gated (Kv) potassium channels in epithelial cells. *Int J Biochem Cell Biol* 37:1578-1594, 2005

95. Smart SL, Lopantsev V, Zhang CL, *et al.*: Deletion of the K(V)1.1 potassium channel causes epilepsy in mice. *Neuron* 20:809-819, 1998
96. Browne DL, Brunt ER, Griggs RC, *et al.*: Identification of two new KCNA1 mutations in episodic ataxia/myokymia families. *Hum Mol Genet* 4:1671-1672, 1995
97. Browne DL, Gancher ST, Nutt JG, *et al.*: Episodic ataxia/myokymia syndrome is associated with point mutations in the human potassium channel gene, KCNA1. *Nat Genet* 8:136-140, 1994
98. Chen H, von Hehn C, Kaczmarek LK, *et al.*: Functional analysis of a novel potassium channel (KCNA1) mutation in hereditary myokymia. *Neurogenetics* 8:131-135, 2007
99. Demos MK, Macri V, Farrell K, *et al.*: A novel KCNA1 mutation associated with global delay and persistent cerebellar dysfunction. *Mov Disord* 24:778-782, 2009
100. Eunson LH, Rea R, Zuberi SM, *et al.*: Clinical, genetic, and expression studies of mutations in the potassium channel gene KCNA1 reveal new phenotypic variability. *Ann Neurol* 48:647-656, 2000
101. Imbrici P, Gualandi F, D'Adamo MC, *et al.*: A novel KCNA1 mutation identified in an Italian family affected by episodic ataxia type 1. *Neuroscience* 157:577-587, 2008
102. Kinali M, Jungbluth H, Eunson LH, *et al.*: Expanding the phenotype of potassium channelopathy: severe neuromyotonia and skeletal deformities without prominent Episodic Ataxia. *Neuromuscul Disord* 14:689-693, 2004
103. Klein A, Boltshauser E, Jen J, *et al.*: Episodic ataxia type 1 with distal weakness: a novel manifestation of a potassium channelopathy. *Neuropediatrics* 35:147-149, 2004
104. Poujois A, Antoine JC, Combes A, *et al.*: Chronic neuromyotonia as a phenotypic variation associated with a new mutation in the KCNA1 gene. *J Neurol* 253:957-959, 2006
105. Shook SJ, Mamsa H, Jen JC, *et al.*: Novel mutation in KCNA1 causes episodic ataxia with paroxysmal dyspnea. *Muscle Nerve* 37:399-402, 2008
106. Zuberi SM, Eunson LH, Spauschus A, *et al.*: A novel mutation in the human voltage-gated potassium channel gene (Kv1.1) associates with episodic ataxia type 1 and sometimes with partial epilepsy. *Brain* 122 (Pt 5):817-825, 1999
107. Rajakulendran S, Tan SV, Matthews E, *et al.*: A patient with episodic ataxia and paramyotonia congenita due to mutations in KCNA1 and SCN4A. *Neurology* 73:993-995, 2009
108. Knight MA, Storey E, McKinlay Gardner RJ, *et al.*: Identification of a novel missense mutation L329I in the episodic ataxia type 1 gene KCNA1--a challenging problem. *Hum Mutat* 16:374, 2000
109. Scheffer H, Brunt ER, Mol GJ, *et al.*: Three novel KCNA1 mutations in episodic ataxia type I families. *Hum Genet* 102:464-466, 1998
110. Lee H, Wang H, Jen JC, *et al.*: A novel mutation in KCNA1 causes episodic ataxia without myokymia. *Hum Mutat* 24:536, 2004
111. Zerr P, Adelman JP, Maylie J: Episodic ataxia mutations in Kv1.1 alter potassium channel function by dominant negative effects or haploinsufficiency. *J Neurosci* 18:2842-2848, 1998
112. Shamotienko OG, Parcej DN, Dolly JO: Subunit combinations defined for K⁺ channel Kv1 subtypes in synaptic membranes from bovine brain. *Biochemistry* 36:8195-8201, 1997
113. Liman ER, Hess P, Weaver F, *et al.*: Voltage-sensing residues in the S4 region of a mammalian K⁺ channel. *Nature* 353:752-756, 1991
114. Pathak MM, Yarov-Yarovoy V, Agarwal G, *et al.*: Closing in on the resting state of the Shaker K(+) channel. *Neuron* 56:124-140, 2007
115. Long SB, Tao X, Campbell EB, *et al.*: Atomic structure of a voltage-dependent K⁺ channel in a lipid membrane-like environment. *Nature* 450:376-382, 2007
116. Creighton TH: *Proteins: structures and molecular properties*, in, edited by Freeman WH, San Francisco, 1993
117. Panyi G, Sheng Z, Deutsch C: C-type inactivation of a voltage-gated K⁺ channel occurs by a cooperative mechanism. *Biophys J* 69:896-903, 1995
118. Yellen G, Sodickson D, Chen TY, *et al.*: An engineered cysteine in the external mouth of a K⁺ channel allows inactivation to be modulated by metal binding. *Biophys J* 66:1068-1075, 1994

119. Planells-Cases R, Ferrer-Montiel AV, Patten CD, *et al.*: Mutation of conserved negatively charged residues in the S2 and S3 transmembrane segments of a mammalian K⁺ channel selectively modulates channel gating. *Proc Natl Acad Sci U S A* 92:9422-9426, 1995
120. Grubbs RD: Intracellular magnesium and magnesium buffering. *Biometals* 15:251-259, 2002
121. Yoshitomi K, Shimizu T, Taniguchi J, *et al.*: Electrophysiological characterization of rabbit distal convoluted tubule cell. *Pflugers Arch* 414:457-463, 1989
122. Mennitt PA, Wade JB, Ecelbarger CA, *et al.*: Localization of ROMK channels in the rat kidney. *J Am Soc Nephrol* 8:1823-1830, 1997
123. Iliev IG, Marino AA: Potassium channels in epithelial cells. *Cell Mol Biol Res* 39:601-611, 1993
124. Warth R: Potassium channels in epithelial transport. *Pflugers Arch* 446:505-513, 2003
125. Glaudemans B, van der Wijst J, Scola RH, *et al.*: A missense mutation in the Kv1.1 voltage-gated potassium channel-encoding gene KCNA1 is linked to human autosomal dominant hypomagnesemia. *J Clin Invest* 119:936-942, 2009
126. Gulbis JM: The beta subunit of Kv1 channels: voltage-gated enzyme or safety switch? *Novartis Found Symp* 245:127-141; discussion 141-125, 165-128, 2002
127. Sokolov MV, Shamotienko O, Dhochartaigh SN, *et al.*: Concatemers of brain Kv1 channel alpha subunits that give similar K⁺ currents yield pharmacologically distinguishable heteromers. *Neuropharmacology* 53:272-282, 2007
128. Zhu J, Watanabe I, Gomez B, *et al.*: Heteromeric Kv1 potassium channel expression: amino acid determinants involved in processing and trafficking to the cell surface. *J Biol Chem* 278:25558-25567, 2003
129. Bockenbauer D, Feather S, Stanescu HC, *et al.*: Epilepsy, ataxia, sensorineural deafness, tubulopathy, and KCNJ10 mutations. *N Engl J Med* 360:1960-1970, 2009
130. Scholl UI, Choi M, Liu T, *et al.*: Seizures, sensorineural deafness, ataxia, mental retardation, and electrolyte imbalance (SeSAME syndrome) caused by mutations in KCNJ10. *Proc Natl Acad Sci U S A* 106:5842-5847, 2009
131. Ito M, Inanobe A, Horio Y, *et al.*: Immunolocalization of an inwardly rectifying K⁺ channel, K(AB)-2 (Kir4.1), in the basolateral membrane of renal distal tubular epithelia. *FEBS Lett* 388:11-15, 1996
132. Reichold M, Zdebik AA, Lieberer E, *et al.*: KCNJ10 gene mutations causing EAST syndrome (epilepsy, ataxia, sensorineural deafness, and tubulopathy) disrupt channel function. *Proc Natl Acad Sci U S A*
133. Loffing J, Vallon V, Loffing-Cueni D, *et al.*: Altered renal distal tubule structure and renal Na⁽⁺⁾ and Ca⁽²⁺⁾ handling in a mouse model for Gitelman's syndrome. *J Am Soc Nephrol* 15:2276-2288, 2004
134. Lemmink HH, Knoers NV, Karolyi L, *et al.*: Novel mutations in the thiazide-sensitive NaCl cotransporter gene in patients with Gitelman syndrome with predominant localization to the C-terminal domain. *Kidney Int* 54:720-730, 1998
135. Lemmink HH, van den Heuvel LP, van Dijk HA, *et al.*: Linkage of Gitelman syndrome to the thiazide-sensitive sodium-chloride cotransporter gene with identification of mutations in Dutch families. *Pediatr Nephrol* 10:403-407, 1996
136. Whang R, Whang DD, Ryan MP: Refractory potassium repletion. A consequence of magnesium deficiency. *Arch Intern Med* 152:40-45, 1992
137. Gomez-Hernandez JM, Lorra C, Pardo LA, *et al.*: Molecular basis for different pore properties of potassium channels from the rat brain Kv1 gene family. *Pflugers Arch* 434:661-668, 1997
138. Drakenberg T: *Physical methods for studying the biological chemistry of magnesium*. New York, VCH, 1995
139. Cohn M, Hughes TR, Jr.: Nuclear magnetic resonance spectra of adenosine di- and triphosphate. II. Effect of complexing with divalent metal ions. *J Biol Chem* 237:176-181, 1962
140. Luthi D, Gunzel D, McGuigan JA: Mg-ATP binding: its modification by spermine, the relevance to cytosolic Mg²⁺ buffering, changes in the intracellular ionized Mg²⁺ concentration and the estimation of Mg²⁺ by ³¹P-NMR. *Exp Physiol* 84:231-252, 1999

141. Lanter F, Erne D, Ammann D, *et al.*: Neutral carrier based ion-selective electrode for intracellular magnesium activity studies. *Anal Chem* 52:2400-2402, 1980
142. Hu ZM, Buhner T, Muller M, *et al.*: Intracellular magnesium ion selective microelectrode based on a neutral carrier. *Anal Chem* 61:574-576, 1989
143. Gunzel D, Schlue WR: Determination of $[Mg(2+)]_i$ - an update on the use of Mg(2+)-selective electrodes. *Biometals* 15:237-249, 2002
144. Rink TJ, Tsien RY, Pozzan T: Cytoplasmic pH and free Mg^{2+} in lymphocytes. *J Cell Biol* 95:189-196, 1982
145. Schachter D: The fluorometric estimation of magnesium in serum and in urine. *J Lab Clin Med* 54:763-768, 1959
146. Raju B, Murphy E, Levy LA, *et al.*: A fluorescent indicator for measuring cytosolic free magnesium. *Am J Physiol* 256:C540-548, 1989
147. Murphy E: Measurement of intracellular ionized magnesium. *Miner Electrolyte Metab* 19:250-258, 1993
148. Gunther T, Vormann J, Konstanczak P, *et al.*: Interactions of polyamines in the measurement of free magnesium concentration by mag-fura-2 and ^{31}P -NMR. *Biochim Biophys Acta* 1192:281-285, 1994
149. Grubbs RD, Beltz PA, Koss KL: Practical considerations for using mag-fura-2 to measure cytosolic free magnesium. *Magnes Trace Elem* 10:142-150, 1991
150. Science IL: *The Molecular Probes Handbook - A Guide to Fluorescent Probes and Labeling Technologies*, 2009-2011
151. Komatsu H, Iwasawa N, Citterio D, *et al.*: Design and synthesis of highly sensitive and selective fluorescein-derived magnesium fluorescent probes and application to intracellular 3D Mg^{2+} imaging. *J Am Chem Soc* 126:16353-16360, 2004
152. Jin J, Desai BN, Navarro B, *et al.*: Deletion of *Trpm7* disrupts embryonic development and thymopoiesis without altering Mg^{2+} homeostasis. *Science* 322:756-760, 2008
153. Kubota T, Shindo Y, Tokuno K, *et al.*: Investigation of intracellular magnesium mobilization pathways I PC12 cells B simultaneous Mg-Ca fluorescent imaging. *J Am Coll Nutr* 23:742S-744S, 2004
154. Zhou H, Clapham DE: Mammalian MagT1 and TUSC3 are required for cellular magnesium uptake and vertebrate embryonic development. *Proc Natl Acad Sci US A* 106:15750-15755, 2009



Nederlandse samenvatting

List of abbreviations

Curriculum vitae

List of publications

Dankwoord

Introductie

Het menselijk lichaam bestaat uit miljoenen cellen, die elk verschillen in grootte en functie. De cel kan gezien worden als kleinste georganiseerde eenheid in een organisme. Alle cellen worden omgeven door een plasmamembraan, die een afscheiding vormt tussen het interne en externe milieu. De plasmamembraan is opgebouwd uit hydrofobe (waterafstotende) vetten en hydrofiele (wateraantrekkende) moleculen. De hydrofobe vetten vormen een barrière voor het membraantransport van hydrofiele en elektrisch geladen moleculen (ionen). In de jaren '50 en '60 zijn er speciale transporteiwitten ontdekt, die ionen door de plasmamembraan kunnen vervoeren. Deze eiwitten worden ionkanalen genoemd. Het transport van ionen door ionkanalen in de plasmamembraan kan gemeten worden als elektrische activiteit. De ontwikkeling van een techniek genaamd patch clamp maakt het mogelijk om de elektrische activiteit van een enkel ionkanaal in een levende cel te meten. Op deze manier kan de ionenstroom door het ionkanaal bepaald worden.

In de laatste decennia heeft onderzoek op dit gebied geleid tot de ontdekking van vele verschillende ionkanalen. De Transient Receptor Potential (TRP) transporteiwitten vormen een familie van ionkanalen. Er bestaan 28 TRP kanalen, die kunnen worden onderverdeeld in zes subfamilies: canonical (TRPC), vanilloïd (TRPV), polycystin (TRPP), mucolipin (TRPML), ankyrin (TRPA) en melastatin (TRPM). De TRPM6 en TRPM7 kanalen zijn essentieel voor het behoud van een gezonde Mg^{2+} balans in het lichaam. TRPM6 is voornamelijk gelokaliseerd in een speciaal segment van de nier, het distaal convoluut, waar het zorgt voor Mg^{2+} opname vanuit de voorurine. Deze opname, ook wel Mg^{2+} resorptie genoemd, bepaalt de uiteindelijke Mg^{2+} concentratie in het bloed. Genetisch onderzoek heeft uitgewezen dat TRPM6 frequent aangetast is in erfelijke aandoeningen met verlaagde bloed Mg^{2+} spiegels (hypomagnesiëmie). Een defect in het TRPM6 gen leidt tot een disfunctionerend TRPM6 kanaal, waardoor de patiënten onvoldoende Mg^{2+} resorberen vanuit de voorurine naar het bloed. Dit leidt tot de aandoening hypomagnesiëmie met secundaire hypocalcëmie (HSH). In tegenstelling tot TRPM6 komt TRPM7 in de meeste weefsels in het lichaam voor en speelt een belangrijke rol bij de algemene cellulaire Mg^{2+} huishouding.

De TRPM6 en TRPM7 eiwitten bestaan uit de unieke combinatie van een porievormend domein voor iontransport en een α -kinase domein. De α -kinases moduleren andere eiwitten door een fosfaatgroep toe te voegen (fosforylatie), waarmee deze eiwitten geactiveerd worden. Er is echter nog weinig bekend over de functionele rol van dit α -kinase domein in de regulatie van de TRPM6 kanaalfunctie. Daarnaast is er nog verder onderzoek vereist naar de regulatie van TRPM6 door bindingseiwitten, hormonen en andere factoren. Het onderzoek beschreven in dit proefschrift heeft als doel meer inzicht te bieden in de moleculaire regulatie van het epitheliale Mg^{2+} kanaal TRPM6 om zodoende de kennis over het proces van actieve Mg^{2+} resorptie in de nier te vergroten.

RACK1 als eerste bindingspartner van het TRPM6 α -kinase domein

Receptor for Activated C Kinase 1 (RACK1), ontdekt als bindingseiwit van Protein Kinase C (PKC), komt samen met TRPM6 voor in de Mg^{2+} -transporterende distaal convoluut cellen in de nier. Door binding aan het α -kinase domein van TRPM6 is RACK1 in staat de TRPM6 kanaalactiviteit te remmen (**Hoofdstuk 2**). Verlaging van endogeen RACK1 in de cel leidde tot stimulatie van de TRPM6 activiteit, hetgeen de directe remming van TRPM6 door RACK1 aantoonde. De inhibitie door RACK1 was afhankelijk van fosforylatie van een TRPM6 threonine residu (Thr¹⁸⁵¹) door het TRPM6 α -kinase domein (autofosforylatie). Deze autofosforylatie van Thr¹⁸⁵¹ beïnvloedde tevens de Mg^{2+} gevoeligheid van de TRPM6 kanaalactiviteit en de α -kinase autofosforylatie activiteit. De binding tussen RACK1 en het TRPM6 α -kinase domein werd sterk verminderd door activering van PKC, dat vervolgens het remmend RACK1-effect op de TRPM6 kanaalactiviteit kon opheffen. In deze studie is een nieuw model beschreven waarbij RACK1 de TRPM6-gedreven Mg^{2+} influx reguleert via interactie met het α -kinase domein, met een belangrijke rol voor de fosforylatie status van het Thr¹⁸⁵¹ residu.

TRPM6 regulatie door REA en oestrogeen

De naam ‘Repressor of Estrogen receptor Activity’ (REA) duidt de oorspronkelijk beschreven functie van het eiwit aan. REA onderdrukt namelijk de transcriptionele activiteit van oestrogeenreceptoren door binding aan de receptor. In het onderzoek beschreven in **Hoofdstuk 3** van dit proefschrift is REA als bindingspartner van het TRPM6 α -kinase domein geïdentificeerd, waarbij het aan dezelfde regio bindt als het eerder beschreven RACK1. Daarnaast bevindt REA zich in hetzelfde niersegment als TRPM6, wat de fysiologische rol van het eiwit benadrukt. REA was in staat om de TRPM6 kanaalactiviteit te remmen, maar had geen effect heeft op een kinase-inactieve TRPM6 mutant (K¹⁸⁰⁴R), die wel in staat was om REA te binden. De functie van REA werd bovendien niet aangetast door het wegvallen van de TRPM6 kinase activiteit, want REA werd niet gefosforyleerd door TRPM6. Daarnaast had REA geen effect op de autofosforylatie activiteit van TRPM6, dus de remmende werking van REA op de kanaalactiviteit kan niet het gevolg zijn van een eventueel remmend effect op autofosforylatie. Deze gegevens wijzen op een nog onbekende indirecte regulatie van TRPM6 door REA. Een mogelijke schakel in dit geheel zou het eiwit PKC kunnen zijn, aangezien activering van dit kinase zorgde voor extra remming van REA op TRPM6. Een interessante bevinding was de rol die oestrogeen in dit proces speelde. Toevoeging van de synthetische variant van oestrogeen, 17 β -estradiol, verstoorde de interactie tussen REA en TRPM6. Door verstoring van deze interactie was 17 β -estradiol in staat de TRPM6 kanaalactiviteit te stimuleren. In een eerdere studie is al aangetoond dat muizen die langdurig behandeld werden met 17 β -estradiol een toegenomen hoeveelheid TRPM6 kanalen in de nier aanmaakten. Hoofdstuk 3 van dit proefschrift beschrijft een geheel nieuw kort tijdspad waarop oestrogeen TRPM6 kan stimuleren. Tevens is REA ontdekt als

negatieve factor in de regulatie van de TRPM6-gedreven Mg^{2+} resorptie, met oestrogeen als belangrijke schakel in dit proces.

TRPM6, MsrB1 en oxidatieve stress

Methionine sulfoxide reductase B1 (MsrB1) behoort tot de Msr familie van eiwitten die bestaat uit MsrA en drie MsrB leden. Deze eiwitten komen met name voor in de nier, de lever, het hart en in het zenuwstelsel. Ze beschermen cellen tegen oxidatieve stress, doordat ze beschadigde eiwitten in de cel kunnen repareren. Deze schade ontstaat door de vorming van zogenaamde 'reactive oxygen species' (ROS), ofwel zuurstofradicalen die ontstaan uit normale metabole reacties. Er is echter steeds meer bewijs dat ROS niet alleen schadelijke producten zijn van deze reacties, maar ook een essentiële rol vervullen voor signalen in de cel. MsrB1, dat methioninesulfoxide reduceert tot methionine, zou een dynamische rol kunnen spelen in deze signaalpaden. MsrB1 is geïdentificeerd als derde bindingspartner van het TRPM6 α -kinase domein (**Hoofdstuk 4**). Onder normale metabole condities had MsrB1 geen effect op de TRPM6 kanaalactiviteit. Inductie van oxidatieve stress door toediening van waterstofperoxide (H_2O_2) veroorzaakte echter een drastisch remmend effect op de TRPM6 kanaalactiviteit. Het methionine residu (Met¹⁷⁵⁵) in TRPM6 was van belang voor het H_2O_2 effect. Verandering van deze methionine in alanine (Met¹⁷⁵⁵Ala, een residu dat niet geoxideerd kan worden) was in staat de remming op de TRPM6 kanaalactiviteit grotendeels op te heffen. Bovendien kon het remmend effect gedeeltelijk worden hersteld door MsrB1. Deze data geven aan dat MsrB1 een rol speelt bij de regulatie van TRPM6 gedurende oxidatieve stress. Het grote aantal mitochondria in de distaal convoluutcellen, een belangrijke bron voor H_2O_2 , zou een fysiologische verklaring kunnen zijn voor de link tussen TRPM6 en MsrB1.

Het effect van Erlotinib op TRPM6-gedreven Mg^{2+} transport

Het is bekend dat receptoren van de epidermale groei factor (EGFR) bij verschillende typen kanker overvloedig aanwezig zijn in de cel en voor ongecontroleerde celgroei zorgen. Deze ongecontroleerde groei kan geblokkeerd worden door het gebruik van monoklonale antilichamen tegen EGFR of specifieke remmers van de zogenaamde tyrosine kinase functie van de EGFR. Cetuximab, een bekende blokker van de EGFR, wordt regelmatig gebruikt tegen darmkanker en het uit recente studies blijkt dat deze behandeling tot hypomagnesiëmie kan leiden. Naast de EGFR antilichamen, zoals Cetuximab, zijn er ook patiënten die behandeld worden met tyrosine kinase-remmers, waaronder Erlotinib. Er is tot dusver niks bekend over het potentiële effect van Erlotinib op de Mg^{2+} huishouding. In **Hoofdstuk 5** van dit proefschrift is het effect van Erlotinib op de regulatie van de Mg^{2+} balans bestudeerd. Gedurende 23 dagen hebben muizen een supra-fysiologische doses Erlotinib toegediend gekregen. Vervolgens werden de Mg^{2+} waarden in bloed en urine gemeten en de hoeveelheid TRPM6 eiwit in de nier bepaald. De muizen vertoonden een verlaagde bloed Mg^{2+}

waarde, terwijl er geen verandering in Mg^{2+} concentratie in de urine zichtbaar was. Dit suggereert een defect in de nieren. Er was bovendien geen verandering waarneembaar in de hoeveelheid TRPM6 eiwit in de nier. Om het effect van Erlotinib op TRPM6 verder te onderzoeken is de kanaalactiviteit gemeten. Er is al eerder aangetoond dat EGF in staat is de TRPM6 kanaalactiviteit te vergroten door transport van TRPM6 eiwitten vanuit het cytoplasma naar de plasmamembraan te stimuleren. Onze studie toonde aan dat Erlotinib deze EGF-gedreven stimulatie van TRPM6 kanaalactiviteit ophief. De remmende werking van Erlotinib is te wijten aan het blokkeren van de EGF-gedreven beweging van TRPM6 kanalen naar de plasmamembraan. De effecten van Erlotinib zijn concentratieafhankelijk, aangezien lagere Erlotinib concentraties (zoals ze worden toegediend aan patiënten) geen effect hebben op de EGF stimulatie. Dit verklaart het feit dat patiënten die Erlotinib voorgeschreven krijgen geen hypomagnesiëmie ontwikkelen. Er zou desondanks extra oplettendheid geboden moeten worden bij patiënten die meer gevoelig zijn om hypomagnesiëmie te ontwikkelen, door combinatie-gebruik van Mg^{2+} -verlagende medicijnen.

Kv1.1 als nieuw ionkanaal in de regulatie van de Mg^{2+} balans

Voltage-afhankelijke kalium (K^+) kanalen behoren tot een veelzijdige familie van ionkanalen, Kv genaamd, die een belangrijke rol spelen bij de elektrische signalen in de cel. Ze gaan open en dicht als gevolg van veranderingen in de elektrische lading over de plasmamembraan van de cel (membraanpotentiaal). In **Hoofdstuk 6** van dit proefschrift wordt een familie beschreven, die aan een erfelijke aandoening van renaal Mg^{2+} verlies lijdt, als gevolg van een mutatie in het gen dat codeert voor Kv1.1. De aangedane familieleden hebben zeer lage bloed Mg^{2+} spiegels (< 0.40 mM, normaal $0.70-0.95$ mM) en hebben al vanaf jonge leeftijd last van spierkrampen, tetanie, spierzwakte en myokymie. Tot dusver zijn er enkel mutaties beschreven in Kv1.1 die leiden tot de ziekte episodische ataxie (EA1) en onze studie toont voor het eerst een link aan tussen Kv1.1 en hypomagnesiëmie. Er is aangetoond dat Kv1.1 evenals TRPM6 voorkomt op de plasmamembraan aan de voorurine zijde van de distaal convoluutcellen. De mutatie die gevonden is in de patiënten van bovenstaande familie resulteert in de aminozuurverandering Asn²⁵⁵ Asp. Het gemuteerde kanaal bevindt zich nog wel op de plasmamembraan, maar kan niet meer normaal functioneren. Hierdoor is het defecte Kv1.1 kanaal niet meer in staat om de membraanpotentiaal van de cel te handhaven. Aangezien er geen verschil is tussen Mg^{2+} concentraties aan beide zijden van de plasmamembraan (chemische gradiënt), is een negatieve membraanpotentiaal essentieel om een elektrische gradiënt te creëren voor Mg^{2+} opname via TRPM6 vanuit de urine. De hypothese in deze studie is dat Kv1.1 de membraanpotentiaal van de distaal convoluutcellen verzorgt en dat de mutatie in Kv1.1 dit proces verstoort, zodat er een verminderde Mg^{2+} resorptie plaatsvindt die de hypomagnesiëmie in deze familie verklaart.

Functionele gevolgen van de Kv1.1 N²⁵⁵D mutatie

Zoals hierboven beschreven, leidt de mutatie in Kv1.1 tot een ‘dood’ kanaal, terwijl de hoeveelheid kanalen op de plasmamembraan niet verminderd was. Daarom is het onderzoek beschreven in **Hoofdstuk 7** gericht op het belang van het bovengenoemde asparagine residu (N²⁵⁵) voor de Kv1.1 kanaalfunctie. Hiervoor werden er diverse aminozuurveranderingen aangebracht op de positie van het N²⁵⁵ residu om het effect van verandering van lading, verlies van waterstofbrugvorming en sterische hindering te bestuderen. Geen van de aminozuurveranderingen had een effect op het vervoer van Kv1.1 kanalen naar het plasmamembraan. De hypothese dat een negatieve lading op het 255 residu de kanaalfunctie zou veranderen, is onderzocht door vervanging van de neutrale asparagine door een negatief geladen glutaminezuur (N²⁵⁵E) of een positief geladen histidine (N²⁵⁵H). Daarbij werd tevens als controle voor structurele hindering van het grotere glutaminezuur het effect van een ongeladen glutamine (N²⁵⁵Q) onderzocht. De N²⁵⁵E en N²⁵⁵Q kanalen konden geen K⁺ meer konden transporteren, terwijl het N²⁵⁵H kanaal normaal functioneerde. Dit laat zien dat er geen specifieke link is tussen lading op het 255 residu en kanaalfunctie. Een andere optie die werd onderzocht, is dat een aminozuurverandering op het 255 residu de vorming van waterstofbruggen met ander residuen opheft, wat gevolgen heeft voor de kanaalfunctie. Daarom werden de gemuteerde Kv1.1 kanalen N²⁵⁵A (asparagine naar alanine), N²⁵⁵V (asparagine naar valine) en N²⁵⁵T (asparagine naar threonine) getest. De aminozuurveranderingen bleken geen effect te hebben op de activiteit van het kanaal, maar tasten zowel de kinetiek van het openen en sluiten van de kanalen aan, als ook de gevoeligheid voor veranderingen in de membraanpotentiaal. Er kan echter geen duidelijke correlatie worden gelegd tussen enerzijds de aminozuurverandering die leidt tot verschillen in grootte van het aminozuur, verlies van waterstofbrugvorming of introductie van lading, en anderzijds de verandering van de kinetiek en voltage-gevoeligheid voor het openen en sluiten van het Kv1.1 kanaal. Er kan geconcludeerd worden het N²⁵⁵ residu essentieel is voor een normale Kv1.1 kanaalfunctie, aangezien de aminozuurveranderingen significante verschillen vertoonden in bovenstaande karakteristieken van het kanaal. Een meer gedetailleerde analyse van de structuur en de betrokkenheid van andere aminozuren is echter noodzakelijk om de link tussen het N²⁵⁵ residu en Kv1.1 kanaalfunctie te ontrafelen.

Conclusie en toekomstperspectieven

Het doel van het onderzoek, beschreven in dit proefschrift, is het vergroten van de kennis en inzicht in de (patho)fysiologische aspecten en moleculaire regulatie van actieve Mg²⁺ resorptie in de nier. Tijdens de diverse studies zijn verschillende regulatoren van TRPM6 gevonden, waaronder bindende eiwitten, hormonen en specifieke medicijnen. Bovendien is Kv1.1 ontdekt als cruciaal ionkanaal in de nier voor het behoud van de Mg²⁺ balans. Dit draagt bij aan de opheldering van de regulatiemechanismen die betrokken zijn bij het proces van Mg²⁺ resorptie. Desondanks zijn

verscheidene aspecten in dit proces nog onbekend, zoals het eiwit dat Mg^{2+} vanuit de distaal convoluitcel naar het bloed vervoert en een eiwit dat betrokken is bij de Mg^{2+} diffusie en/of buffer in de cel. Nieuwe genen, coderend voor Mg^{2+} -transporterende eiwitten, kunnen worden ontdekt middels genetische studies naar aandoeningen met erfelijk verlaagde bloed Mg^{2+} spiegels, zoals in dit proefschrift is gedaan. Daarnaast zijn er in de afgelopen jaren al enkele Mg^{2+} -transporterende eiwitten ontdekt en nader onderzoek naar deze eiwitten kan de mogelijke fysiologische rol in de Mg^{2+} huishouding ontrafelen. Er ligt ook een interessante uitdaging om de rol van de TRPM6 α -kinase verder op te helderen. Nieuwe projecten kunnen gericht zijn op de bestudering van een directe link tussen TRPM6 kanaalfunctie en de functie van het α -kinase domein. Gezamenlijk zullen de toekomstige studies de kennis vergroten rondom het moleculaire mechanisme van actieve Mg^{2+} resorptie en regulatie hiervan door het TRPM6 kanaal en α -kinase domein. Dit kan uiteindelijk worden gebruikt om nieuwe therapieën te ontwikkelen voor hypomagnesiëmie en andere Mg^{2+} -gerelateerde aandoeningen.

List of abbreviations

[Mg ²⁺] _i	intracellular Mg ²⁺ concentration
2-ABP	2-amino-ethoxydiphenyl borate
ANOVA	analysis of variance
ATP	adenosine 5'-triphosphate
ATPase	adenosine 5'-triphosphatase
bp	base pairs
Ca ²⁺	calcium ion
cAMP	cyclic adenosine monophosphate
CD	collecting duct
cDNA	complementary deoxyribonucleic acid
Cl ⁻	chloride ion
CLC-Kb	Cl ⁻ channel Kb
<i>CLDN16</i>	gene encoding claudin 16
<i>CLDN19</i>	gene encoding claudin 19
CNT	connecting tubule
cM	centi-Morgan
DCT	distal convoluted tubule
DMEM	dulbecco's modified eagle medium
EDTA	ethylenediaminetetraacetate
EGF	epidermal growth factor
EGFR	epidermal growth factor receptor
FTMS	fourier transform ion cyclotron resonance mass spectrometry
GFP	green fluorescent protein
GST	glutathione S-transferase
HEK293	human embryonic kidney cells
HEPES	4-(2-hydroxyethyl)-1-piperazineethanesulfonic acid
HSH	hypomagnesemia with secondary hypocalcemia
IC ₅₀	half maximal inhibitory concentration
IRH	isolated recessive renal hypomagnesemia
I/V	current-voltage relationship
K ⁺	potassium ion
KCl	potassium chloride
<i>KCNA1</i>	gene encoding Kv1.1
kDa	kilo dalton

List of abbreviations

Kv1.1	voltage-gated K ⁺ channel 1.1, <i>shaker</i> , member 1
MDCK cells	madin darby canine kidney cells
Mg ²⁺	magnesium ion
Mg ²⁺ ·ATP	Mg ²⁺ bound to ATP
mRNA	messenger ribonucleic acid
MsrB1	methionine sulfoxide reductase B1
mTAL	medullary thick ascending limb of Henle's loop
Na ⁺	sodium ion
NaCl	sodium chloride
NCC	Na ⁺ ,Cl ⁻ -cotransporter
PBS	phosphate-buffered saline
PCR	polymerase chain reaction
PIP ₂	phosphatidylinositol 4,5-bisphosphate
PKA	protein kinase A
PKC	protein kinase C
PLC	phospholipase C
PMA	phorbol 12-myristate 13-acetate
PT	proximal tubule
RACK1	receptor for activated c-kinase 1
REA	repressor of estrogen receptor activity
RRS	ras recruitment system
RT-PCR	reverse-transcriptase polymerase chain reaction
SDS-PAGE	sodium dodecyl sulphate polyacrylamide gel electrophoresis
SEM	standard error of the mean
TAL	thick ascending limb of Henle's loop
TIRF	total internal reflection fluorescence
TM	transmembrane segment
Tris	tris(hydroxymethyl)aminomethane
TRP	transient receptor potential channel
TRPA	transient receptor potential channel, subfamily ankyrin
TRPC	transient receptor potential channel, subfamily canonical
TRPM	transient receptor potential channel, subfamily melastatin
TRPML	transient receptor potential channel, subfamily mucolipin
TRPP	transient receptor potential channel, subfamily polycystin
TRPV	transient receptor potential channel, subfamily vanilloid
YFP	yellow fluorescent protein

Curriculum vitae

Jenny van der Wijst werd geboren op 25 september 1983 te Oss. Zij behaalde in 2001 het VWO examen aan het Udens college te Uden. Vervolgens studeerde ze Biologie aan de Radboud Universiteit Nijmegen. Tijdens deze opleiding verrichtte zij een mini-stage van 3 maanden op de afdeling Cellulaire Dierfysiologie (onder leiding van Dr. W.J. Scheenen en Prof. Dr. E.W. Roubos). Ze vervolgde haar studie met een stage van 9 maanden op de afdeling Celbiologie (onder leiding van Dr. A.P. Theuvenet en Prof. Dr. E.J. van Zoelen). Haar laatste stage werd opgedeeld over twee tijdsperiodes, waarbij ze startte bij de afdeling Fysiologie (onder leiding van Dr. G. Cao) om vervolgens de laatste 4 maanden van haar stage werkzaam te zijn op de afdeling 'Kidney and Acid-base Physiology' van Fysiologie Instituut aan de Universiteit van Zürich in Zwitserland (onder leiding van Prof. Dr. C.A. Wagner). In 2006 behaalde ze haar doctoraal examen. Aansluitend startte ze in oktober 2006 als onderzoeker in opleiding (OIO) op de afdeling Fysiologie van het UMC St Radboud, onder leiding van Prof. dr. J.G.J. Hoenderop en Prof. Dr. R.J.M. Bindels, wat heeft geleid tot het in dit proefschrift beschreven onderzoek. Tijdens haar promotieonderzoek begeleidde ze een student van de internationale masteropleiding "Molecular Mechanisms of Disease" en werd er een bijdrage geleverd aan demonstratiepractica voor bachelor en masterstudenten. Daarnaast was ze in de periode 2007-2009 actief als lid van de PhD commissie van het Nijmegen Centre for Molecular Life Sciences (NCMLS) en organiseerde ze in dit kader de jaarlijkse NCMLS PhD retraite. Tevens heeft ze in april 2009 de prijs voor beste poster presentatie verkregen op de jaarlijkse NCMLS PhD retraite en is in december 2009 het Frye stipendium van de Radboud Universiteit Nijmegen aan haar uitgereikt. Per maart 2011 zal ze als post-doc werkzaam zijn op het lab van Dario Alessi in de Protein Phosphorylation Unit (Dundee, Schotland), gefinancierd via een EMBO long-term fellowship van the European Molecular Biology Organization.

List of publications

Groenestege W.M, Thebault S, **van der Wijst J**, van den Berg D, Janssen R, Tejpar S, van den Heuvel LP, van Cutsem E, Hoenderop JG, Knoers NV, Bindels RJ. Impaired basolateral sorting of pro-EGF causes isolated recessive renal hypomagnesemia. *J Clin Invest* 117: 2260-2267, 2007

Cao G*, Thebault S*, **van der Wijst J**, van der Kemp A, Lasonder E, Bindels RJ, Hoenderop JG. RACK1 inhibits TRPM6 activity via phosphorylation of the fused alpha-kinase domain. *Curr Biol* 18: 168-176, 2008 *contributed equally to this work

van der Wijst J*, Glaudemans B*, Scola RH, Lorenzi PJ, Heister A, van der Kemp AW, Knoers NV, Hoenderop JG, Bindels RJ. A missense mutation in the Kv1.1 voltage-gated potassium channel-encoding gene KCNA1 is linked to human autosomal dominant hypomagnesemia. *J Clin Invest* 119: 936-942, 2009 *contributed equally to this work

van der Wijst J*, Cao G*, van der Kemp A, van Zeeland F, Bindels R.J, Hoenderop J.G. Regulation of the epithelial Mg²⁺ channel TRPM6 by estrogen and the associated repressor protein of estrogen receptor activity (REA). *J Biol Chem* 284: 14788-14795, 2009 *contributed equally to this work

van der Wijst J, Hoenderop JG, Bindels RJ. Epithelial Mg²⁺ channel TRPM6: insight into the molecular regulation. *Magnes Res* 22: 127-132, 2009

van der Wijst J, Glaudemans B, Venselaar H, Nair A, Forst A, Hoenderop JG, Bindels RJ. Functional analysis of the Kv1.1 N255D mutation associated with autosomal dominant hypomagnesemia. *J Biol Chem* 285: 171-178, 2010

Cao G*, Lee KP*, **van der Wijst J**, de Graaf M, van der Kemp A, Bindels RJ, Hoenderop JG. MsrB1 recovers TRPM6 channel activity during oxidative stress. *J Biol Chem* 285: 26081-26087, 2010 *contributed equally to this work

Dimke H, **van der Wijst J**, Alexander TR, Meijer IMJ, Mulder GM, van Goor H, Tejpar S, Hoenderop JG, Bindels RJ. Effects of the Epidermal Growth Factor Receptor (EGFR) kinase inhibitor Erlotinib on renal and systemic magnesium handling. *J Am Soc Nephrol* 21: 1309-1316, 2010

Vermeer S, Hoischen A, Meijer RP, Gilissen C, Neveling K, Wieskamp N, de Brouwer A, Koenig M, Anheim M, Assoum M, Drouot N, Todorovic S, Milic-Rasic V, Lochmüller H, Stevanin G, Goizet C, David A, Durr A, Brice A, Kremer B, van de Warrenburg BP, Schijvenaars MM, Heister A, Kwint M, Arts P, **van der Wijst J**, Veltman J, Kamsteeg EJ, Scheffer H, Knoers N. Targeted Next-Generation Sequencing of a 12.5 Mb Homozygous Region Reveals ANO10 Mutations in Patients with Autosomal-Recessive Cerebellar Ataxia. *Am J Hum Genet* (in press)

Dankwoord

Wat zijn de jaren voorbij gevlogen als ik terugkijk, zoveel geleerd en zoveel gegroeid, op wetenschappelijk én op persoonlijk vlak. Het is fijn om op deze laatste pagina's van m'n proefschrift alle mensen (collega's, vrienden en familie) te bedanken die daaraan hebben bijgedragen.

Allereerst wil ik mijn promotores Prof. dr. **René** Bindels en Prof. dr. **Joost** Hoenderop bedanken. Ik heb 'n goede tijd gehad op de afdeling Fysiologie.

Beste **René**, ik wil je bedanken voor de mogelijkheid om mijn promotieonderzoek hier te doen. Jouw inzicht in de fysiologie, slagvaardigheid, en organisatietalent zijn bewonderenswaardig en een fundament voor het succes van de afdeling. Ik heb veel geleerd van je kritische blik en daarnaast heeft je vertrouwen in mijn werk me gesteund. De EMBO fellowship voelt als 'n kroon op dit alles en laat het maar een goede start zijn van 'n mooie nieuwe periode.

Beste **Joost**, jouw inzet en enthousiasme voor onderzoek zijn onnavolgbaar. Het is enorm fijn geweest om het gevoel te hebben altijd bij je binnen te kunnen stappen. Daarnaast wil ik je bedanken voor alles wat je me geleerd hebt op het gebied van presentatie- en schrijfvaardigheden.

Ook gaat mijn dank uit naar Prof. dr. **Nine** Knoers. Door samenwerking met de afdeling Antropogenetica zijn er mooie publicaties tot stand gekomen. Ik wil je verder heel veel succes wensen met je nieuwe baan in Utrecht.

Een andere prettige samenwerking is die met het CMBI. Ik wil graag Prof. dr. **Gert Vriend** en **Hanka Venselaar** bedanken voor alle behulpzaamheid en de verhelderende blik op de structuur van het TRPM6 kinase domein, maar vooral voor de modeling van Kv1.1.

Hierbij wil ik ook mijn student Anna-Lena Forst betrekken. **Anna-Lena**, bedankt voor je enorme inzet tijdens je stage en alle uitleg over de structuurveranderingen van Kv1.1, het heeft tot 'n mooie publicatie geleid.

I would like to thank all my colleagues of the department of Physiology for support, nice talks, good drinks, fruitful discussions and for creating an 'gezellige' atmosphere. I would especially like to thank a couple of people that were closer related to my daily lab activities over the past four years.

Gang, your enthusiasm for science is great! It was great having you as my supervisor for the student internship. This is where our collaborative studies started on your TRPM6 kinase babies. I enjoyed working with you, thanks a lot!

Dankwoord

Wouter, wat was 't goed om bij jou in de unit te belanden als student. Eerst voornamelijk met m'n mond vol tanden staan, maar ik heb flink wat opgestoken van jou directe en adremme opmerkingen, bedankt! Je heldere blik en humor doen 't trouwens nog steeds goed, tegenwoordig onder genot van 'n biertje en veel gezelligheid.

Kirsten, het was fijn dat jij ook in Zürich zat toen ik daar als naïeve student stage kwam lopen. Ik heb je leren kennen als 'n lieve, warme persoon en wil je alle succes wensen met je nieuwe uitdaging in Utrecht komend jaar!

Rob (J.), ik ben blij dat we contact zijn blijven houden. Het is altijd erg fijn en gezellig om je weer te zien en spreken. En wat was New York tof!! Ik hoop over vier jaar ook jouw boekje te mogen ontvangen, succes met je promotietraject in Amsterdam!

Todd, I have fond memories of the time you spend in Nijmegen, I cherish your goodbye email and I hope to see you this year, either in Nijmegen or in Alberta, Canada.

AnneMiete en Irene, jullie draaien al 'n aantal jaren mee op de afdeling. **AnneMiete**, jouw bijdrage in het onderzoek is in nagenoeg ieder hoofdstuk van dit proefschrift terug te vinden, bedankt hiervoor. **Irene**, ik wil je bedanken voor je bijdrage in de vorm van het altijd tijd vrij maken voor alle bestellingen en vragen. Daarnaast wil ik jullie vooral bedanken voor de interesse die altijd getoond werd tijdens de koffiepauzes.

Femke en Mark, jullie zijn 'n belangrijke spil op de afdeling en ik bewonder de manier hoe jullie flexibel tussen verschillende projecten switchen. Ook wil ik jullie beide bedanken voor de extra experimenten die vaak nodig waren voor alle rebuttals van de artikelen in dit proefschrift.

Silvia en Anke, I really enjoyed our dinner nights/afternoons (together with Leonie)! I wish you all the best with finishing your PhD thesis at the department, you will do great!

Mannen uit 't hetzelfde startjaar: **Anne, Theun, Henrik**, wat was 't fijn om gezamenlijk deze promotietijd te doorlopen. **Anne**, jouw positiviteit is geweldig! Een hoop gezelligheid met jou op 't lab en daarbuiten. Ik herinner me genoeg mooie bieravondjes en toffe feestjes op de Molenweg. **Theun**, ik vond 't altijd fijn om met je praten en voel veel herkenning. Jij bent er ook bijna met je boekje en ik wens je veel succes met de vervolgstap. **Henrik**, "my Unit-partner", I cannot think of a better one:-) Thanks for your support and good laughs!

Patch team: **Stephanie**, thanks for helping me out in the starting period as patcher. **Catalin**, jij was de eerste met wie ik dagenlang in de patchruimte heb doorgebracht, erg fijn en leerzaam! **Kyu pil**, I got to know you as very clever and technically skilled patcher, thanks for all the things you have learned

me in this field. **Anil**, I admire your bright vision on both daily lab work and daily life. I appreciate your warm and caring personality. It's fantastic that you'll be standing next to me as paranimf. **Sjoerd**, jouw positieve instelling is super! Ik vond 't enorm fijn om met je samen te werken en om daarnaast portjes en biertjes met je te drinken, top! **Sergio**, you are the newest member of the patch-team and your quick way of mingling, both inside and outside of the lab, is wonderful.

Onmisbaar voor een succesvolle OIO periode is de tijd die je nog spendeert buiten het lab met 'n aantal zeer mooie en lieve vrienden:

Bobby, jij hebt deze periode van zeer dichtbij meegemaakt en wat hebben we de afgelopen tweeënhalf jaar veel beleefd in ons paleisje in hartje Nijmegen; gediscussieerd, steun gezocht en gevonden, gelachen, gehuild (ik dan), geleerd met en van elkaar, onvergetelijk! 'Een bonte tijd' als ik erop terugkijk....Bij jou zal 't leven nooit kleurloos worden, je bent 'n bijzonder en mooi persoon, Bob! Ik heb er alle vertrouwen in dat je 't helemaal gaat maken in Zürich (en kijk al uit naar onze bezoeken).

Minja, sweetie, I will always remember our coffee breaks during working hours, which could be either helpful for serious stuff or just fun for juicy details;-) I cherish our lazy dinner/movie nights, as well as the ones we went out for dancing that mostly started off with great photos at your place. Let's keep on visiting each other, anywhere in the world!

Goric, wat is het goed dat er PhD retraites bestaan, vooral die van 2009! Erg fijn dat we elkaar hebben leren kennen. Je bent een lieve vriendin en een topper in je werk, ik heb alle vertrouwen in je! En **Ad**, wat was New York 'n toffe ervaring, ik ben blij je daar te hebben leren kennen en laten we 't zien als 'n mooie start voor de toekomst. We gaan gedrieën vast nog veel mooie dingen beleven onder het genot van lekkere wijntjes.

An, ik ben zo enorm blij dat we elkaar zijn tegengekomen! Jouw enthousiasme, stralende lach en open blik naar de wereld doen 't altijd goed. Leven staat met 'n hele grote L in ons woordenboek!!

Leo, ik wil je bedanken voor alle momenten dat je voor me hebt klaargestaan. En daarbij voor al je gezelligheid natuurlijk! Je moet weten dat je ook altijd bij mij terecht zal kunnen.

En voor jullie samen **An en Leo**, ik ga nog vaak terugdenken aan onze enorm gezellige 'eet-klets-of-sauna-avondjes', die blijven we doen hoor!

Marie, jij maakte 't extra fijn om thuis te komen in Uden. Ondanks onze drukke schema's van de afgelopen jaren, heb ik onze 'dates' altijd heel erg gewaardeerd, supergezellig en verhelderd. Je ben 'n schat!

Frouk, wat zijn onze levens toch veranderd vergeleken met zo'n 10 jaar geleden. We zien elkaar niet zo vaak meer als vroeger, maar je moet weten dat ik 't altijd heel leuk vind om samen te komen. Grote hoeveelheden vlees eten bij Marc's BBQ of de Griek moeten we er gewoon in houden;-)!

Rob (P.), ik heb jou leren kennen in m'n studietijd en het voelt daarom als 'n cirkel rondmaken met jou als paranimf. Het is fijn om te weten dat er iemand is die minstens zo perfectionistisch is als ik;-) Ik zou eigenlijk alleen willen zeggen: "maak je niet te druk, **Erwin** en jij zijn samen top!"

Job, jij bent een belangrijke pilaar geweest tijdens m'n studie en start van m'n promotie. Ik heb heel goede herinneringen aan onze tijd samen. Je hebt een mooi plekje in m'n hart!

Freek en Lisa, ik had me geen betere afsluiting van m'n promotietijd voor kunnen stellen dan met jullie door Laos en Cambodja te reizen. Ik heb er enorm van genoten en het heeft me veel nieuwe energie gegeven om verder te gaan. Het is zeker jammer dat jullie niet bij de verdediging zullen zijn, maar zoals afgesproken zien we elkaar weer in Schotland!

En natuurlijk, **paps en mams**, wil ik jullie enorm bedanken! Ik ben misschien niet even gemakkelijk voor jullie geweest in de afgelopen hectische periode, maar het geeft 'n enorm goed gevoel om te weten dat jullie altijd onvoorwaardelijk achter me staan en trots zijn op wat ik doe. Dit maakt mede tot wie ik ben en waar ik sta. Jullie steun is ontzettend belangrijk voor me, dank jullie wel!!